ANL/NE-16/19

Argonne NATIONAL LABORATORY

The SAS4A/SASSYS-1 Safety Analysis Code System

Nuclear Engineering Division

About Argonne National Laboratory

Argonne is a U.S. Department of Energy laboratory managed by UChicago Argonne, LLC under contract DE-AC02-06CH11357. The Laboratory's main facility is outside Chicago, at 9700 South Cass Avenue, Argonne, Illinois 60439. For information about Argonne and its pioneering science and technology programs, see www.anl.gov.

Document Availability

Online Access: U.S. Department of Energy (DOE) reports produced after 1991 and a growing number of pre-1991 documents are available free via DOE's SciTech Connect (http://www.osti.gov/scitech/)

Reports not in digital format may be purchased by the public from the National Technical Information Service (NTIS):

U.S. Department of Commerce
National Technical Information Service
5301 Shawnee Rd
Alexandria, VA 22312
www.ntis.gov
Phone: (800) 553-NTIS (6847) or (703) 605-6000
Fax: (703) 605-6900
Email: **orders@ntis.gov**

Reports not in digital format are available to DOE and DOE contractors from the Office of Scientific and Technical Information (OSTI):

U.S. Department of Energy
Office of Scientific and Technical Information
P.O. Box 62
Oak Ridge, TN 37831-0062
www.osti.gov
Phone: (865) 576-8401
Fax: (865) 576-5728
Email: **reports@osti.gov**

Disclaimer

ANL/NE-16/19

The SAS4A/SASSYS-1 Safety Analysis Code System

Chapter 14:
Non-Voided Channel Fuel Motion Analysis – PLUTO2

Nuclear Engineering Division
Argonne National Laboratory

March 31, 2017

TABLE OF CONTENTS

LIST OF FIGURES

LIST OF TABLES

NOMENCLATURE

Symbol	Definition	Units
ℓ	Linear	
n	Time step n	
′	Prime always indicates that a quantity refers to a unit of generalized smear volume	
Subscripts		
ac	Acoustic	
an	Annular	
bb	Bubbly or bubble	
bk	Lower boundary of node K	
ca	Cavity	
ch	Coolant channel	
cl	Cladding	
co	Condensation	
deet	De-entrainment	
drag	Drag	
ej	Ejected or ejection	
et	Entrained or entrainment	
fc	Fuel/clad interface	
ff	Frozen fuel	
ffcl	Frozen fuel on cladding	
ffsr	Frozen fuel on structure	
fi	Free fission gas in coolant channel	
fica	Free fission gas in molten pin cavity	
ficaxx	Used for special fission gas volume fraction calculation (see Eq. 14.2-38a)	
fm	Film (stationary liquid sodium film or moving annular fuel film)	
fr	Friction	
friction	Friction	
FR1	Flow regime 1 - particulate fuel flow	
FR3	Flow regime 3 - partially or fully annular flow	
FR4	Flow regime 4 - bubbly fuel flow	

Symbol	Definition	Units
fsca	Dissolved fission gas in the molten pin cavity	
fs	Dissolved fission gas in the coolant channel	
fu	Liquid and/or mobile solid fuel in the coolant channel	
fuca	Mobile fuel in the molten pin cavity	
fuch	Mobile fuel in the coolant channel (including fuel vapor)	
fufi	Fuel and fission gas	
fv	Fuel vapor in the coolant channel	
fvca	Fuel vapor in the molten pin cavity	
fz	Freezing, frozen	
hoop	Hoop (stress)	
Ht	Heat transfer	
i	Axial coolant channel index, specific enthalpy	
IB	Uppermost slug segment of lower sodium slug	
if	Interface	
in	Inner (middle) clad node or structural node facing neighboring hexan wall	
inlet	Subassembly inlet	
IT	Lowermost slug segment of upper sodium slug	
K	Axial pin or cavity index	
k	Material component k; this can also be cladding or structure	
l	Dummy index	
liq	Liquidus	
ls	Lower slug	
m	m = 1 indicates upward flow, m = 2 downward flow	
me	Melting, melt-in	
mi	Mixture of sodium and fission gas	
min	Minimum	
mv	Moving	
mx	Maximum	
Na	Sodium	
Nl	Liquid sodium	
Nm	Moving sodium liquid and sodium vapor	

Symbol	Definition	Units
node	Node	
Nv	Sodium vapor	
op	Open channel - channel volume or cross section remaining open after plateout has occurred	
or	Orifice	
os	Outer surface of clad or structure of fuel film or fuel crust. All these surfaces are facing the coolant channel.	
outlet	Subassembly outlet	
p	Subscript of specific heat for constant pressure	
Pa	Fuel particle	
pin,pi	Pin	
PL	PLUTO2	
power	Power	
radial	Radial	
rl	Dissolved fission-gas release	
S′	Sink or source per unit of generalized smear volume	
sol	Solidus	
sonic	Sonic	
sr	Structure	
un	Uncompressed	
us	Upper liquid sodium slug	
UTS	Ultimate tensile strength	
vg	Vapor and gas	
vi	Viscous	
x	Auxiliary subscript	
z	Axial location z	
zi	Designates bottom of a liquid sodium slug segment	
Greek Symbols	**Definition**	**Units**
α	Void fraction	
β	Delayed neutron fraction	
γ	C_p/C_v	
δ	Partial derivative	

Symbol	Definition	Units
Δ	Derivative in finite differences	
κ	Compressibility	
π	Circumference of a circle divided by its diameter	
ρ	Theoretical density	
ρ′	Generalize linear density	
σ	Surface tension	
θ	Generalized volume fraction	
Regular Symbols	**Description**	**Units**
A	Cross section area	
A′	Interaction or surface area per unit of generalized smear volume	
AFR	Input, liquid sodium friction coefficient	
AFRV	Input, sodium vapor friction coefficient	
AHELP	Auxiliary quantity in momentum conservation	
AMIIN	Auxiliary quantity in momentum conservation	
ARCH	Cross section area of coolant channel per pin	
ARCL	Cladding surface area per unit of generalized smear volume	
AREA	Area	
ARFF	Cross section area of plated-out fuel pin	
ARMF	Cross section area of moving fuel per pin	
ARSR	Structure surface area per unit of generalized smear volume	
AXMX	Input, reference cross section area; recommended input value is subassembly cross section area	
BFR	Input, exponent of liquid friction coefficient	
BFRV	Input, exponent of vapor friction coefficient	
BHELP	Auxiliary quantity in the momentum equation	
BMIIN	Auxiliary quantity in the momentum equation	
C	Specific heat	
CDFU	Input, fuel conductivity	
CDNL	Input, liquid sodium conductivity	
CDVG	Input, conductivity of sodium vapor	

Symbol	Definition	Units
CFCOFV	Input, fuel vapor condensation coefficient	
CFFFCL	Fraction of channel perimeter covered by plated-out fuel	
CFFRMF	Friction coefficient for annular fuel	
CFFUCL	Fraction of cladding and structure covered by moving or plated-out fuel	
CFMELT	Fraction of frozen fuel remelting per PLUTO2 time step	
CFMFCL	Fraction of channel perimeter covered by moving fuel	
CFMFFF	Fraction of plated-out fuel covered by moving fuel	
CFNACL	Fraction of channel perimeter that is in contact with sodium	
CFNACN	Input, sodium vapor condensation coefficient	$J/(m^2 \cdot s \cdot K)$
CFNAEV	Input, sodium evaporation coefficient	$J/(m^2 \cdot s \cdot K)$
CIANIN	Input, determines when a complete annular fuel flow begins	
CIA1	Input, constant in the fuel particle-to-sodium heat transfer	
CIA2	Input, constant in the fuel particle-to-sodium heat transfer	
CIA3	Input, constant in the Deissler heat-transfer correlation	
CIA4	Input, controls range of interpolation between boiling heat transfer coefficient and single-phase gas heat-transfer coefficient	
CIA5	Input, controls drag dependence in void fraction in the particulate flow regime	
CIA6	Input, controls drag in the bubbly flow regime	
CIBBIN	Input, controlling onset of bubbly flow regime	
CIETFU	Input, controls effect of fuel particles on sodium film entrainment	
CIFRFU	Input, part of the fuel friction calculation	
CIFUFZ	Input, controls mode of fuel freezing	
CIFUMO	Input, controls axial fuel momentum low on ejection from pin	
CINAFO	Input, initial and maximum sodium film fraction	
CIREFU	Input, Reynolds number above which fully turbulent fuel flow is assumed for friction calculation	

Symbol	Definition	Units
CIRTFS	Input, controls dissolved gas release	1/s
CIVOID	Input, controls liquid sodium fraction below which single-phase heat-transfer and friction laws are used	
CMFU	Input, liquid fuel compressibility	1/Pa
CMNL	Input, liquid sodium compressibility	1/Pa
COFICH	Convective fission-gas mass flux in coolant channel	$kg/(s \cdot m^2)$
COFUCH	Convective fuel mass flux in coolant channel	$kg/(s \cdot m^2)$
COFUOS	Convective fuel energy flux in the channel	$J/(s \cdot m^2)$
CONACH	Convective sodium mass flux in coolant channel	$kg/(s \cdot m^2)$
CPFU	Input, fuel heat capacity	$J/(s \cdot m^2)$
CTFRFU	Fraction of the moving fuel that is in contact with clad or plated-out fuel	
C1	Input, part of liquid sodium heat-transfer correlation	
C2	Input, part of liquid sodium heat-transfer correlation	
C3	Input, part of liquid sodium heat-transfer correlation	
C1VIPR	Input, used for the artificial viscous pressure calculation in the pin	
C2VIPR	Input, used for the artificial viscous pressure calculation in the pin	
D	Diameter, hydraulic diameter	m
DEFICH	Generalized smear density of free fission gas in the coolant channel	kg/m^3
DEFUCH	Generalized smear density of the moving fuel in the coolant channel	kg/m^3
DEFVCH	Generalized smear density of fuel vapor in the coolant channel	kg/m^3
DENACH	Generalized smear density of sodium in the coolant channel	kg/m^3
DENMCH	Generalized smear density of moving sodium in the coolant channel	kg/m^3
DZPLIN	Input, minimum length of a Lagrangian edge cell	m
e	Internal energy	J/kg
EGBBLY	Input, internal fuel energy below which fuel freezing begins	J/kg
EGFULQ	Input, internal fuel energy at the solidus	J/kg
EGFUSO	Input, internal fuel energy at the solidus	J/kg

Symbol	Definition	Units
EGMN	Input, internal fuel energy below which fuel cannot switch from the particulate to a continuous flow regime	J/kg
EPCH	Input, controls use of advanced pressure in in-pin calculation	
f	Factor used in interphase drag term	
F	Friction factor	
FF	Mass of fuel ejected per time step and per unit of generalized smear volume	kg/m^2
FIFNGB	Input, fraction of fission gas on grain boundaries which becomes available as free gas upon fuel melting	
FNARME	Input, cross section area of pin cavity/cross section area of fuel above which failure of this node is allowed to occur	
FNFUAN	Input, controls when annular fuel flow in molten pin cavity is assumed	
FNMECA	Fraction of node width of radial heat-transfer node on cavity boundaries which melts in pure PLUTO2 time step	
FNMELT	Input, controls locus of cavity boundary	
FNPI	Fraction of all the pins in a subassembly which have failed	
FNPOHE	Relative power level	
FN	Fraction of the molten fuel in a ejection cell which is ejected per PLUTO2 time step	
FUELMS	Initial fuel mass in a radial fuel-pin mode	kg
FUMASS	Initial total fuel mass in an axial fuel node	kg
FUMS	Current fuel mass in the radial fuel pin node on the cavity boundary	kg
F.R. 1	Particulate fuel flow regime	
F.R. 3	Partially or fully annular flow regime	
F.R. 4	Bubbly fuel flow regime	
g	Gravity	m/s^2
GAMSS	Input, fraction of power going into direct heating of structure	

Symbol	Definition	Units
GAMTNC	Input, fraction of power going into direct heating of coolant	
GAMTNE	Input, fraction of power going into direct heating of cladding	
h	Heat-transfer coefficient	J/(m²·s·K)
H	Heat-transfer coefficient times heat-transfer area	J/(s·K)
HCCLMI	Input, heat-transfer coefficient between hot cladding and a two-phase sodium/gas mixture	J/(m²·s·K)
HCFFMI	Input, heat-transfer coefficient between frozen fuel crust surface and two-phase sodium/gas mixture	J/(m²·s·K)
HCFUBB	Input, heat-transfer coefficient between the interior of the molten fuel and bubble surface	J/(m²·s·K)
h1	Auxiliary heat-transfer coefficient	J/(m²·s·K)
h2	Auxiliary heat-transfer coefficients	J/(m²·s·K)
I	Axial node index in coolant channel	
IB	Channel zone in which the uppermost segment of the lower slug is located	
IDIFF	Offset between pin and channel grid. The first pin node is at the same elevation as channel node IDIFF + 1	
IFLAG	Pointer array which gives the flow regime number for each axial channel node	
IMAX	Uppermost slug segment of upper sodium slug	
IT	Channel zone in which the lowermost segment of the upper slug is located	
k	Conductivity	J/(m·s·K)
K	Axial index in the pin	
KKMX	Uppermost node in the molten pin cavity	
KZPIN	Coolant channel zone which contains the fuel pins	
KK1	Lowermost node in the molten pin cavity	
L	Length	m
L1	Length of the Lagrangian node at one end of the interaction region	m

Symbol	Definition	Units
L2	Length of Lagrangian node at the other end of the interaction region	m
N′	Number per unit of generalized smear volume	
NCPLEV	Input, number of cladding nodes which have to be molten in to lead to switch to LEVITATE	
NGRDSP	Input, number of grid spacers in the channel zone containing fuel pins	
NRPI	Number of pins per subassembly	
NT	Number of radial fuel pin nodes	
Nu	Nusselt number	
P	Pressure	Pa
PECH	Perimeter of the coolant channel associated with one pin	M
PORFR	Porosity fraction	
POW	Input, power in highest rated axial fuel pin node	W
POWCOF	Exponent in the exponential function which give the power history during main time step	
PRFAIL	Input, failure pressure for non-mechanistic clad failure Propagation	Pa
Pr	Prandtl number	
PSHAPE	Input, axial pin power shape	
PSHAPR	Input, radial power shape in a pin	
Q	Fission heat source	W/kg
r	Radius	M
R	Gas constant or radius	J/(kg·K)
RAFPLA	Input, radius of large particles	m
RAFPSM	Input, radius of small particles (which have been generated due to the decay of the larger particles after TIFP seconds)	kg
RETFG2	Retained fission-gas mass in the original radial fuel-pin node at the cavity boundary before it began melting into the cavity	
Re	Reynold's number	
RGAS	Input, gas constant for fission gas	J/(kg·K)
RGNA	Sodium vapor gas constant which is a calculated quantity in PLUTO2	J/(kg·K)

Symbol	Definition	Units
S	Mass sink or source	kg/s
S′	Mass sink or source per unit of generalized smear volume	kg/(s·m^3)
St	Stanton number	
t	Time	s
T	Temperature	K
TECLMN	Input, cladding temperature above which frozen fuel will not stick to the cladding	K
TECLRL	Input, cladding temperature above which the frozen fuel crust will be released	K
TEFAIL	Input, cladding failure temperature in nonmechanistic failure criteria	K
TESOL	Input, steel solidus temperature	K
TIFP	Input, time delay for fragmentation of large particles into small ones	s
TKFF	Thickness of frozen fuel crust	m
u	Velocity	m/s
UFCH	Fuel velocity in the channel	m/s
UMCH	Sodium/gas mixture velocity in the channel	m/s
VCONST	Auxiliary quantity in the sodium film entrainment calculation	
VFNALQ	Input, liquid sodium fraction below which a particulate flow regime can become a continuous one	
VFNARE	Input, liquid sodium fraction below which a particular flow regime can become a continuous one	
VIFG	Input, viscosity of sodium vapor	kg/(m·s)
VIFULQ	Input, viscosity of liquid sodium	kg/(m·s)
VOLUME	Volume	m^3
w	Width	m
W	Mass flow rate	kg/s
x	Sodium quality	
XKORGD	Input, orifice coefficient of a single grid spacer	
XKORV	Input, expansion, contraction, or orifice coefficient	
z	Axial coordinate	m

NON-VOIDED CHANNEL FUEL MOTION ANALYSIS - PLUTO2

14.1 Introduction and Overview

14.1.1 Historical Background and Description of the Physical Model

The PLUTO2 module calculates the post-failure fuel motion and sodium voiding in subassemblies experiencing an overpower condition leading to significant fuel melting, fuel-pin failures and fuel ejection into unvoided or partially voided coolant channels. The degree of fuel-pin disruption is limited to cladding ruptures through which molten fuel can be ejected into the coolant channels. Thus, this model will be appropriate for treating the early post-pin-failure phase of higher ramp rate transient overpower (TOP) accidents and the entire post-failure phase of lower ramp rate TOPs if no complete pin disintegration or extensive cladding melting occurs. Of additional importance is the module's application to the early post-pin-failure fuel motion and sodium voiding in unvoided or partially voided subassemblies experiencing a Loss-of-Flow driven TOP (LOF'd'TOP). Once complete pin disintegration, high fuel vapor pressures, or molten cladding motion have to be considered, a switch to the LEVITATE module, which is designed to treat these phenomena, is made. This compatibility between PLUTO2 and LEVITATE is important for a consistent continuation of the analysis of the transient. This compatibility did not exist between the corresponding SAS3D modules SAS/FCI [14-1] and SLUMPY [14-2] which could never be used sequentially to treat the same fuel pin.

The PLUTO2 module can be used in all situations for which the SAS/FCI module of SAS3D was used. Moreover, the PLUTO2 fuel pins can fail into partially voided coolant channels, which was not possible with SAS/FCI. The models in PLUTO2 are considerably more mechanistic than those used in SAS/FCI. For example, fuel motion in SAS/FCI was largely treated with a lumped parameter approach, whereas PLUTO2 has one-dimensional models of the fuel motion inside the pins and in the coolant channels. Moreover, PLUTO2 treats phenomena that were not addressed in SAS/FCI such as continuous molten fuel flow regimes and the plateout of freezing fuel.

The PLUTO2 module is an outgrowth of the earlier PLUTO code [14-3, 14-4] which has been successfully used to simulate the early sodium voiding and fuel motion in TOP experiments [14-5, 14-6]. Therefore, the basic PLUTO concept has been retained in PLUTO2. However, as mentioned above, PLUTO2 is also designed to analyze the longer-term phenomena in mild TOPs and the early phases of LOF'd'TOPs. Moreover, PLUTO2 has an Eulerian hydrodynamic treatment which eliminates most of the cumbersome rezoning that was necessary in the Lagrangian PLUTO code. The Eulerian treatment has allowed the incorporation of axial cladding rupture propagation, fuel plateout, and variable cross section flow. Furthermore, PLUTO2 is considerably more economical to run than PLUTO; this is of importance for a module of a whole-core analysis code.

The PLUTO2 (and LEVITATE) coolant-channel treatment considers the entire subassembly cross section with all associated cladding and structure although the treatment is still one-dimensional. This is somewhat different from the concept that is

used in the pre-fuel motion phase in SAS4A. The latter considers the coolant flow area, cladding and structure associated with only one pin.

Schematics of the PLUTO2 model when used for a mild TOP calculation and for a LOF'd'TOP condition are shown in Figs. 14.1-1 and 14.1-2, respectively. These schematics are for a single pin with a coolant channel that can belong to one or more pins. Although the PLUTO2 channel treatment is one-dimensional (i.e., there is a common treatment of all subchannels), not all of the fuel pins in a subassembly have to fail simultaneously. A number of the pins, as specified by input, can remain intact. A treatment of the delayed failure of these pins is not yet operational. In cases that assume that only some of the pins in a subassembly fail, the fuel and gas ejection from these failed pins will be added to all coolant subchannels since all subchannels in a sub-assembly are treated alike. This has prompted the use of the above-mentioned concept in PLUTO2 in which the basic channel cell has a cross section equal to the entire coolant flow area in a subassembly.

The PLUTO2 model addresses three major modeling areas pertinent to the post-pin-failure behavior. The first area is the in-pin fuel motion toward a cladding rupture, the second is the fuel and gas ejection through the cladding rupture, and the third is the multi-component, multi-phase hydrodynamics treatment in the coolant channel.

The basic assumption for the in-pin motion is the treatment of the molten fuel region inside the pin (see Figs. 14.1-1 and 14.1-2) as a pressurized cavity containing fuel and fission gas, which flow toward a cladding rupture. This general concept was already used in SAS/FCI, PLUTO, and EPIC [14-7, 14-8]. The key PLUTO2 features in the modeling of the in-pin flow are:

A1) Treatment of the two-phase, two-component flow as a compressible homogeneous flow with variable flow cross section and strong mass sinks (due to fuel ejection) and mass sources (due to the addition of melting fuel).

A2) Modeling of the radial and axial growth of the molten fuel cavity due to additional fuel melt-in determined by a heat-transfer calculation in the solid fuel annulus which is performed by subroutine PLHTR.

A3) The treatment of two types of fission-gas bubbles in the molten cavity. These are the large fission-gas bubbles on the grain boundaries which are assumed to act like free gas and exert pressure in the molten cavity and very small intragranular bubbles which do not affect the cavity pressure directly because they are assumed to be totally constrained by surface tension. However, these small bubbles can coalesce into large bubbles and thus contribute to the cavity pressurization in a delayed fashion. In the code, the rate of coalescence is controlled by an input time constant. Up to the time of pin failure, when PLUTO2 is initiated, the relative fractions of these two types of gas bubbles in the solid fuel and molten fuel cavity are calculated by DEFORM. DEFORM has the same two-bubble fission-gas treatment and uses the same input grain-boundary gas fraction and time constant for small bubble coalescence. Once PLUTO2 is active, additional fuel can melt into the cavity which brings fission gas with it. The total amount of fission gas in the melting fuel node is known from the steady-state

DEFORM calculation. In the solid fuel, the DEFORM calculation tracks grain boundary gas (large bubbles) and intragranular gas (small bubbles) separately. The input fraction (FIFNGB) should roughly correspond to the fraction of gas on the grain boundaries in the solid fuel as determined from post-irradiation examinations of fuel pins.

A4) A simple fuel vapor pressure calculation which is based on the radially averaged temperature in a cavity node is performed. The fuel vapor pressure and the fission-gas pressure are assumed to be additive. A better fuel vapor pressure calculation would be based on the maximum fuel temperature in a node. However, computing the latter in a moving fluid is difficult. Also, it is not clear that any significant radial temperature gradients remain present after the onset of fuel motion. This problem will be addressed in future SAS4A work.

The fuel ejection from the pins is based on the assumption that the cavity pressure in the node behind the cladding rupture of the failed pins equilibrates instantaneously with the coolant channel pressure at the same elevation by ejecting appropriate amounts of fuel and gas. The latter are ejected with the same volume ratio as present in the cavity nodes. If the pressure in the coolant channel becomes temporarily higher than the pressure in the failed cavity nodes, the fuel and gas ejection is halted. Backflow of fuel, gas or sodium into the pins is not allowed. Two items concerning pin failure coherency and the axial pin-failure propagation are of importance:

B1) There is an option to fail only some of the pins in a subassembly. The other pins remain intact. This option is relevant for mild TOPs. Because of the common one-dimensional treatment of all subchannels, this requires that the failed pins are reasonably well distributed over the subassembly cross section (see Fig. 14.1-3). A problem with this option is that LEVITATE cannot be switched on after PLUTO2 because LEVITATE assumes that all pins in a subassembly are failed.

B2) The cladding failures can enlarge axially; this is also referred to as axial pin-failure propagation. There is a nonmechanistic pin-failure propagation option available which is keyed on input fuel melt fraction, cladding temperature, and required pressure difference between cavity and channel. The mechanistic option compares the calculated cladding hoop stress with an ultimate tensile strength function. Moreover, an input fuel melt fraction has also to be exceeded.

The axial pin-failure propagation is of key importance for lower power channels experiencing a high overpower condition due to an LOF accident (LOF′d′TOP). In this case, the cladding can be relatively soft along a considerable length of the channel at the time of the initial failure. This may lead to rapid axial failure propagation. For milder overpower conditions, the axial failure propagation would be slower and mostly caused by the overheating of the cladding by molten fuel that has been ejected into the coolant channels.

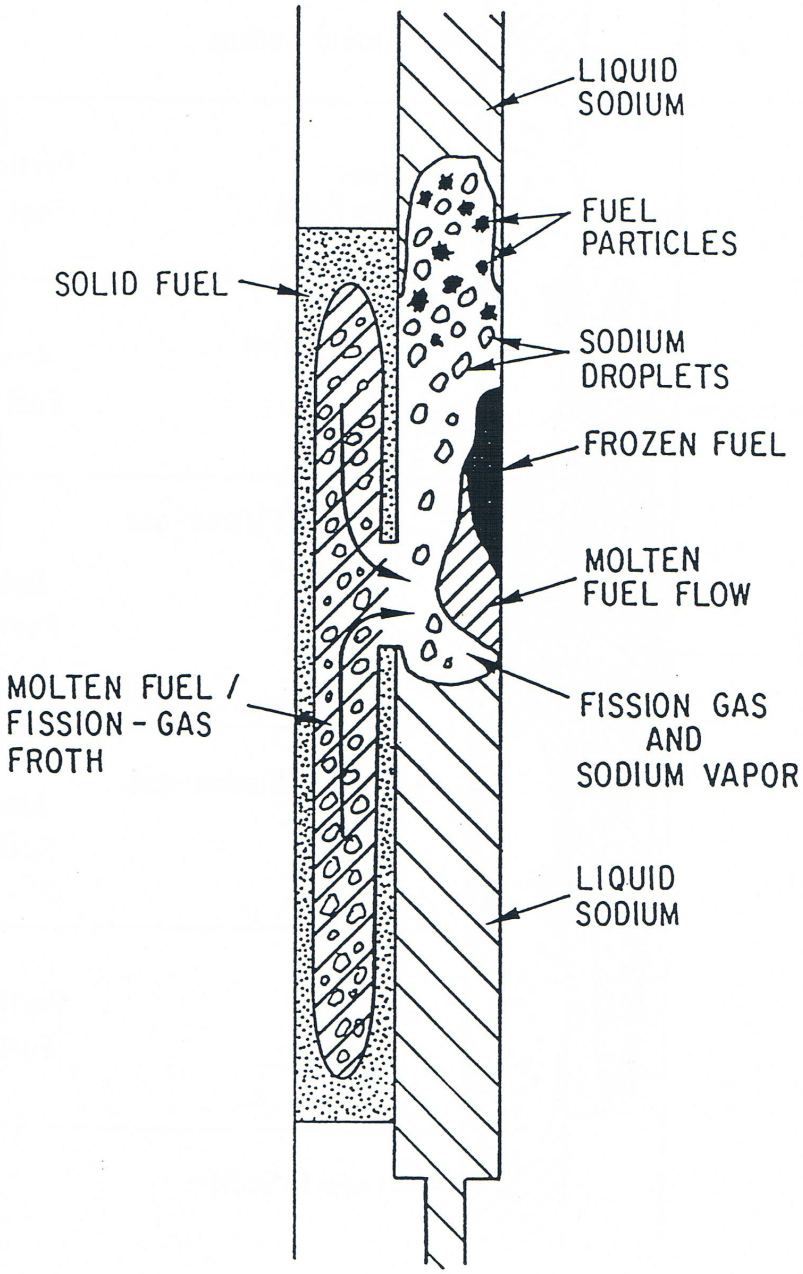

Fig. 14.1-1. PLUTO2 Schematic for Transient Overpower Conditions

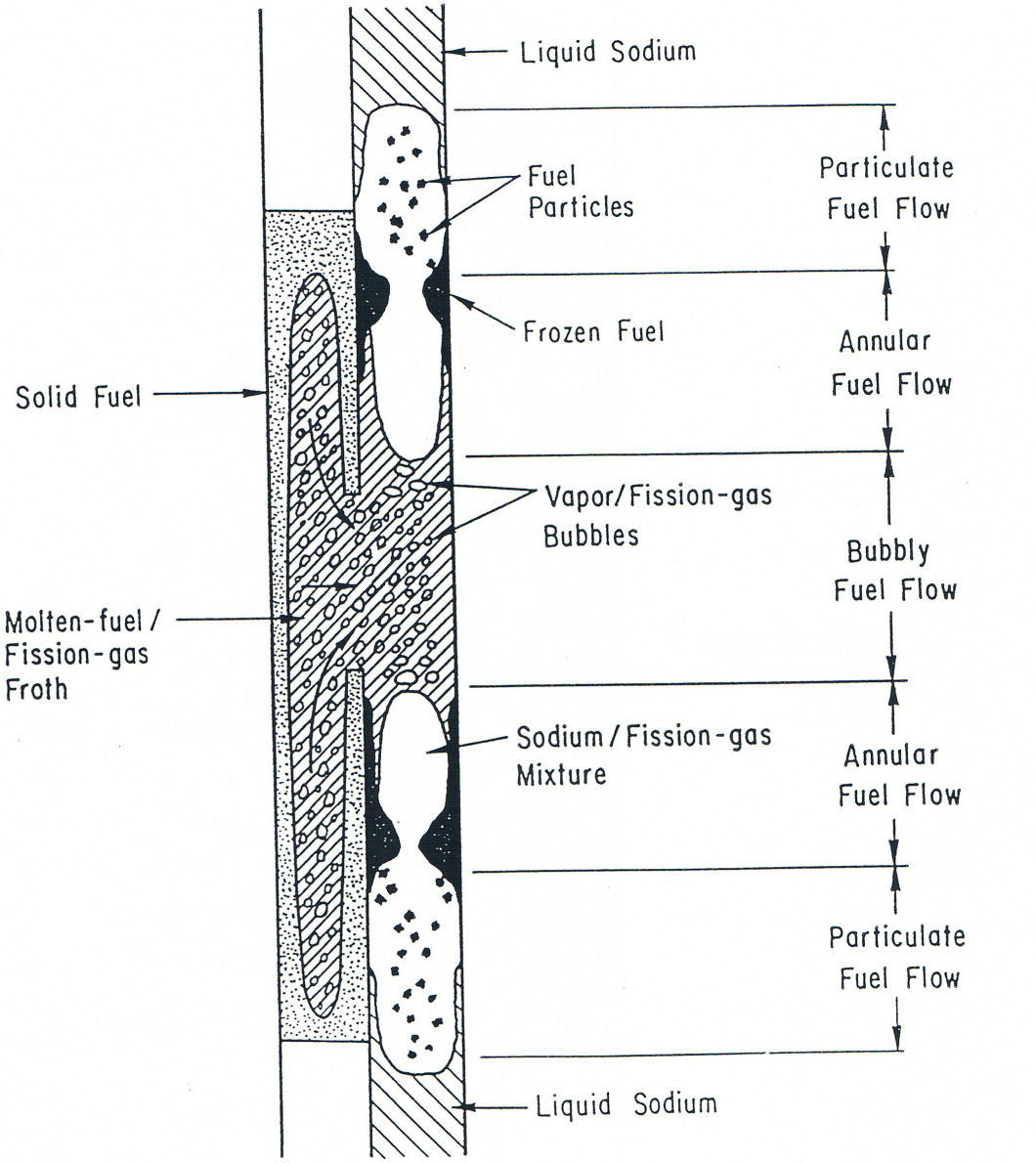

Fig. 14.1-2. PLUTO2 Schematic for Loss of Flow Driven Transient Overpower Conditions

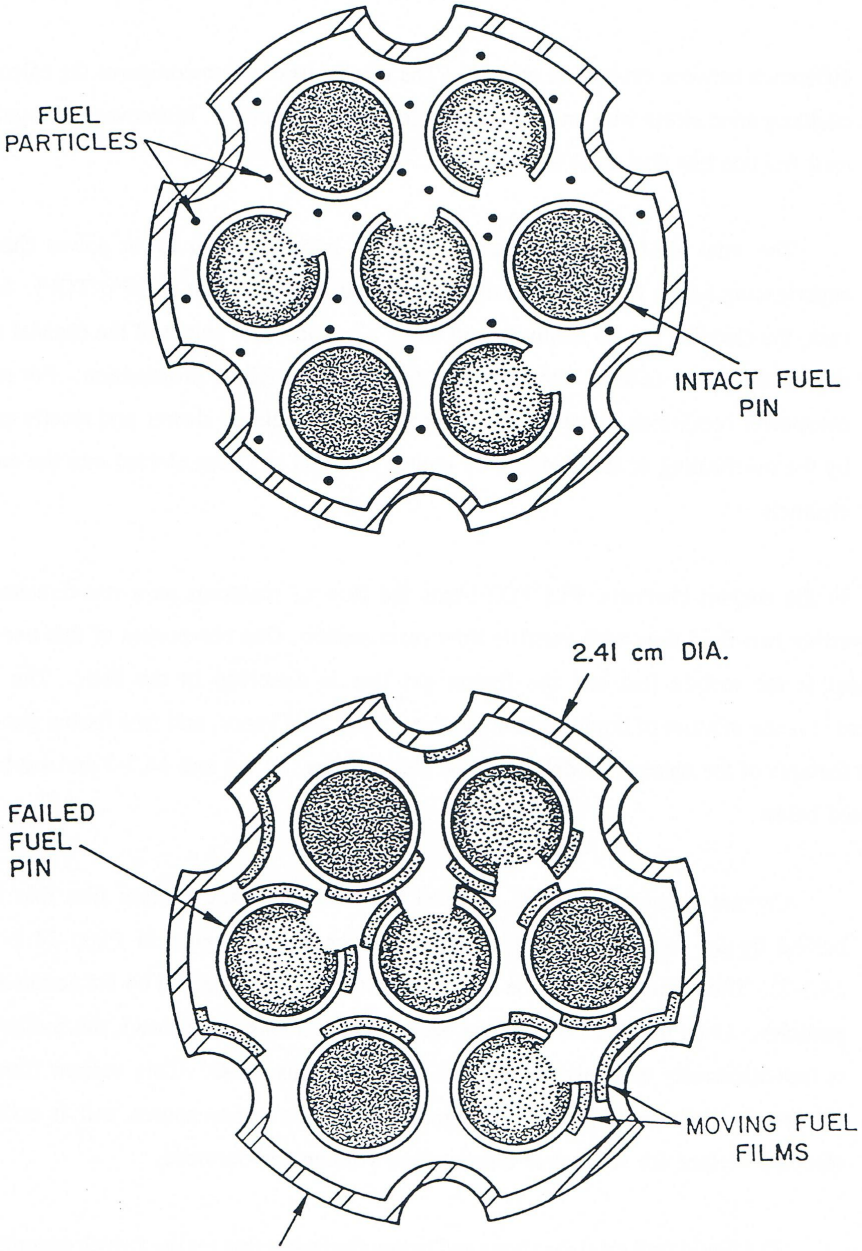

Fig. 14.1-3. Illustration of Particulate Fuel Flow Regions (Upper Figure) and Partial Annular Fuel Flow Regime (Lower Figure) for a Seven-Pin Bundle in Which Only Four Pins Are Assumed to Have Failed

In the coolant channels, PLUTO2 treats the flow of materials as a one-dimensional, compressible two-fluid flow with variable flow cross section. One component of this two-fluid treatment is the mobile fuel and the fission gas that is dissolved in the fuel. The other component is the mixture of liquid sodium, sodium vapor, fuel vapor, and free fission gas. The salient features of the channel modeling can be seen in Figs. 14.1-1 and 14.1-2 and are briefly discussed below.

C1) Coolant channel boiling is modeled by treating a static sodium film that is left behind by the expelled coolant slugs (see upper voided region in Figs. 14.1-1 and 14.1-2). The sodium film can be entrained by vapor streaming and by the action of fuel particles. Once the fuel flow regime becomes continuous (see below), the sodium film is instantaneously entrained as droplets in the gaseous phase. This sodium film is of importance because it provides a significant sodium vapor source and it cools the cladding surface for some time after sodium voiding has occurred.

C2) The liquid sodium slugs above and below the interaction region (which encompasses all the two-phase sodium, fuel, and fission gas) are treated as incompressible slugs with variable flow cross section. However, during the first few milliseconds after failure, an acoustic approximation is made to determine the slug interface velocities.

C3) Three different fuel flow regimes are treated in PLUTO2: particulate, partially or fully annular, and bubbly. The flow regime selection is mainly keyed to the liquid sodium fraction and to the channel fuel volume fraction.

The fuel motion in TOP accidents has been traditionally modeled as a particulate fuel suspension in a two-phase sodium/fission-gas mixture. However, the breakup of fuel into droplets or particles is likely only when the liquid sodium fraction is fairly high. From TREAT experiments, it can be concluded that continuous molten fuel flow regimes exist in voided regions. In PLUTO2, continuous fuel flow regimes are, therefore, considered in addition to the particulate flow regime. The treatment of a partially annular fuel flow regime is not a common approach but has been prompted by the notion that a relatively small amount of molten fuel in a voided channel will not cover the entire cladding and structure perimeter, but will rather behave like a single or multiple rivulet flow. For higher fuel fractions, a complete annular fuel flow regime is assumed and for an even higher fuel volume fraction, a bubbly fuel flow is modeled. Figure 14.1-3 illustrates the particulate and partially annular flow regime models for a seven-pin TREAT test bundle for the case in which only a certain fraction of the pins has failed. For the particulate or bubbly fuel flows, the fuel is simply uniformly distributed in all subchannels. For the partially annular flow, the fuel mass is assumed to be distributed between the pin cladding and structure in proportion to the cladding-to-structure surface area ratio. The cladding of all failed and unfailed pins is assumed to be covered by equal amounts of fuel film with equal film thickness. The fraction of the cladding perimeters covered by the fuel films is dependent on the fuel volume fraction and the input constant CIANIN. Where this fuel is exactly located on the pin perimeters is not relevant since there is no azimuthal cladding temperature distribution calculated. The fraction of the fuel covering the structure is of considerable

importance in small bundles. Once frozen fuel crusts are generated (see below), they are also distributed in the same manner. Once the fuel fraction is high enough to lead to a fully annular flow, all cladding and structure in a given node is covered by the fuel films. The fuel flow regimes will be discussed in more detail in Section 14.4.2. Figure 14.4-1, which is shown later in Section 14.4, illustrates the fuel flow regimes in more detail for an equivalent cylindrical geometry.

Modeling these different fuel flow regimes explicitly has the advan-tage that one has all interaction areas for heat, mass, and momentum transfer readily available.

C4) Frozen fuel plateout is treated in PLUTO2 because there is over-whelming evidence from in-pile and out-of-pile experiments that fuel freezing and plateout are key phenomena. In PLUTO2, only fuel in the continuous flow regime can plate out on cladding and structure upon fuel freezing. The fuel particles are not allowed to stick to cladding and structure because the fuel particles are assumed to have a solid shell due to their interaction with liquid sodium.

The modeling of the fuel plateout in PLUTO2 can either be of the bulk-freezing type or conduction-limited type. This is controlled by input parameter CIFUFZ, which also allows intermediate modes. Frozen fuel crusts can also become mobile after remelting. In addition, frozen fuel crusts are released into the moving fuel stream if the underlying clad or structure becomes significantly molten.

C5) The Fuel-Coolant Interaction (FCI) treatment depends on the fuel flow regime. In the particulate flow regime, the FCI treatment is largely based on the Cho-Wright approach [14-9] which considers the heat flow resistance in the fuel particles and ignores the resistance of liquid sodium. Moreover, the resistance due to vapor blanketing is treated in a parametric fashion in PLUTO2. In the code, separate FCI calculations are done for every numerical cell, whereas the Cho-Wright model is a lumped-parameter approach. Of importance for the FCI treatment in PLUTO2 is also the treatment of the slip between fuel and liquid sodium which mitigates the strength of the FCI's.

In the annular fuel flow regimes in PLUTO2, the convective heat transfer between the hot fuel film and/or fuel crusts and the two-phase sodium/fission-gas mixture is considered. Since the fuel surface area for the annular flow is significantly smaller than that for the particulate flow, this type of FCI is much milder.

In the bubbly fuel flow regime high heat-transfer rates between fuel and liquid sodium are possible, but the bubbly fuel flow regime is usually generated at an axial elevation where no liquid sodium is present. The penetration of liquid sodium into a bubbly fuel flow regime is also unlikely in the one-dimensional PLUTO2 because the cladding near a node with bubbly flow is usually too hot to allow reentry of liquid sodium.

The numerical grids on which the hydrodynamics equations are solved are shown in Fig. 14.1-4. The stationary Eulerian grid in the molten pin cavity is aligned with the stationary Eulerian grid in the coolant channel. The cavity grid can expand

continuously in the radial direction due to fuel melt-in and stepwise (by whole cells) in the axial direction. The grid on which the reactivity calculations are done covers the pin and blankets and the adjacent coolant channel cells from K = 1 to K = MZ. Outside the molten cavity region, this grid is also subdivided radially for the heat-transfer calculation in the solid fuel and cladding. The interaction region in the coolant channel can expand or contract continuously in the axial direction, which requires a partially Lagrangian treatment for the edge cells of the interaction region. The channel fuel region and the fission-gas region also expand or contract continuously in the axial direction. However, when they have moved into a new cell, the fuel or fission gas is assumed to be homogeneously distributed in that cell for calculating the pressure, heat transfer, momentum change, and reactivity. On the mesh grids above and below the interaction region, only the liquid sodium temperatures are calculated. The momentum change of the liquid sodium slugs is calculated in an integral fashion.

The current status of the PLUTO2 validation and its future validation needs are discussed in the SAS4A Validation and Verification Plan [14-10]. Here only an enumeration of the integral validation efforts already performed will be given. As mentioned earlier, the PLUTO code has been successfully used to simulate the early sodium voiding and fuel motion in two in-pile TOP experiments [14-5, 14-6]. PLUTO2 comparison calculations with PLUTO showed good agreement for the early fuel motion and sodium voiding [14-11]. An intercode comparison with the EPIC code for LOF′d′TOP conditions showed that the two codes compare rather well when several of the advanced features in PLUTO2, such as fuel flow regimes and fuel plateout, are switched off [14-12]. PLUTO2 was also used in the EEC-WAC TOP comparative exercise [14-20]. Because its advanced features were active in this comparison exercise, the PLUTO2 results differed considerably from those calculated with simpler models.

A reasonably good post-test simulation of the major flow event in the H6 50 ¢/s TOP TREAT test [14-13] was achieved through input parameter adjustments [14-6]. However, some uncertainty with regard to the mode of the FCI observed in this test could not be resolved. A good post-test simulation of the L8 LOF′d′TOP TREAT Test [14-14, 14-15, 14-12] was also achieved after introduction of a model for frozen fuel crust release from molten cladding. This was prompted by a pre-test analysis which underpredicted the fuel dispersal [14-16]. Other pretest predictions with PLUTO2 were made for the AX1 $3/s TOP test using carbide fuel [14-17], the W2 10 ¢/s TOP test in the ETR [14-18], and the 37-pin bundle P4 pin-failure propagation test in ETR [14-19]. The prediction for the AX1 test was quite reasonable, whereas the prediction for W2 suffered from the assumption of too coherent pin failures. The PLUTO2 P4 pretest analysis predicted a complete sweepout of the fuel ejected from the three fuel canisters used in this test, whereas the experiment led to very little sweepout and a sizable frozen fuel blockage. Possible explanations of the observed behavior include sodium bypass effects in a large bundle or the fuel canister ejecting the fuel more violently than the fuel pins in TOP tests.

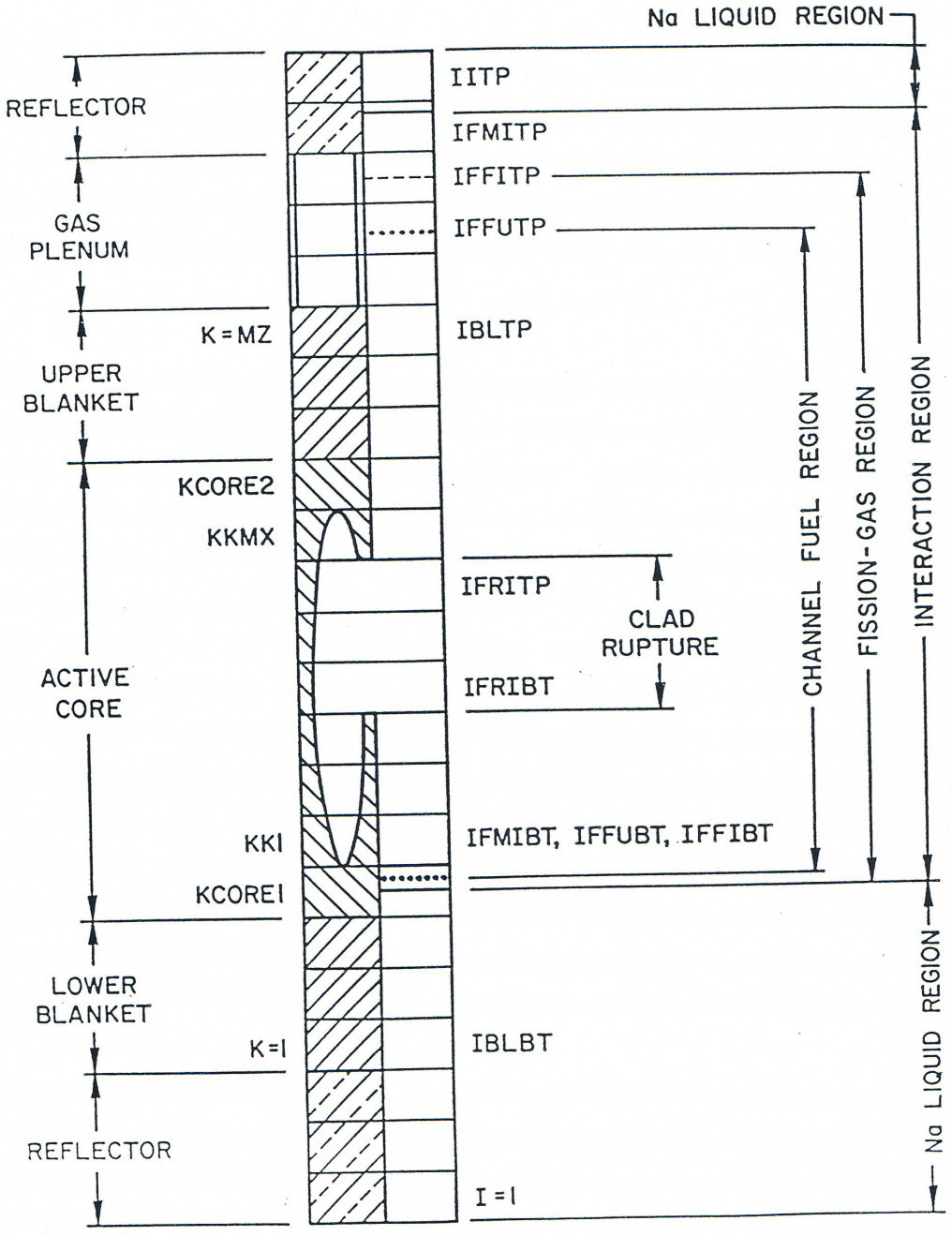

Fig. 14.1-4. Axial Mesh Cells Used in the Pin and the Coolant Channel for the Numerical Solution of Conservation Equations. Also Shown Are the Different Component Regions in the Channel

14.1.2 Overview of the Program Flow

Either PLUTO2 or LEVITATE is initiated once the subroutine FAILUR has predicted pin failure and a minimum fuel melt fraction equal to the input parameter FMELTM exists at the failure node. Subroutine FAILUR is usually called from the driver of the DEFORM pin-behavior module. However, in the case when cladding motion has already begun, it is directly called from the transient SAS4A driver routine TSTHRM. The decision as to which one of the two modules, PLUTO2 or LEVITATE, is to be initiated depends on the existence and size of a boiling region at the time of pin failure and whether the pins are predicted to fail into a voided or unvoided region of the coolant channel. If there is no boiling, as in an intermediate ramp rate TOP accident or if the pins fail into the liquid region of a partially voided channel, PLUTO2 will be initiated because of its capability of treating FCI's and sweepout of particulate fuel. For the case of fuel failing into a multibubble boiling region, PLUTO2 will only be initiated if the average void fraction in this region is less than 70%. If the average void fraction is larger or if cladding motion has begun, LEVITATE will be initiated.

The PLUTO2 initialization is described in more detail in Section 14.7.1. The subroutines involved in this procedure are PLINPT, PLSET, PLSETl, and PLSAIN. In these routines all permanent PLUTO2 variables are either set to input values or values calculated by the single-phase hydraulics, the pin heat-transfer routines, the pin behavior module DEFORM, or the boiling module. It should also be mentioned here that the flag ICALC, which designates which major module is currently active, will be set to 3 if PLUTO2 has been initialized and to 2 if LEVITATE has been initialized.

Once the PLUTO2 initialization routines have been executed and the flag ICALC has been set to 3, the transient SAS4A driver TSTHRM (see flow diagram in Chapter 2) will call PLUDRV (PLUTO2 DRIVER SUBROUTINE). PLUDRV will retain control and advance the solution using PLUTO2 time steps until the end of the primary-loop time step is reached. If another SAS4A channel is using PLUTO2 at this time, its solution will also be advanced until the end of the current primary-loop time step.

The flowcharts in Figs. 14.1-5 and 14.1-6 show the logic of the PLUTO2 driver. They are complete except for an option for switching off all subroutines performing the material velocity calculations. This option is discussed later in this section. If the flag MODEPL, which controls this option, is zero, the flow diagrams in Figs. 14.1-5 and 14.1-6 are appropriate.

If the flag ILEPLI has been set to 1 in the PLUTO2 initialization (see Fig. 14.7-2 in Section 14.7), LEVITATE will have to be initiated via PLUTO2. In this case, the PLUTO2 driver calls LEPLIN which is the interface routine between PLUTO2 and LEVITATE. The flag ICALC is then set to 2 and control is returned to TSTHRM. The latter will call the LEVITATE driver at the beginning of the next coolant time step upon encountering ICALC = 2 for the channel under consideration (see flow diagram of TSTHRM in Chapter 2).

If ILEPLI is not equal to 1, subroutine PLSET2 will be called (see Fig. 14.1-5). In this subroutine, all temporary arrays (i.e., arrays which can be overwritten once control is returned to TSTHRM) are initiated. Moreover, temporary integers are set.

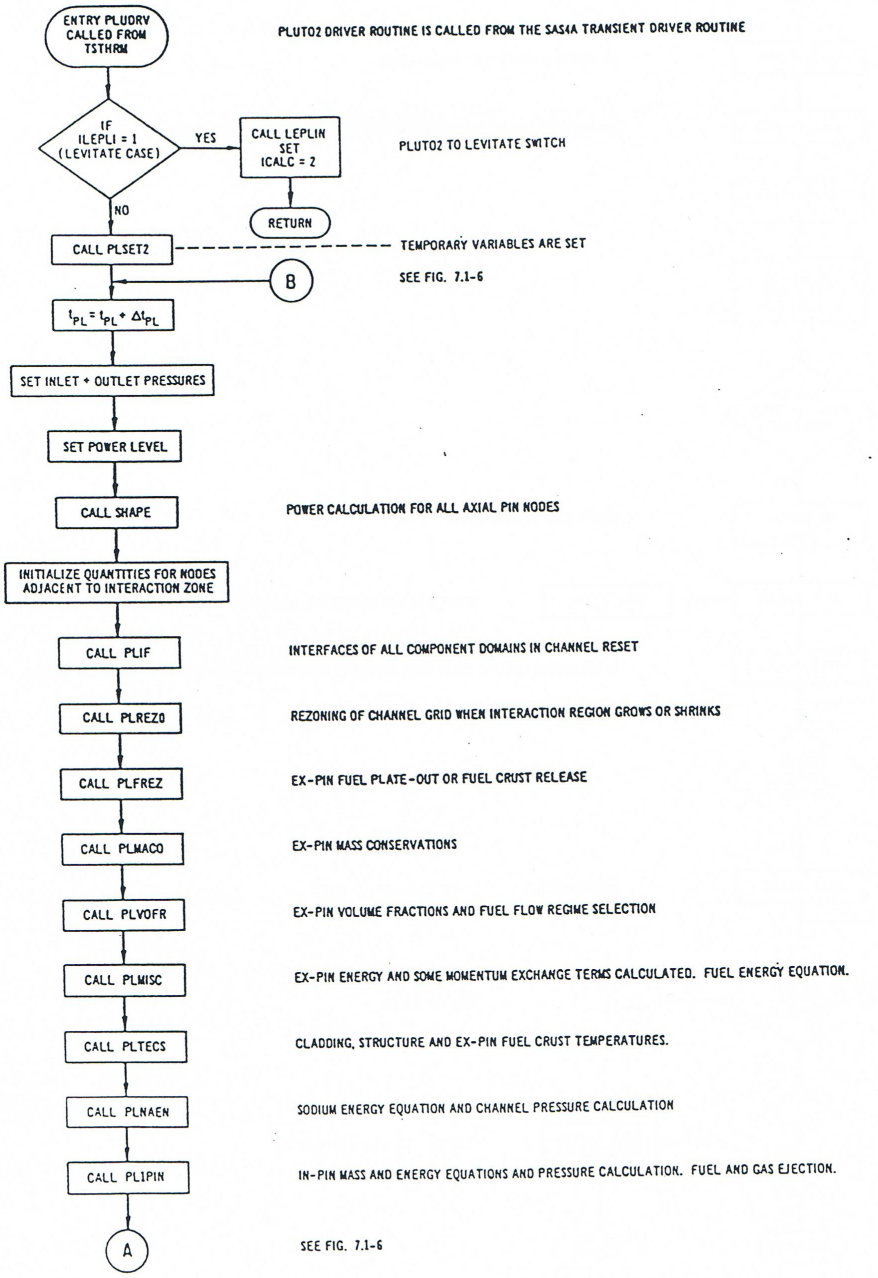

Fig. 14.1-5. First Part of the Flow Chart of the PLUTO2 Driver Subroutine, PLUDRV, Showing the Functions of the Major Subroutines

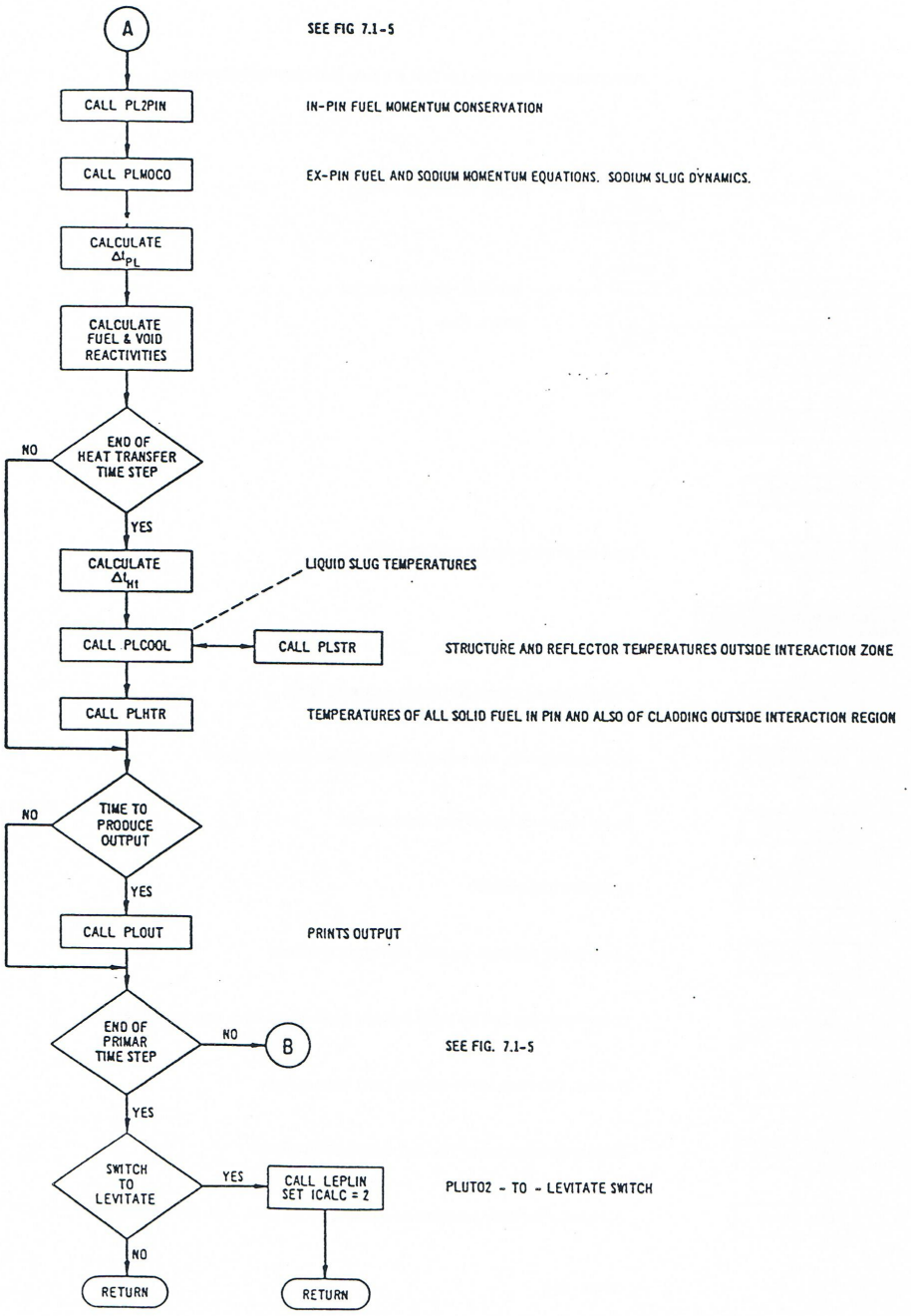

Fig. 14.1-6. Second Part of the Flow Chart of the PLUTO2 Driver Subroutine, PLUDRV, Showing the Functions of the Major Subroutines

Next, the PLUTO2 time is advanced by adding the PLUTO2 time-step size to the time at the beginning of the PLUTO2 cycle. The time-step increment for the very first PLUTO2 cycle is an input value which is also the minimum PLUTO2 time-step size. Later, in the logic flow, the time-step size is calculated.

Next, the inlet and outlet pressures at the end of the PLUTO2 time step are determined from the PRIMAR calculated inlet and outlet pressures and rates of inlet and outlet pressure changes.

Next, the power level at the end of the PLUTO2 time step is calculated from an exponential fit of the power-time history that takes the power level at the beginning of the previous and the current main time steps and the precalculated power level at the end of the current main time step into account. By using the calculated power level and the axial input power distribution, the specific power for each axial pin node is calculated. The same specific power is set for the corresponding channel nodes.

In subroutine PSHAPE, which is not a PLUTO2 subroutine, the total power for all axial fuel-pin nodes is calculated assuming that the pin is still intact. This is needed for the heat-transfer calculation in the solid fuel annulus in the pin.

Next, cladding and structure temperatures in the nodes adjacent to the interaction region are initialized in order to make sure that they will be available if the interaction zone expands into one of these nodes.

In subroutine PLIF (PLUTO2 INTERFACES), the axial displacements of the sodium slug interfaces, the interfaces of the fission-gas region and the interfaces of the regions containing fuel are reset. The actual calculations of the velocities needed for this resetting are performed later in subroutine PLMOCO. The initial sodium velocities come from the single-phase hydraulics or the boiling model and are set in PLSAIN. Fission gas and mobile sodium velocities are always the same in PLUTO2. Subroutine PLIF also calculates the axial pin-failure propagation and resets the pointer array IDISR(I) which indicates which pin nodes have failed.

In subroutine PLREZO (PLUTO2 REZONE), mesh cells are added to an expanding interaction region or deleted from a shrinking interaction region. Moreover, it cuts off short columns of liquid sodium slugs which are attempting to reenter into a cell of the interaction zone containing frozen fuel or ruptured cladding. The liquid sodium is added homogeneously to such cells. If fuel pins fail into the lower sodium slug, PLREZO will enlarge the interaction region downwards.

In subroutine PLFREZ (PLUTO2 FREEZING ROUTINE), the amount of fuel plating out per time step and per node is calculated. Moreover, PLFREZ calculates the amount of crust released because of remelting or because the underlying cladding has become molten. The released fuel crusts, which have an axial velocity of zero, are mixed with the moving fuel and an updated velocity is calculated by momentum averaging.

In PLMACO (PLUTO2 MASS CONSERVATION), the mass conservation equations for the moving components in the channels are solved. This includes a combined mass conservation for solid or liquid fuel and fuel vapor, and mass conservations for the sodium, free fission gas and dissolved fission gas. There is a special treatment for the

top and bottom cells of the channel. Fuel, sodium and fission-gas will be taken out and stored in a reservoir if the interaction region has extended into the lowermost or uppermost channel cell.

In subroutine PLVOFR (PLUTO2 VOLUME FRACTIONS), the entrainment of the static sodium film by the flow of the two-phase sodium/fission-gas mixture and of the fuel particles as well as the de-entrainment of liquid droplets onto the film, is calculated. PLVOFR also sets the volume fractions of the various components based on the results of the plateout and crust release calculation in PLFREZ and the results of the mass conservation equations. The final section of subroutine PLVOFR is devoted to the selection of the fuel flow regime.

In subroutine PLMISC (PLUTO2 MISCELLANEOUS), several important items are calculated. First, the molten- and frozen-fuel configurations in the flow channel are determined (see Fig. 14.4-1). Second, most energy and some momentum exchange terms between the various flow components, cladding and structure are calculated. Because many of these interaction terms depend on the fuel flow regimes, three different exchange coefficients are needed for several of the components. Third, the mobile fuel energy equation is solved.

In subroutine PLTECS (PLUTO2 TEMPERATURE CALCULATION OF CLADDING AND STRUCTURE}, the cladding, reflector, and structure temperatures within the interaction zone are calculated. This calculation is preceded by the determination of the energy exchange coefficients for the frozen fuel crust and the solution of the frozen crust energy equation. Since the energy exchange between fuel crust and moving fuel was not considered in subroutine PLMISC, an updating of the moving fuel energies is also performed here.

In subroutine PLNAEN (PLUTO2 NA ENERGY EQUATION), the two-phase and single-phase enthalpy equations for the mixture of sodium and fission gas are solved. From the resulting temperatures and the previously calculated volume fractions (see PLVOFR), the liquid-phase sodium pressure or the sodium saturation or superheated sodium vapor pressure, as well as the free fission gas pressure, are calculated. In addition, the total end-of-time-step pressure, which includes the fuel vapor pressure, is calculated.

In subroutine PLlPIN (PLUTO2 NO.1 PIN EQUATIONS}, the mass and energy equations for the in-pin fuel motion are solved. At first, the fuel and free and dissolved fission-gas mass sources due to fuel melt-in are calculated and the in-pin cavity enlargement is determined. Moreover, the free fission-gas mass sources due to dissolved gas coalescence and the corresponding sinks for the dissolved gas are evaluated. Following these, the fuel mass and energy conservation equations and the free fission-gas mass conservation equation are solved. Then, a preliminary end-of-time-step pressure is calculated for all cavity cells. This pressure calculation takes the prior-calculated end-of-time-step densities and temperatures into account. Only the pressures in the ejecting nodes will be further updated; in the other cells, the "preliminary end-of-time-step pressure" is the pressure that will actually be used in the momentum equation. The last major item in PLlPIN is the calculation of the mass of fuel

and fission gas ejected from all cavity cells that have failed cladding and a pressure higher than that in the corresponding channel cell. The masses of fuel and free and dissolved fission gases in these cavity cells are then reduced and the pressure is updated. The fuel and free and dissolved fission-gas masses in the channel cells are correspondingly increased and the end-of-time-step pressures in the channel nodes receiving fuel and/or fission gas are updated. The fuel energy in the channel nodes receiving fuel is also updated due to the addition of fuel with a higher temperature.

In subroutine PL2PIN (PLUTO2 NO. 2 PIN EQUATIONS), the momentum equation for the homogeneous fuel/fission gas mixture in the molten pin cavity is solved. Next, the mass conservation equation for the dissolved fission gas is solved. This could have been solved earlier in PLlPIN but that routine had become too crowded. The calculation of the time-step size for the in-pin calculation during the next time step is also performed in PL2PIN.

In subroutine PLMOCO (PLUTO2 MOMENTUM CONSERVATION), many quantities which were previously needed only at the cell centers have to be defined at the cell edges. Moreover, most of the momentum exchange terms and, in particular, the drag between the fuel and the two-phase sodium/fission-gas mixture are evaluated for the particulate and bubbly fuel flow regimes. The main section of this routine deals with the simultaneous solution of the two momentum equations at all cell edges in the interaction region. Moreover, momentum equations will also be solved for fuel particles at either end of the fuel region if the end nodes of the fuel region are in a particulate flow regime. Another section of PLMOCO deals with the calculation of the interaction zone interface velocities. This includes an acoustic approach in the liquid slugs during the first few milliseconds after pin failure and later an incompressible variable-cross-section treatment of the upper and lower coolant slugs. Also calculated in PLMOCO are instantaneous coolant slug flow rates for the entire calculational channel, as well as the integrated channel flow rates over a PRIMAR time step. These quantities are needed by the PRIMAR4 module for recalculating the inlet and outlet pressures.

The next task in the PLUTO2 driver routine is the time-step size determination in the coolant channel. This is compared with the time-step size calculated for the in-pin motion and the smaller of the two will be the PLUTO2 time-step size for the next calculational step.

The next task of PLUDRV is to calculate the transient mass distributions for the fuel and voiding reactivities. This calculation will be described in the next section on the interaction with other SAS4A modules.

If the time at the end of a PLUTO2 time step coincides with the end of the heat-transfer time step, several heat-transfer routines are called. This "coincidence" is forced to occur whenever the calculated PLUTO2 time step would overshoot the end of the heat-transfer time step. In this case, the PLUTO2 time step is set to coincide with the end of the heat-transfer time step. This is actually done right after the time-step size calculation described above.

The heat-transfer time step is determined next. Its maximum value is based on a characteristic heat-transfer time of the cladding and can be further limited by small primary-loop time steps which will be small in high power situations because the main (or point kinetics) time step becomes small. Since the heat-transfer time step is also used for the liquid slug temperature calculations, it can be further limited by a Courant condition based on the slug velocities.

In subroutine PLCOOL (PLUTO2 COOLANT SLUG TEMPERATURE), the temperature in all numerical nodes in the liquid sodium slugs is calculated. This involves the calculation of heat-transfer exchange terms between liquid sodium and cladding, plenum cladding, reflectors, and structure, and the solution of an energy equation. Moreover, PLCOOL checks whether a node in the lower sodium slug has started to boil.

In subroutine PLSTR (PLUTO2 STRUCTURE TEMPERATURE CALCULATION), the temperatures of the structure, the plenum cladding, and the reflectors outside of the interaction region are calculated.

In subroutine PLHTR (PLUTO2 HEAT TRANSFER), calculations are made of the temperature fields in the solid fuel annulus surrounding the molten fuel cavity, in the unmelted fuel and blanket cells, and in the fuel and blanket cladding outside the interaction region. The heat-transfer boundary condition at the interface between the molten cavity and the solid fuel annulus is treated by applying a time-integrated heat flow rate term whose contributions were calculated and summed up in subroutine PLlPIN. The boundary condition between the inner cladding and the outer fuel surface is also based on such an integrated heat flow rate term. The latter is calculated and summed up in subroutine PLTECS, in which the cladding temperature field in the interaction region is calculated using the PLUTO2 time step.

If it is time to produce output, subroutine PLOUT (PLUTO2 OUTPUT) will be called. If the end of the PRIMAR time step has not yet been reached, the logic flow will return to point B (see Fig. 14.1-5).

If the end of the PLUTO2 time step coincides with the end of the primary loop time step, a check is made whether the conditions require a switch to the LEVITATE module. This will be necessary if extensive cladding melting has occurred or if complete fuel-pin disruption is imminent or if the fuel vapor pressures have become quite high. In this case, the LEVITATE-PLUTO2 interface routine LEPLIN is called and the integer flag ICALC is set to 2 which will assure the calling of the LEVITATE driver routine LEVDRV at the beginning of the next PRIMAR step. Whether a switch to LEVITATE is made or not, control will now be returned to the transient driver TSTHRM.

An option, which is not shown in the flow charts in Figs. 14.1-5 and 14.1-6, allows the user to set all material velocities to small values and to shut off all the subroutines or subroutine sections that are calculating the motion of materials in PLUTO2. This option, which allows an economical but very simplistic continuation of a PLUTO2 calculation for several tens of seconds, is useful for the later treatment of a lead channel failing long before other channels in a low-ramp-rate TOP calculation. This situation is most likely to occur when the negative reactivity introduced due to fuel sweepout from the lead channel is not enough to insure permanent subcriticality. This option may be

reasonable for subassemblies that are completely blocked by frozen fuel as long as they do not lose much heat to neighboring subassemblies (this subassembly-to-subassembly heat loss should eventually be modeled in SAS4A). Moreover, if the fuel in the disrupted assembly heats up too much, it could also become mobile again; this is not currently treated. The above-mentioned PLUTO2 option will be activated if the input time TIPLMX is exceeded by the PLUTO2 time.

14.1.3 Interaction with other SAS4A Modules

During the PLUTO2 initialization, data from several other modules are transferred to PLUTO2 (see Fig. 14.1-7). When PLUTO2 is used for a TOP calculation, it requires data from the single-phase hydraulics, the DEFORM pin behavior module, and the pin heat-transfer module for non-boiling conditions (whose driver routine is TSHTRN). When PLUTO2 is used in a SAS4A channel experiencing a LOF'd'TOP condition, data may also be needed from the boiling module and the heat-transfer module for boiling conditions (whose driver routine is TSHTRV). The PLUTO2 initialization has already been briefly discussed at the beginning of Section 14.1.2 and will be described in more detail in Section 14.7.1.

Once PLUTO2 is active, there will only be an interaction with the point kinetics module and also with the primary loop module if the PRIMAR-4 module has been selected (see Fig. 14.1-7). Moreover, there is an interaction with the PLHTR pin heat-transfer calculation which is virtually a PLUTO2 routine but uses a different time step than PLUTO2 (see Section 14.1.2). There is no interaction with other modules because PLUTO2 calculates the motion of the liquid sodium slugs (in PLMOCO), has the capability to treat sodium boiling in regions which are not yet occupied by fuel, and also has a simplified calculation of the axial cladding failure propagation (in PLIF).

When PLUTO2 is active, it uses the user input axial fission power distribution with the magnitude calculated by the point kinetics module. PLUTO2 provides the point kinetics module with the sodium and fuel axial mass distributions for all channels in which PLUTO2 is active. Moreover, the Doppler reactivity calculation is based on PLUTO2 calculated average fuel temperatures. The details of these calculations are given in Section 14.6.1.

If the PRIMAR-1 option is chosen PLUTO2 will use a constant outlet coolant plenum pressure which is input and an inlet coolant plenum pressure which is calculated by PRIMAR-1 at the beginning of the transient and later modified by an input table PLUTO2 will not feed back and information to the primary-loop module if the PRIMAR-1 option has been chosen.

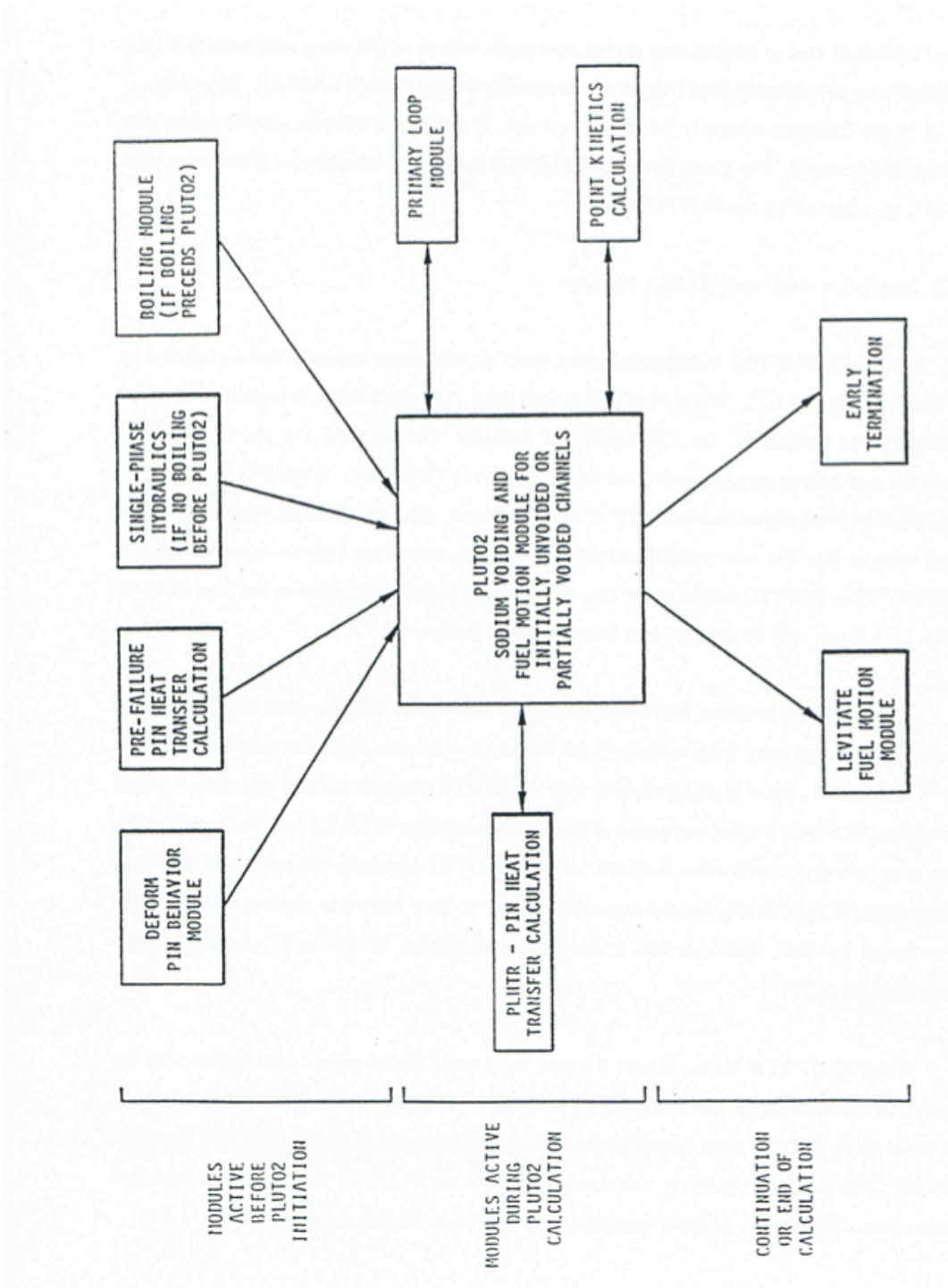

Fig. 14.1-7. Data Transfer Between the PLUTO2 Module and the Other SAS4A Module

If the PRIMAR-4 option has been chosen, PLUTO2 uses the time-dependent inlet and outlet plenum pressures and temperatures which are calculated by PRIMAR-4. PLUTO2 feeds back to the PRIMAR-4 module the sodium masses ejected into or received from the inlet and outlet plena during a PRIMAR time step. PLUTO2 also provides the PRIMAR-4 module with the energy of the sodium ejected into the plena and with the liquid sodium flowrates at the end of the PRIMAR time step. This is described in more detail in Section 14.6.2.

The PLUTO2 calculation will be taken over by the LEVITATE module if extensive cladding melting has occurred or if complete pin disruption is imminent or if the fuel vapor pressure becomes quite high. This transition, which can be controlled by input, is necessary because PLUTO2 is not designed to treat these situations. However, the transition to LEVITATE will not occur if only some of the pins have failed in PLUTO2. This PLUTO2 option, which is useful for mild TOP conditions, causes problems for LEVITATE because the latter assumes that all pins have failed when it is initiated.

14.2 In-Pin Fuel Motion

14.2.1 Overview and Assumptions

When LMFBR fuel pins melt in an overpower accident, the interiors of the pins melt first and form cavities containing molten fuel and fission gas. Some of this fission gas is dissolved in the molten fuel and the remainder is free fission gas which resides in bubbles too large to be constrained by surface tension. The decrease in the void volume, caused by the density decrease of the melting fuel and also of the molten fuel, which is further heated, compresses the free fission gas and causes a hydrostatic cavity pressurization which loads the cladding. This cavity pressure increases further when more free gas becomes available due to additional fuel melting and release of dissolved gas, and when fuel vaporization occurs. This leads eventually to cladding failure. The subsequent fuel and fission-gas ejection from the fuel pin and the local depressurization in the cavity caused by this ejection leads to fuel motion inside the pin toward the failure location. If the pin failure location for driver fuel is above the core midplane, this in-pin fuel motion reduces reactivity; if it is near the midplane, it can cause a reactivity addition.

The concept of a pressurized molten pin cavity, which was originally developed for TOP accidents, is also reasonable for LOF accidents which lead to a power rise and fuel melting before the cladding melts. Therefore, this cavity concept is used not only in PLUTO2 but also in LEVITATE. However, in an LOF accident, leading only to a few times nominal power or less, cladding motion and fuel swelling will precede fuel melting. In this case, the fuel pin is likely to disrupt completely into a mixture of molten fuel, gas, and solid fuel chunks once fuel melting has begun. This is only modeled in LEVITATE.

The in-pin fuel motion in the molten pin cavity in both PLUTO2 and LEVITATE is treated as a one-dimensional, compressible flow with a time dependent and spatially variable flow cross section. The fuel/fission gas flow is considered to be homogeneous and the fission gas is assumed to be in thermal equilibrium with the fuel.

Special attention had to be given to the potentially large mass sinks due to fuel and fission-gas ejection from the molten pin cavity. Mass sources due to fuel melt-in which cause flow cross section changes are also considered. The fuel which is melting into the cavity brings with it dissolved (intragranular) and free (intergranular) gas. These two types of gas are treated separately in the PLUTO2 and LEVITATE in-pin motion models. The free gas is considered not to be constrained by surface tension and to act as an ideal gas that is at the local fuel temperature. The dissolved gas, which is in the form of small bubbles, is assumed to be strongly constrained by surface tension, and its contribution to the local pressure depends on the input variable PRSFTN. If PRSFTN $\leq 10^7$ then the model assumes that the volume of the small bubbles containing the dissolved gas is negligible and thus the dissolved gas does not immediately affect the local pressure. If PRSFTN $>10^7$, the pressure calculation takes into account the volume of the dissolved gas bubbles, as described in Section 14.2.6. The dissolved gas is released (coalesces) according to a decay type law using an input decay constant. The amount released during each time step is added to the free gas. The fission-gas pressure calculation takes the compressibility of the liquid fuel into account and reduces to a liquid-fuel single-phase pressure calculation for no fission gas and zero void volume. The total pressure includes the fission-gas pressure and fuel vapor pressure. The fuel vapor pressure is based on the radially averaged fuel temperature.

Incoherency of the pin failures is mainly an issue in lower ramp rate TOP accidents. In these accidents, pin failure incoherency should be helpful for the post-accident coolability. If not all pins fail in the lead assemblies during a slow TOP, some subchannels may remain open and provide coolant paths. However, if near-midplane failures are assumed in slow TOPs in higher void worth cores, there may be a potential for exacerbating the accident due to pin failure incoherency. This is because the first pin failures will probably lead to some rapid fuel sweepout but may also cause significant voiding. Pins failing later will inject fuel into partially voided regions and this fuel may not experience rapid sweepout.

There are two major reasons for the incoherency in pin failures. One is the stochastic nature of pin failures and the other is due to differences in the power, flow, or coolant temperatures experienced by different pins. For example, the outer two fuel-pin rows in a subassembly see colder coolant temperatures due to the proximity of the hexcan wall. Many subassemblies in an LMFBR also see considerable radial power skews. In PLUTO2 an attempt has been made to treat the stochastic pin failures by allowing different pin failure groups. However, currently only one pin group can fail, and the other two groups of pins have to remain unfailed; (see input variables NRPIl, NRPI2, and NRPI3). The treatment of the delayed fuel expulsion and in-pin fuel motion for the two additional pin groups is not yet operational.

14.2.2 Initial Conditions for the In-pin Calculation from DEFORM and the Pre-Failure Pin Heat-transfer Calculation

Before pin failure, the molten fuel/fission-gas cavity is treated by the DEFORM pin behavior module. In the DEFORM treatment, the initially present central fuel hole is considered and the closing of this central hole due to the expansion of the molten fuel is

calculated. Although DEFORM does not calculate axial fuel redistribution inside the molten cavity, an axially uniform pressure is assumed for the entire molten cavity and found by considering the total gas and volume available. (An option is also available in DEFORM to use the nodal pressures for loading the cladding. This option is relevant only for very high power situations in which the molten cavity grows to a large size within a few milliseconds.) When pin failure is predicted by DEFORM or because an input melt-fraction or failure time have been reached, PLUTO2 is initialized from DEFORM conditions. These include the uniform cavity pressure (or the axial pressure distribution if the special DEFORM option was used), the dissolved and free fission-gas densities, and the molten cavity geometry. However, PLUTO2 will have exactly the same cavity geometry as DEFORM only if the PLUTO2 input option FNMELT = 0.0 is chosen. This value means that the radial cavity boundary is defined by the location of the fuel solidus temperature (an assumption in DEFORM). However, it is recommended for PLUTO2 to use a higher melt fraction (FNMELT > 0.5) for the definition of the location of the cavity boundary. This is because the analysis of TREAT test E8 [14-5, 14-6] showed that fuel, which had not yet undergone significant melting, did not move. This can probably be explained by a high viscosity of partially molten fuel.

When the regular DEFORM option of a uniform cavity pressure is used, there is an inconsistency in the DEFORM/PLUTO2 transition due to the lack of an axial in-pin fuel motion model in DEFORM. The nodal pressures calculated in PLUTO2 which use the pressure-generating free fission gas and the nodal volume obtained from DEFORM can be different from the average cavity pressure. Since the latter is considered more realistic for all but very high power situations, the free fission-gas content of the PLUTO2 nodes is adjusted to give the DEFORM calculated average cavity pressure. When the axially nonuniform pressure option in DEFORM is chosen (only relevant for very high power situations), the PLUTO2-calculated nodal pressure can still be somewhat different from the one calculated by DEFORM and has to be slightly adjusted. This is because DEFORM takes into account the radial temperature, fuel density, and porosity profiles in the molten fuel cavity, whereas PLUTO2 uses a radially averaged temperature, fuel density and porosity in the cavity nodes. The above-mentioned inconsistencies in the transition from DEFORM to PLUTO2 are not considered to be serious. To remove them would require the inclusion of pre-failure in-pin fuel motion in DEFORM and the accounting of the radial temperature profile in the molten cavity in PLUTO2 or LEVITATE.

The initialization of the PLUTO2 and LEVITATE cavity is done in subroutines PLINPT (PLUTO2 INPUT) and PLSET (PLUTO2 SETUP). DEFORM calculated cavity dimensions and free and dissolved fission-gas densities are transferred to PLUTO2 in these routines. Also, the radially averaged cavity temperatures are determined from the temperature profiles obtained from the heat-transfer routines, TSHTRN or TSHTRV.

14.2.3 Coupling of the In-pin Motion Calculation with the PLHTR Heat Transfer Calculation

For the calculation of the growth of the molten fuel cavity, it is important that a fuel temperature calculation is performed in the solid fuel surrounding the molten fuel

cavity. This temperature calculation is performed with the PLHTR (PLUTO2 HEAT TRANSFER) routine which is a modified version of the transient heat-transfer subroutine TSHTRV. (The latter is used to calculate fuel-pin temperatures during the sodium boiling phase of a LOF accident). In the PLHTR heat conduction calculation, the fuel node adjacent to the molten cavity boundary receives heat from the molten cavity in the form of a heat source. This heat source is the total energy convected to the cavity wall from the molten fuel flow during a heat-transfer time step divided by the heat-transfer time-step size. If a solid fuel node reaches the input melt fraction criterion FNMELT, this node will be gradually added to the molten cavity. The rate of fuel addition depends on the temperature gradient between the node adjacent to the cavity wall and its neighboring solid fuel node.

14.2.4 Overview of the Numerical Approach for the In-pin Fuel Motion Calculation and Description of Subroutines PLlPIN and PL2PIN

There are several requirements for the solution algorithm for this one dimensional, compressible flow problem with variable flow cross section: (a) it had to be able to handle large mass sinks (due to fuel ejection from the pins), (b) it had to conserve mass perfectly, and (c) it had to run efficiently. This was achieved with a predominantly explicit Eulerian solution method. All convection mass, energy, and momentum fluxes are treated explicitly (i.e., the beginning of time-step values are used). However, the solution sequence of the different equations introduces a certain implicitness which is of importance for treating the strong mass sinks.

For the in-pin motion calculation three mass, one energy and one momentum conservation equations are solved. The mass conservation equations are for the fuel and the free and the dissolved fission gas. The fuel and free fission-gas mass conservation equations are solved first, followed by the fuel energy conservation equation. The fission-gas temperature change is assumed to be the same as the fuel temperature change. From the results of the mass and energy conservation equations, a new pressure is calculated. This is not the true end-of-time-step pressure because the velocity changes during the time step have not been included. However, it is a proper prediction for the end-of-time- step value in an explicit sense. In the fuel-ejecting nodes, this new pressure and the advanced densities and energies are used for calculating the fuel and fission-gas ejection rates. The pressure in the ejection nodes is then decreased in order to account for the fuel and gas losses. The adjusted new pressures are then used in the fuel/fission-gas momentum equation. There is an input option in PLUTO2 to use a combination of the new and the old pressures. This option lets the pressure, P, be:

$$P = (1 - \text{EPCH}) \bullet \text{beginning-of-time-step pressure} + \text{EPCH} \bullet \text{advanced pressure} \qquad (14.2\text{-}1)$$

The recommended input value is EPCH=1 because the calculation remained stable for longer time steps in test problems involving shock propagation and shock reflection

when this input value was used [14-21]. In these test calculations, it was also attempted to iterate on the convective fluxes by repeating most of the in-pin calculation for each time step. This seemed to make the results somewhat smoother, but did not allow a time step as long as the one allowable with the above-described explicit scheme.

The time-step criterion in this compressible calculation is the sonic Courant condition. This does not require particularly small time steps because the sonic velocity in two-phase mixtures is fairly low for the void fractions encountered in pin blowdown calculations.

A staggered numerical grid with the densities, energies, and temperatures defined at the cell centers and the velocities at the cell edges is used. The spatial differencing uses full donor cell differencing. Although this is not as accurate as higher order differencing, it makes the calculation stable because it introduces a numerical diffusion effect. It is interesting to note that this stabilizing effect was not enough to keep two-phase test calculations stable for shock reflections from a rigid wall. Although these test calculations could be stabilized by introducing an artificial viscous pressure into the calculations [14-21], the artificial viscous pressure is not necessary for regular pin blowdown calculations. It could even cause problems if the input constants, which affect the magnitude of the artificial viscous pressure, are set too high. The two relevant input parameters, C1VIPR and C2VIPR, should therefore be set to small values such as 10^{-3}.

The free fission-gas mass conservation, the fuel mass conservation, and the fuel energy equation are solved in subroutine PLIPIN (PLUTO2 1st PIN ROUTINE). PLIPIN also computes the molten cavity geometry changes due to fuel melt-in, and the fuel and fission-gas ejection from the pins (see Section 14.3). The fuel/fission-gas momentum equation and the dissolved fission-gas mass equation are solved in PL2PIN (PLUTO2 2nd PIN ROUTINE). This routine also calculates the sonic velocities for each node. The minimum time step found is the predicted time step for the next cycle. However, the actual PLUTO2 time step, which is used both in the pin and in the channel calculation, is the smaller of the pin and channel hydrodynamics time steps. The channel time step is usually the smaller one, and thus, dominates the time-step selection.

14.2.5 Definition of the Generalized Smear Densities for the In-pin Calculation

The use of generalized smear densities in PLUTO2 (and LEVITATE) has been prompted by the many different moving and stationary components in this problem. Its use also simplifies the differential and finite difference equations for variable cross section flow. The pie chart in Fig. 14.2-1 gives an example of the relative cross sectional areas within a subassembly or experimental loop at a certain axial elevation.

If the total area of the subassembly is AXMX, the generalized volume fraction of a certain component k is:

$$\theta_k(z,t) = A_k(z,t) \,/\, AXMX \qquad (14.2\text{-}2)$$

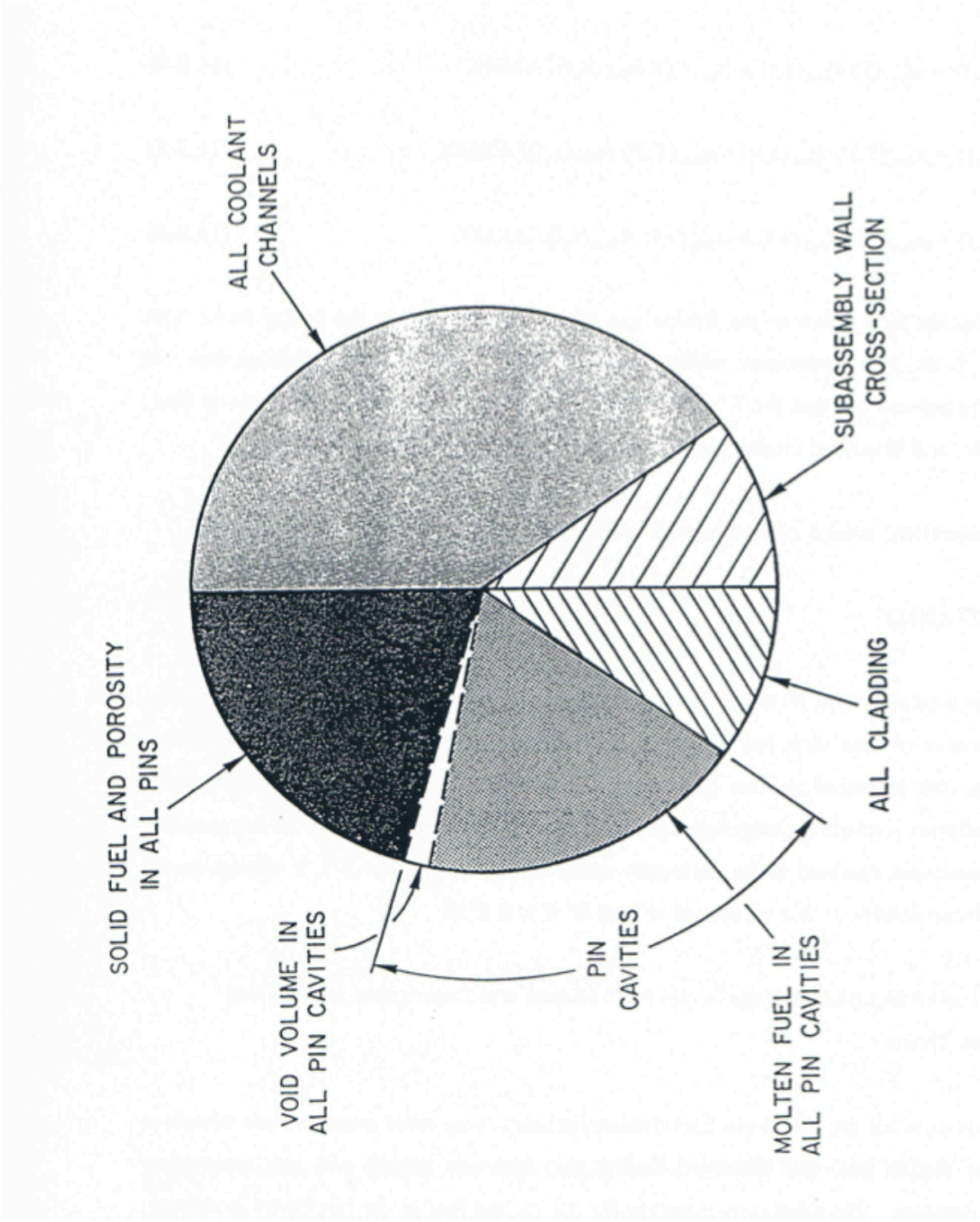

Fig. 14.2-1. The Left-hand Side of This Pie Chart Illustrates the Possible Material Cross Sectional Areas in the Fuel Pin, the Whole Pie Representing an Area AXMW Which is an Input Parameter

where A_k is the cross sectional area occupied by component k (the latter refers, e.g., to the cavities or the moving fuel in all failed pins within the subassembly cross section). The reference area AXMX, which is an input quantity, can be arbitrarily chosen. This is because the code is invariant to the choice of AXMX (i.e., as long as it is not varied by several orders of magnitude which can lead to differences due to truncation errors). However, the recommended value of AXMX is the cross sectional area of a subassembly or experiment test section (including the can wall) because the volume fractions of the different components that appear in the PLUTO2 output are better understood in this case.

The generalized volume fraction of the free fission gas and fuel vapor in the cavity is the difference between the cavity volume fraction and the fuel volume fraction.

$$\theta_{fica}(z,t) = \theta_{ca}(z,t) - \theta_{fuca}(z,t) \tag{14.2-3}$$

where

θ_{fica} = generalized volume fraction of the free fission gas and fuel vapor in the cavities of the failed pins.

θ_{ca} = generalized volume fraction of the molten cavities in all failed pins which can be calculated from A_{ca}/AXMX

θ_{fuca} = generalized volume fraction of the fuel in the cavities of all failed pins

Generalized smear densities, which are always marked by a prime, are defined as products of physical densities and generalized volume fractions:

$$\rho'_{fuca}(z,t) = \rho_{fuca}(T)\,\theta_{fuca}(z,t) = \rho_{fuca}(T)\,A_{fuca}(z,t)/AXMX \tag{14.2-4}$$

$$\rho'_{fica}(z,t) = \rho_{fica}(T,P)\,\theta_{fica}(z,t) = \rho_{fica}(T,P)\,A_{fica}(z,t)/AXMX \tag{14.2-5}$$

$$\rho'_{fsca}(z,t) = \rho_{fsca}(z,t)\,\theta_{fuca}(z,t) = \rho_{fsca}(z,t)\,A_{fuca}(z,t)/AXMX \tag{14.2-6}$$

where the subscript *fsca* refers to the fission gas which is dissolved in the cavity fuel. The temperature T is the fuel temperature, which should actually be written with subscript *fuca*. It should again be pointed out that the A's refer to total cross section areas of all the cavity fuel, free fission gas, and dissolved fission gas in the failed pins of one subassembly.

The generalized source or sink term is written as:

$$S' = S^{\ell}/AXMX \tag{14.2-7}$$

where the source or sink term S^{ℓ} represents a mass source or sink per unit time and unit length. The primed source or sink term has the dimension of mass per unit time and per unit smear volume. This unit of smear volume is a m^3 of the cell volume $AXMX \cdot \Delta z$ in which all relevant components (including components in all failed pins, the components in all the channels and the structure) are assumed to be uniformly smeared. From Eq. 14.2-7, a change in the generalized smear density ρ' due to source or sink S' it just $S'\Delta t$.

14.2.6 Differential Equations for the In-pin Fuel Motion and Description of Sink and Source Terms

The equation set for the in-pin fuel motion includes three mass conservation equations (for fuel, free fission gas, and dissolved fission gas) and one energy and one momentum conservation equation. The continuity equation for the molten fuel in the pin cavity is written:

$$\frac{\partial}{\partial t}(\rho_{fuca}A_{fuca}) = -\frac{\partial}{\partial_z}\left(\rho_{fuca}A_{fuca}u_{fuca}\right) + S^{\ell}_{fuca,me}(z,t) - S^{\ell}_{fuca,ej}(z,t) \qquad (14.2\text{-}8)$$

where the subscripts *me* and *ej* refer to fuel melting into and fuel ejection from the pin cavities of all failed pins, respectively. By dividing by *AXMX* and using the definitions of the generalized smear densities and source and sink terms, Eq. 14.2-8 becomes:

$$\frac{\partial}{\partial t}\rho'_{fuca} = -\frac{\partial}{\partial_z}\left(\rho'_{fuca}u_{fuca}\right) + S'_{fuca,me} - S'_{fuca,ej} \qquad (14.2\text{-}9)$$

where the primed sources and sinks are per unit time and per unit smear volume (see Eq. 14.2-7). The integrated source term, $S'_{fuca,me}\,\Delta t_{PL}$, which is actually needed in the finite difference equations of the code, is calculated from

$$S'_{fuca,me}\Delta t_{PL} = \rho_{fu,cabd}\Delta A_{me}\,NRPI \cdot FNPI / AXMX \qquad (14.2\text{-}10a)$$

here

Δt_{PL} = PLUTO2 time step

$\rho_{fu,cabd}$ = fuel density (including porosity) adjacent to the cavity boundary,

ΔA_{me} = area of fuel (including porosity) melted into the cavity per PLUTO2 time step per pin

$NRPI$ = number of pins per subassembly,

$FNPI$ = fraction of the pins which are failed.

When the solid fuel node adjacent to the cavity has not yet exceeded an input melt fraction value FNMELT:

$$S'_{fuca,me}\Delta t_{PL} = 0 \tag{14.2-10b}$$

The ΔA_{me} in Eq. 14.2-10a is related to a change in the cavity diameter by

$$\Delta A_{me} = \frac{\pi}{4}\Delta D_{ca}\left(2D_{ca} + \Delta D_{ca}\right) \tag{14.2-11a}$$

In order to avoid adding the whole radial node instantaneously upon meeting the input melt fraction criterion *FNMELT*, the radial node is added gradually beginning at the time *FNMELT* is reached and the addition is completed once the melt fraction has exceeded *FNMELT* + 0.1. Once the melt fraction has become greater than *FNMELT*, the change in cavity diameter is calculated from

$$\Delta D_{ca} = FNMECA \cdot 2 \cdot \Delta r_{node} \tag{14.2-11b}$$

where Δr_{node} is the width of the heat-transfer node adjacent to the cavity wall before it is melted into the cavity. *FNMECA* is the fraction of this node width that has melted into the cavity per PLUTO2 time step.

$$\begin{aligned} FNMECA &= \Delta t_{PL}\left(\left(T_{cabd}^{n+1} - T_{cabd}^{n}\right)/\Delta t_{Ht}\right)/\left(0.1\cdot\left(T_{fu,liq} - T_{fu,sol}\right)\right) \\ &= \Delta T_{PL}/\left(0.1\cdot\left(T_{fu,liq} - T_{fu,sol}\right)\right) \end{aligned} \tag{14.2-12}$$

where

$T_{cabd}^{n}, T_{cabd}^{n+1}$ are the temperatures of the fuel node adjacent to the cavity at the beginning and at the end of the heat-transfer time step Δt_{Ht}, respectively.

$T_{fu,liq}, T_{fu,sol}$ are fuel liquidus and solidus temperatures, respectively. The difference between the two is the melting band width.

Δt_{PL} is the PLUTO2 time step.

ΔT_{PL} is the temperature change of the fuel adjacent to the cavity during a PLUTO2 time step.

Equation 14.2-12 implies that the whole heat-transfer node will be melted into the cavity after its temperature has risen by 1/10 of the melting band width beyond the input value FNMELT. Moreover, it is checked whether the neighboring solid fuel node also has exceeded the input melt fraction criterion FNMELT. If this is the case, the entire remaining node currently melting into the cavity is added immediately to the cavity. This situation can occur in TREAT experiments.

The sink term $S'_{fuca,ej}$ that is due to fuel ejection is also the source term for the coolant channel equations. It will be described in detail in Section 14.3. Its integrated form is similar to Eq. (14.2-10a)

$$S'_{fuca,ej} \cdot \Delta t_{PL} = \rho'_{fuca} \cdot FN \tag{14.2-13}$$

where

FN = fraction of the fuel in an ejecting cavity cell that is actually ejected during a PLUTO2 time step.

The free fission-gas mass conservation equation is written

$$\frac{\partial}{\partial t}\left(\rho_{fica} A_{fica}\right) = -\frac{\partial}{\partial z}\left(\rho_{fica} A_{fica} u_{fuca}\right) + S^{\ell}_{fica,me}(z,t) - S^{\ell}_{fica,ej} + S^{\ell}_{fsca,rl} \tag{14.2-14}$$

where the subscripts *fsca* and $r\ell$ refer to fission gas in solution and to the release of this dissolved fission gas, respectively. Dividing by *AXMX* and by using the definition of the generalized smear densities and source and sink terms yields

$$\frac{\partial}{\partial t}\rho'_{fica} = -\frac{\partial}{\partial z}\left(\rho'_{fica} u_{fuca}\right) + S^{\ell}_{fica,me} - S^{\ell}_{fica,ej} + S^{\ell}_{fsca,rl} \tag{14.2-15}$$

The integrated source term for free fission gas due to fuel melt-in is similar to that in Eq. 14.2-10a:

$$S'_{fica,me}\,\Delta t_{PL} = \rho_{fifs,cabd}\,\Delta A_{me}\left(NRPI \cdot FNPI / AXMX\right) \cdot FIFNGB \tag{14.2-16}$$

where ΔA_{me} is the calculated change in cavity cross sectional area described before (see Eq. 14.2-11a), $\rho_{fifs,cabd}$ is the density of all the gas in the fuel node adjacent to the cavity, and *FIFNGB* is an input parameter determining the fraction of all the gas entering the cavity with the molten fuel which instantaneously becomes free gas. This is an input parameter because DEFORM does not currently discriminate between intra-granular and grain-boundary gas. The ratio of the grain-boundary gas to the total gas in a node may be similar to the fraction of the gas that becomes free upon melting into the cavity. However, it seems more likely that only a smaller fraction will be instantaneously available because some of the grain-boundary bubbles may not be large enough to be considered free gas as soon as the fuel melts.

The quantity $\rho_{fifs,cabd}$ is calculated from:

$$\rho_{fifs,cabd} = RETFG2_{cabd}\left(FUMS_{cabd} / FUELMS_{cabd}\right) / VOLUME_{cabd} \tag{14.2-16a}$$

where

$RETFG2_{cabd}$ is the total retained fission-gas mass in the original radial fuel-pin node at the cavity boundary before it has actually melted in,

$FUMS_{cabd}$ is is the current fuel mass in the melting radial fuel-pin node at the cavity boundary,

$FUELMS_{cabd}$ is the original fuel mass of the radial fuel-pin node at the cavity boundary before any fuel is removed due to melt-in,

$VOLUME_{cabd}$ is the current volume of the melting radial fuel-pin node at the cavity boundary.

The free fission-gas sink term due to fuel ejection in Eq. 14.2-15 is described in detail in Section 14.3. Its form is similar to that of the sink term for fuel ejection (Eq. 14.2-13):

$$S'_{fica,ej} \cdot \Delta t_{PL} = \rho'_{fica} \cdot FN \tag{14.2-17}$$

The term *FN* used in this equation is the same as in Eq. 14.2-13 because it is assumed in *PLUTO2* that fission gas and fuel are ejected with the same volume fractions that exist in the ejecting cavity node.

The source term due to dissolved fission-gas release in Eq. 14.2-15 is:

$$S'_{fsca,r\ell} = \rho'_{fsca} \cdot CIRTFS \tag{14.2-18}$$

where *CIRTFS* is a release constant for dissolved fission gas which is input and has the dimensions s^{-1}. (The same release constant is also used for the dissolved fission-gas release in the coolant channels - see Eq. 14.4-20). This is a relatively simple exponential decay-type approach to treat the release of the gas dissolved in molten fuel. However, the understanding of the mechanism of dissolved gas release from molten fuel is still very limited.

The dissolved fission-gas mass conservation equation is:

$$\frac{\partial}{\partial t}\left(\rho_{fsca} A_{fuca}\right) = -\frac{\partial}{\partial z}\left(\rho_{fsca} A_{fuca} u_{fuca}\right) + S^{\ell}_{fsca,me} - S^{\ell}_{fsca,ej} - S^{\ell}_{fsca,rl} \tag{14.2-19}$$

By dividing this equation by *AXMX* and using the definitions of the generalized smear density and sources and sinks, one obtains:

$$\frac{\partial}{\partial t}\rho'_{fsca} = -\frac{\partial}{\partial z}\left(\rho'_{fica} u_{fuca}\right) + S^{\ell}_{fsca,me} - S^{\ell}_{fsca,ej} - S^{\ell}_{fsca,rl} \tag{14.2-20}$$

where

$$S'_{fsca,me} = S'_{fica,me}\left(1 - FIFNGB\right)/\, FIFNGB \tag{14.2-21}$$

and $S'_{fica,me}$ and *FIFNGB* are defined for Eq. 14.2-16. The ejection term is connected to the one for the free fission-gas ejection, which is given in Eq. 14.2-17:

$$S'_{fsca,ej} = S'_{fica,ej}\rho'_{fsca} / \rho'_{fica} \tag{14.2-22}$$

The absolute value of the sink term due to the dissolved fission-gas release has been described in Eq. 14.2-18.

The fuel energy conservation equation is written:

$$\begin{aligned}\frac{\partial}{\partial t}\left(\rho_{fuca} e_{fuca} A_{fuca}\right) = &-\frac{\partial}{\partial z}\left(\rho_{fuca} e_{fuca} A_{fuca} u_{fuca}\right) + S^{\ell}_{fuca,me} e_{fu,cabd} \\ &- S'_{fuca,ej} e_{fuca} + Q\, A_{fuca}\rho_{fuca} \\ &- h_{fuca,cabd}\cdot\left(T_{fuca} - T_{fu,cabd}\right)\pi\, D_{ca}\; NRPI\cdot FNPI\end{aligned} \tag{14.2-23}$$

Dividing Eq. 14.2-23 by *AXMX* and using the definitions of the generalized smear densities and sources and sinks produces:

$$\begin{aligned}\frac{\partial}{\partial t}\left(\rho'_{fuca} e_{fuca}\right) = &-\frac{\partial}{\partial z}\left(\rho'_{fuca} e_{fuca} u_{fuca}\right) + S'_{fuca,me} e_{fu,cabd} \\ &- S^{\ell}_{fuca,ej} e_{fuca} + Q\,\rho'_{fuca} \\ &- h_{fuca,cabd}\cdot\left(T_{fuca} - T_{fu,cabd}\right)\pi\, D_{ca} NRPI\cdot FNPI / AXMX\end{aligned} \tag{14.2-24}$$

By rewriting the left-hand side of Eq. 14.2-24 as

$$\frac{\partial}{\partial t}\left(\rho'_{fuca} e_{fuca}\right) = \rho'_{fuca}\frac{\partial}{\partial t} e_{fuca} + e_{fuca}\frac{\partial}{\partial t}\rho'_{fuca} \tag{14.2-24a}$$

and by using the mass conservation Eq. 14.2-8, one obtains

$$\begin{aligned}\rho'_{fuca}\frac{\partial}{\partial t} e_{fuca} = &-\frac{\partial}{\partial z}\left(\rho'_{fuca} e_{fuca} u_{fuca}\right) + e_{fuca}\frac{\partial}{\partial z}\left(\rho'_{fuca}\, u_{fuca}\right) \\ &+ S'_{fuca,ej}\left(e_{fu,cabd} - e_{fuca}\right) + Q\,\rho'_{fuca} \\ &- h_{fuca,cabd}\left(T_{fuca} - T_{fu,cabd}\right)\pi\, D_{ca} NRPI\cdot FNPI / AXMX\end{aligned} \tag{14.2-25}$$

where Q is the fission heat source per kg of fuel

$$Q = FNPOHE \cdot POW \cdot PSHAPE(K) \cdot (1 - GAMSS - GAMTNC - GAMTNE) \cdot F_{POWER} / FUMASS(K) \quad (14.2\text{-}25a)$$

In Eq. 14.2-25a,

$$FNPOHE = \exp\left[POWCOF(1) + \Delta t(POWCOF(2) + \Delta t_x POWCOF(3))\right] \quad (14.2\text{-}25b)$$

where Δt_x is the time between the current *PLUTO*2 time and the beginning of the current main (point kinetics) time step. The *POWCOF*s are the coefficients that are found by fitting an exponential function to the power levels at the end of the last three point kinetics time step.

POW = steady-state power in the peak axial fuel-pin segment (see SAS4A input description)

PSHAPE(K) = ratio of pin power at axial node *K* to *POW* (see SAS4A input description)

GAMSS, GAMTNC, GAMTNE = fractions of total power for the direct heating of structure, coolant, and cladding, respectively. (See SAS4A input description)

FUMASS(K) = initial total fuel mass in axial pin segment *K*

F_{POWER} = power reduction factor if there is a radial power gradient in the pin (as is common in TREAT experiments):

$$F_{POWER} = \frac{\sum_{I=1}^{I_{cabd}} PSHAPR(I) \cdot FUELMS(I,K) / \sum_{I=1}^{I_{cabd}} FUELMS(I,K)}{\sum_{I=1}^{NT} PSHAPR(I) \cdot FUELMS(I,K) / \sum_{I=1}^{NT} FUELMS(I,K)} \quad (14.2\text{-}26)$$

where

NT= number of radial pin nodes

I_{cabd}= number of radial pin nodes in the cavity

PSHAPR(I) = mass normalized radial power distribution in radial node *I* (See SAS4A input description)

FUELMS(I,K) = initial fuel mass in the radial fuel-pin node *I,K*.

The heat-transfer coefficient in Eq. 14.2-23 is the sum of a convective and a conduction heat transfer term.

$$h_{fuca,cabd} = \left(h_1 + h_2\right)$$

where

$$h_1 = \frac{k_{fu}}{D_{ca}} \cdot St \cdot \mathrm{Pr} \cdot \mathrm{Re} \tag{14.2-27}$$

This comes from the definition of the Nusselt number

$$Nu = St \cdot \mathrm{Pr} \cdot \mathrm{Re} \tag{14.2-27a}$$

where

St = Stanton number = $h/(\rho u C_p)$

Pr = Prandtl number = $\mu C_p / k$

Re = Reynolds numbers = $D\rho u/\mu$

The Deissler correlation [14-22, 14-23] was used for finding the relationship between the three nondimensional numbers on the right-hand side of Eq. 14.2-27a. The Prandtl number for fuel is about 2.2. By using this value in the Deissler correlation, it can be shown that

$$St \approx 0.0158\ \mathrm{Re}^{-0.2} \tag{14.2-28}$$

By using Eq. 14.2-28 and the definition of the Prandtl number,

$$h_1 = \frac{1}{D_{ca}} \cdot \mu_{fu,liq} \cdot C_{p,fu} \cdot CIA3 \cdot \mathrm{Re}_{ca}^{0.8} \tag{14.2-29}$$

where

k_{fu} = conductivity of fuel which is input (CDFU)

$\mu_{fu,liq}$ = liquid fuel viscosity which is input (VIFULQ)

$CIA3$ = input constant. A value of 0.0158 is recommended because of

$$\mathrm{Re}_{ca} = \left(\left| u_{fuca} \right| D_{ca} \rho'_{fuca} / \theta_{ca} \right) / \mu_{fu,liq} \tag{14.2-30}$$

The conduction heat-transfer coefficient, h_2, which is relevant for a low flow or a stagnant flow condition (the stagnant condition is assumed in the simplified *PLUTO*2 node — see Section 14.1.2), is of the following form

$$h_2 = \frac{k_{fu}}{D_{ca}} 4 \tag{14.2-31}$$

The pressure calculation in the fuel-pin cavity is based on the assumption that the fission-gas pressure and fuel-vapor pressure can be added. The total cavity pressure is:

$$P_{ca} = P_{fica}\left(T_{fuca}, \rho_{fica}\right) + P_{fvca}\left(T_{fuca}\right) \tag{14.2-32}$$

where the fission-gas pressure is calculated form a special form of the ideal-gas equation which takes the compressibility of the liquid fuel into account:

$$P_{fica} = R_{fi} \cdot T_{fuca} \rho'_{fica} / \left(\theta_{ca} - \theta_{fuca} + \theta_{fuca} K_{fu} \cdot P_{fica}\right) \tag{14.2-33}$$

where

R_{fi} = the universal gas constant divided by the molecular weight of the mixture of fission gas and helium fill gas. R_{fi} is equal to an input value RGAS which should take into account the relative amounts of krypton, xenon, and helium. The latter may be important for near-fresh fuel.

K_{fu} = liquid fuel compressibility which is input (see CMFU).

The physically reasonable solution of the quadratic Eq. 14.2-33 is:

$$P_{fica} = \frac{-\left(\theta_{ca} - \theta_{fuca}\right) + \sqrt{\left(\theta_{ca} - \theta_{fuca}\right)^2 + 4\theta_{fuca} K_{fu} \cdot R_{fi} \cdot T_{fuca} \rho'_{fica}}}{2\theta_{fuca} K_{fu}} \tag{14.2-34}$$

There is also a second solution with a minus sign in front of the square root, which does not give a physically reasonable result. Equation 14.2-34 reduces to a single-phase liquid pressure solution for no fission gas and $\theta_{fuca} > \theta_{ca}$:

$$P_{fica} = -\left(\theta_{ca} - \theta_{fuca}\right) / \left(\theta_{fuca} K_{fu}\right) \tag{14.2-35}$$

which is equivalent to the definition of the fuel compressibility. For void fractions greater than 30% the fission-gas pressure is calculated from a modified Eq. 14.2-33 in which the term with K_{fu} is dropped.

If the dissolved fission gas present in the molten fuel cavity is assumed to occupy a negligible volume, in comparison with the volume occupied by the free gas then the θ_{fuca} in Eq. 14.2-33 and 14.2-34 reflects the actual volume occupied by the molten fuel. This assumption is justified when the ambient cavity pressure is significantly smaller than the bubble surface tension pressure, as was the case in all TREAT experiments analyzed

with SAS4A. When this assumption is used, the dissolved fission gas does not affect the cavity pressure until it is released, in a gradual manner, to the free gas field.

However, during a transient characterized by a rapid increase in the power level, the cavity pressures can reach higher values, so that the influence of the dissolved fission gas becomes important. In order to address this issue the dissolved fission gas modeling in the pin cavity was introduced as described below.

The dissolved fission gas is assumed to exist in the form of small bubbles, with the gas inside the bubbles at the pressure P_{bubble}:

$$P_{bubble} = P_{surface\ tension} + P_{cavity}\ .$$

The quantity $P_{surface\ tension}$ is an input to the code (PRSFTN). Its value can be determined as:

$$P_{surface\ tension} = \frac{2\sigma}{r},$$

where:

σ = bubble surface tension,

r = bubble radius.

The recommended value for $P_{surface\ tension}$ is 4 x 10^7 Pa, corresponding to σ = 0.4 N/m (400 dyne/cm) and r = 2 x 10^{-8} m (200 Å). The surface tension pressure is assumed to remain constant during the calculations. Furthermore, in order to simplify the calculations, the pressure P_{cavity} used in the calculation of the bubble pressure P_{bubble} is the cavity pressure at the end of the previous time step. The volume occupied by the dissolved gas in the axial cavity cell i is then calculated using the equation:

$$V_{D,i} = \frac{M_{D,i} \cdot R \cdot T_i}{m \cdot P_{bubble,i}} = \frac{R}{m} \cdot \frac{M_{D,i} \cdot T_i}{P_{bubble,i}}$$

where:

$M_{D,I}$ = mass of dissolved fission gas in cell i,

R/m = universal gas constant divided by molar mass,

T_i = gas temperature in cell i, assumed to be equal to the molten fuel temperature,

$P_{bubble,I}$ = the pressure of the gas contained in the small bubbles, calculated above.

The fuel and dissolved gas are assumed to form a homologous mixture, with the volume given by:

$$V_{fuel}^{mixture} = V_{fuel,i} + V_{D,i},$$

where:

$V_{fuel,I}$ = molten fuel volume in cell *i*,

$V_{D,i}$ = dissolved gas volume in cell *i*.

The calculation then proceeds as before, using the volume $V_{fuel,i}^{mixture}$ instead of $V_{fuel,i}$ to determine the value of θ_{fuca} used in Eqs. 14.2-33 and 14.2-34.

When there is little molten fuel in an axial cavity cell, i.e., the gas occupies a large fraction of the cell volume, a perfect gas equation is used to determine the free gas pressure. The underlying assumption is that the compressibility of the fuel/dissolved-gas-mixture has a negligible effect under these circumstances. However, if larger amounts of molten fuel are present, the pressure calculation takes into account the molten fuel compressibility. In this case, the dissolved fission gas and molten fuel volumes are lumped together and assumed to have the same compressibility as the molten fuel. This is a simplifying assumption, but is conservative in the sense that the molten fuel/dissolved gas mixture is likely to have a higher compressibility than the molten fuel itself and thus would lead to somewhat lower cavity pressures during rapid power excursions.

This treatment of the dissolved fission gas has also been implemented in DEFORM-4, LEVITATE, and PLUTO2. If the input constant PRSFTN is less than 10^7 the effect of the dissolved fission gas on the ambient pressure is ignored.

The momentum conservation equation for the fuel/fission-gas mixture is:

$$\begin{aligned}
&\frac{\partial}{\partial t}\left(\rho_{fuca}A_{fuca}u_{fuca} + \rho_{fica}A_{fica}u_{fuca}\right) \\
&\quad = -\frac{\partial}{\partial z}\left(\rho_{fuca}A_{fuca}u_{fuca}^2 + \rho_{fica}A_{fica}u_{fuca}^2\right) \\
&\qquad - A_{ca}\cdot\left(\frac{\partial P_{ca}}{\partial z} + \frac{\partial P_{vi}}{\partial z}\right) - g\left(\rho_{fuca}A_{fuca} + \rho_{fica}A_{fica}\right) \\
&\qquad - u_{fuca}\left|u_{fuca}\right|\cdot\left(\rho_{fuca}A_{fuca}/A_{ca} + \rho_{fica}A_{fica}/A_{ca}\right)A_{ca}\cdot F_{friction}/\left(2D_{ca}\right) \\
&\qquad - \left(S_{fuca,ej}^{\ell} + S_{fica,ej}^{\ell}\right)u_{fuca}
\end{aligned} \tag{14.2-36}$$

Dividing Eq. 14.2-36 by AXMX and using the definitions for the generalized smear densities and mass sinks gives:

$$\frac{\partial}{\partial t}\left[u_{fuca}\left(\rho'_{fuca}+\rho'_{fica}\right)\right]=\frac{\partial}{\partial z}\left[u^2_{fuca}\left(\rho'_{fuca}+\rho'_{fica}\right)\right]$$
$$-\theta_{ca}\left(\partial P_{ca}/\partial z+\partial P_{vi}/\partial z\right)-g\left(\rho'_{fuca}+\rho'_{fica}\right)$$
$$-u_{fuca}\left|u_{fuca}\right|\cdot\left(\rho'_{fuca}+\rho'_{fica}\right)F_{friction}/\left(2D_{ca}\right)$$
$$-\left(S'_{fuca,ej}+S'_{fica,ej}\right)u_{fuca} \qquad (14.2\text{-}37)$$

u_{fuca} = vertically upward fuel velocity in the cavity (see the sign of the gravity head term in Eq. 14.2-36).

P_{vi} = artificial viscous pressure for stabilizing test problems involving shock wave propagation and shock reflection from a rigid boundary. Not necessary for regular cavity blowdown problems.

If the net free fission-gas mass flux into a numerical node is negative (i.e., for net outflow), then $P_{vi} = 0$.

If the net convective free fission-gas mass flux into a numerical cell is positive [14-27]:

$$P_{vi}=C2VIPR\cdot 0.5\cdot\left(p'_{fu,K}+p'_{fi,K}\right)\cdot\left(u_{fuca,K+1}-u_{fica,K}\right)^2/\theta_{ficaxx,K} \qquad (14.2\text{-}38)$$

where

K = index of the axial cavity node for which P_{vi} is being evaluated

$C2VIPR$ = input constant which determines the magnitude of the numerical damping.

$$\theta_{ficaxx}=\begin{cases}\theta_{fica} & \text{for}\ \theta_{fica}>\theta_{ca}\cdot C1VIPR\\ \theta_{ca}-C1VIPR & \text{for}\ \theta_{fica}<\theta_{ca}\cdot C1VIPR\end{cases} \qquad (14.2\text{-}38a)$$

where

C1VIPR = Input constant

The Moody friction factor $F_{friction}$ in Eq. (14.2-37) depends on the Reynolds number

$$\mathrm{Re}_{pi}=\left|u_{fuca}\right|D_{ca}\cdot\left(\rho'_{fuca}+\rho'_{fica}\right)/\left(\theta_{cs}\cdot VIFULQ\right) \qquad (14.2\text{-}39)$$

where *VIFULQ* is the viscosity of liquid fuel which is input. The friction factor is

$$F_{friction} = \begin{cases} 64/\mathrm{Re}_{pi} & \text{for } \mathrm{Re}_{pi} \; CIREFU \\ \mathrm{CIFRFU} & \text{for } \mathrm{Re}_{pi} \; CIREFU \end{cases} \qquad (14.2\text{-}39a)$$

where *CIREFU* and *CIFRFU* are both input and should be made consistent in order to avoid a jump in the friction factor at Re_{pi} = *CIREFU*.

The last term in Eq. 14.2-37 is necessary because the total momentum in the cell decreases due to ejection and this has to be considered in a momentum equation written in conservative form. There is no term accounting for the fuel melt-in because this fuel is added to the cavity with zero axial velocity, and therefore does not change the total momentum. However, since the generalized fuel smear density will change in a cell with melt-in, this will lead to a velocity decrease in such a cell.

14.2.7 Finite Difference Equations for the In-pin Motion

In the overview of the numerical scheme given in Section 14.2.4, it was pointed out that full donor cell spatial differencing and a largely explicit time differencing are used for treating the in-pin motion. The implicit aspect of the solution is that the mass and energy conservation equations are solved first and then a pressure is calculated on the basis of the mass and energy equation results. This advanced pressure is used in the momentum conservation equation.

The finite differencing of all the mass conservation equations is the same. The fuel mass conservation is used as an illustration.

$$\left(\rho'^{n+1}_{fuca,K} - \rho'^{n}_{fuca,K}\right)/\Delta t_{PL} = -\left((\rho' u)_{fuca,K+1} - (\rho' u)_{fuca,K}\right)/\Delta z_K + \sum_k S'_{K,k} \qquad (14.2\text{-}40)$$

where

$$(\rho' u)_{fuca,K} = \begin{cases} \rho'_{fuca,K-1}\, u_K & \text{for } u_K > 0 \\ \rho'_{fuca,K}\, u_K & \text{for } u_K < 0 \end{cases} \qquad (14.2\text{-}40a)$$

u_K= fuel velocity at the mesh cell boundary *K*.

$\rho'_{fuca,K-1}$ = generalized fuel smear density at the mesh cell midpoint below boundary *K*

$\rho'_{fuca,K}$ = generalized fuel smear density at the mesh cell midpoint above boundary *K*

The numerical grid used in the program was discussed in Section 14.2.4, which gives an overview of the numerical scheme. Densities are at the cell centers and velocities at the cell edges (see schematic before the momentum conservation Eq. 14.2-48). The source

and sink terms have already been described in their finite difference form in the previous section.

The convective fluxes at the lower and upper boundaries of the cavity that are located in the end cells *KK*1 and *KKMX*, respectively, are

$$\left(\rho' u\right)_{fuca,KK1} = 0 \tag{14.2-41}$$

and

$$\left(\rho' u\right)_{fuca,KKMX+1} = 0 \tag{14.2-42}$$

The end cells are not always the same during a *PLUTO*2 run because the molten cavity can extend axially. When a new cell is added to the cavity, mass can only flow into this end cell if its cross section is at least 20% of that of the neighboring cell in the molten cavity. This had to be done because of problems with overcompression of cells with a very small cross section.

The finite difference form of the fuel energy Eq. 14.2-25 is:

$$\begin{aligned}\rho'_{fuca,K}\left(e^{n+1}_{fuca,K} - e^{n}_{fuca,K}\right)/\Delta t_{PL} = -\Big[&\left(\rho'_{fuca}\, e_{fuca}\, u_{fuca}\right)^{n}_{K+1} \\ &-\left(\rho'_{fuca}\, e_{fuca}\, u_{fuca}\right)^{n}_{K}\Big]/\Delta z_K + e^{n}_{fuca,K}\Big[\left(\rho'_{fuca}\, u_{fuca}\right)^{n}_{K+1} \\ &-\left(\rho'_{fuca}\, u_{fuca}\right)^{n}_{K}\Big]/\Delta z_K + S'^{n}_{fuca,me,K}\left(e^{n}_{fu,cabd,K} - e^{n}_{fuca,K}\right) \\ &+Q^{n}_{K}\,\rho'^{n}_{fuca,K} - h^{n}_{fuca,cabd,K}\left(T^{n}_{fuca,K} - T^{n}_{fu,cabd,K}\right)\pi\, D^{n}_{ca,K}\;\; NRPI\cdot FNPI / AXMX\end{aligned} \tag{14.2-43}$$

The fuel cavity temperature T_{fuca} in the above equation has to be calculated from the internal energy:

For $e_{fu,sol} < e_{fuca} < e_{fu,liq}$,

$$T_{fuca} = T_{fu,sol} + \left(T_{fu,liq} - T_{fu,sol}\right)\cdot\left(e_{fuca} - e_{fu,sol}\right)/\left(e_{fu,liq} - e_{fu,sol}\right) \tag{14.2-44}$$

For $e_{fuca} > e_{fu,liq}$,

$$T_{fuca} = T_{fu,liq} + \left(e_{fuca} - e_{fu,liq}\right)/C_{p,fu}$$

where $C_{p,fu}$ is the fuel specific heat which is the single input value CPFU. The convective energy flux at cell boundary K in Eq. (14.2-43) in calculated as:

$$\left(\rho'_{fuca} e_{fuca} u_{fuca}\right)_k = \begin{cases} \left(\rho'_{fuca} e_{fuca}\right)_{K-1} u_{fuca,K} & \text{for } u_{fuca,K} > 0 \\ \left(\rho'_{fuca} e_{fuca}\right)_K u_{fuca,K} & \text{for } u_{fuca,K} < 0 \end{cases} \tag{14.2-45}$$

At the lower and upper cavity ends that are in cells KK1 and KKMX, the convective energy fluxes are zero.

$$\left(\rho'_{fuca} e_{fuca} u_{fuca}\right)^n_{KK1} = 0 \tag{14.2-45a}$$

and

$$\left(\rho'_{fuca} e_{fuca} u_{fuca}\right)^n_{KKMX+1} = 0 \tag{14.2-45b}$$

By using the convective fluxes from Eqs. 14.2-40a and Eqs. 14.2-45, and the definitions of the energy gain and loss terms given earlier, and by differencing the second term of Eq. 14.2-43 like the first, Eq. 14.2-43 can be solved for $e^{n+1}_{fuca,K}$. Fuel temperatures that are shown in the PLUTO2 output are calculated by using Eqs. 14.2-44 and 14.2-44a.

For the finite difference form of the momentum equation the following quantities have to be defined at the edges of the numerical cells: the combined fuel/fission-gas generalized smear density and the cavity volume fraction. These quantities become:

$$\rho'_{fufi,bk} = 0.5\left(\rho'_{fuca,K-1} + \rho'_{fuca,K}\right) + 0.5\left(\rho'_{fica,K-1} + \rho'_{fica,K}\right) \tag{14.2-46}$$

$$\theta_{ca,bk} = 0.5\left(\theta_{ca,K} + \theta_{ca,K-1}\right) \tag{14.2-47}$$

where the subscript *bk* indicates that these quantities are at the lower boundaries of cell *K*. This is shown on the schematic below. On the numerical grid the velocities are also defined on the cell boundaries, whereas the pressures, densities and volume fractions are defined at the cell centers. This is also shown in the following schematic.

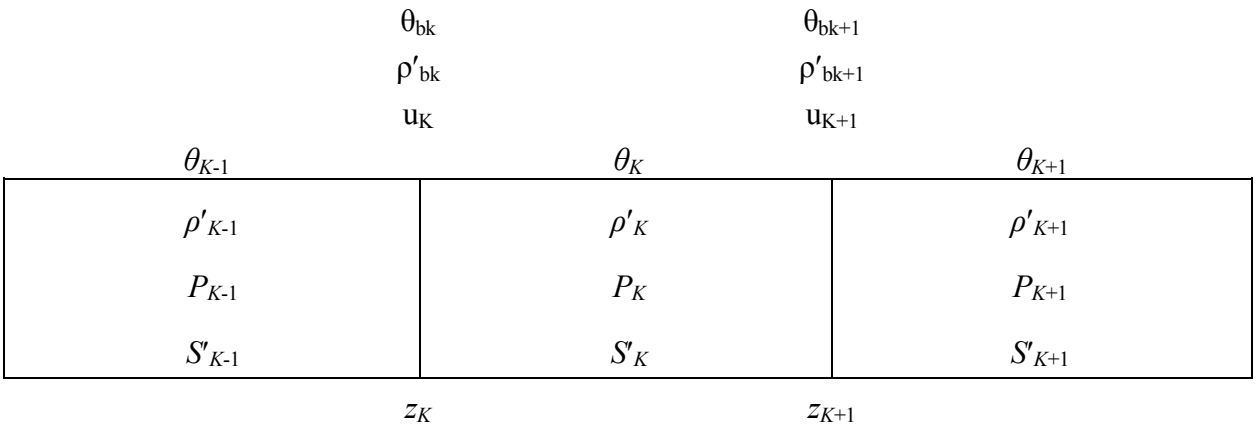

The finite difference form of the momentum conservation Eq. 14.2-37, is written using the definitions 14.2-46 and 14.2-47 as:

$$\begin{aligned}
&\left(\rho'^{n+1}_{fufi,bk}\,u^{n+1}_{fuca,K}-\rho'^{n}_{fufi,bk}\,u^{n}_{fuca,K}\right)/\Delta t_{PL}=-\Big[\left(u^2_{fuca}\,\rho'_{fufi}\right)^{n}_{K}\\
&-\left(u^2_{fuca}\,\rho'_{fufi}\right)^{n}_{K-1}\Big]/\Delta z-\theta_{ca,bk}\Big[\left(1-\varepsilon\right)\cdot\left(P^{n}_{ca,K}-P^{n}_{ca,K-1}\right)\\
&+\varepsilon\cdot\left(P^{n+1}_{ca,K}-P^{n+1}_{ca,K-1}\right)+\left(P^{n}_{vi,K}-P^{n}_{vi,K-1}\right)\Big]/\Delta z-g\,\rho'_{fufi,bk}\\
&-u^{n+1}_{fuca,K}\left|u^{n}_{fuca,K}\right|\rho'^{n}_{fufi,bk}\,F_{friction,bk}/\left(2D_{ca}\right)-\left(S'^{n+1/2}_{fuca,ej,K-1}\right.\\
&\left.+S'^{n+1/2}_{fuca,ej,K}+S'^{n+1/2}_{fica,ej,K-1}+S'^{n+1/2}_{fica,ej,K}\right)\cdot\left(u^{n+1}_{fuca,K}+u^{n}_{fuca,K}\right)\cdot 0.25
\end{aligned}\qquad (14.2\text{-}48)$$

where

ε = Input value EPCH that can be between zero and one (see Eq. 14.2-1),

and Δz implies $0.5(\Delta z_{K-1}+\Delta z_K)$.

By defining

$$S'^{n+1/2}_{fuca,ej,bk}=\left(S'^{n+1/2}_{fica,ej,K-1}+S'^{n+1/2}_{fica,ej,K}+S'^{n+1/2}_{fica,ej,K-1}+S'^{n+1/2}_{fica,ej,K}\right)\cdot 0.5 \qquad (14.2\text{-}49$$

and by collecting all terms with u^{n+1}_{uica} on the left-hand side of the equation, one obtains

$$
\begin{aligned}
u_{fuca,K}^{n+1}\Big[\rho'^{n+1}_{fufi,bk}/\Delta t_{PL} + \Big|u_{fuca,K}^{n}\Big|\rho'^{n}_{fufi,bk}F_{friction,bk}/(2D_{ca})\\
+ S'^{n+1/2}_{fufi,ej,bk}\cdot 0.5\Big] = \rho'^{n}_{fufi,bk}\,u_{fuca,K}^{n}/\Delta t_{PL}\\
-\Big[\left(u_{fuca}^{2}\,\rho'_{fufi}\right)_{K}^{n} - \left(u_{fuca}^{2}\,\rho'_{fufi}\right)_{K-1}^{n}\Big]/\Delta z\\
-\theta_{ca,bk}\Big[(1-\varepsilon)\cdot\left(P_{ca,K}^{n} - P_{ca,K-1}^{n}\right)\\
+\varepsilon\left(P_{ca,K}^{n+1} - P_{ca,K-1}^{n+1}\right) + \left(P_{vi,K}^{n} - P_{vi,K-1}^{n}\right)/\Delta z - g\,\rho'_{fufi,bk}\\
-S'^{n+1/2}_{fuca,ej,bk}\,u_{fuca,K}^{n}\cdot 0.5
\end{aligned}
\qquad (14.2\text{-}50)
$$

The convective momentum flux in Eq. 14.2-50 is calculated as

$$
\left(u_{fuca}^{2}\,\rho'_{fufi}\right)_{K} = \begin{cases} \rho'_{fufi,K}\,u_{fuca,K}^{2} & \text{if } \left(u_{fuca,K} + u_{fuca,K+1}\right) > 0 \\ \rho'_{fufi,K}\,u_{fuca,K+1}^{2} & \text{if } \left(u_{fuca,K} + u_{fuca,K+1}\right) < 0 \end{cases} \qquad (14.2\text{-}51)
$$

$$
\left(u_{fuca}^{2}\,\rho'_{fufi}\right)_{K-1} = \begin{cases} \rho'_{fufi,K-1}\,u_{fuca,K-1}^{2} & \text{if } \left(u_{fuca,K-1} + u_{fuca,K}\right) > 0 \\ \rho'_{fufi,K-1}\,u_{fuca,K}^{2} & \text{if } \left(u_{fuca,K-1} + u_{fuca,K}\right) < 0 \end{cases} \qquad (14.2\text{-}51a)
$$

where

$$
\rho'_{fufi,K} = \rho'_{fuca,K} + \rho'_{fica,K} \qquad (14.2\text{-}52)
$$

The momentum fluxes for the lower and upper end cells of the cavity, which are designated by KK1 and *KKMX*, are:

$$
\left(u_{fuca}^{2}\,\rho'_{fufi}\right)_{KK1} = \begin{cases} \rho'_{fufi,KK1}\,u_{fuca,KK1+1}^{2}\cdot 0.25 & \text{if } u_{fuca,KK1+1} > 0 \\ \rho'_{fufi,KK1}\,u_{fuca,KK+1}^{2} & \text{if } u_{fuca,KK1+1} < 0 \end{cases} \qquad (14.2\text{-}53)
$$

$$
\left(u_{fuca}^{2}\,\rho'_{fufi}\right)_{KKMX} = \begin{cases} \rho_{fufi,KKMX}\,u_{fuca,KKMX}^{2} & \text{if } u_{fuca,KKMX} > 0 \\ \rho_{fufi,KKMX}\,u_{fuca,KKMX}^{2}\cdot 0.25 & \text{if } u_{fuca,KKMX} < 0 \end{cases} \qquad (14.2\text{-}54)
$$

The factor 0.25 in the above convection terms comes from the assumption of a zero velocity at the end of the cavity.

The momentum Eq. 14.2-50 can be solved for $u_{fuca,K}^{n+1}$ if Eqs. 14.2-46, 14.2-47, and 14.2-51 through 14.2-54 are used.

14.2.8 Time-step Determination for the In-Pin Motion

The PLUTO2 time step Δt_{PL} used in the numerical solution of all the in-pin and channel conservation equations is restricted by the sonic Courant conditions for both the in-pin and channel flows. The sonic Courant condition for the channel flow and the determination of the PLUTO2 time step Δt_{PL} is given at the end of the channel flow description in Section 14.4.6.4. In the present section, only the restriction imposed by the sonic Courant condition for the in-pin flow is described.

The time-step size for the in-pin motion is computed to be a fraction, 0.4, of the minimum time step based on the sonic Courant condition

$$\Delta t_{PL,pin} = 0.4 \cdot \min\left[\Delta z_K / \left(v_{sonic,K} + \left| u_{fuca,K} \right|\right)\right]_{K=KK1,KKMX} \tag{14.2-55}$$

The minimum in Eq. 14.2-55 is evaluated over all the axial cells of the molten fuel cavity. The sonic velocity is calculated from an expression for an adiabatic, homogeneous two-component gas-liquid mixture which is based on Eq. 27 in Reference [14-28].

$$\begin{aligned} v_{sonic}^2 = \gamma_{fi} P_{fica} / \Big\{ & \left[\alpha_{fica}^2 \cdot \rho_{fica} + \alpha_{fica}\left(1-\alpha_{fica}\right)\rho_{fuca}\right] \\ & + \left[\left(1-\alpha_{fica}\right)^2 \rho_{fica} + \alpha_{fica}\left(1-\alpha_{fica}\right)\rho_{fica}\right] \gamma_{fi} P_{fica} K_{fu} \Big\} \end{aligned} \tag{14.2-56}$$

where

α_{fica} = $\theta_{fica}/\theta_{ca}$ = void fraction in the cavity

γ_{fi} = $C_{p,fi}/C_{v,fi}$ = 1.4 (value assumed in PLUTO2)

K_{fu} = $CMFU$ = input liquid fuel compressibility

The above equation holds for adiabatic gas behavior, although the in-pin fission-gas treatment in PLUTO2 is isothermal (the gas temperature is assumed to be always equal to the fuel temperature). However, the sonic velocity for adiabatic gas behavior is higher than that for isothermal gas behavior, and thus, leads to a more conservative (i.e., smaller) time step. Moreover, if a pure gas flow were treated in sections of pins with a prefabricated central hole, the current time-step determination would actually be necessary.

14.3 Fuel and Fission-gas Ejection from the Pins

14.3.1 Physical Model and Assumptions

In the previous section, the sinks for the in-pin motion due to fuel and fission-gas ejection appeared in the fuel, free fission gas, and dissolved fission-gas mass

conservation equations (see Eqs. 14.2-9, 14.2-15, and 14.2-20). These sink terms are, of course, source terms in the channel thermal-hydraulics treatment.

The approach taken for the calculation of the fuel and fission-gas ejection from the pins is based on the assumption that there will always be pressure equilibrium established between a cavity node and the adjacent channel node if fuel and fission-gas ejection occurs. This assumption is justified for cladding ruptures with dimensions larger than one-pin diameter because of the very short distance between cavity nodes and corresponding coolant channel nodes. For pin-hole type failures leading to a pure gas release, which is not currently treated in PLUTO2, an orifice equation for calculating this gas release may be more appropriate. In the older PLUTO code [14-1, 14-3, 14-4], both an asymptotic orifice equation and an ejection calculation, based on pressure equilibration, were computed for the fuel and gas ejections, and the smaller of the two predictions was used. The asymptotic orifice equation usually predicted the higher ejection rates. These were causing a higher pressure in the channel node than in the adjacent cavity node which was considered non-physical.

To achieve the pressure equilibrium between the cavity and channel nodes in PLUTO2, an estimated amount of fuel and gas (with the same volume ratio as present in the cavity node) is ejected into the channel and the resulting cavity and channel pressures are calculated. This calculation is repeated several times with updated estimates for the ejected fuel and fission-gas masses until a pressure equilibrium is achieved. This approach does not consider (or require) the cladding rupture area, which is an advantage because the evolution of the cladding rupture is not known. The cladding rupture sizes found in the post-test examinations of TREAT tests H5 [14-24] and J1 [14-25], which were terminated at a time when the pins were still largely intact, show large enough rupture sizes to justify the assumption of pressure equilibration between the cavity node behind the rupture and the adjacent channel node. Moreover, these rupture areas are considerably larger than the cross section of the molten cavity (50% areal melt fraction in an FFTF type pin means a molten cross sectional area of about 0.1 cm^2; cladding rupture areas in H5 and J1 are about 1 cm^2). This means that the controlling aspect of the fuel and gas ejection (at least in mild TOP accidents) is really the cross sectional area of the cavity, which is taken into account in the in-pin motion calculation in PLUTO2. In the SAS3D model SAS/FCI, which does not consider the in-pin motion mechanistically, the cross sectional area for the orifice equation, used in the calculation of the SAS/FCI fuel and gas ejection, has to be set to about twice the cross sectional area of the cavity near the failure location [14-3]. Under LOF-driven-TOP conditions, when axial cladding rupture propagation is likely (see Section 14.3.3), the in-pin motion is not dominant in controlling the ejection because several contiguous cavity nodes may eject fuel and gas simultaneously. In addition, the time scales are very short under these conditions, leading to less axial fuel and gas convection into an ejection node than can actually be ejected.

Fuel and fission gas are being ejected from the fuel pins with the same volume ratio as exists in the ejecting cavity node. For conditions involving high void fractions in the ejecting cavity node, it is possible that fission gas or fuel vapor will be ejected preferentially because the remaining fuel may be in an annular flow configuration.

Another assumption about the fuel and gas ejection is that no backflow of materials from the channel to the pin is allowed when the pressure in the coolant channel node adjacent to the rupture becomes higher than the pressure in the ejection node. To model this backflow would be difficult and is not warranted because only a small amount of liquid sodium flowing back into the pin would lead to enough vaporization and pressurization to inhibit further backflow of materials. However, the potential pressure increase in the cavity node may diminish the in-pin fuel motion. This could be beneficial if midplane failures are assumed. However, most channel pressurizations that have been observed experimentally and that may be due to FCIs are not sufficient in magnitude or duration to cause concern about this assumption.

14.3.2 Numerical Solution of the Fuel and Gas Ejection Calculation

The numerical evaluation of the amount of fuel and fission gas ejected during a PLUTO2 time step is performed as a second step after the fuel mass conservation Eq. 14.2-9 has been solved and advanced to the end of the time step without accounting for the ejection term $S'_{fuca,ej}$. This section describes how the fuel smear density value obtained at the end of the time step without accounting for ejection ρ'^{old}_{fuca} is corrected for fuel ejection, thus obtaining the actual fuel smear density at the end of time step the ρ'^{new}_{fuca} and the resulting equilibrated pressure of the ejecting cavity cell.

If FN_k is the fraction of the fuel in a cavity node that is ejected during a time step, the new generalized fuel smear density in the cavity node will be:

$$\rho'^{new}_{fuca} = \rho'^{old}_{fuca} - \rho'^{old}_{fuca} \cdot FN_k = \rho'^{old}_{fuca} - FF \tag{14.3-1}$$

where $FF = \rho'^{old}_{fuca} \cdot FN_K$ and is actually the same as the sink term for fuel ejection, $S'_{fuca,ej} \cdot \Delta t_{PL}$ (see Eq. 14.2-13).

Since the fission gas and fuel are assumed to be ejected with the same volume ratio as present in the ejecting cell, the new generalized free-fission-gas smear density is

$$\rho'^{new}_{fica} = \rho'^{old}_{fica} - \rho'^{old}_{fica} \cdot FN_k = \rho'^{old}_{fica} - FF \cdot \rho'^{old}_{fica} / \rho'^{old}_{fuca} \tag{14.3-2}$$

The new cavity fuel fraction will be

$$\theta^{new}_{fica} = \theta^{old}_{fica} - FF / \rho_{fuca} \tag{14.3-3}$$

where $\rho_{fuca} = \rho_{fuca}(T_{fuca})$ is the theoretical fuel density.

By using Eqs. 14.3-1, 14.3-2, and 14.3-3 in the cavity pressure calculation of Eqs. 14.2-32 and 14.2-33 and by dropping the superscripts "old", one obtains

$$P_{ca}^{new} = P_{fvca} + R_{fi} \cdot T_{fuca} \cdot \left(\rho'_{fica} - FF \cdot \rho'_{fica} / \rho'_{fuca}\right) \\ / \left\{\theta_{ca} - \theta_{fuca} + FF / \rho_{fuca}(T) + \left[\theta_{fuca} - FF / \rho_{fuca}(T)\right] K_{fu} \cdot \left(P_{ca}^{new} - P_{fuca}\right)\right\} \quad (14.3\text{-}4)$$

where

$\theta_{ca} - \theta_{fuca} = \theta_{fica}$

By collecting the terms with *FF* on the left-hand side one obtains

$$FF \cdot \left[\left(P_{ca}^{new} - P_{fvca}\right) / \rho_{fuca} + \rho'_{fica} / \rho'_{fuca} \cdot R_{fi} \cdot T_{fuca} \right. \\ \left. - K_{fu} / \rho_{fu} \cdot \left(P_{ca}^{new} - P_{fvca}\right)^2\right] = R_{fi} \cdot T_{fuca} \cdot \rho'_{fica} \quad (14.3\text{-}5) \\ - \theta_{fica}\left(P_{ca}^{new} - P_{fvca}\right) - \theta_{fica} \cdot K_{fu} \cdot \left(P_{ca}^{new} - P_{fvca}\right)^2$$

This equation is used to calculate the fuel ejection *FF* for an estimated P_{ca}^{new}. *FF* is used, in turn, to update the fission-gas and fuel densities in the channel node adjacent to the ejecting cavity node. A new channel pressure is then calculated based on the updated fuel and gas densities. The method of calculating the channel pressures is discussed in Section 14.4.5. If the new channel pressure is not within 1% of the estimated new cavity pressure, a better estimate for the new cavity pressure is made and the calculational sequence for the fuel and gas ejection is repeated.

Because the conditions in the coolant channel node can vary from normal coolant flow to fully voided, the procedure of estimating the new cavity pressure is somewhat complex. It has evolved through trial and error and it usually leads to convergence in a few iterations. If the iteration does not converge, it usually indicates that a non-physical condition has developed in the pin or channel. When the axial extent of the cladding rupture includes more numerical nodes as a result of axial pin failure propagation (which is likely under LOF'd'TOP conditions), the ejection calculation will be performed for each of the axial failure nodes.

The ejection calculation from the pins was originally formulated to allow a simultaneous ejection from the three pin failure groups at any given axial location. As mentioned earlier, the second and third pin failure groups are not yet operational. Because of the complexity of the current ejection calculation from only one pin failure group, it is expected that a simultaneous ejection from three pin failure groups into the same coolant channel node may become too complicated. Therefore, a simpler approach, which would only allow the ejection from the cavity node with the highest pressure during a PLUTO2 time step, may have to be adopted. In this approach it would, of course, still be possible for the different pin failure groups to eject fuel simultaneously at different axial locations.

The fuel and gas ejection calculation is done at the end of subroutine PL1PIN which was discussed in Section 14.1.2. The ejection calculation is done in the calculational

sequence after all in-pin as well as channel mass and energy conservation have been solved and before the momentum equations for both the in-pin and channel flows are solved. The ejection calculation thus provides updated pressures for the momentum equations.

14.3.3 Axial Pin Failure Propagation

Rapid axial pin failure propagation due to the stress concentrations at the edges of the initial rupture (zipper-type failure propagation) has not been accepted as a mechanism for rapid axial failure propagation (i.e., on a millisecond or submillisecond time scale) [14-26]. However, if the conditions in a fuel-pin node are such that failure of the cladding should occur irrespective of cladding stress concentrations due to an adjacent cladding rupture and whether the potential new failure node location is adjacent to the initial failure or not, there is no reason to disallow this type of failure propagation.

The failure of nodes other than the initial one is determined by PLUTO2 because the DEFORM calculation is not done in a calculational channel once PLUTO2 (or LEVITATE) has been initiated. There are two options for pin failure propagation in PLUTO2. The first option is a mechanistic one based on the burst strength of the cladding. The second option allows the pin failure propagation to proceed according to a combination of input failure criteria based on fuel melt fraction, cladding temperature, and pressure differential between cavity and channel.

The mechanistic option (KFAILP=0) assumes that the solid fuel surrounding the molten cavity is completely cracked and that the radial stress at the fuel-cladding interface can therefore be calculated by reducing the cavity pressure by a geometrical reduction factor.

$$\sigma_{radial,fc,K} = P_{ca,K} \cdot D_{ca,K} / \left(2R_{cl,fc,K}\right) \tag{14.3-6}$$

where

$R_{cl,fc,K}$ is the inner radius of the cladding at axial node K.

$D_{ca,K}$ is the diameter of the molten cavity at axial node K.

The hoop stress in the cladding can be calculated from

$$\sigma_{hoop,K} = \left(\sigma_{radial,fc,K} - P_{ch,i}\right) R_{cl,fc,K} / \Delta R_{cl,K} \tag{14.3-7}$$

where $\Delta R_{cl,K}$ is the cladding thickness at axial node K, and subscript i refers to the channel node which is adjacent to cavity node K; $i = K + IDIFF$ where $IDIFF$ is the number of channel nodes below cavity node $K = 1$.

By substituting Eq. 14.3-6 for the radial stress in Eq. 14.3-7,

$$\sigma_{hoop,K} = \left(P_{ca,K} \cdot D_{ca,K} - 2 \cdot P_{ch,i} \cdot R_{cl,fc,K}\right) / \left(2\Delta R_{cl,K}\right) \quad (14.3\text{-}8)$$

Failure is assumed to occur when the following two conditions are satisfied:

$$\sigma_{hoop,K} > \sigma_{UTS}\left(T_{cl,in,K}\right) \quad (14.3\text{-}9)$$

$$AREA_{ca,K} > FNARME \cdot \pi \cdot R_{cl,fc,K}^2 \quad (14.3\text{-}10)$$

where

FNARME = an input melt fraction (or more precisely cavity cross sectional area divided by cross sectional area of the fuel) which should be set to ≥ 0.2 because the PLUTO2 in-point motion model requires a moderately sized cavity diameter to run well.

σ_{UTS} = the burst strength of the cladding that is a function of cladding temperature. This is calculated from the middle cladding node temperature in function subroutine UTS, which is described in Chapter 8 on fuel behavior.

A problem with this burst failure criterion is that it is not compatible with a melt fraction failure criterion, cladding strain failure criterion or any other criteria that are not directly related to the cladding strength. Since these latter criteria may be used in DEFORM to predict the initial failure, care has to be taken that the cladding will not rip open along sizable length as soon as PLUTO2 takes over the calculation. For example, this could happen if the initial pin failure was assumed to occur due to a melt fraction criterion at a time when the cavity pressure was already high enough to burst the cladding at several axial elevations. If a melt fraction criterion was chosen for the initial failure prediction, the problem that several nodes will instantaneously rupture once PLUTO2 initiates, can be avoided by setting the input parameter FNARME (see Eq. 14.3-10) equal to or greater than the input melt fraction criterion for the initial failure.

The non-mechanistic input failure propagation criterion (KFAILP=1) involves several separate criteria. Failure occurs when the cladding middle node and outer surface temperatures, the cross sectional area of the cavity, and the pressure difference between cavity and channel exceed input criteria.

$$T_{cl,in,K} \text{ and } T_{cl,os,K} > TEFAIL \quad (14.3\text{-}11)$$

and

$$AREA_{ca,K} > FNARME \cdot \pi \cdot R_{cl,fc,K}^2 \quad (14.3\text{-}12)$$

and

$$P_{ca,K} > P_{ch,i} + PRFAIL \qquad (14.3\text{-}13)$$

where

TEFAIL, *FNARME*, and *PRFAIL* are input parameters.

Subscripts *in* and *os* refer to the middle and outer cladding nodes, respectively. This combined criterion can of course be simplified by setting some of the input values to extreme numbers. For example, if *TEFAIL* is set to zero and *PRFAIL* to -10^{20}, this criterion will reduce to a pure melt fraction criterion. This input failure propagation criterion may be useful for comparison calculations with codes that allow failure propagation only according to one of the above non-mechanistic criteria. Moreover, if the initial failure criterion is a melt fraction criterion, one may also want to do the failure propagation based on a melt fraction criterion or on a melt fraction criterion combined with the condition that some overpressure has to exist in the molten cavity nodes.

14.3.4 Complete Pin Disruption and Switch to LEVITATE

Once the cladding has melted at a certain axial location and extensive fuel melting has also occurred at the same location, complete fuel-pin disruption will eventually occur. This cannot be treated with PLUTO2, and therefore, a switch to LEVITATE is made under these conditions. For each pin node, PLUTO2 checks whether the middle and outer cladding temperatures have exceeded the liquidus and whether the fuel-surface temperature has exceeded the solidus.

$$T_{cl,in,K} > T_{cl,liq}$$

and

$$T_{cl,os,K} > T_{cl,liq}$$

and

$$T_{fu,os,K} > T_{fu,sol}$$

where

cl,*in* refers to the middle cladding node,

cl,*os* refers to the outer cladding node,

fu,*os* refers to the outermost fuel node.

If the above conditions are met, control will be transferred from PLUTO2 to LEVITATE. These checks are performed at the end of the PLUTO2 driver routine. At that location in the code, it is also checked whether cladding melting has occurred in more than NCPLEV nodes (NCPLEV is input). If this criterion is met, a switch to

LEVITATE will also occur. Moreover, a switch to LEVITATE is also made if the fuel temperature in the cavity or in the channel exceeds 4000 K because significant fuel vapor pressures will develop beyond this temperature.

14.4 Channel Hydrodynamics Model

14.4.1 Overview and Definition of Generalized Smear Densities

The treatment of the material motion in the coolant channels is more complex than that inside the pins because several material components (fuel, sodium, fission gas) and three different phases (solid, liquid, and gas) are involved. Of particular importance are the mass, energy and momentum interactions between the components and phases of this multi-component, multi-phase flow. These are largely determined by the local fuel configurations, which are in turn determined by the fuel flow regimes. Figure 14.4-1 depicts the possible fuel and liquid sodium configurations in an equivalent cylindrical channel. The outer perimeter of this equivalent cylindrical channel represents outer cladding surfaces and inner subassembly wall surfaces. The fuel flow regimes are extensively discussed in Section 14.4.3.1. Table 14.4-1 gives an overview of the interactions between the various channel components that are described in detail in Section 14.4.3.4.

A one-dimensional two-fluid approach with variable flow cross section is used to calculate the momentum changes in the coolant channels. This means that two momentum conservation equations are solved. One of them calculates the velocity changes of the mixture of liquid sodium, sodium vapor, fission gas, and fuel vapor; the other calculates the velocity changes of the moving liquid or solid fuel. This approach is taken because the fuel-to-liquid sodium density ratio is more than 10, and a relatively rapid separation of these two components is likely. This is quite important for treating fuel coolant interactions (FCI's) because it may be one of the major limiting processes.

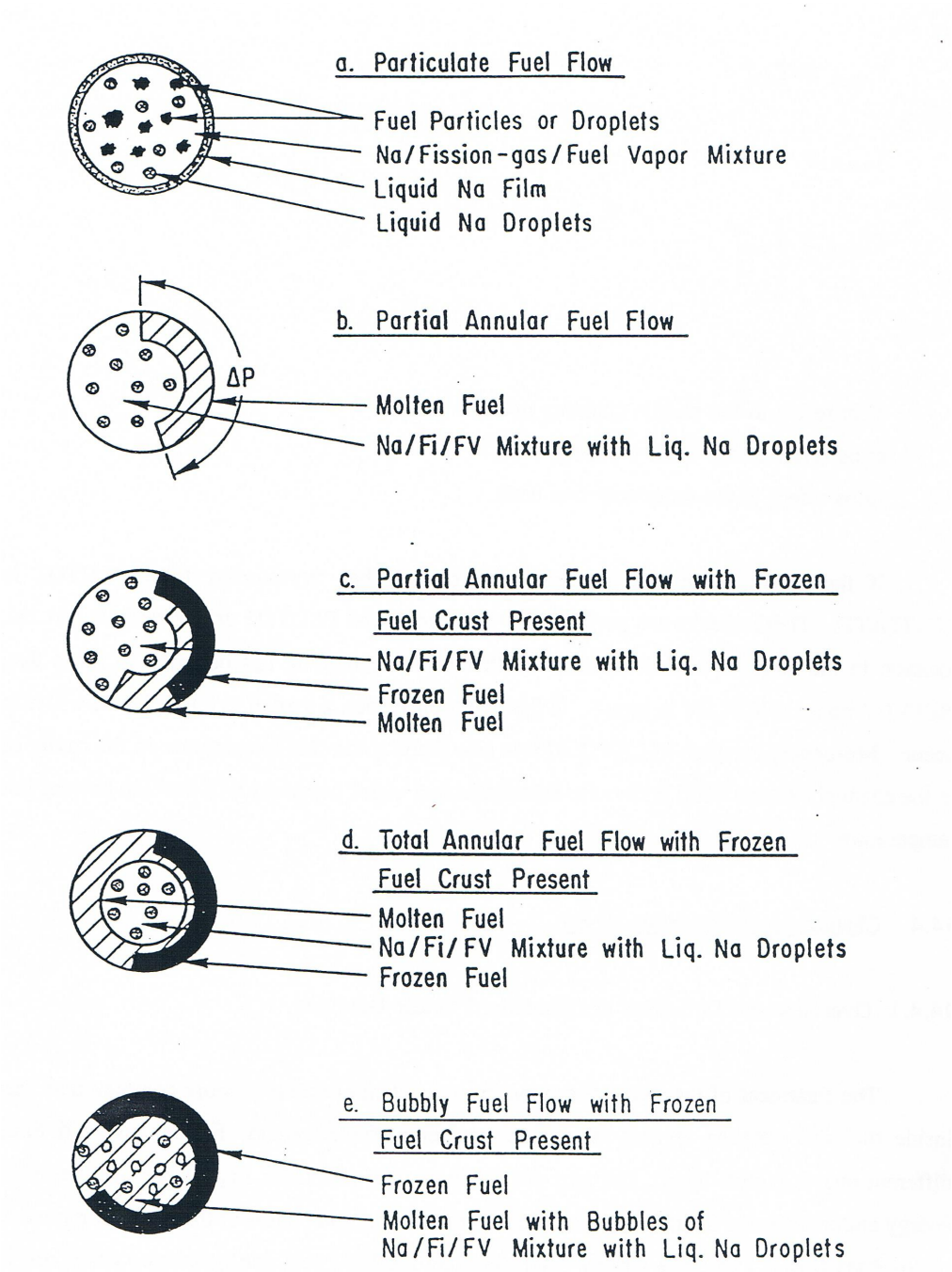

Fig. 14.4-1. Illustration of the Possible Sodium and Fuel Flow Regimes as Well as the Fuel Freezing Patters in the PLUTO2 Model of the Coolant Channel

Table 14.4-1. Overview of the Interaction Between the Channel Components in PLUTO2

Components	Symbols	Moving or Stationary		fu	fs	N ℓ	Nv	fi	Fv*	c ℓ	sr	ff	fsff	fm
Mobile Liquid or Solid Fuel	fu	Moving Components	UFCH			Ht Mo	Ht Mo	Ht Mo	Mo Ma	Ht Mo	Ht Mo	Ht Mo Ma		Ht
Dissolved gas in Mobile fuel	fs							Ma					Ma	
Moving Liquid Sodium	N ℓ ,mv		UMCH	Ht Mo			Ma	Eq	Ht	Ht Mo	Ht Mo	Ht Mo		Ma
Sodium Vapor	Nv			Ht Mo		Ma		Eq	Ht	Ht Mo	Ht Mo	Ht Mo		Mo Ma
Free Fission gas	fi			Ht Mo	Ma	Eq	Eq			Ht Mo	Ht Mo	Ht Mo		Mo
Fuel Vapor*	fv			Mo Ma		Ht				Ht Mo	Ht Mo	Ht Mo		Ht Mo
Cladding	c ℓ	Stationary		Ht Mo		Ht Mo	Ht Mo	Ht Mo	Ht Mo			Ht		Ht
Subassembly Wall	sr			Ht Mo Ma		Ht Mo	Ht Mo	Ht Mo	Ht Mo			Ht		Ht
Frozen Fuel Crusts	ff			Ht Mo Ma		Ht Mo	Ht Mo	Ht Mo	Ht Mo	Ht	Ht			
Dissolved fission Gas in crusts	fsff				Ma									
Liquid Sodium Film	fm			Ht		Ma	Mo Ma	Mo	Ht Mo	Ht	Ht			

*Not yet operational.

Legend

Ht = Heat transfer
Mo = Momentum transfer
Ma = Mass transfer
Eq = Thermal and Velocity Equilibrium

There are four mass conservation equations for tracking moving components in PLUTO2; (a) for liquid or solid fuel and for fuel vapor*, (b) for liquid sodium and sodium vapor, (c) for free fission gas, and (d) for fission gas still dissolved in the fuel. There are also mass conservation equations for the stationary fuel crust (i.e., plated-out solid fuel) and for the stagnant sodium film.

A single energy conservation equation is solved for the mixture of liquid sodium (including the stagnant sodium film), sodium vapor, and free fission gas, which are all assumed to be in thermodynamic equilibrium. An energy conservation equation is solved for the moving solid fuel or for the two-phase mixture of liquid fuel and fuel vapor. The latter two are assumed to be in thermodynamic equilibrium in the region where the fuel vapor pressure is larger than 10^{-2}MPa. Outside this region, no fuel vapor is considered. There is also an energy equation for the solid fuel crusts.

The equation-of-state calculates the pressure for cells containing (a) liquid-phase sodium, (b) two-phase sodium, two-phase fuel and fission gas, and (c) superheated vapor and fission gas.

Although Eulerian hydrodynamics is generally employed in the formulation of the equations, a Lagrangian treatment is used to track the moving upper and lower boundaries of the multiphase region. All finite difference equations are written in conservative form. A staggered mesh grid, with the velocities at the cell edges, and pressures, densities, and temperatures at the cell centers, is used. The spatial derivatives are evaluated by full donor cell differencing, which is also known as second upwind differencing. This approach is more stable for very non-continuous conditions that are quite common in PLUTO2 applications although this is not as accurate as higher order schemes [14-30, 14-31].

The time differencing is mainly explicit, but there are also important implicit features involved. First, advantage is taken of the solution sequence of the conservation equations. The results of the mass conservation equations which are solved first, are used in the energy conservation equations. The results of these two sets of conservation equations and the results from the calculation of the fuel and gas ejection from the pins are used in the equation-of-state and provide an estimate of the channel pressure at the end of the time step. This is then used in the solution of the momentum conservation equations.

Another implicit feature that is of key importance for a stable velocity calculation of the lighter component is the simultaneous solution of the two momentum equations. The lighter component can experience strong and opposing pressure gradient and drag forces, which lead to oscillatory behavior for low density mixtures if a simultaneous solution is not performed [14-32]. Also important is the implicit treatment of the potentially large heat transfer between the various hot and cold components.

The explicit aspect of the solution method is that the conservation equations at different axial locations are not solved in a coupled fashion. This means, for example,

*Fuel vapor is not yet operational.

that a new velocity calculated at one mesh cell boundary does not have an immediate effect on the new velocity at the neighboring boundary. By not solving the equation sets simultaneously, one can avoid three potential problems. First, an iterative solution for the inversion of a complicated matrix, which can have convergence problems or may require many iterations, can be avoided. (A direct solution through Gaussian elimination does not seem to be easily feasible for more than two coupled equation sets.) Second, the later addition of certain terms to the equation set is relatively straightforward for explicit schemes but can be complicated for implicit schemes. Terms may have to be added to the equation set in order to make a code such as PLUTO2 work for heretofore unforeseen conditions or because the importance of additional terms may have to be investigated. Third, the matrix elements of an implicit solution technique for multi-phase, multicomponent flows are usually complex and have no direct physical meaning. Therefore, they can complicate the debugging of such implicit solution schemes. However, a very stable implicit scheme that would decrease the code running time and diminish the truncation error introduced by the many time steps in an explicit scheme is desirable. This may not be a practical goal for the solution of the entire equation set in PLUTO2 but it would be a reasonable goal for selected equations such as the mass and momentum conservations of the light components.

Definition of the Generalized Smear Densities. A special feature of the PLUTO2 module (and of the LEVITATE module) is the use of generalized smear densities. This has been prompted by the presence of the many different components and the simplification of the differential and finite difference equations. The volume fractions are lumped together with the physical densities of the materials and therefore do not appear in the equations. Details about the smear densities in the fuel pin have already been described in Section 14.2.5. The pie chart in Fig. 14.4-2 gives an example of the relative cross sectional areas involved at a certain axial location.

As discussed in Section 14.2.1, the same total cross sectional area of the pie, which is an input value AXMX, is used at all axial locations of the subassembly or the experimental loop considered. The relative sizes of the pie pieces can vary at different axial locations; pieces such as the pin piece can actually disappear at elevations above or below the pin bundles. There is no empty piece in the pie if one assumes the total area of the pie, AXMX, to be the total cross sectional area of a subassembly or an experimental loop. However, at elevations where the cross sectional area of the subassembly or the experimental loop is smaller than AXMX, an empty pie piece is necessary.

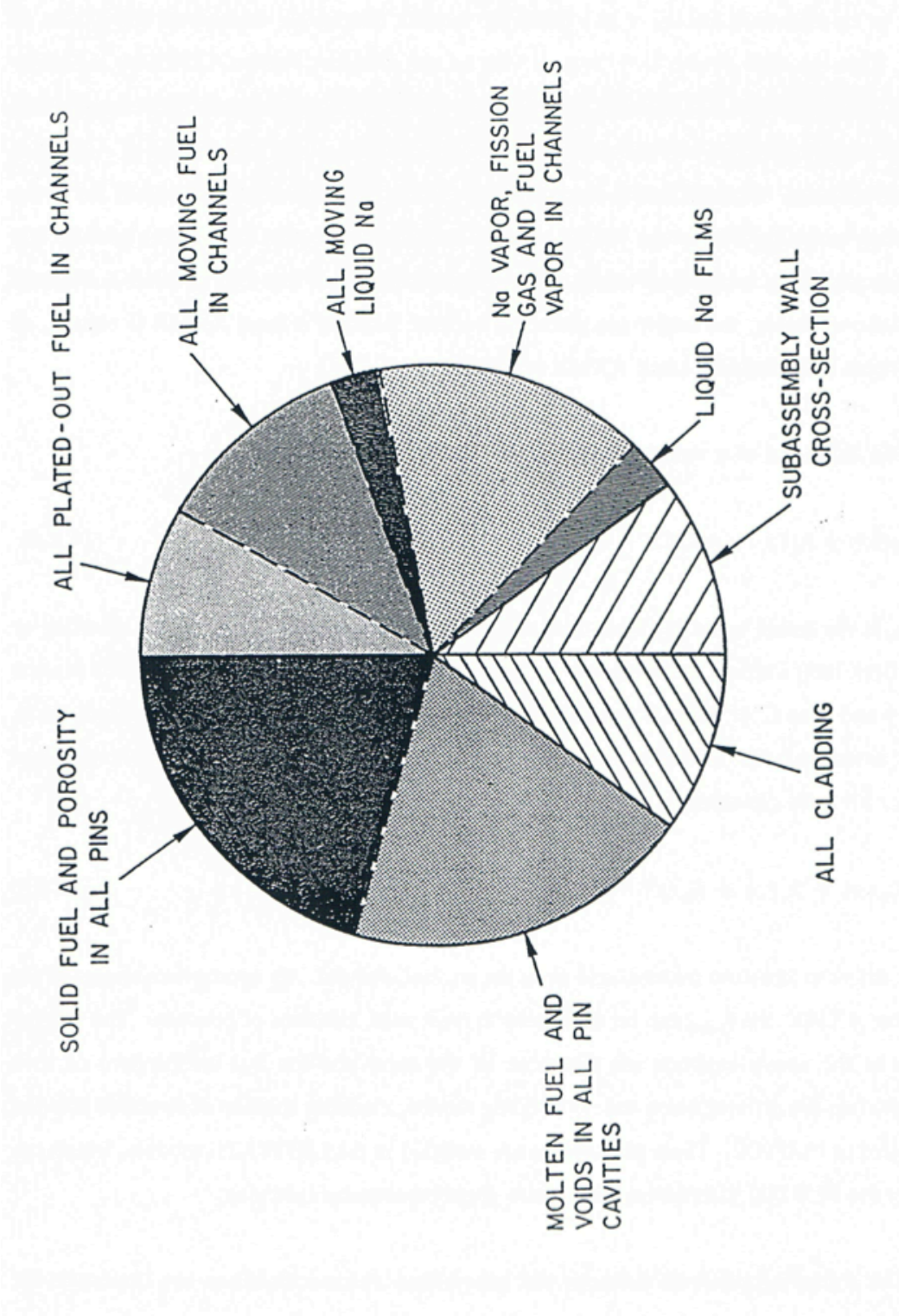

Fig. 14.4-2. The Right-hand Side of This Pie Chart Illustrate the Possible Material Cross Sectional areas in the Coolant Channel, the Whole Pie Representing an Area AXMX, which is an Input Parameter

The calculational results of the PLUTO2 module should not depend on the choice of AXMX. This has been shown to be true as long as one does not change AXMX by too many orders of magnitude. If one changes AXMX very much, small differences in the results can occur due to differences in truncation errors. Thus, the choice of the input value of AXMX is one of convenience. The best choice for AXMX is usually the cross sectional area of the entire subassembly including the hexcan wall at an axial location where pins are present because this will lead to physically meaningful values of the volume fraction. If one uses an AXMX different from the above choice, the empty pie piece can become larger if a large AXMX is chosen, or even negative if a relatively small AXMX is chosen.

The definition of a volume fraction of a certain component k is:

$$\theta_k(z,t) = A_k(z,t)/\,AXMX \tag{14.4-1}$$

where A_k is the actual cross sectional area occupied by component k (e.g., all the cladding or all the frozen fuel) inside a fuel assembly or inside the can wall of an experimental loop at axial location z and time t. If AXMX was chosen to be the entire subassembly cross section, the θ_k gives the actual volume fraction of component k in a slice of a subassembly or an experimental loop. For all axial elevations,

$$\theta_{pin}(z)+\theta_{sr}(z)+\theta_{ch}(z)+\theta_{empty}(z)=1 \tag{14.4-2}$$

where *sr* refers to structure material and *ch* to the coolant channel. By appropriate choice of the input value AXMX, the θ_{empty} can be made zero at most axial locations of concern. The volume fractions in the above equation are functions of the axial position but independent of time because no fuel-pin disintegration and no cladding motion, cladding ablation or structure ablation are modeled in PLUTO2. These phenomena are modeled in the LEVITATE module, which can take over the PLUTO2 calculation when these phenomena come into play.

The following relations between the generalized volume fractions are important for writing the channel hydrodynamics equations in PLUTO2:

$$\theta_{pin}(z) = \theta_{ch,op}(z,t)+\theta_{ff}(z,t) \tag{14.4-3}$$

where

θ_{ch} is the generalized coolant channel volume fraction which is always equal to the values at pin failure in PLUTO2;

$\theta_{ch,op}$ is the generalized volume fraction of the open channel (i.e., the part of the channel available for the mobile components);

θ_{ff} is the generalized volume fraction of the frozen fuel crusts;

$$\theta_{ch,op}(z,t) = \theta_{fu}(z,t) + \theta_{N1}(z,t) + \theta_{vg}(z,t) \tag{14.4-4}$$

where

θ_{fu} is the generalized volume fraction of the mobile liquid or solid fuel in the channel;

θ_{N1} is the generalized volume fraction of the liquid sodium;

θ_{vg} is the generalized volume fraction of the vapor/gas (i.e., void) space in the channel;

$$\theta_{N1}(z,t) = \theta_{N1,mv}(z,t) + \theta_{fm}(z,t) \tag{14.4-5}$$

where

$\theta_{N1,mv}$ is the generalized volume fraction of the moving liquid sodium;

θ_{fm} is the generalized volume fraction of the liquid sodium film.

The following generalized smear densities are defined:

$$\begin{aligned}\rho'_{fuch}(z,t) &= \rho_{fu}(T)\theta_{fu}(z,t) + \rho_{fv}(T)\,\theta_{vg}(z,t) \\ &= \rho_{fu}(T)A_{fu}(z,t)/\,AXMX + \rho_{fv}(T)A_{vg}(z,t)/\,AXMX\end{aligned} \tag{14.4-6}$$

where

ρ'_{fuch} is the generalized smear density of all the mobile fuel (solid, liquid and vapor) in the channel;

ρ_{fu} is the theoretical density of the liquid or solid fuel;

ρ_{fv} is the physical fuel vapor density;

$$\rho'_{ff} = \rho_{ff}(T)\theta_{ff}(z,t) \tag{14.4-7}$$

where

ρ'_{ff} is the generalized smear density of the frozen fuel crust.

$$\rho'_{Na} = \rho_{N1}(T)\theta_{N1}(z,t) + \rho_{Nv}(T)\theta_{vg}(z,t) \tag{14.4-8}$$

where

ρ'_{Na} is the generalized smear density of all the sodium (moving liquid, stationary liquid film, and vapor).

$$\rho'_{Nm} = \rho'_{Na} - \rho_{N1}(T)\theta_{fm}(z,t) \qquad (14.4\text{-}9$$

where

ρ'_{Nm} is the generalized smear density of the sodium vapor and the mobile liquid sodium.

$$\rho'_{fi} = \rho_{fi}(T,p)\theta_{vg}(z,t) \qquad (14.4\text{-}10)$$

where

ρ'_{fi} is the generalized smear density of the free fission gas in the channel.

$$\rho'_{fi} = \rho_{fv}(T,p)\theta_{vg}(z,t) \qquad (14.4\text{-}11)$$

where

ρ'_{fv} is the generalized smear density of the fuel vapor in the channel.

$$\rho'_{Mi} = \rho'_{Nm} + \rho'_{fi} + \rho'_{fv} \qquad (14.4\text{-}12)$$

where

ρ'_{Mi} is the total generalized smear density of all moving "light components" (liquid sodium, sodium vapor, free fission gas, and fuel vapor).

$$\rho'_{fs} = \rho_{fs}\,\theta_{fu}(z,t) \qquad (14.4\text{-}13)$$

where

ρ'_{fs} is the generalized smear density of the dissolved fission gas in the moving liquid or solid fuel.

All the variables and subscripts are described in the list of symbols at the beginning of Chapter 14. The subscript *ch,op* requires some additional explanation. It designates the open channel cross section which is occupied by the moving materials in the channel including the sodium film. The basic definition of $\theta_{ch,op}$ will become clearer if one rewrites Eq. 14.4-3 with $\theta_{ch,op}$ on the left-hand side of the equation.

In Eq. 14.4-6, the definition of the volume fractions, which is given in Eq. 14.4-1, is used to rewrite the right-hand side of this equation. The initial forms of the conservation equations described in the following sub-sections contain products of the

physical densities and the cross-sectional areas associated with each component. After dividing these equations by AXMX, one can make use of the above definitions for the volume fractions and generalized linear densities to simplify the conservation equations.

For the generalized source or sink terms,

$$S' = S^{\ell} / AXMX \tag{14.4-14}$$

where the source or sink terms S^{ℓ} are the mass sources and sinks per unit time and per unit length.

14.4.2 Mass Conservation for Fuel, Sodium, and Free and Dissolved Fission-gas

14.4.2.1 Moving Components: Differential Equation

14.4.2.1.1 Fuel and Fuel Vapor Mass Conservation

The differential equation for the mass conservation of all the moving fuel, including fuel vapor** is:

$$\begin{aligned}\frac{\partial}{\partial t}\left(\rho_{fu}A_{fu}+\rho_{fv}A_{vg}\right)+\frac{\partial}{\partial z}\left(\rho_{fu}A_{fu}u_{fu}+\rho_{fv}A_{vg}u_{Mi}\right)\\ =\left(S^{\ell}_{fu,ej}+S^{\ell}_{fu,me}-S^{\ell}_{fu,ff}\right)\end{aligned} \tag{14.4-15}$$

where the source terms denoted by S^{ℓ} are the mass sources and sinks per unit time and per unit length. The source term due to fuel ejection has been discussed in Section 14.3. The source and sink terms due to fuel freeze-out and frozen fuel remelting, respectively, will be discussed in Section 14.4.3.2.

By dividing the above mass conservation equation by AXMX and by using the definitions for the generalized volume fractions and smear densities one arrives at:

$$\begin{aligned}\frac{\partial}{\partial t}\rho'_{fuch}+\frac{\partial}{\partial z}\left(\rho'_{fuch}u_{fu}\right)+\frac{\partial}{\partial z}\left(\rho'_{fv}u_{Mi}\right)-\frac{\partial}{\partial z}\left(\rho'_{fv}u_{fu}\right)\\ =S'_{fu,ej}+S'_{fu,me}-S'_{fu,ff}\end{aligned} \tag{14.4-16}$$

where

$$\rho'_{fuch}=\rho'_{fu}+\rho'_{fv} \tag{14.4-17}$$

is the total generalized mobile fuel smear density in the channel including solid and liquid fuel and fuel vapor. The primed source and sink terms represent the mass

**Fuel vapor is not yet operational.

sources and sinks per unit time and unit volume. The latter is a m^3 of the cell volume $AXMX \cdot \Delta z$ in which all components (including pin, structure and channel components) are assumed to be uniformly smeared.

Fuel vapor streaming into regions with no fuel or with fuel which is not generating significant fuel vapor pressure (i.e., less than 10^{-2} MPa) is not currently considered in PLUTO2.

14.4.2.1.2 Dissolved Fission-gas Mass Conservation

The mass conservation for the dissolved fission gas (or matrix fission gas) in the moving liquid or solid fuel reads:

$$\frac{\partial}{\partial t}\left(\rho_{fs} A_{fu}\right)+\frac{\partial}{\partial z}\left(\rho_{fs} A_{fu} u_{fu}\right)=\left[\left(S^{\ell}_{fu,ej}\ \rho_{fsca}\ A_{fuca}\right)\right.$$
$$\left./\left(\rho_{fuca} A_{fuca}\right)-\left(S^{\ell}_{fu,ff}\ \rho_{fs}\ A_{fu}\right)/\left(\rho_{us} A_{fu}\right)-S^{\ell}_{fs,rl}\right] \qquad (14.4\text{-}18)$$

where the fuel mass sources $S^{\ell}_{fu,ej}$ and $S^{\ell}_{fu,ff}$ have been multiplied by the dissolved gas-to-fuel mass ratios in the molten pin cavity and in the channel, respectively, to obtain the dissolved gas sources. The areas and densities with the subscripts *fsca* and *fuca* are for the molten pin cavity. The sink term $S^{\ell}_{fs,rl}$ is the rate of dissolved fission-gas release. Its generalized form is described in Eq. 14.4-20. By dividing Eq. 14.4-18 by AXMX and by using the definitions for the generalized smear densities, one arrives at:

$$\frac{\partial}{\partial t}\rho'_{fs}+\frac{\partial}{\partial z}\rho'_{fs}u_{fu}=\left[\left(S'_{fu,ej}\ \rho'_{fsca}\right)/\ \rho'_{fuca}\right.$$
$$\left.-\left(S'_{fu,ff}\ \rho'_{fs}\right)/\ \rho'_{fu}-S'_{fs,rl}\right] \qquad (14.4\text{-}19)$$

$$S'_{fs,rl}=\begin{cases}\rho'_{fs}\cdot CIRTFS & \text{for}\ T_{fu}>T_{fu,sol}\\ 0 & \text{for}\ T_{fu}<T_{fu,sol}\end{cases} \qquad (14.4\text{-}20)$$

where *CIRTFS* is a dissolved gas release time constant which is input and has the dimensions s^{-1}. The same gas release time constant is used for releasing the dissolved gas in the molten pin cavity (see Section 14.2.6).

14.4.2.1.3 Two-phase Sodium Mass Conservation

The mass conservation equation of the sodium liquid and vapor including the sodium film is given by

$$\frac{\partial}{\partial t}\left(\rho_{Na} A_{ch}\right)+\frac{\partial}{\partial z}\left(\rho_{Nm,ch} A_{Nm} u_{Mi}\right)=0 \qquad (14.4\text{-}21)$$

where

ρ_{Na} is the total sodium smear density, including the sodium films, in the channel. Note that this is not a generalized smear density.

$\rho_{Nm,ch}$ is the smear density of the mobile sodium referring to the cross section A_{Nm} of the moving sodium mixture.

$$A_{Nm} = A_{ch} - A_{Na,fm} - A_{fu} - A_{ff} \tag{14.4-21a}$$

where

A_{ch} is the cross sectional area of the channel;

$A_{Na,fm}$ is the cross sectional area of the liquid Na films;

A_{ff} is the cross sectional area of frozen fuel.

By dividing the mass conservation Eq. 14.4-21 by AXMX and using the definitions for the generalized smear densities, one obtains:

$$\frac{\partial}{\partial t}\rho'_{Na} + \frac{\partial}{\partial z}\rho'_{Nm,ch}u_{Mi} = 0 \tag{14.4-22}$$

$$\text{where } \rho'_{Nm} = \rho'_{Na} - \rho_{N\ell}\,\theta_{fm} \tag{14.4-23}$$

The calculation of the volume fraction of the sodium film, θ_{fm}, considers vapor condensation, film evaporation and film entrainment. This is described in Section 14.4.2.2.

14.4.2.1.4 Free Fission-gas Mass Conservation

$$\frac{\partial}{\partial t}\left(\rho_{fi}A_{vg}\right) + \frac{\partial}{\partial z}\left(\rho_{fi}A_{vg}u_{Mi}\right) = \left(S^{\ell}_{fi,ej} + S^{\ell}_{fs,rl}\right) \tag{14.4-24}$$

where the two source terms are due to fission-gas ejection from the fuel pins and due to the release of fission gas dissolved in the fuel. The rate of fuel ejection from the pins is described in Section 14.3. The release of the dissolved fission gas is described in Eq. 14.4-20. Dividing by AXMX and using the generalized smear density definitions, one obtains:

$$\frac{\partial}{\partial t}\rho'_{fi} + \frac{\partial}{\partial z}\rho'_{fi}\,u_{Mi} = S'_{fi.ej} + S'_{fs.rl} \tag{14.4-25}$$

14.4.2.2 Finite Difference Forms of the Mass Conservations and Subroutine PLMACO

For the free fission gas and the dissolved fission gas, the form of the differential mass conservation is:

$$\frac{\partial \rho'_k}{\partial t} + \frac{\partial (\rho'_k u_k)}{\partial z} = \sum_n S_{k,n} \tag{14.4-26}$$

where *k* designates a specific component and n the different types of source or sink terms for this component.

For the numerical solution of these equations, a staggered mesh with the velocities at the edges and the densities at the mesh centers is used (on the numerical grid, which is actually used in the code, the half indices have to be avoided; see later in this section).

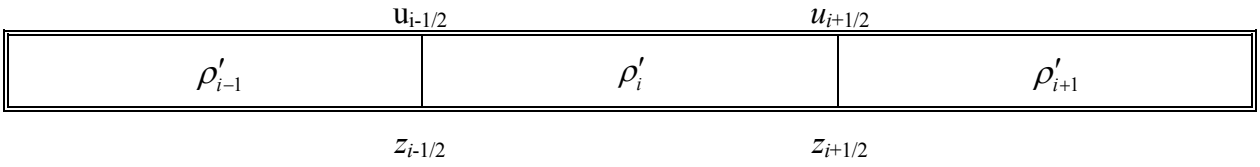

By spatially integrating over the control volume for $z_{i-1/2}$ to $z_{i+1/2}$ one obtains

$$\frac{\partial \rho'_{k,i}}{\partial t} \Delta z_i + \left[(\rho' u)_{k,i+1/2} - (\rho' u)_{k,i-1/2} \right] = \sum_n S'_{k,n,i} \Delta z_i \tag{14.4-27}$$

By performing the time integration over the length of the time step, Δt, we obtain:

$$\rho'^{n+1}_{k,i} = \rho'^{n}_{k,j} - \left[(\rho' u)_{k,i+1/2} - (\rho' u)_{k,i-1/2} \right] \frac{\Delta t}{\Delta z_i} + \sum_n S'_{k,n,i} \cdot \Delta t \tag{14.4-28}$$

It should be noted that this finite difference form of mass conservation is in a conservation form that prevents any mass losses. It should be noted that this mass conservation actually includes a variable flow cross-section treatment because the primed generalized smear densities include the flow cross-section areas.

Full donor cell differencing is used for evaluating the convective fluxes. Although this is not as accurate as higher order approaches, it tends to increase the stability of the solution [14-30, 14-31]. This is important because of the very complicated flow condition which can be encountered in PLUTO2 calculations. The convective terms in Eq. 14.4-28 are calculated in the following manner:

$$(\rho' u)_{k,i+1/2} = \begin{cases} \rho'_{k,i} u_{k,i+1/2} & \text{if } u_{k,i+1/2} > 0 \\ \rho'_{k,i+1} u_{k,i+1/2} & \text{if } u_{k,i+1/2} < 0 \end{cases} \tag{14.4-29}$$

$$(\rho' u)_{k,i-1/2} = \begin{cases} \rho'_{k,i}\, u_{k,i-1/2} & \text{if } u_{k,i-1/2} > 0 \\ \rho'_{k,i+1}\, u_{k,i-1/2} & \text{if } u_{k,i-1/2} < 0 \end{cases} \tag{14.4-30}$$

In the above equations, half indices are used that can be located on the previous schematic of the mesh grid. However, since half indices cannot be used in a computer program, the indices used in the code are arranged on the numerical grid as follows:

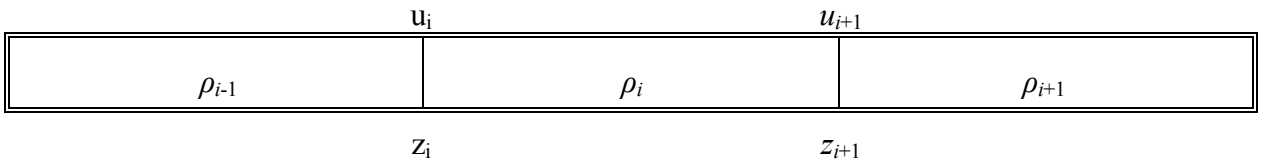

When using FORTRAN variable names, the convective flux for the free fission gas at i-1/2 is therefore:

$$COFICH(I) = \begin{cases} DEFICH(I-1)\cdot UMCH(I) & \text{if } UMCH(I) > 0 \\ \\ DEFICH(I)\cdot UMCH(I) & \text{if } UMCH(I) < 0 \end{cases} \tag{14.4-31}$$

The convective fluxes are set to zero at the edges of the component domains. The location of the upper and lower interfaces of each component domain is calculated in PLUTO2. The integers designating the lowermost and uppermost nodes containing free fission gas are designated IFFIBT and *IFFITP*, respectively, and the convective fluxes are set to zero at these locations:

$$COFICH(IFFIBT) = 0 \tag{14.4-32}$$

$$COFICH(IFFITP+1) = 0 \tag{14.4-33}$$

Eq. 14.4-15 is the fuel mass conservation in differential form. It can be rearranged to give

$$\begin{aligned} &\frac{\partial}{\partial t}\rho'_{fuch} + \frac{\partial}{\partial z}\left[\left(\rho'_{fuch} - \rho'_{fv}\right)u_{fu}\right] + \frac{\partial}{\partial z}\left(\rho'_{fv}\, u_{Mi}\right) \\ &= S'_{fu,ej} + S'_{fu,me} - S'_{fu,ff} \end{aligned} \tag{14.4-34}$$

By integrating over Δz_i and Δt, one obtains:

$$\rho'^{n+1}_{fuch,i} = \rho'^{n}_{fuch,j} - \left\{\left[\left(\rho'_{fuch} - \rho'_{fv}\right)u_{fu}\right]_{i+1/2} - \left[\left(\rho'_{fuch} - \rho'_{fv}\right)u_{fu}\right]_{i-1/2} + \left(\rho'_{fv}\,u_{Mi}\right)_{i+1/2} - \left(\rho'_{fv}\,u_{Mi}\right)_{i-1/2}\right\}\frac{\Delta t}{\Delta z_i} + \left[S'_{fu,ej,i} + S'_{fu,me,i} - S'_{fu,ff,i}\right]\Delta t \qquad (14.4\text{-}35)$$

In the code, the convective flux term $\left[\left(\rho'_{fuch} - \rho'_{fv}\right)u_{fu}\right]_{i-1/2}$ is written as:

$$COFUCH(I) = \begin{cases} \left[DEFICH(I-1) - DEFVCH(I-1)\right]\cdot UFCH(I) & \text{if } UFCH(I) > 0 \\ \left[DEFUCH(I) - DEFVCH(I)\right]\cdot UFCH(I) & \text{if } UFCH(I) < 0 \end{cases} \qquad (14.4\text{-}36)$$

The two-phase sodium mass conservation equation (Eq. 14.4-22) includes the generalized smear density of the moving mixture in the convective term and not the total sodium smear density which includes the sodium film. The value of the density is evaluated according to eq. 14.4-23. When using the FORTRAN variable names, the convective flux at the boundary *i*-1/2 is:

$$CONACH(I) = \begin{cases} \left[DEFICH(I-1)\right]\cdot UMCH(I) & \text{if } UMCH(I) > 0 \\ \left[DENMCH(I)\right]\cdot UMCH(I) & \text{if } UMCH(I) < 0 \end{cases} \qquad (14.4\text{-}37)$$

All of the above mass conservation equations are solved in subroutine PLMACO (PLUTO2 MASS CONSERVATION). However, sink or source terms related to fuel plateout and frozen fuel crust release are considered earlier in the calculational sequence in subroutine PLFREZ. Fuel and fission-gas ejection terms are considered later when subroutine PL1PIN, which calculates these terms, is called. Besides solving the mass conservation equations, PLMACO also contains a special treatment for the numerical cells at the bottom and top of the channel, which comes into play only when the interaction zone extends to the subassembly inlet or outlet. For example if the interaction zone has reached the subassembly outlet and if the pressure in the top node is larger than the outlet pressure, appropriate amounts of fuel, sodium and fission gas are taken out of the top nodes in order to reduce the pressure to the outlet pressure. The same procedure is performed for the inlet node if the interaction zone extends into it. The total component masses taken out of the end nodes are shown in the PLUTO2 output.

14.4.2.3 Determination of the Axial Extent of the Component Regions in Subroutine PLIF and Mesh Rezoning in Subroutine PLREZO

Before the above mass conservation equations are solved in subroutine PLMACO, the axial extent of the different component regions has to be determined. In subroutine PLIF (PLUTO2 INTERFACE), the interface locations of the interaction region are reset (the velocity calculations of the liquid sodium slugs above and below this region, which determine the interface velocities, are actually done later in the sequence in PLMOCO). The resetting of the interaction zone interface locations is not quite straightforward because the sodium slugs leave a liquid sodium film behind on the cladding and structure when the interaction zone expands. Because the dynamic slug calculation in PLMOCO is done for the entire channel cross section area, the interface displacement is increased by a factor of 1/(1 - liquid film cross section/channel cross section). This conserves the sodium voiding calculated for the entire cross section. For a sodium slug reentering over an existing film the slug interface displacement is increased by multiplying by (1 + liquid film cross section/channel cross section). PLIF also resets the lower and upper interface locations of the fuel region which can be inside the interaction region or at the interaction zone boundaries. If the latter are being penetrated by the fuel, they are set to the fuel interfaces in subroutine PLREZO, as discussed below (the actual velocity calculation of the fuel interfaces is done in PLMOCO). Furthermore, the upper and lower interface locations of both the free fission gas and the fuel vapor region are calculated in the subroutine PLIF (these interfaces can also be at the edges of the interaction region or inside it; the velocities of these interfaces are assumed to be equal to the local sodium/fission gas/fuel vapor mixture velocities). Besides calculating the extent of the component regions, the subroutine PLIF also calculates the axial fuel-pin failure propagation (see Section 14.3). If the fuel pins fail into the liquid sodium slugs outside the interaction zone, the interaction zone is enlarged in subroutine PLREZO. This is discussed below.

In subroutine PLREZO (PLUTO2 REZONE), mesh cells are added to an expanding interaction region or deleted from a shrinking interaction region. In the schematic below it is shown that the end cells of the interaction region can be shorter or longer than the regular cell lengths. The small cell 6 in the schematic exists because L1 is greater than the input value DZPLIN, which has to be shorter than any regular mesh cell used in a given calculation. Cell 9 is larger than the regular cell length at this location because it has not yet extended enough into cell 10 (L2 < DZPLIN). Creating a new cell or collapsing a small cell with a neighboring one is a complicated procedure because it requires redistributing liquid sodium and fission gas in a manner that no significant pressure disturbances are introduced. The SAS4A reactivity calculation refers only to the regular mesh grid and not the Lagrangian edge cells. The material in a particular cell grid such as cell No. 6 is assumed to be homogeneously mixed with the liquid sodium sluglet to the left of it for the reactivity calculation. The materials in the section L2 of cell 9 are assumed to be homogeneously mixed with cell 10 for the reactivity calculation.

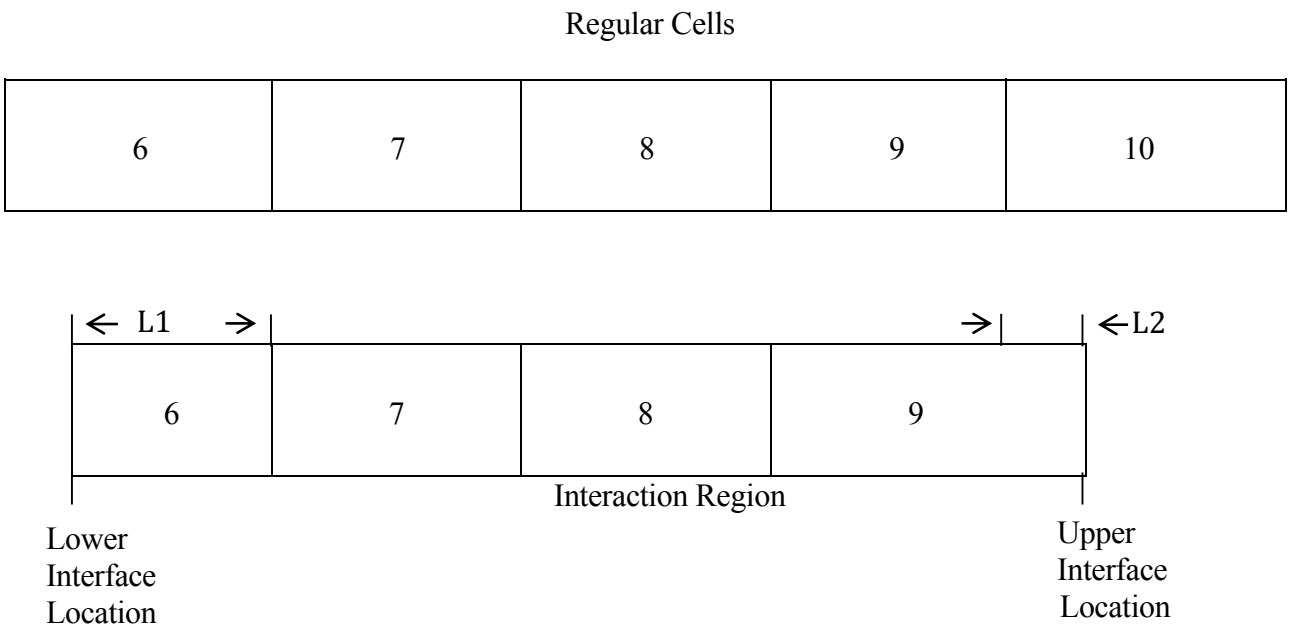

Subroutine PLREZO also expands the interaction zone when fuel penetrates the liquid sodium slugs. The liquid sodium that has been penetrated by the fuel is added to the edge cell and homogeneously distributed into it.

PLREZO also has the following treatment for slug interfaces (with the interaction region) crossing into cells that contain frozen fuel crusts or cells into which fuel can be ejected from adjacent ruptured fuel pin nodes: the liquid sodium that has crossed into such a cell is homogeneously distributed in it and the slug interface location is reset to the edge of the cell containing frozen fuel or the ejection cell, respectively.

14.4.2.4 Stationary Sodium Films and Subroutine PLVOFR

The liquid sodium films that are left behind by the ejected coolant slugs are of importance for keeping the cladding cool in voided regions of the coolant channel. Moreover, when fuel moves into voided regions in which a liquid sodium film is still present, the fuel-to-liquid sodium heat transfer will increase the liquid sodium evaporation, and thus the sodium vapor pressure.

In PLUTO2, the liquid sodium film is assumed to be stationary. It can become thinner due to sodium evaporation or to entrainment caused by the drag from the moving vapor/gas/sodium droplet/fuel particle mixture. Once an annular fuel flow regime develops in a coolant channel node, the entire sodium film in that node is added to the moving vapor/gas/sodium droplet flow (This assumption should be further investigated). Liquid sodium films can grow due to sodium vapor condensation and sodium droplet de-entrainment, i.e., deposition on the film. However, the maximum thickness of the liquid film cannot be larger than the initial film thickness, which is determined by the input liquid film fraction CINAFO.

The evaporation of, or the condensation on, the liquid sodium film is taken into account in the sodium energy equation and contributes to the change of the liquid

sodium fraction in a numerical cell. Once the liquid sodium fraction is below the input film fraction, the sodium film fraction will approach and eventually be equal to the current liquid fraction if the node considered is in the de-entrainment mode. If the sodium film is being entrained, the sodium film thickness is determined by this mechanism.

In order to determine whether sodium entrainment or de-entrainment occurs, the superficial velocity (i.e., the volumetric flux divided by the entire channel cross section) of the fission-gas/two-phase sodium/fuel particle mixture has to be evaluated. The following momentum averaging suggested by Ishii [14-58] is performed to arrive at an average velocity of all the moving components:

$$\bar{u}_{Mi,fu} = \left\{ \frac{\left| \left(CIETFU \cdot \rho'_{fu} / \theta_{ch} \cdot u_{fu} \left| u_{fu} \right| + \rho'_{Mi} / \theta_{ch} \cdot u_{Mi} \left| u_{Mi} \right| \right) \right|}{\left(CIETFU \cdot \rho'_{fu} / \theta_{ch} + \rho'_{Mi} / \theta_{ch} \right)} \right\}^{1/2} \tag{14.4-38}$$

where CIETFU is an input value which can be between zero and one. This input variable has been introduced because of the uncertainty about the influence of the fuel particles on the entrainment of the film. If one assumes that the fuel particle mass can be smeared over the entraining mixture cross section and that it would act like a dense gas, CIETFU = 1.0 has to be chosen. If one assumes that the fuel particles are less efficient in entraining the film, a lower value should be used. A value of 0.1 is recommended because it was used successfully in experiment analyses of TREAT tests L8 and H6 [14-15, 14-12].

The entrainment limit $u_{et,min}$ used in the code is based on a correlation given in Reference [14-33, 14-34] for the inception of entrainment of a rough turbulent film flow:

$$u_{et,\min} = \begin{cases} VCONST^{0.8} \cdot \sigma_{N1} / \mu_{N1} \cdot \sqrt{\rho_{N1} / \rho_{mi,fu}} & \text{if VCONST} < 1/15 \\ 0.1146 \cdot \sigma_{N1} / \mu_{N1} \cdot \sqrt{\rho_{N1} / \rho_{mi,fu}} & \text{if VCONST} > 1/15 \end{cases} \tag{14.4-39}$$

where the viscosity number VCONST is defined by

$$VCONST = \mu_{N1} / \left\{ \rho_{N1} \sigma_{N1} \left[\sigma_{N1} / \left(g \cdot \left(\rho_{N1} - \rho_{Mi,fu} \right) \right) \right]^{1/2} \right\}^{1/2} \tag{14.4-40}$$

μ_{N1} = viscosity of liquid sodium

σ_{N1} = surface tension of liquid sodium

ρ_{N1} = density of liquid sodium

$\rho_{Mi,fu}$ = CIETFU $\cdot \rho'_{fu} / \theta_{ch} + \rho'_{Mi} / \theta_{ch}$

In the entrainment mode:

$$\left|\bar{u}_{Mi,fu}\right| > u_{et,\min} \tag{14.4-40a}$$

The amount of sodium film entrained is computed using the following equation.

$$\theta_{Mi,fu}^{new} = \theta_{fm}^{old} - CINAFO \cdot \theta_{ch,op} \cdot \Delta t_{PL} / 5\,ms \tag{14.4-41}$$

where

$CINAFO \cdot \theta ch,op$ = initial and maximum liquid sodium film generalized volume fraction (CINAFO is input);

$\Delta t_{PL}/5\ ms$ = fraction of the initial and maximum film volume fraction which is entrained during a PLUTO2 time step.

The entrainment time constant of 5 milliseconds will lead to a complete entrainment of the liquid film in 5 milliseconds if the mixture velocity stays above the entrainment limit during that time. Since the entrained liquid sodium droplets are assumed to be instantaneously in velocity equilibrium with the moving mixture, the velocity of the latter can decrease due to the entrainment. This may temporarily lead to a de-entrainment period, which is characterized by:

$$\bar{u}_{Mi,fu} < u_{et,\min}$$

and

$$\theta_{fm}^{new} = \theta_{fm}^{old} + CINAFO \cdot \theta_{ch,op} \cdot \Delta t_{PL} / 5\,ms \tag{14.4-42}$$

Subroutine PLVOFR. Subroutine PLVOFR (PLUTO2 VOLUME FRACTIONS) calculates the sodium entrainment/de-entrainment discussed above. Two other tasks are performed in this routine. One is concerned with the setting of most channel volume fractions and the other with the selection of the fuel flow regimes. The latter will be discussed in the next section.

Since PLVOFR is called after PLMACO and PLFREZ, the volume fractions calculated in PLVOFR already reflect the component mass changes due to convection and due to fuel plateout and fuel crust release. Volume fractions set in this routine include the moving fuel volume fraction θ_{fu}, the volume fraction of the open channel $\theta_{ch,op} = \theta_{ch} - \theta_{ff}$, the liquid sodium volume fraction θ_{Nl}, the vapor/gas volume fraction when the liquid sodium is assumed to be uncompressed $\theta_{vg,un}$, the vapor/gas volume fraction for properly compressed liquid sodium θ_{vg}, and also the sodium film volume fraction θ_{fm} as discussed above. Moreover, the sodium quality is calculated in this routine. It is based on the following definition:

$$1/\rho_{Na} = x_{Na}/\rho_{Nv} + (1 - x_{Na})/\rho_{N1} \tag{14.4-43}$$

The last equation can be solved for x_{Na}:

$$x_{Na} = \frac{(\rho_{N1} - \rho_{Na}) \cdot \rho_{Nv}}{(\rho_{N1} - \rho_{Nv}) \cdot \rho_{Na}} \tag{14.4-44}$$

where

$$\rho_{Na} = \rho'_{Na}/(\theta_{ch,op} - \theta_{fu})$$

The sodium void fraction is also set in PLVOFR. It is based on the definition

$$\rho_{Na} = \alpha_{Na}\,\rho_{Nv} + (1 - \alpha_{Na})\rho_{N1} \tag{14.4-45}$$

This leads to

$$\alpha_{Na} = (\rho_{N1} - \rho_{Na})/(\rho_{N1} - \rho_{Nv}) \tag{14.4-46}$$

The volume fraction of the vapor/gas mixture for the case of uncompressed liquid sodium is

$$\theta_{vg,un} = (\theta_{ch,op} - \theta_{fu}) \cdot \alpha_{Na} \tag{14.4-47}$$

The gas/vapor volume fraction for compressed liquid sodium is

$$\theta_{vg} = \theta_{vg,un} + K_{N1} \cdot \theta_{N1} \cdot (P_{ch} - P_{Nv}) \tag{14.4-48}$$

where

K_{N1} = CMNL which is a single input value for the isothermal liquid sodium compressibility.

The θ_{vg} calculated in this routine is not allowed to be smaller than $\theta_{ch,op}/1000$. This is done because θ_{vg} is used in the denominator of certain interaction terms. Later in the fission-gas pressure calculation in subroutine PLNAEN, the θ_{vg} is implicitly used without the above-mentioned restriction.

14.4.3 Fuel Flow Regimes, Fuel Plateout and Frozen Crust Release, Plated-out and Moving Fuel Configurations, and Energy and Momentum Exchange Terms

14.4.3.1 Fuel Flow Regimes

Based on the evidence from TREAT TOP experiments, only a fraction of the fuel ejected into the coolant channels fragments into particles or droplets that get rapidly swept upwards. The other fuel does not break up but moves in the channels in the form of a continuous flow that tends to plate out on the cladding and structure upon freezing. Particulate debris with only little plated-out fuel was found in TOP tests R12 [14-35] and J1 [14-25] in which the power transients were cut soon after the first indication of pin failure. This suggests that the fuel that is ejected first from the pins and contacts liquid sodium tends to break up. The fuel that is ejected later into a locally voided channel tends to stay together although liquid sodium reentering from below can cause a delayed fragmentation. This was concluded from the analysis of TREAT test H4 [14-37, 14-36].

The CAMEL out-of-pile tests [14-38, 14-39] also show rapid particulate fuel sweepout. The fuel that does not fragment tends to plate out very close to the fuel ejection site in these out-of-pile tests. The regions with plated-out fuel found in the post-test examination of most TREAT TOP tests, however, extend considerably above the cladding failure site. This indicates the temporary existence of a continuous fuel flow in TREAT experiments. The likely reasons why the plated-out fuel does not extend further upwards in CAMEL tests are (a) the lack of continued fission heating of the fuel in these out-of-pile tests, (b) the amount of fuel ejected into the channels in these tests was relatively small, and thus, had little stored heat, and (c) the relatively cold cladding and structure in these tests may rapidly cool the fuel. Two further items may have promoted the rather localized plateout in the CAMEL tests. First, the ejection of the thermite fuel in several CAMEL tests was accompanied by excessive amounts of gas. Second, the CAMEL ejection pressure was high for longer times than expected for fuel ejection from prototypic pins. Both these items cause coolant channel voiding and lack of fragmentation.

In PLUTO2, one particulate and two continuous fuel flow regimes are modeled. The latter include annular flow (which can be a total or a partial annular flow) and bubbly flow. Flow regime in a cell is determined based on flow conditions in that cell, and can vary from cell to cell. All possible PLUTO2 flow regimes are depicted in Fig. 14.4-1. The use of these flow regimes has the advantage of providing a geometry which allows a more straighforward determination of the mass, momentum, and energy exchange terms than in models not explicitly treating different flow regimes.

The particulate or droplet flow regime has been traditionally assumed in fuel-coolant interaction (FCI) models such as the Cho-Wright model [14-9], the Board-Hall model [14-40], and the MURTI model [14-41]. Whole-core modules assuming particulate flow include the SAS/FCI module of SAS3D [14-1] and the EPIC code [14-7, 14-8] which has been coupled with the SAS3D code. It is also interesting to note that the SIMMER-II disassembly and transition phase code [14-29] treats all its moving

liquid or solid components as droplet or particulate flows. However, some attempts are made to account for the effect of flow regimes on exchange terms.

The PLUTO code [14-3, 14-4], which is the predecessor of PLUTO2, assumed exclusively particulate or droplet flow. It was nevertheless successful in analyzing the fuel motion and sodium voiding during the first few tens of milliseconds after pin failure in the E8 \$3/s TOP experiment [14-5, 14-6] and also the fuel motion and voiding during the first event of the H6 \$0.5/s TOP experiment [14-6].

The particulate flow regime has therefore been retained in PLUTO2. The fuel ejected into liquid sodium is assumed to instantaneously fragment into droplets or particles of radius RAFPLA if the liquid sodium fraction θ_{N1} > VFNALQ $\cdot\ \theta_{ch,op}$. Both RAFPLA and VFNALQ are input. All particles can, later on, simultaneously further fragment (after an input time delay of TIFP after pin failure) into smaller particles with radius RAFPSM, which is also input. Moreover, if the liquid sodium fraction in a certain channel node exceeds the input value VFNARE, mobile fuel, which was previously in a continuous flow regime (i.e., annular or bubbly flow), will instantaneously fragment into droplets in this node. This is an attempt to simulate delayed FCIs generated by sodium slugs reentering from below.

The continuous fuel flow regime in PLUT02 will develop if considerable local voiding has occurred (θ_{N1} < VFNALQ $\cdot\ \theta_{ch,op}$) and if the fuel energy is above the input fuel energy EGMN. For the latter a value somewhat above the solidus energy is suggested. This is because particles with an average energy corresponding to the solidus may already have a frozen outer crust which will prevent them from splattering on cladding and will thus not lead to an annular film flow. For the input value VFNALQ, which is the liquid sodium fraction below which a continuous fuel flow can develop, a value of 0.33 is recommended because it was used in the successful L8 post-test analysis [14-15, 14-12].

Once a continuous fuel flow has developed and is not yet occupying most of the coolant channel open cross sectional area at a certain elevation, a partially or fully annular fuel flow regime is assumed at that elevation. The partially annular flow regime was introduced because it appears unlikely that a relatively small amount of liquid fuel would spread around the entire perimeter of the coolant channel (see Eq. 14.4-74). Once the fuel volume fraction at a certain axial elevation becomes higher than the input value CIBBIN (for which a value of 0.7 is recommended), the development of a bubbly fuel flow is assumed to occur. This bubbly flow is then assumed to exist until the fuel volume fraction drops below 2/3 of the input volume fraction CIBBIN. This is because surface tension effects can maintain the bubbly flow down to a lower fuel volume fraction compared to the value required to cause the onset of the bubbly flow. The decision about flow regime changes is made at the end of subroutine PLVOFR. The logic flow for deciding whether the flow regime in a certain node should remain the same or whether it should change to another one is shown in Fig. 14.4-3. The sequence of "if" checks and statements is exactly the same as in the program. The input parameters appearing in the flowchart have already been described above. The meaning of the Flow Regime [F.R.] numbers is the following:

F.R. 1 particulate or droplet flow regime

F.R. 3 partially or fully annular fuel flow

F.R. 4 bubbly fuel flow

The flow regime labels for each node i are stored in the code in pointer array IFLAG(I). The value 2 has been reserved for a possible future PLUTO2 version in which cladding motion is considered and in which the number 2 would designate nodes with moving cladding. In the LEVITATE module, flow regime 2 is operational and designates molten cladding flow with imbedded fuel drops or chunks.

In explaining the flow chart logic, it is best to start at the time of PLUTO2 initiation when the flow regime in all nodes is set to 1 (particulate flow). The fuel will remain in flow regime 1 at least until the fourth diamond from above leads to a "no". However, if the fuel particles are already cold enough, the third diamond from above will keep them in particulate form. If both the third and fourth diamond lead to "no", the logic flow will drop straight through, lead to a complete entrainment of the liquid sodium film in the node considered and then switch to the annular flow regime (F.R. = 3). If the lowermost diamond leads to a "no", a switch to the bubbly flow regime (F.R. = 4) will be made. If such a switch occurs, the vapor/gas/sodium droplets mixture velocity will be set to the fuel velocity. This is done at the moment of bubbly flow regime initiation only. This helps to initialize a well-behaved two-fluid bubbly flow calculation. Starting with the previous vapor/gas/sodium droplets mixture velocity from the annular flow, which can be fairly high, can cause problems with the inertial terms in the bubbly flow calculation.

Once an annular or bubbly flow regime has been established in a node, the only way to get back to the particulate or droplet regime is via the first diamond. The latter will make it a particulate flow only if enough liquid sodium has reentered into the node considered. Once a bubbly flow regime has been established, it will get back to the annular flow regime only if the second lowest diamond leads to a "no". Overall, it has been attempted to keep the numerical nodes in the same flow regime for a reasonable length of time. This has helped to stabilize the overall calculation.

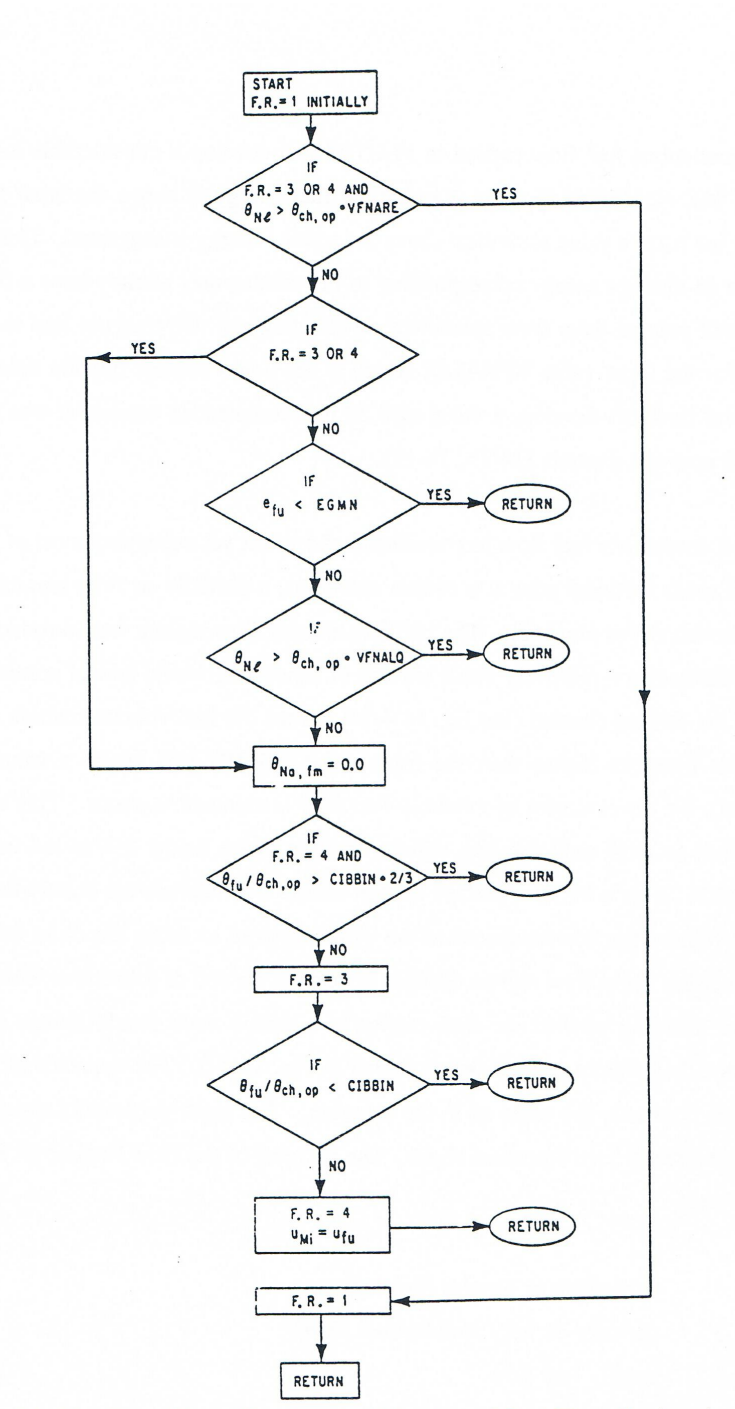

Fig. 14.4-3. Flow Chart Showing the Selection of Fuel Flow Regime in a Coolant Channel Mesh Cell

14.4.3.2 Fuel Plateout and Frozen Fuel Crust Release in Subroutine PLFREZ

In subroutine PLFREZ (PLUTO2 FREEZING ROUTINE), the amount of fuel plating out on cladding and structure as well as the amount of frozen fuel crust released from an underlying melting cladding are calculated. This information is later used in subroutine PLMISC to update the frozen fuel geometry. PLFREZ is called before the mass conservation equations and it can therefore provide updated densities and velocities of the moving components for the mass conservation. (The velocity change of the moving mixture due to frozen crust release is calculated in PLFREZ). However, since PLFREZ uses data from the end of the last time step, it could also have been called at the end of the calculational sequence as it is done in LEVITATE.

Fuel plateout on the cladding and structure of channel node i can only occur if there is either an annular or bubbly fuel flow regime in that node. Solid particles or particles with a reasonably thick solid outer crust are not believed to be able to stick to a cold surface, and molten droplets can exist in PLUTO2 only if there is a significant liquid sodium volume fraction ($\theta_{N1} > VFNALQ \cdot \theta_{ch,op}$; see previous section). The liquid sodium and, in particular, the liquid sodium film are assumed to prevent molten fuel droplets from sticking to cold surfaces because the droplets should form thin solid crusts due to the contact with the liquid sodium. The assumption that liquid droplets which are surrounded by significant amounts of liquid sodium will not plate out on cold surfaces may be questionable when a jet of fuel droplets hits a cold wall with a reasonably high velocity. In this case, the droplets may splatter on the cold wall and form a moving liquid film, which soon freezes and sticks despite the presence of liquid sodium. Such a high-velocity impingement of fuel may have occurred in the P4 test [14-42] or during the later stages of some of the CAMEL tests [14-38, 14-39]. This high-velocity impingement is not modeled in PLUTO2, but its effect can be roughly simulated by using for the input value VFNALQ, which is the sodium liquid fraction above which droplet or particle flow is allowed, a value close to 1, and for the input value VFNARE, also a value close to 1 and greater than VFNALQ. In the P4 pre-test analysis with PLUTO2, VFNALQ = 0.33 was used (similar values had been used in the successful PLUTO2 analyses of H6 [14-6] and L8 [14-15, 14-12]). This input choice led to the prediction of total fuel sweepout because only flow regime 1 (particulate or droplet flow) was selected by the code. The P4 experiment, however, showed extensive plateout and little sweepout. The above explanation of a high-velocity fuel jet hitting the cladding, however, is not the only possible explanation. Another explanation for this preferential plateout may be that the sodium could have bypassed the ejected fuel in this relatively large bundle test and, therefore, not exerted the full inlet pressure on it.

To be in the annular or bubbly flow regime is only one of the necessary conditions for initiating plateout. The other ones are:

$$e_{vu} < EGBBLY \tag{14.4-49}$$

and

$$T_{ffcl} < T_{fu,sol} \tag{14.4-50}$$

and

$$T_{cl,os} < TECLMN \tag{14.4-51}$$

and

$$\theta_{ch,op} > 0.3\ \theta_{ch} \tag{14.4-51a}$$

Moreover, the moving fuel volume fraction is not allowed to drop below 0.01 of the channel volume fraction due to fuel plateout. This is done to avoid problems with zero amounts of moving fuel.

The condition 14.4-49 states that the moving that the moving fuel energy should be below the input value EGBBLY which has to be within the melting band of the fuel. A value in the lower part of the melting band is recommended, based on the L8 analysis with PLUTO2 [14-15, 14-12]. One should be careful that the input value EGMN, below which a continuous flow regime cannot develop (see Fig. 14.4-3), is smaller than EGBBLY because this can inhibit plateout.

The condition 14.4-50 states that the temperature of the fuel crust on the cladding should be below the fuel solidus temperature in order to allow plateout. Fuel should not plate out on already molten fuel crusts (layers), and, as soon as the fuel crust temperature has increased half way into the melting band, this fuel crust will actually be ablated by the moving fuel field (see below).

The condition 14.4-51 states that fuel plateout will occur only if the cladding surface temperature is less than the input value TECLMN. This value should be set to the steel solidus temperature TESOL (which is input) or somewhat above it. It is believed that freezing fuel will not stick to a molten cladding surface but rather slide over it. However, it will probably also ablate some of the molten steel which is not treated in PLUTO2. If one wants to consider this phenomenon, one will have to switch to the LEVITATE module, which is treating steel ablation. This can be done by setting the input value NCPLEV to a low integer number.

The condition 14.4-51a limits the frozen fuel fraction in a node to 70% of the nodal volume. Thus a complete plugging of a coolant channel is not allowed in PLUTO2. This is done because the PLUTO2 equations are written for relatively smoothly varying flow cross sections. If all the above-mentioned conditions are met in a channel cell, then fuel plateout will occur in that cell. There are two possibilities:

(a) If

$$e_{fu,sol} < e_{fu} < \text{EGBBLY},$$

the amount of mobile fuel which will be plated out in node *i* during Δt_{PL} is calculated from:

$$\Delta\rho'_{fu,i} = \rho'_{fu,i} \cdot \frac{EGBBLY - e_{fu,i}}{EGBBLY - e_{fu,sol}} \tag{14.4-52}$$

The input parameter (EGBBLY) appeared already in Eq. 14.4-49. It has to be between the fuel solidus and liquidus energies. The latter are the input values EGFUSO and EGFULQ, respectively. It was mentioned earlier that a value in the lower part of the melting range is recommended based on the PLUTO2 L8 analysis [14-15, 14-12]. The fuel which plates out is assumed to have a temperature of

$$T_{fu,fz,i} = T_{fu,sol} \tag{14.4-53}$$

This assumption leads to a temperature increase of the mobile fuel when plateout occurs and is accounted for in the code. The underlying assumption is that the mobile fuel has a radial temperature gradient with the freezing fuel being at the fuel solidus temperature.

(b) If

$e_{fu} < e_{fu,sol}$,

the fraction of the mobile fuel plated out in a PLUTO2 time step of Δt_{PL} second will be calculated from

$$\Delta\rho'_{fu,i} = \rho'_{fu,i}\,\Delta t_{PL} \cdot \frac{1}{2\ ms} \tag{14.4-54}$$

which causes a near complete fuel plateout of the mobile fuel in 2 ms. This situation can occur when frozen fuel crusts, which were released in another cell due to melting cladding, slide into a cell in which cladding has not yet melted. The assumption is that these fuel crusts will bring with them some liquid steel that will make them stick on still-unmelted cladding. The temperature of the plated-out fuel in this case equals the temperature of the moving fuel.

$$T_{fu,fz,i} = T_{fu,i} \tag{14.4-55}$$

For both cases, the temperature changes of the frozen fuel crusts on cladding and structure are calculated in the same way by making use of the assumptions about $T_{fu,fz}$ in Eqs. 14.4-53 and 14.4-55.

$$T_{ffci,i}^{new} = \frac{T_{fu,fz,i}\,\Delta\rho'_{fu,i} + T_{ffcl,i}^{old}\,\rho'_{ff,i}}{\rho'_{ff,i} + \Delta\rho'_{fu,i}} \tag{14.4-56}$$

and

$$T_{ffsr,i}^{new} = \frac{T_{fu,fz,i}\,\Delta\rho'_{fu,i} + T_{ffsr}^{old}\,\rho'_{ff,i}}{\rho'_{ff,i} + \Delta\rho'_{fu,i}} \tag{14.4-57}$$

Because the relative fractions of the fuel plating out on cladding and on structure and the relative fractions of fuel already plated out on cladding and structure are assumed to be the same, the above two equations are very similar. This is because the fraction of the fuel plating out on cladding cancels out in Eq. 14.4-56, and the fraction of fuel plating out on the structure cancels out in Eq. 14.4-57. Although separate temperatures for the frozen film on the cladding and structure are tracked in PLUTO2, only one common smear density is tracked for the frozen films. This should be improved in a future PLUTO2 version.

When fuel plateout has occurred, the generalized densities of the mobile and frozen fuel, the generalized volume fractions $\theta_{ch,op}$, θ_{fu}, and θ_{vg} of the open channel, mobile fuel, and the vapor/gas mixture are updated. Moreover, the channel hydraulic diameter is updated:

$$D_{ch}^{new} = D_{ch}^{old} \cdot \left(\theta_{ch,op} - \Delta\rho'_{fu} / \rho_{fu,sol}\right) / \theta_{ch,op} \tag{14.4-58}$$

This change in the hydraulic diameter is based only on the changes in the open channel cross-section area because the perimeter of the open channel will remain approximately the same whether a fuel crust is present or not. This is a reasonable approximation for an actual subchannel, but it would not be good for a cylindrical pipe.

Fuel crusts can also be released and added back into the moving fuel field. One apparent reason is that the fuel crust can become re-melted due to fission heating and/or the heat flux from the moving fuel. In the code, the crust release due to remelting is initiated when the fuel crust temperature is half way through the melting band. The fraction CFMELT of the crust released per PLUTO2 time step is calculated from:

$$CFMELT = \frac{T_{ffcl,i} - \left(T_{fu,liq} + T_{fu,sol}\right)/2}{T_{fu,liq} - \left(T_{fu,liq} + T_{fu,sol}\right)/2} \tag{14.4-59}$$

The new generalized smear density of the fuel crust is

$$\rho'_{ff,i} = \rho'^{old}_{ff,i} - \Delta\rho_{ff,i} \tag{14.4-60}$$

where

$$\Delta\rho'^{old}_{ff,i} = \rho'^{old}_{ff,i} \cdot CFMELT \tag{14.4-61}$$

A melting fuel crust is assumed to have a higher temperature at the interface with the gas/vapor mixture than at the interface with the cladding because the cladding cannot be significantly molten since this would have led to crust ablation (see below). Therefore the crust thickness is reduced in this case of crust melting:

$$TKFF = TKFF^{old} \cdot \left(1 - CFMELT\right) \tag{14.4-62}$$

The other reason for releasing a fuel crust in PLUTO2 is the melting of the underlying cladding. The frozen fuel crust in mesh cell *i* will be released in PLUTO2 when the temperature of the middle cladding node has exceeded the input value TECLRL in cell *i*. A value in the upper part of the cladding melting band is recommended. The frozen crust is rapidly released in this case according to

$$\Delta\rho'_{ff,i} = \rho_{fu,sol}\,\theta_{ch}\,\Delta t_{PL} \cdot \frac{1}{5\,ms} \tag{14.4-63}$$

This means that a crust which would initially fill the entire channel would be completely released in 5 *ms*. A crust occupying only a fraction FN_{ff} of the channel would be released in $FN_{ff} \cdot 5$ *ms*. The change in the generalized densities of the fuel crust and also the mobile fuel are calculated with Eqs. 14.4-60 and 14.4-61. In this case of frozen crust release, it is likely fuel pieces with the full crust thickness will get released and that only the fraction of the channel perimeter, which is covered by frozen crust, which is *CFFFCL*, gets reduced:

$$CFFFCL(I) = CFFFCL(I) \cdot \rho'^{new}_{ff} / \rho'^{old}_{ff} \tag{14.4-64}$$

It is important to note that the treatment of frozen crust release after the underlying cladding has melted and also the disallowing of fuel plateout on molten cladding made the successful L8 post-test analysis with PLUTO2 possible [14-15, 14-12]. In the pre-test analysis, these phenomena were not considered and led to a considerable underprediction of the fuel dispersal [14-43, 14-16]. The current treatment, however, is not yet ideal because the released frozen crust pieces are homogenized with the mobile fuel in the node considered. Ideally, these frozen fuel pieces should be treated in a separate chunk field. Such a treatment is being incorporated in the chunk version of the LEVITATE module. Once this version has been made compatible with the SAS4A release version, one can switch to it via the NCPLEV input parameter. This input parameter specifies the number of axial cladding nodes which have to be fully molten before a switch from PLUTO2 to LEVITATE occurs.

For both the remelting of a crust and the release of a frozen crust, energy and velocity adjustments for the moving fuel are made in the lower section of subroutine PLFREZ. Although these adjustments could also be made later in the fuel energy and momentum equations, it is easier to do it in this subroutine because several local variables that are needed would have to become part of the common blocks. The energy adjustment for the moving fuel is:

$$e_{fu,i}^{new} = \frac{e_{fu,i}^{old}\,\rho'_{fu,i} + e_{fu,rl,i}^{old}\Delta\rho'_{ff,i}}{\rho'_{fu,i} + \Delta\rho'_{ff,i}} \tag{14.4-65}$$

where

$$e_{fu,r1} = \begin{cases} \mathrm{e}_{\mathrm{fu,liq}} & \text{for a melting crust} \\ e_{ff} & \text{for a crust which is released due to clad melting} \end{cases}$$

The calculation of the velocity adjustments for the moving fuel at the lower and upper boundaries of the mesh cell *i* is as follows:

$$u_{fu,i}^{new} = u_{fu,i}^{old} \cdot \frac{\rho'_{fu,i-1} + \rho'_{fu,i}}{\rho'_{fu,i-1} + \rho'_{fu,i} + \Delta\rho'_{ff,i-1} + \Delta\rho'} \tag{14.4-66}$$

$$u_{fu,i+1}^{new} = u_{fu,i+1}^{old} \cdot \frac{\rho'_{fu,i} + \rho'_{fu,i+1}}{\rho'_{fu,i1} + \rho'_{fu,i+1} + \Delta\rho'_{ff,i} + \Delta\rho'_{ff,i+1}} \tag{14.4-67}$$

If the release of a fuel crust has taken place, the generalized volume fractions $\theta_{ch,op}$, θ_{fu}, and θ_{vg} of the open channel, the mobile fuel, and the vapor/gas, respectively, are updated at the end of subroutine PLFREZ. Moreover, the hydraulic diameter of the channel is updated

$$D_{ch}^{new} = D_{ch}^{old} \cdot \left(\theta_{ch,op} - \Delta\rho'_{ff} / \rho_{fu,sol}\right) / \theta_{ch,op}^{old} \tag{14.4-68}$$

This change in the hydraulic diameter is based only on changes in the open channel cross-section area because the perimeter of a real sub-channel will be approximately the same whether a fuel crust is present or has been released.

14.4.3.3 Plated-Out and Moving Fuel Configurations

The different configurations of the plated-out and moving fuel in PLUTO2 are shown in Fig. 14.4-1 at the beginning of Section 14.4.1. These configurations are shown in a cylindrical geometry although the areas and wetted perimeters used in the code are based on the actual subchannel values. The outer perimeter of the cylindrical channel shown in Fig. 14.4-1 represents mostly cladding but also some structure. The various fuel configurations are of importance for calculating the energy and momentum

exchange terms because the interface areas are largely determined by the fuel configurations. The fuel flow regime selection has already been described in Section 14.4.3.1. In the present section, the assumptions about the specific fuel configuration in each flow regime are described. In the code, these are implemented near the front of subroutine PLMISC (PLUTO2 MISCELLANEOUS).

In the particulate flow regime [see configuration (a) in Fig. 14.4-1], the only assumption is that the particles are uniformly distributed in a numerical cell. With regard to the heat transfer between fuel and liquid sodium, both the liquid sodium film and the sodium droplets are also assumed to be uniformly distributed. The heat-transfer area between fuel and liquid Na per unit of generalized smear volume is assumed to be

$$A'_{fi.N1} = A'_{Pa} \cdot \left(\theta_{N1} / \theta_{ch,op}\right)^{CIA2} \qquad (14.4\text{-}69$$

where

$$A'_{Pa} = N'_{Pa} \cdot 4\pi r_{Pa}^2$$

$$N'_{Pa} = \frac{\rho'_{fu}}{\frac{4}{3}\pi r_{Pa}^3 \rho_{fu,sol}}, \text{ number of fuel particles in a generalized smear volume}$$

θ_{N1} = the generalized liquid sodium volume fraction which includes the moving sodium droplets and the static sodium film.

*CIA*2 = input constant (see Eq. 14.4-98).

The heat-transfer area between fuel particles and the vapor/gas mixture is:

$$A'_{fu,vg} = N'_{Pa}\, 4\pi_{Pa}^2 \cdot \left[1 - \left(\theta_{N1} / \theta_{ch,op}\right)^{CIA2}\right] \qquad (14.4\text{-}70)$$

For the continuous flow regimes [see (b) through (e) in Fig. 14.4-1], the assumed interaction areas between the various components are considerably more complicated than for the particulate flow regime. Several important Fortran variables describing the different configurations for continuous fuel flow will be explained first.

$$ARCH = \theta_{ch} \cdot AXMX / NPIN \qquad (14.4\text{-}70a)$$

where *ARCH* is the coolant channel cross section area associated with one pin. *AXMX* has already been described in Section 14.4.2.1. *NPIN* is the number of pins per subassembly. Both *AXMX* and *NPIN* are input.

$$ARMF = ARCH \cdot \theta_{fu} / \theta_{ch} \tag{14.4-71}$$

where *ARMF* is the cross-sectional area of moving fuel associated with one pin.

$$ARFF = ARCH \cdot \left(\theta_{ch} - \theta_{ch,op}\right) / \theta_{ch} \tag{14.4-72}$$

where *ARFF* is the cross-sectional area of plated-out fuel which is associated with one pin.

$$PECH = \left(ARCL' + ARSR'\right) \cdot AXMX / NPIN \tag{14.4-73}$$

where *PECH* is the channel perimeter associated with one pin. This also includes a fraction of the structure perimeter. The quantities *ARCL'* and *ARSR'* are the cladding and structure surface areas per unit of generalized smear volume. Moreover, they are also the total perimeters of the cladding and structure (times one meter) in a unit of generalized smear volume.

The fraction of the cladding and structure which is covered by either molten or plated-out fuel, *CFFUCL*, has the value 1.0 in the bubbly flow regime. In the annular flow regime (see b,c, and d in Fig. 14.4-1), *CFFUCL* is taken to be a linear function of the total (moving fuel + fuel crust) fuel volume fraction.

$$CFFUCL = \frac{ARMF + ARFF}{ARCH} \cdot \frac{1}{CIANIN} \tag{14.4-74}$$

or if *CFFUCL* calculated from Eq. 14.4-74 is greater than 1.0:

$$CFFUCL = 1.0 \tag{14.4-74a}$$

The latter value applies to condition d in Fig. 14.4-1. The input parameter *CIANIN* in Eq. 14.4-74 determines the fuel volume fraction above which a complete annular fuel flow will exist (i.e., condition d in Fig. 14.4-1). A value of 0.5 is recommended, based on the L8 TREAT test analysis with PLUTO2 [14-15, 14-12].

In the annular flow regimes, the thickness *TKFU* of the layer containing both moving and plated-out fuel is also important. Its calculation is based on the conservation of fuel volume:

$$TKFU = \left(ARFF + ARMF\right) / \left(PECH \cdot CFFUCL\right) \tag{14.4-75}$$

The frozen fuel crust, which is important in both the annular and the bubbly flow regimes is also characterized by two variables. These are the frozen fuel crust thickness *TKFF* and the fraction *CFFFCL* of the channel perimeter that is covered by frozen fuel crust. Both *TKFF* and *CFFFCL* are permanent arrays in the code (which are updated

during the time steps), whereas the thickness and coverage fraction of the layer including all the fuel are recalculated every PLUTO2 time step. The calculation of the change in the frozen fuel cross-sectional area due to remelting or release has been described in the previous section. The change of the frozen fuel cross section due to freezing can cause both an increase in the frozen crust thickness *TKFF* and in the coverage fraction CFFFCL. How much either one increases depends on whether bulk type freezing or conduction-limited freezing [14-44, 14-45, 14-46] is more appropriate. In PLUTO2 the mode of plateout of fuel for the partially annular, totally annular and bubbly flow regime is controlled by an input parameter (*CIFUFZ*) which allows both extremes or values anywhere between these two extremes. The increase in the crust thickness is calculated from:

$$\Delta TKFF = \frac{\Delta ARFF}{CFFFCL \cdot PECH} \cdot \frac{H_{fu,ff} \cdot \left(T_{fu} - T_{ff}\right)}{H_{fu,ff} \cdot \left(T_{fu} - T_{ff}\right) + H_{fu,cl} \cdot \left(T_{fu} - T_{cl,os}\right) \cdot CIFUFZ} \tag{14.4-76}$$

where

$\Delta ARFF$ = the change in the frozen fuel cross section during one PLUTO2 time step.

CFFFCL = the fraction of the channel perimeter covered by plated-out fuel at the beginning of the PLUTO2 time step.

CIFUFZ = an input parameter whose value should be between 0 and 1.0. A value of zero leads to pure bulk-type freezing (i.e., the crust grows till it reaches the thickness of the total molten fuel layer thickness before the coverage fraction *CFFFCL* increases). A value of 1 leads to a conduction-type freezing. *CIFUFZ* = 0 was used in the L8 analysis [14-15, 14-12] because no other option was available at that time.

and the moving fuel-to-frozen-fuel heat flux per unit temperature difference and per unit of generalized smear volume is given by

$$H_{fu,ff} = h_{fu,ff} \cdot CFFFCL \cdot CFMFFF \cdot PECH \tag{14.4-76a}$$

where

$h_{fu,ff}$ = the heat-transfer coefficient between molten fuel and frozen fuel which takes the resistance in the fuel crust into account. It is described in the following section on exchange terms.

$$\text{CFMFFF} = \text{ARMF}/(\text{ARMF} + \text{ARFF}) \tag{14.4-77}$$

In Eqs. 14.4-76a and 14.4-77, *CFMFFF* is the fraction of the frozen crust that is assumed to be covered with moving fuel. In the bubbly flow regime, *CFMFFF* is always 1.0. The moving fuel-to-cladding heat flux required in Eq. 14.4-76 is given by

$$H_{fu,cl} = h_{fu,cl}\ (CFFUCL - CFFFCL) \cdot PECH \tag{14.4-78}$$

where

$h_{fu,cl}$ is the heat-transfer coefficient between moving fuel and cladding, which is described in the following section on exchange coefficients.

The initialization of the crust thickness during the first time step when plateout commences is also affected by the input parameter *CIFUFZ* that was discussed above:

$$TKFF = \frac{ARMF + ARFF}{PECH \cdot CFFUCL} \cdot (1 - CIFUFZ) + \frac{ARFF}{PECH \cdot CFFUCL} \cdot CIFUFZ \tag{14.4-79}$$

where the first term on the right-hand side would lead to the maximum initial crust thickness for *CIFUFZ* = 0 and the second term gives the minimum thickness if *CIFUFZ* = 1. The latter will cause the frozen fuel coverage fraction of the channel perimeter (*CFFFCL*) to be the same as the one for the total (moving + frozen) fuel, *CFFUCL*. Since *TKFF* and *CFFFCL* are permanent arrays in the code, the initial values of these variables are quite important. The frozen fuel coverage fraction of the channel perimeter is calculated, based on frozen fuel volume conservation:

$$CFFFCL = ARFF / (TKFF \cdot PECH) \tag{14.4-79a}$$

If *CFFFCL* > *CFFUCL*, *CFFFCL* and *TKFF* will be:

$$CFFFCL = CFFUCL \tag{14.4-79b}$$

and

$$TKFF = ARFF / (PECH \cdot CFFUCL) \tag{14.4-79c}$$

The crust dimension calculations described above hold in all continuous flow regimes.

14.4.3.4 Energy and Momentum Exchange Terms in Subroutine PLMISC

Besides calculating the moving and frozen fuel configurations, subroutine PLMISC (PLUTO2 MISCELLANEOUS) also calculates many heat-transfer and friction coefficients that are later used in the calculation of the fuel energy equations, the sodium energy equation, and in the channel momentum equation. The latter also requires several drag coefficients which are determined in the subroutine calculating the channel momentum equation, PLMOCO. However, some of the variables needed for the drag coefficients are also calculated in subroutine PLMISC.

Several heat and momentum exchange terms described below are still in a simplified or preliminary form. Additional validation efforts, which are outlined in the SAS4A validation plan [14-10], will be necessary to improve certain heat and momentum exchange terms. However, the reasonably successful analyses of TREAT experiments L8 and H6 [14-15, 14-12, 14-6] may be an indication that all of the more important exchange terms are treated properly.

14.4.3.4.1 Heat-transfer and Momentum Exchange Terms Between Sodium and Cladding, and Sodium and Structure

14.4.3.4.1.1 Near-Liquid Sodium

If $\alpha_{Na} < CIVOID$, where *CIVOID* is an input parameter, liquid single-phase correlations will be used if there is still cladding or structure that is not covered by fuel (i.e., particulate or partially annular fuel flow). The input parameter *CIVOID* determines the sodium void fraction below which these correlations will be used. A value of 0.5 is recommended based on the L8 analysis [14-15, 14-12]. The heat-transfer coefficient that is used for low-void fraction sodium flow which has a low Prandtl number of about 0.005, is based on Ref. 14-47.

$$h_{Na,c1,i} = \left[Cl \cdot \left(D_{N1} \cdot \rho_{N1} \cdot \left| u_{Mi,i} + u_{Mi,i+1} \right| \cdot 0.5 \cdot C_{p,N1} / k_{N1} \right)^{C2} + C3 \right] \cdot \frac{k_{N1}}{D_{ch}} \cdot CFNACL \tag{14.4-80}$$

where all variables without axial indexes are calculated at the center of cell *i*

$C1$, $C2$ and $C3$ are input constants, and

k_{N1} = *CDNL* which is a constant input value for the liquid sodium thermal conductivity

$C_{p,N1}$ = liquid sodium heat capacity whose temperature dependence is described in the material property section of Chapter 12.

D_{n1} = $D_{ch} \cdot \theta_{N1} / \theta_{ch,op}$ is the hydraulic diameter for the liquid sodium which is assumed to be in an annular flow regime.

D_{ch} = hydraulic diameter of the open coolant channel which takes the presence of a fuel crust into account (see Eq. 14.4-58)

CFNACL = fraction of the channel perimeter that is wetted by sodium. When the particulate flow regime exists, a fraction of the perimeter can be covered by frozen fuel. The value of *CFNACL* is in this case

$$CFNACL = \left(1 - CFFFCL\right) \tag{14.4-80a}$$

If an annular flow regime exists

$$CFNACL = (1 - CFFUCL) \tag{14.4-80b}$$

The CFNACL should actually be lumped together with the heat-transfer area. However, to lump such terms together with heat-transfer coefficients has the advantage that the total heat flow rates, which are calculated at the end of subroutine PLMISC, include only the total cladding or structure areas.

The heat-transfer coefficient between low-void fraction sodium and the structure is set equal to that between low-void fraction sodium and cladding

$$h_{NA,sr,i} = h_{Na,cl,i} \tag{14.4-81}$$

The friction factor used for the low-void fraction sodium and fission-gas mixture is:

$$F_{Mi} = AFR \cdot (\mathrm{Re}_{Mi})^{BFR} \tag{14.4-82}$$

where

AFR, BRF are input constants

Re_{Mi} Reynolds number of the mixture of sodium and fission gas which is calculated from:

$$\mathrm{Re}_{Mi} = \left\{ D_{ch} \cdot \left| u_{Mi,i} + u_{Mi,i+1} \right| \cdot 0.5 \cdot \rho'_{Mi} / \left(\theta_{vg} + \theta_{N1} - \theta_{Na.fm} \right) \right\} / \mu_{Mi} \tag{14.4-83}$$

where the viscosity of the two-phase mixture is evaluated from a formulation suggested by Dukler [14-48]:

$$\mu_{Mi} = \frac{\rho'_{Mi}}{\left(\theta_{vg} + \theta_{N1} - \theta_{Na,fm} \right)} \cdot \left\{ \frac{x_{Mi} \mu_{vg}}{\left(\rho_{Nv} + \rho'_{fi} / \theta_{vg} \right)} + \frac{\left(1 - x_{Mi} \right) \mu_{N1}}{\rho_{N1}} \right\} \tag{14.4-83a}$$

where

μ_{Nl} = VINL, viscosity of liquid sodium which is input

μ_{vg} = VIVG, viscosity of the vapor/gas mixture which is input.

x_{Mi} = $(\theta_{vg}\, \rho_{Nv} + \rho'_{fi}) / \rho'_{Mi}$ quality of moving sodium fission-gas mixture

ρ'_{Mi} = $\rho'_{Na} - \rho_{Nl}\, \theta_{Na,fm} + \rho'_{fi}$

i.e., ρ'_{Mi} is the generalized smear density of the moving sodium and the fission gas.

14.4.3.4.1.2 Liquid Sodium Films Present and a Vapor/Gas Mixture or Two-phase Sodium/Gas Mixture in the Gas Core

If $\theta_{Na,fm} > 0$ and $\alpha_{Na} > CIVOID$,

liquid sodium film evaporation or condensation on the liquid film will take place. A splitting of the currently available liquid film volume fraction, $\theta_{Na,fm}$, into a film volume fraction for the cladding, $\theta_{cl,fm}$, and for the structure, $\theta_{sr,fm}$, is done in the following way:

$$\theta_{sr,fm} = CINAFO \cdot \theta_{ch,op} \cdot \frac{A'_{sr}}{A'_{sr} + A'_{cl}} \tag{14.4-84}$$

$$\theta_{cl,fm} = \theta_{Na,fm} - \theta_{sr,fm} \tag{14.4-84a}$$

where $CINAFO$ is an input constant which gives the initial and maximum film volume fraction. However, if $\theta_{cl,fm} \le 0$,

$$\theta_{sr,fm} = \theta_{Na,fm} \tag{14.4-84b}$$

This means, that the structure film has its maximum value as long as a liquid film exists on the cladding. If $T_{Na} > Tl_{cl,os}$

$$h_{Na,cl} = CFNACN \cdot (1 - CFFFCL) \tag{14.4-85}$$

where

$CFNACN$ is the sodium condensation coefficient which is input

and for

$CFFFCL$ see Eq. 14.4-76

If $T_{Na} < T_{cl,os}$

$$h_{Na,cl} = \frac{1}{(1/CFNAEV) + w_{cl,fm}/CDNL} \cdot (1 - CFFFCL) \tag{14.4-86}$$

where

$CFNAEV$ is the sodium evaporation coefficient which is input and which should be larger than $CFNACN$ which is discussed above

$w_{cl,fm}$ is the thickness of the sodium film on the clad

CDNL liquid sodium conductivity which is input

The sodium-to-structure heat-transfer coefficient, $h_{Na,sr}$, is set equal to the $h_{Na,cl}$ calculated from Eq. 14.4-86 as long as the structure has a lower temperature than the sodium. In the unlikely case that the structure is hotter than the sodium, an equation similar to Eq. 14.4-86 is used but with the structure film thickness, $w_{sr,fm}$, instead of $w_{cl,fm}$.

The friction factor for the case when liquid sodium films are present is based on Ref. 14-49, page 320, and is calculated in the following way:

$$F_{Mi} = AFRV \cdot \left(\mathrm{Re}_{Mi}\right)^{BFRV} \cdot \left\{1+\left(1-CFFUCL\right) \cdot \frac{300\left(w_{cl,fm} \cdot A'_{cl} + w_{sr,fm} \cdot A'_{sr}\right)}{D_{ch} \cdot \left(A'_{cl} + A'_{sr}\right)}\right\} \qquad (14.4\text{-}86a)$$

where

AFRV and *BFRV* are input constants

Re_{Mi} Reynolds number for the sodium/gas mixture (see Eq. 14.4-83)

14.4.3.4.1.3 No Sodium Films Left and Sodium Temperature Below the Outer Cladding Temperature

This condition is common in the annular fuel flow regime in which liquid sodium films are not allowed. Moreover, in the particulate flow regime, the sodium films may have been completely entrained or evaporated. Two conditions have to be considered. First, there can be a flow of sodium droplets, vapor, and gas in the coolant channels or just a flow of vapor and gas. For void fractions larger than the input value CIA4 (which has to be larger than the input value *CIVOID*), the heat-transfer coefficient used is a linear interpolation between a convective heat-transfer coefficient for a pure vapor/gas moisture, $h_{vg,cl}$, and a boiling heat-transfer coefficient *HCCLMI* which is input. For void fractions smaller than CIA4 and larger than *CIVOID*, a constant value is used:

$$h_{Na,cl} = HCCLMI \cdot CFNACL \qquad (14.4\text{-}87)$$

where

CFNACL is the fraction of the channel perimeter which is in contact with the two-phase sodium (see also Eq. 14.4-88)

HCCLMI is an input heat-transfer coefficient describing the forced convection heat transfer between sodium droplets and cladding. *HCCLMI* should be definitely smaller than the evaporation coefficient *CFNAEV* and probably also smaller than the condensation coefficient *CFNACN*. It should also be remembered here that for sodium void fractions less than the input value *CIVOID*, a single-phase convective heat-transfer coefficient is used

for the calculation of $h_{Na,c\ell}$ (see Eq. 14.4-80). Therefore, CIA4 should be larger than *CIVOID*.

For α_{Na} > CIA4, the above-mentioned linear interpolation is done:

$$h_{Na,cl} = \frac{\left[HCCLMI \cdot \left(1-\alpha_{Na}\right) + h_{vg,cl} \cdot \left(\alpha_{Na} - CIA4\right)\right] \cdot CFNACL}{\left(1-CIA4\right)} \tag{14.4-88}$$

where

α_{Na}= ($\theta_{ch,op}$ - θ_{N1} - θ_{fu}) / ($\theta_{ch,op}$ - θ_{fu})

HCCLMI = input heat-transfer coefficient (see Eq. 14.4.87)

$$CFNACL = \begin{cases} 1 = CFFFCL & \text{for the particulate fuel flow regime (see Eq. 14.4-76)} \\ 1 = \text{CFFUCL} & \text{for the annular fuel flow regime (see Eq. 14.4-74)} \end{cases}$$

$h_{vg,c1}$ = convective heat-transfer coefficient between a vapor/gas mixture and cladding which is calculated from a simplified Dittus-Boelter equation in which a Prandtl number of 0.7 is assumed [14-50]:

$$h_{vg,cl} = 0.02 \cdot \frac{k_{vg}}{D_{Mi}} \cdot \left(\text{Re}_{Mi}\right)^{0.8} \tag{14.4-89}$$

where

$$\text{Re}_{Mi} = \frac{D_{Mi} \cdot \rho_{vg} \cdot \left|u_{Mi,i} + u_{Mi,i+1}\right|}{2\,VIVG}$$

VIVG = viscosity for the vapor/gas mixture which is input.

$$\rho_{vg} = \begin{cases} \rho'_{Mi} / \left(\theta_{ch,op} - \theta_{fu}\right) & \text{for } \alpha < 1 \\ \left(\rho_{Nv} \cdot \theta_{vg} + \rho'_{fi}\right) / \left(\theta_{ch,op} - \theta_{fu}\right) & \text{for } \alpha = 1 \end{cases}$$

k_{vg} = *CDVG*, the input thermal conductivity for a vapor/gas mixture.

$$D_{Mi} = D_{ch} \cdot \left(\theta_{ch,op} - \theta_{fu}\right) / \theta_{ch,op} \tag{14.4-89a}$$

For the calculation of the latter quantity, it is assumed that only the cross-sectional area of the open channel is reduced due to a molten fuel film, but not the perimeter.

14.4.3.4.1.4 No Liquid Sodium Films Present and Sodium Temperature Higher Than Cladding Temperature

If $\theta_{cl,fm} = 0$, $T_{Na} > T_{cl,os}$, and $\alpha_{Na} > CIVOID$

$$h_{Na,cl} = CFNACN \cdot CFNACL \tag{14.4-90}$$

i.e., the sodium vapor condensation heat transfer is not decreased with increasing void fraction.

Since the calculation of the heat transfer between sodium and cladding is quite complicated, an overview is given in Table 14.4-2.

14.4.3.4.1.5 Heat Transfer Between Sodium and Structure

The calculation of the heat-transfer coefficient between sodium and structure, $h_{Na,sr}$, is based on the same equations as indicated in Table 14.4-2. This table should be slightly modified by replacing $T_{cl,os}$ by $T_{sr,os}$ and by replacing "Na film present on cladding" by "Na film present on structure" in order to make it appropriate as an overview for the sodium-to-structure heat-transfer coefficient.

Heat fluxes per unit of temperature and per unit of generalized smear volume are later needed in the energy equations. They are calculated towards the end of subroutine PLMISC and are simply:

$$H_{Na,cl} = h_{Na,cl} \cdot A'_{cl} \tag{14.4-90a}$$

$$H_{Na,sr} = h_{Na,sr} \cdot A'_{sr} \tag{14.4-90b}$$

14.4.3.4.1.6 Friction Coefficient When No Liquid Sodium Film is Present

Friction coefficients for calculating the friction on the sodium/gas mixture have already been given for the situation when much liquid sodium is present in the channels (Eq. 14.4-82) and for the case when liquid sodium films are still present (Eq. 14.4-86a).

When no liquid films are present, Eq. 14.4-86a leads to:

$$F_{Mi} = AFRV \cdot \left(\mathrm{Re}_{Mi}\right)^{BFRV} \tag{14.4-91}$$

This equation is appropriate for the particulate fuel flow regime. In the annular fuel flow regime, the momentum exchange between the moving fuel film and the sodium/gas mixture is included in the drag term, which describes this momentum exchange. Thus, the friction of the mixture due to the interaction with the stationary cladding or fuel crust has to be reduced from that of the whole channel perimeter.

$$F_{Mi} = AFRV \cdot \left(\mathrm{Re}_{Mi}\right)^{BFRV} \cdot \left(1 - CFMFCL - CFMFFF \cdot CFFFCL\right) \qquad (14.4\text{-}92)$$

where the quantities in the parentheses (*CFMFCL*, *CFMFFF* and *CFFFCL*) are explained in Eqs. 14.4-100, 14.4-77, and 14.4-79a.

Table 14.4-2. Overview of the Calculation of the Sodium-to-Cladding Heat Transfer

Void Fraction	Equation
$\alpha_{Na} < CIVOID$	Eq. (14.4-80) (Single-Phase Correlation)
$CIVOID \le \alpha_{Na} \le CIA4$	If liquid *Na* film present on cladding (only F.R. = 1): For $T_{Na} > T_{cl,os}$ Eq. (14.4-85) For $T_{Na} < T_{cl,os}$ Eq. (14.4-86) If no liquid *Na* film left (F.R. = 1 or F.R. = 3): For $T_{Na} > T_{cl,os}$ Eq. (14.4-90) For $T_{Na} < T_{cl,os}$ Eq. (14.4-87)
$CIA4 < \alpha_{Na} < 1$	If liquid Na film present on cladding (only F.R. = 1): For $T_{Na} > T_{cl,os}$ Eq. (14.4-85) For $T_{Na} < T_{cl,os}$ Eq. (14.4-86) If no liquid *Na* film (F.R. = 1 or F.R. = 3): For $T_{Na} > T_{cl,os}$ Eq. (14.4-90) For $T_{Na} < T_{cl,os}$ Eq. (14.4-88)
$\alpha_{Na} = 1$	If $T_{Na} > T_{cl,os}$ Eq. (14.4-90) If $T_{Na} < T_{cl,os}$ Eq. (14.4-89)

14.4.3.4.2 Fuel-to-Coolant Heat Transfer

14.4.3.4.2.1 Fuel-to-Coolant Heat Transfer in the Particulate Fuel Flow Regime

The heat flow rate per unit of temperature and unit of generalized smear volume is calculated from

$$H_{fu,Na} = h_{fu,N1} \cdot A'_{Pa} \cdot f_{fu,N1} + h_{fu,vg} \cdot A'_{Pa}\left(1 - f_{fu,N1}\right) \qquad (14.4\text{-}93)$$

where $f_{fu,N1}$ is the fraction of fuel which is in contact with liquid sodium which is discussed below. The A'_{Pa} was discussed in Eq. 14.4-69. The above heat-transfer coefficient between fuel and liquid sodium is based on the original Cho-Wright model which considered only the thermal resistance in the fuel [14-9]:

$$h_{fu,N1} = CIA1 \cdot k_{fu} / r_{Pa} \tag{14.4-94}$$

where

CIA1 is an input constant. A value of 1.0 is recommended based on the L8 and H6 analyses [14-15, 14-12, 14-6]. However, when Eq. 14.4-94 is compared to analytical solutions, a value between 3 and 5 would be appropriate [14-51].

r_{Pa} is the radius of the fuel particles or droplets (see input quantities *RAFPLA* and *RAFPSM*)

The heat-transfer coefficient between fuel particles and a vapor/gas mixture is calculated from:

$$\frac{1}{h_{fu,vg}} = \frac{1}{h_1} + \frac{(r_{Pa} \cdot 0.1)}{k_{fu}} \tag{14.4-95}$$

where the heat-transfer coefficient h_1, which determines the heat transfer between the fuel surface and the vapor/gas mixture is based on Ref. 14-22 and a Prandtl number of 0.7

$$h_1 = \frac{k_{vg}}{2r_{Pa}} \left[2.0 + 0.54 \cdot \left(\frac{2r_{Pa} \cdot \left| u_{Mi} - u_{fu} \right| \cdot \rho_{vg}}{\mu_{vg}} \right)^{1/2} \right] \tag{14.4-96}$$

where

μ_{vg} = *VIVG*, viscosity of the vapor/gas mixture which is input

$\rho_{vg} = \rho_{Nv} + \rho'_{fi} / \theta_{vg}$

The heat-transfer coefficient h_{fuvg} considers only 1/10 of the possible heat resistance in the fuel particles. This is because the heat capacity of a vapor/gas mixture is so low that only the outer skin of the particles will be affected by the heat loss of the vapor.

The particle surface area per unit of generalized smear volume is

$$A'_{Pa} = N'_{Pa} \cdot 4\pi r_{Pa}^2 \tag{14.4-97}$$

N'_{Pa} = number of fuel particles in a generalized smear volume (see Eq. 14.4-69)

The contact fraction between fuel and liquid sodium is calculated in the following way:

$$f_{fu,N1} = \left(\theta_{N1} / \theta_{ch,op}\right)^{CIA2} \tag{14.4-98}$$

where

CIA2 is an input constant. A value of 2.0 is recommended based on the H6 and L8 analysis [14-15, 14-12, 14-6]. A value of 1.0 appears to be too low, because it implies that the liquid sodium appears to be too low, because it implies that the liquid sodium in a partially voided node is heated at the same rate as if the cell were full of sodium. This is because both the effective fuel surface area and the sodium mass (and thus, the sodium heat capacity) are reduced by the same factor in this case.

When the fuel vapor pressure of the moving fuel is above 10^{-2} MPa, fuel vapor condensation on liquid sodium is considered. The heat flow rate per unit of temperature and unit of generalized smear volume is

$$H_{fv,N1} = \begin{cases} 0 & \text{if } P_{fv} < 10^{-2}\ MPa \\ \left[\mathrm{CFCOFV}\cdot\left(\mathrm{f}\cdot \mathrm{A}'_{\mathrm{cl}} + A'_{sr}\right)\cdot \dfrac{\theta_{vg}}{\theta_{ch,op} - \theta_{Na,fm}}\right] & \text{if } P_{fv} > 10^{-2}\ MPa \end{cases} \tag{14.4-98a}$$

where

P_{fv} = fuel vapor pressure

$CFCOFV$ = fuel vapor condensation coefficient which is input

f = is a multiplier which is zero when $\theta_{fm,cl} = 0$ and 1 when $\theta_{fm,cl} > 0$

$h_{fu,N1}$ and A'_{Pa} are described in Eqs. 14.4-94 and 14.4-97.

This is a rather simple formulation that is at the one extreme limited by the condensation on liquid sodium and at the other extreme by the heat resistance in the fuel droplets.

14.4.3.4.2.2 Fuel-to-Coolant Heat Transfer in the Annular Fuel Flow Regime

In this fuel flow regime, the contact area between the fuel and the sodium is significantly reduced from that in the particulate regime. The heat flow rate per unit of temperature and per unit of generalized smear volume is calculated from

$$H_{fu,Na} = A'_{fu} \cdot \left(\frac{1}{1/h_1 + 1/h_2}\right) \tag{14.4-99}$$

where

A'_{fu} is the surface area of the molten fuel film per unit of the generalized smear volume which is calculated from:

$$A'_{fu} = \left(A'_{cl} + A'_{sr}\right) \cdot \left(CFMFCL + CFFFCL \cdot CFMFFF\right) \tag{14.4-99a}$$

where

$$CFMFCL = CFFUCL - CFFFCL \tag{14.4-100}$$

i.e., *CFMFCL* is the fraction of the cladding covered by molten fuel. Regarding *CFFUCL*, see Eq. 14.4-74; for *CFFFCL*, see Eq. 14.4-79a.

CFMFFF = fraction of the frozen fuel perimeter covered by molten fuel (see Eq. 14.4-77).

The term h_1 in Eq. 14.4-99 is the heat-transfer coefficient between the bulk of the moving fuel film and the surface of the moving film. It is based on the Deissler correlation [14-23, 14-22] and it is very similar to Eq. 14.2-28, except that a different hydraulic diameter and a different Reynolds number are used (see derivation of Eq. 14.2-29).

$$h_1 = \frac{1}{D_{fu}} \cdot \mu_{fu,liq} \cdot C_{p,fu} \cdot CIA3 \left(\mathrm{Re}_{fu,Mi}\right)^{0.8} \tag{14.4-101}$$

where

$\mu_{fu,liq}$ = liquid fuel viscosity for which the input constant VIFULQ is used

$C_{p,fu}$ = liquid fuel specific heat for which the input constant CPFU is used

*CIA*3 = input constant (see Eq. 14.2-29)

$$D_{fu} = 4 \cdot ARMF / \left(PECH \cdot CFFUCL\right) \tag{14.4-101a}$$

where

ARMF= cross-sectional area of moving fuel per pin (see Eq. 14.4-71)

PECH = channel perimeter associated with one pin (see Eq. 14.4-73)

CFFUCL = fraction of the channel perimeter covered by fuel (see Eq. 14.4-74)

$$\mathrm{Re}_{fu,Mi} = \frac{\rho'_{fu}}{\theta_{fu}} \cdot \frac{\left|u_{Mi,i} - u_{fu,i}\right| + \left|u_{Mi,i+1} - u_{fu,i+1}\right|}{2} \cdot \frac{D_{fu}}{\mu_{fu,liq}} \qquad (14.4\text{-}102)$$

The value of the heat-transfer coefficient h_2 in Eq. 14.4-99 for sodium void fractions less than the input value *CIA*4 is

$$h_2 = HCFFMI \quad \text{for } \alpha_{Na} < CIA4 \qquad (14.4\text{-}102a)$$

where

HCFFMI is an input variable which is the convective heat-transfer coefficient between the moving fuel film surface and the sodium droplet/vapor gas mixture

For sodium void fractions larger than *CIA*4, an interpolation between the above value and a heat-transfer coefficient between the fuel film and a pure vapor/gas mixture is done similarly to the one in Eq. 14.4-88:

For $\alpha_{Na} > CIA4$

$$h_2 = \frac{\left[HCFFMI \cdot \left(1 - \alpha_{Na}\right) + h_{vg,fu}\left(\alpha_{Na} - CIA4\right)\right]}{\left(1 - CIA4\right)} \qquad (14.4\text{-}103)$$

α_{Na} = sodium void fraction

*CIA*4 = input void fraction above which the above interpolation 14.4-103 is done. In the L8 and H6 analyses [14-15, 14-12] a value of 0.5 was used for CIA4, because no other option was available at that time. Using a higher CIA4 should boost the pure vapor/gas temperatures which appeared to be on the low side in the L8 and H6 analyses. A higher value may actually lead to a better agreement with the downward voiding observed in the L8 experiment.

$h_{vg,fu}$ = is the heat transfer coefficient between the vapor/gas mixture and the mobile fuel which is based on the same Dittus-Boelter correlation as used for $h_{vg,cl}$ (see Eq. 14.4-89).

$$h_{vg,fu} = 0.02 \cdot \frac{k_{vg}}{D_{Mi}} \cdot \left(\mathrm{Re}_{vg,fu}\right)^{0.8} \qquad (14.4\text{-}104)$$

where

$$\mathrm{Re}_{vg,fu} = \frac{D_{Mi} \cdot \rho_{vg} \cdot \left| u_{Mi,i} - u_{fu,i} + u_{Mi,i+1} - u_{fu,i+1} \right|}{VIVG \cdot 2} \tag{14.4-105}$$

$$\rho_{vg} = \begin{cases} \rho_{Nv} + \rho'_{fi} / \theta_{vg} & \text{for } \alpha_{Na} < 1 \\ \rho'_{Mi} / \left(\theta_{ch,op} - \theta_{fu} \right) & \text{for } \alpha_{\mathrm{Na}} = 1 \end{cases}$$

$VIVG$ = viscosity of the vapor/gas mixture which is input

D_{Mi} = hydraulic diameter for the mixture flow

Equation 14.4-104 comes from the Dittus-Boelter equation in which a Prandtl number to the power 0.4 appears [14-50]. Since Prandtl numbers for gases are in a narrow range and since the exponent of the Prandtl number further minimizes the dependency of the heat transfer on Prandtl numbers, an average Prandtl number of 0.686 is used to arrive at Eq. 14.4-105.

The fuel vapor to the sodium/gas mixture heat flow rate term per unit of temperature and unit of smear volume is assumed to be limited by the heat resistance in the molten fuel film:

$$H_{fv,Na} = \begin{cases} 0 & \text{if } P_{fv} < 10^{-2}\ MPa \\ h_1 \cdot A'_{fu} & \text{if } P_{fv} > 10^{-2}\ MPa \end{cases} \tag{14.4-105a}$$

h_1, A'_{fu} are described in Eqs. 14.4-99 and 14.4-99a

14.4.3.4.2.3 Fuel Crust-to-Sodium/Fission-gas Heat Transfer for the Case of Particulate or Annular Fuel Flow Regime

The heat-transfer coefficient between the fuel crust and a two-phase sodium/fission-gas mixture is calculated from

$$\frac{1}{h_{ff,Mi}} = \frac{1}{h_1} + \frac{TKFF}{k_{fu} \cdot 2} \tag{14.4-106}$$

where

$TKFF$ is the frozen fuel crust thickness (see Eq. 14.4-76)

For $\alpha_{Na} < CIA4$, $h_1 = HCFFMI$ (see Eq. 14.4-102)

For $\alpha_{Na} > CIA4$, h_1 is based on an interpolation between $HCFFMI$ and a single-phase gas/vapor heat-transfer coefficient (see also Eq. 14.4-103)

$$h_2 = \frac{\left[HCFFMI \cdot \left(1-\alpha_{Na}\right) + h_{vg,os}\left(\alpha_{Na} - CIA4\right)\right]}{\left(1-CIA4\right)} \tag{14.4-107}$$

where

$$h_{vg,os} = 0.02\frac{k_{vg}}{D_{Mi,ff}}\left(\mathrm{Re}_{vg,ff}\right)^{0.8} \tag{14.4-108}$$

where

$$D_{Mi,ff} = \frac{D_{ch}}{\left(1-\theta_{ff}/\theta_{cf}\right)} - 2\cdot TKFF \tag{14.4-108a}$$

D_{ch} is hydraulic diameter of the open coolant channel (see Eq. 14.4-57a). By dividing it by the term in the brackets, one gets back to the original hydraulic diameter.

$TKFF$ is the thickness of the frozen fuel crust (see Eq. 14.4-76)

$$\mathrm{Re}_{vg,ff} = \frac{D_{Mi}\cdot\rho_{vg}\cdot\left|u_{Mi.i}+u_{Mi,i+1}\right|}{\mu_{vg}\cdot 2} \tag{14.4-109}$$

The latter Reynolds number calculation is very similar to that in Eq. 14.4-105 and several variables are explained there.

The fuel crust-to-sodium/fission-gas heat flow rate per unit temperature and per unit of generalized smear volume is split into a heat transfer to the crust on the cladding and the crust on the structure because temperature are calculated for both crusts.

$$H_{ffcl,Na} = h_{ff,Mi}\cdot A'_{cl}\cdot CFFFCL\cdot\left(1-CFMFFF\right) \tag{14.4-110}$$

$$H_{ffsr,Na} = h_{ff,Mi}\cdot A'_{sr}\cdot CFFFCL\cdot\left(1-CFMFFF\right) \tag{14.4-111}$$

where

$CFFFCL$ is the fraction of the channel perimeter covered by frozen fuel (see Eq. 14.4-79a)

CFMFFF is the fraction of CFFFCL covered by moving fuel, which is zero in the particulate fuel flow regime (see Eq. 14.4-77)

14.4.3.4.2.4 Fuel-to-Sodium/Fission-gas Heat Transfer in the Bubbly Fuel Flow Regime

The description of this heat-transfer process will require some more investigation. On the one hand, the bubble temperatures should quickly adjust to the surrounding fuel temperature. On the other hand, if liquid sodium is entrapped by the bubbly fuel, the achievement of high temperatures will lead to exaggerated sodium vapor pressures that will rapidly disperse fuel. This may be realistic but the premise that significant amounts at liquid sodium can be entrapped by a bubbly fuel flow is still unclear. Sudden fuel dispersal of denser fuel masses such as observed in the SLSF experiment P2 [14-52] or in the TREAT tests L3 and L4 [14-53, 14-54] may have been due to non-prototypical lateral injections of liquid sodium into the molten fuel masses. (However, such lateral injections of liquid sodium may be prototypical in the transition phase.) The current heat-transfer calculation in PLUTO2 is relatively straightforward and can be limited via an input parameter.

For the calculation of the heat transfer between fuel and the sodium/fission-gas mixture in the bubbly fuel flow regime, an estimate of the bubble radius is needed. For the maximum bubble radius, it is assumed that

$$r_{bb,mx} = D_{Mi} \cdot 0.5$$

This implies that a string of spherical bubbles is assumed for larger void fractions, rather than one or a few elongated bubbles. For decreasing void fractions, the bubble radius is assumed to be:

$$r_{bb} = r_{bb,mx} \cdot \left[0.05 + (1 - 0.05) \cdot \exp\left(- \frac{1 - CIBBIN - \alpha_{bb}}{\alpha_{bb}} \right) \right] \qquad (14.4\text{-}112)$$

where

CIBBIN is the input void fraction above which a bubbly fuel regime can be initiated.

$$\alpha_{bb} = \left(\theta_{ch,op} - \theta_{fu} \right) / \theta_{ch,op}$$

When α_{bb} goes to zero, r_{bb} goes to $r_{bb,mx} \cdot 0.05$. This is the assumed minimum bubble radius. For the heat-transfer coefficient between bubbly fuel and the two-phase mixture, it is assumed that

$$\frac{1}{h_{fu,Mi}} = \frac{1}{HCFUBB} + \frac{r_{bb}}{k_{Mi}} \qquad (14.4\text{-}113)$$

where

HCFUBB is an input heat-transfer coefficient describing the heat transfer between the bulk of the fuel and the bubble surfaces. It is also used to control the heat transfer between fuel vapor and the mixture (see Eq. 14.4-116a).

and

$$k_{Mi} = \frac{\theta_{N1} \cdot CDNL + \theta_{vg} \cdot CDVG}{\theta_{N1} + \theta_{vg}} \tag{14.4-114}$$

where

CDNL, CDVG
are input conductivities for liquid sodium and the vapor/fission-gas mixture, respectively.

The heat flow rate per unit of temperature and unit of generalized smear volume is:

$$H_{fu,Mi} = A'_{fu,Mi} \cdot h_{fu,Mi} \tag{14.4-115}$$

where

$$A'_{fu,Mi} = 3 \cdot \left(\theta_{ch,op} - \theta_{fu}\right) / r_{bb} \tag{14.4-116}$$

which is the total bubble surface area in a unit of smear volume. $\left(\theta_{ch,op} - \theta_{fu}\right)$ is the total bubble volume in a unit of generalized smear volume.

The heat flow rate term between fuel vapor and the bubbles is assumed to be controlled by the input heat-transfer coefficient HCFUBB

$$H_{fv,Mi} = \begin{cases} 0 & \text{for } P_{fv} < 10^{-2}\ MPa \\ HCFUBB \cdot A'_{fu,Mi} & \text{for } P_{fv} > 10^{-2}\ MPa \end{cases} \tag{14.4-116a}$$

14.4.3.4.3 Moving Fuel-to-Cladding, Moving Fuel-to-Structure, and Moving Fuel-to-Fuel-crust Heat Transfer

In the particulate fuel flow regime, no heat transfer between moving fuel and cladding, structure, or fuel crust is considered. However, fuel-vapor condensation on cladding and structure is considered when there is no liquid sodium film left on the cladding or structure. The heat flow rates per unit of temperature and per unit of generalized smear volume are

$$H_{fv,cl} = \begin{cases} 0 & \text{if } P_{fv} < 10^{-2} \text{ MPa or } \theta_{fm,cl} = 0 \\ CFCOFV \cdot A'_{c1} \cdot CFNACL & \text{if } P_{fv} > 10^{-2} \text{ MPa and } \theta_{fm,cl} > 0 \end{cases} \quad (14.4\text{-}117)$$

$$H_{fv,sr} = \begin{cases} 0 & \text{if } P_{fv} < 10^{-2} \text{ MPa or } \theta_{fm,sr} = 0 \\ CFCOFV \cdot A'_{sr} \cdot CFNACL & \text{if } P_{fv} > 10^{-2} \text{ MPa and } \theta_{fm,sr} > 0 \end{cases} \quad (14.4\text{-}117a)$$

where

CFNACL = 1-*CFFFCL* (see Eq. 14.4-77)

CFCPOFV = fuel vapor condensation coefficient, which is input.

In the annular and bubbly fuel flow regimes, very similar expressions are used for the heat flow rate terms. The difference lies in the different values for the contact coefficients and the Reynolds numbers that are used.

The heat-transfer coefficient for the moving fuel-to-cladding and moving fuel-to-structure coefficient is the same and it is also used for the calculation of the moving fuel-to-fuel-crust heat transfer. It is based on the Deissler correlation [14-23, 14-22] which was already discussed earlier (see Eq. 14.2-28). However, a conduction term was added to this correlation because it is not designed for very slow or stagnant flow conditions. For the partial or fully annular fuel flow, the following relationship holds:

$$h_{fu,cl} = \frac{1}{D_{fu}} \cdot CIA3 \cdot VIFULQ \cdot CPFU \cdot \left(\mathrm{Re}_{fu}\right)^{0.8} + 2\frac{k_{fu}}{TKFU} \quad (14.4\text{-}118)$$

where

TKFU is the thickness of the moving fuel film (see eq. 14.4-75). In the above equation, this film thickness is not allowed to become smaller than 1/10 of the channel hydraulic diameter. Thus, the additional term will not dominate the equation except for very slow or stagnant flow conditions.

*CIA*3, *VIFULQ, CPFU*
are all input constants, which were explained in Eq. 14.2-28.

D_{fu} is the hydraulic diameter of moving fuel film (see Eq. 14.4-101).

$$\mathrm{Re}_{fu} = \frac{\rho_{fu} \cdot D_{fu} \cdot \left| u_{fu,i} + u_{fu,i+1} \right|}{\mu_{fu,liq} \cdot 2} \tag{14.4-119}$$

In the bubbly fuel flow regime, pretty much the same form of the heat-transfer coefficient is used. However, some of the terms are evaluated differently:

$D_{fu} = D_{ch}$

$TKFU = D_{ch}/4$

where D_{cg} is the open channel hydraulic diameter, which takes the frozen crusts into account (see Eqs. 14.4-57a and 14.4-68).

If the energy of the moving fuel film is below the solidus energy, which is possible if solid fuel gets released from an underlying melting cladding, only the pure conduction part of Eq. 14.4-118 will be used. The thickness TKFU is, in this case, always calculated from Eq. 14.4-75 and no lower limit is assumed for it as in Eq. 14.4-118. The calculation of this special heat-transfer coefficient and of the related heat flow rates are performed near the end of PLMISC, whereas the regular coefficients and flow rates are done in the middle section of PLMISC.

The heat flow rates per unit temperature and per unit of generalized smear volume are

$$H_{fu,cl} = h_{fu,c} \cdot A'_{cl} \cdot CFMFCL \tag{14.4-120}$$

and

$$H_{fu,sr} = h_{fu,cl} \cdot A'_{sr} \cdot CFMFCL \tag{14.4-121}$$

where

$$CFMFCL = 1 - CFFUCL - CFFFCL. \tag{14.4-122}$$

CFMFCL is the fraction of the channel perimeter covered with moving fuel (see Eqs. 14.4-74 and 14.4-77). In the case of the bubbly fuel flow regime.

$$CFMFCL = 1 - CFFFCL \tag{14.4-123}$$

because all the structure or cladding which is not covered by frozen fuel is assumed to be in contact with moving fuel in this case.

For the fuel vapor condensation on cladding and structure, heat flow rate terms per unit temperature and per unit smear volume are used which are similar to Eqs. 14.4-117 and 14.4-117a:

$$H_{fv,cl} = \begin{cases} 0 & \text{if } P_{fv} < 10^{-2} \text{ MPa} \\ CFCOFV \cdot A'_{cl} \cdot CFNACL & \text{if } P_{fv} > 10^{-2} \text{ MPa} \end{cases} \quad (14.4\text{-}124)$$

$$H_{fv,sr} = \begin{cases} 0 & \text{if } P_{fv} < 10^{-2} \text{ MPa} \\ CFCOFV \cdot A'_{sr} \cdot CFNACL & \text{if } P_{fv} > 10^{-2} \text{ MPa} \end{cases} \quad (14.4\text{-}124a)$$

where

$CFNACL = 1 - CFFUCL$ (see Eq. 14.4-74).

The heat-transfer coefficient between moving fuel and a frozen fuel crust is calculated form

$$\frac{1}{h_{hu,ff}} = \frac{1}{h_{fu,cl}} + \frac{2 \cdot k_{fu}}{TKFF} \quad (14.4\text{-}125)$$

where

$TKFF$ = the thickness of the frozen fuel crust (see Eqs. 14.4-76 and 14.4-79).

k_{fu} = $CDFU$ which is the input fuel conductivity

The heat flow rates per unit temperature and per unit of smear volume for the annular flow regimes are

$$H_{fu,ffcl} = h_{fu,ff} \cdot A'_{cl} \cdot CFFFCL \cdot CFMFFF \quad (14.4\text{-}126)$$

$$H_{fu,ffsr} = h_{fu,ff} \cdot A'_{sr} \cdot CFFFCL \cdot CFMFFF \quad (14.4\text{-}127)$$

where

$CFFFCL$: see Eq. 14.4-77

$CFMFFF$: see Eq. 14.4-110

In the bubbly fuel flow regime

$$H_{fu,ffcl} = h_{fu,ff} \cdot A'_{cl} \cdot CFFFCL \tag{14.4-128}$$

$$H_{fu,ffsr} = h_{fu,ff} \cdot A'_{sr} \cdot CFFFCL \tag{14.4-129}$$

All the frozen fuel is assumed to be covered with moving fuel in the bubbly flow regime. Therefore, *CFMFFF* is 1.0 in this case.

The multiplication with the A's in the above equations is not done in subroutine *PLMISC*, but in *PLTECS* which is called next in the calling sequence.

14.4.3.5 Partial Momentum exchange Terms Between Annular Fuel and the Sodium/Fission-gas Mixture

The friction coefficient *CFFRMF* for the calculation of the drag between a moving fuel film and the sodium/gas mixture is calculated from

$$CFFRMF = AFRV \cdot \left(\mathrm{Re}_{Mi,fu}\right)^{BFRV} \cdot \left(CFMFCL + CFFFCL \cdot CFMFFF\right) \tag{14.4-130}$$

where

AFRV, BFRV = input constants

$$\mathrm{Re}_{mi,fu} = \frac{D_{ch} \cdot \left| u_{Mi} - u_{fu} \right| \cdot \rho'_{Mi}}{VIVG \cdot \left(\theta_{vg} + \theta_{N1}\right)} \tag{14.4-131}$$

CFMFCL = CFFUCL – CFFFCL

CFFUCL: see Eq. 14.4-74

CFFFCL: see Eq. 14.4-79a

CFMFFF: see Eq. 14.4-77

In subroutine *PLMISC*, a contact coefficient that gives the fraction of the cladding and fuel crust in contact with the moving fuel is also set. It is needed in *PLMOCO* for the calculation of the fuel friction term. In the annular fuel flow regime, it is:

$$CTFRFU = CFMFCL + CFMFFF \cdot CFFFCL \tag{14.4-132}$$

The terms on the right-hand side of this equation were also used in Eq. 14.4-130.

If the bubbly fuel flow regime holds:

$$CTFRFU = 1 \tag{14.4-133}$$

14.4.4 Mobile Fuel and Fuel Crust Energy Equations

14.4.4.1 Mobile Fuel Energy Equation

The mobile fuel energy equation, which is solved at the end of subroutine *PLMISC*, includes only source and sink terms due to heat transfer. The energy changes due to fuel plateout and the energy changes due to the addition of released or remelting fuel crusts are taken into account in subroutine *PLFREZ* which was discussed in Section 14.4.3.2. The energy change due to the addition of fuel ejected from the pins is taken into account in subroutine *PL1PIN*.

The mobile fuel energy equation in differential form reads:

$$\begin{aligned}&\frac{\partial}{\partial t}\left(\rho_{fu}\, e_{fu}\, A_{fu} + \rho_{fv}\, e_{fv}\, A_{vg}\right) + \frac{\partial}{\partial z}\left(\rho_{fu}\, e_{fu}\, u_{fu}\, A_{fu} + \rho_{fv}\, e_{fv}\, u_{Mi}\, A_{vg}\right)\\ &= -\sum_{k} h_{fu,k}\, A^{\ell}_{fu,k} \cdot \left(T_{fu} - T_{k}\right)\\ &\quad -\sum_{l} h_{fv,\ell}\, A^{\ell}_{fv,\ell} \cdot \left(T_{fu} - T_{\ell}\right) + Q \cdot \left(A_{fu}\, \rho_{fu} + A_{vg}\, \rho_{fv}\right)\end{aligned} \qquad (14.4\text{-}134)$$

where

A_{fu}, A_{vg} = cross sectional areas of the mobile liquid or solid fuel and of the vapor/gas mixture, respectively

$A^{\ell}_{fu,k}$ = interaction area between moving fuel and component k per unit length

$A^{\ell}_{fv,\ell}$ = interaction areas between fuel vapor and component ℓ per unit length

ρ_{fv} = saturated fuel vapor density

ρ_{fu} = theoretical density of liquid or solid fuel

e_{fu} = internal energy of liquid or solid fuel

$$e_{fv} = e_{fu} + \lambda_{fv} \qquad (14.4\text{-}135)$$

λ_{fv} = fuel heat of vaporization

Q = fission heat source per kg of fuel that is calculated from Eq. 14.2-25.

However, F_{POWER} is always 1 in this case.

By inserting Eq. 14.4-135 into the first term of Eq. 14.4-134, one obtains:

$$\frac{\partial}{\partial t}(\quad) = \frac{\partial}{\partial t}\left[\left(\rho_{fu}\, A_{fu} + \rho_{fv}\, A_{vg}\right)\cdot e_{fu} + \rho_{fv}\, A_{vg}\, \lambda_{fv}\right] \tag{14.4-136}$$

By inserting Eq. 14.4-136 into 14.4-134 and dividing the resulting equation by *AXMS*, and by also using the definitions of the generalized smear densities, one arrives at:

$$\begin{aligned}&\frac{\partial}{\partial t}\left(\rho'_{fuch}\, e_{fu}\right) + \frac{\partial}{\partial t}\left(\rho'_{fv}\, \lambda_{fv}\right) + \frac{\partial}{\partial z}\left(\rho'_{fu}\, e_{fu}\, u_{fu} + \rho'_{fv}\, e_{fv}\, u_{Mi}\right)\\ &\quad = -\sum_k h_{fu,k}\, A'_{fu,k}\cdot\left(T_{fu} - T_k\right) - \sum_\ell h_{fv,\ell}\, A'_{fu,k}\cdot\left(T_{fu} - T_\ell\right) + Q\,\rho'_{fu}\end{aligned} \tag{14.4-137}$$

where

ρ'_{fuch} = $\rho'_{fu} = \rho'_{fv}$

ρ'_{fu} = generalized smear density of the moving liquid or solid fuel

ρ'_{fv} = generalized smear density of fuel vapor

$A'_{fu,k}$ = interaction area between moving liquid or solid fuel and component *k* in a unit of generalized smear volume

$A'_{fv,\ell}$ = interaction area between fuel vapor and component ℓ in a unit of generalized smear volume

The different heat flow rates which are summed up in Eq. 14.4-137 can be written as:

$H_{fu,na}\cdot(T_{fu} - T_{Ta})$: see Eq. 14.4-93 for particulate fuel flow and Eq. 14.4-99 for annular flow and Eq. 14.4-115 for bubbly flow

$H_{fu,cl}\cdot(T_{fu} - \mathrm{T}_{cl,os})$: see Eqs. 14.4-120 and 14.4-122. For particulate flow this term is zero.

$H_{fu,sr}\cdot(T_{fu} - T_{sr,os})$: see Eqs. 14.4-121 and 14.4-122. For particulate flow this term is also zero.

$H_{fu,ffcl}\cdot(T_{fu} - T_{ffcl})$: see Eqs. 14.4-126, 14.4-128

$H_{fu,ffsr}\cdot(T_{fu} - T_{ffsr})$: see Eqs. 14.4-127, 14.4-129

$H_{fv,N1}\cdot(T_{fu} - T_{Na})$: see Eqs. 14.4-98a, 14.4-105b, and 14.4-116a

$H_{fv,cl}\cdot(T_{fu} - T_{cl,os})$: see Eqs. 14.4-177 and 14.4-125; in the bubbly flow regime this term is zero

$H_{fv,sr} \cdot (T_{fu} - T_{sr,os})$: see Eqs. 14.4-117a and 14.4-124a; in the bubbly flow regime this term is zero

where *H* is heat transfer coefficient times heat transfer area.

The main part of the energy equation for the moving fuel is solved at the end of subroutine *PLMISC*. However, heat-transfer terms between moving fuel and the frozen crust on cladding and structure are only included in subroutine *PLTECS* which is called after *PLMISC*.

Since the moving fuel energy equation is solved explicitly (i.e., using only beginning-of-time step values in the convective terms and in the heat-transfer terms), it is possible to solve this equation for the fuel energy rather than for fuel temperature. This has the advantage that the heat of fusion can be easily taken into account. The moving fuel energy is stored in a permanent array in *PLUTO*2, and fuel temperatures, which are needed in the heat-transfer terms and for calculating fuel vapor pressure, are obtained from function subroutine *TEFUEG*. The equations solved in this subroutine are the following:

If $e_{fu} < e_{fu,sol}$

$$C_{p,fu} = CPFU \tag{14.4-138}$$

$$T_{fu} = T_{fu,sol} - \left(e_{fu,sol} - e_{fu}\right) / C_{p,fu} \tag{14.4-139}$$

If $e_{fu,sol} < e_{fu} < e_{fu,liq}$

$$C_{p,fu} = \left(e_{fu,liq} - e_{fu,sol}\right) / \left(T_{fu,liq} - T_{fu,sol}\right) \tag{14.4-140}$$

$$T_{fu} = T_{fu,sol} + \left(e_{fu} - e_{fu,sol}\right) / C_{p,fu} \tag{14.4-141}$$

If $e_{fu,liq} < e_{fu}$

$$C_{p,fu} = CPFU \tag{14.4-142}$$

$$T_{fu} = T_{fu,liq} + \left(e_{fu} - e_{fu,liq}\right) / C_{p,fu} \tag{14.4-143}$$

The function subroutine TEFUEG is called in subroutine PLSET2, which is called whenever control is transferred to PLUTO2 and which sets all temporary arrays such as the fuel temperature. Moreover, it is called for all nodes containing fuel at the end of subroutine PLTECS after nearly all the updating of the moving fuel energy has been done. In nodes receiving fuel that is ejected from the pins, the fuel energy is further

updated and function subroutine TEFUEG is used again for further updating the fuel temperatures in such nodes.

For the numerical solution of Eq. 14.4-137, the main storage term is rewritten:

$$\frac{\partial}{\partial t}\left(\rho'_{fuch}\, e_{fu}\right) = \rho'_{fuch} \cdot \frac{\partial}{\partial t} e_{fu} + \frac{\partial \rho'_{fuch}}{\partial t} \cdot e_{fu} \tag{14.4-144}$$

In finite difference form, the above equation is written as

$$\frac{\Delta\left(\rho'_{fuch}\, e_{fu}\right)}{\Delta t} = \rho'^{n+1}_{fuch} \cdot \frac{\Delta e_{fu}}{\Delta t} + e^{n}_{fu} \cdot \frac{\Delta \rho'_{fuch}}{\Delta t} \tag{14.4-144a}$$

which can be arrived at by writing

$$\Delta\left(\rho'_{fuch}\, e_{fu}\right) = \left(\rho'_{fuch} + \Delta\rho'_{fuch}\right) \cdot \left(e_{fu} + \Delta e_{fu}\right) - \rho'_{fuch} \cdot e_{fu}$$

The derivative of the generalized smear density in Eq. 14.4-144a is

$$\frac{\Delta \rho'_{fuch}}{\Delta t} = -\frac{\Delta\left[\left(\rho'_{fuch} - \rho'_{fv}\right) u_{fu}\right]}{\Delta z} - \frac{\Delta\left(\rho'_{fv}\, u_{Mi}\right)}{\Delta z} \tag{14.4-145}$$

which is the fuel mass conservation equation without source or sink terms. Since the energy Eq. 14.4-137 does not include loss or gain terms due to mass sinks or sources (these are separately included in the fuel freezing and crust release calculations in subroutine *PLFREZ* and in the fuel ejection calculation in subroutine *PLIPIN*), the density changes in Eq. 14.4-137 are solely due to mass convection. By writing Eq. 14.4-137 in finite difference form and by including Eq. 14.4-144a and Eq. 14.4-145, one arrives at

$$\begin{aligned} \rho'_{fuch} \frac{\Delta e_{fu}}{\Delta t} + \lambda_{fv} \frac{\partial \rho'_{fv}}{\partial T} \frac{\Delta T}{\Delta t} &= e_{fu} \cdot \frac{\Delta\left(\rho'_{pu}\, u_{fu}\right)}{\Delta z} + e_{fu} \cdot \frac{\Delta\left(\rho'_{pv}\, u_{Mi}\right)}{\Delta z} \\ &- \frac{\Delta\left(\rho'_{pu}\, e_{fu}\, u_{fu}\right)}{\Delta z} - \frac{\Delta\left(\rho'_{fv}\, e_{fv}\, u_{Mi}\right)}{\Delta z} \\ &+ \sum_{k} H_{fu,k} \cdot \left(T_{fu} - T_{k}\right) + \sum_{\ell} H_{fv,\ell}\left(T_{fu} - T_{\ell}\right) + Q' \rho_{fu} \end{aligned} \tag{14.4-146}$$

In the second term of the left-hand side, it was assumed that the heat of vaporization is constant over the range considered (3700-5000 K). The temperature change in the second term on the left-hand side of Eq. 14.4-146 can be related to the liquid energy change by

$$\frac{\Delta T}{\Delta t} = \frac{\Delta e_{fu}}{\Delta t \cdot C_{p,fu}} \tag{14.4-146a}$$

By using Eq. 14.4-146a in Eq. 14.4-146, the left-hand side of this equation can be rewritten:

$$\rho'_{fuch} \frac{\Delta e_{fu}}{\Delta t} + \lambda_{fu} \cdot \frac{\partial' \rho_{fv}}{\partial T} \frac{\Delta T}{\Delta t} = \frac{\Delta e_{fu}}{\Delta t} \left(\rho'_{fuch} + \frac{\lambda_{fv}}{C_{p,fu}} \frac{\partial \rho'_{fv}}{\partial T} \right) \tag{14.4-147}$$

The convective terms are evaluated by using full donor cell differencing. The first two terms on the right-hand side are actually the convective fluxes of the fuel mass conservation equation (see Eq. 14.4-34) multiplied by e_{fu} (note that in Eq. 14.4-34, ρ'_{fu} is written as $\rho'_{fuch} - \rho'_{fv}$). These convective mass fluxes are used in the energy equation to evaluate the first two terms on the right-hand side of Eq. 14.4-146. The convective energy flux of the solid or liquid fuel is evaluated in the following way (see the schematic below Eq. 14.4-30).

$$\frac{\Delta\left(\rho'_{fu} e_{fu} u_{fu}\right)}{\Delta z_i} = \left[\left(\rho'_{fu} e_{fu} u_{fu}\right)_{i+1/2} - \left(\rho'_{fu} e_{fu} u_{fu}\right)_{i-1/2}\right] / \Delta z_i \tag{14.4-148}$$

The first term on the right-hand side is evaluated in the following way:

$$\left(\rho'_{fu} e_{fu} u_{fu}\right)_{i+1/2} = \begin{cases} \rho'_{fu,i} e_{fu,i} u_{fu,i+1} & \text{for } u_{fu,i+1} > 0 \\ \rho_{fu,i+1} e_{fu,i+1} u_{fu,i+1} & \text{for } u_{fu,i+1} < 0 \end{cases} \tag{14.4-149}$$

The second term on the right-hand side is evaluated correspondingly. The *FORTRAN* name for the convective energy fluxes is *COFUOS* (I). They are calculated in the subroutine solving the mass conservation equations, *PLMACO*. Equation 14.4-146 is solved for Δe_{fu} at the end of subroutine *PLMISC*. As mentioned earlier, the heat flow terms between fuel and the frozen crust on the cladding and on the structure are only later included in subroutine *PLTECS*, which is called after *PLMISC*. After these additional updates to the energy equations have been made, the fuel temperature is calculated by using function subroutine *TEFUEG* (see Eqs. 14.4-138-14.4-143).

14.4.4.2 Fuel Crust Energy Equations

The energy equations for the stationary fuel crusts on the cladding and structure are solved in subroutine PLTECS (PLUTO2 TEMPERATURE CALCULATION OF CLADDING AND STRUCTURE). The calculation of the fuel crust temperatures is done at the beginning of this routine and provides heat flow rates per unit temperature and unit

smear volume for the cladding and structure calculation which make up the bulk of this routine and are described in Section 14.5.

Only the temperatures of the fuel crusts on cladding and structure (one for each crust) are stored in permanent arrays in PLUTO2. The beginning of time-step energy of the fuel crust on cladding is determined form the beginning of time-step temperature by

$$e^n_{ffcl} = \begin{cases} e_{fu,sol} - \left(T_{fu,sol} - T^n_{ffcl}\right) \cdot C_{p,fu} & \text{for } T_{ffcl} < T_{fu,sol} \\ \text{EGFUTE}\left(T^n_{ffcl}\right) & \text{for } T_{ffcl} > T_{fu,sol} \end{cases} \tag{14.4-150}$$

where

$C_{p,fu}$ = CPFU which is the input value of the fuel specific heat.

EGFUTE
: is a function subroutine to convert form temperatures to energies. It is could be used over the entire temperature range of the fuel, but by calling it only for the rare case when the crust is above the solidus temperature, computer time is save.

The change in the internal energy of the cladding fuel crust per PLUTO2 time step is calculated from:

$$\begin{aligned} \Delta e_{ffc1} \cdot \rho'_{fufm} \cdot f_{ffcl} / \Delta t = Q \cdot \rho'_{fufm} \cdot f_{ffcl} - H_{ff,Na} \cdot \left(T_{ffcl} - T_{Na}\right) \\ - H_{ff,fu} \cdot \left(T_{ffcl} - T_{fu}\right) - H_{ff,cl} \cdot \left(T_{ffcl} - T_{cl,os}\right) \end{aligned} \tag{14.4-151}$$

where

f_{ffcl} = $\dfrac{A'_{c1}}{A'_{c1} + A'_{sr}}$ is the fraction of all the fuel crust which is on the cladding

$H_{ff,Na}$ has been described in Eq. 14.4-110.

$H_{ff,fu}$ has been described in Eq. 14.4-111.

$$H_{ff,cl} = \frac{k_{fu} \cdot 2}{TKFF} \cdot A'_{cl} \cdot CFFFCL \tag{14.4-151a}$$

where

TKFF is the thickness of the frozen fuel crust

CFFFCL is the fraction of the cladding perimeter covered by fuel crust (see Eq. 14.4-76)

After the new internal energy has been calculated from

$$e_{ffcl}^{n+1} = e_{ffcl}^{n} + \Delta e_{ffcl} \tag{14.4-152}$$

the new temperature is calculated from

$$T_{ffc1}^{n+1} = \begin{cases} T_{fu,sol} - e_{ffcl}^{n+1} / C_{p,fu} & \text{for } e_{ffcl} < e_{fu,sol} \\ \text{TEFUEG}\left(e_{ffcl}^{n+1}\right) & \text{for } e_{ffcl} > e_{fu,sol} \end{cases} \tag{14.4-153}$$

The function subroutine TEFUEG for converting from fuel energies to temperatures is only called for the rate case when the crust energy is above the solidus energy in order to save computer running time.

The calculation of the structure crust temperature, T_{ffsr}, is done correspondingly. In this case, the fraction of the crust that is on the structure is assumed to be:

$$f_{ffsr} = A'_{sr} / \left(A'_{sr} + A'_{cl}\right) \tag{14.4-154}$$

14.4.5 Sodium/Fission-gas Energy Equation and Channel Pressure Calculation

The subroutine PLNAEN (PLUTO NA ENERGY) which calculates the sodium temperature change for the two-phase sodium/fission-gas mixture and the single phase sodium/vapor/fission-gas mixture is nearly the same as the LEVITATE sodium energy equation (see section 16.4.3.5) and therefore is not described in detail here. Only the slight differences between the two routines will be discussed.

One difference is due to the fact that LEVITATE treats more components than PLUTO2. These additional components are the moving molten steel films (designated by subscripts *se*) and the moving fuel and steel chunks (designated by subscript *f1* and *s1*, respectively). Because of the presence of these components, three additional heat-transfer terms appear in the LEVITATE sodium energy subroutine LENAEN.

Another difference between the two sodium energy equations is due to the fact that PLUTO2 treats liquid sodium films on the cladding. This has not yet been incorporated in LEVITATE. In PLUTO2, the convective energy fluxes for the two-phase sodium/gas mixture use sodium densities and sodium qualities which exclude the liquid sodium film. The quality of the moving two-phase mixture in PLUTO2 is

$$x_{Mi} = \rho_{Nv} \cdot \theta_{vg} / \left(\rho'_{Na} - \rho'_{Na,fm}\right) \tag{14.4-155}$$

In LEVITATE, the sodium quality x_{Na} is also based on the above equation, but with $\rho'_{Na,fm} = 0$ in all nodes. It should be noted here that the liquid film treatment in PLUTO2 does not come into the energy equation in other ways because the liquid sodium film is considered to be in thermal equilibrium with the moving sodium in a node.

Subroutine PLNAEN includes most of the PLUTO2 channel pressure calculation. However, an updating is done later in subroutine PL1PIN for cells into which fuel and/or gas is injected. Subroutine PLNAEN includes the calculation of fission-gas pressure, sodium saturation pressure or superheated sodium vapor pressure, fuel vapor pressure, and, if necessary, single-liquid-phase pressure of sodium. LEVITATE does not treat the latter because it is not important for voided channel conditions. LEVITATE has a much more refined fuel vapor pressure calculation than PLUTO2, tub this is not performed in the LEVITATE sodium energy equation LENAEN. Moreover, LEVITATE treats steel vapor pressure. But this is also not calculated in LENAEN.

In single-phase liquid sodium pressures do not play a significant role, PLUTO2 will add up the partial pressures according to Dalton's law:

$$P_{ch} = P_{Nv}\left(T_{Na}\right) + P_{fv}\left(T_{fu}\right) + P_{fi}\left(T_{Na,}\rho_{fi}\right) \tag{14.4-156}$$

In the above equation, the fission-gas pressure contribution is based on the ideal-gas equation (see Eqs. 14.4-157 and 14.4-158). The fission gas is assumed to be always in thermal equilibrium with the two-phase sodium mixture. Therefore, no separate fission-gas temperature appears in the equation-of-state. For sodium void fractions greater than 70%, the fission-gas pressure is calculated from the ideal-gas equation:

$$P_{fi} = R_{fi}\,\rho'_{fi}\,T_{Na} / \theta_{vg,un} \tag{14.4-157}$$

where

R_{fi} = RGAS gas constant for fission gas which is the universal gas constant divided by the averaged molecular weight of xenon, krypton, and helium (the latter is only important for near-fresh fuel)

$\theta_{vg,un}$ is the generalized volume fraction of the vapor gas space when the compressibility of liquid sodium is not taken into account.

For sodium void fractions of less than 70%, the fission-gas pressure calculation takes the sodium compressibility into account. This is done by solving the ideal-gas equation which includes the sodium compressibility:

$$P_{fi} = \frac{R_{fi}\,\rho'_{fi}\,T_{Na}}{\theta_{vg,un} + \theta_{N1}\,K_{N1}\,P_{fi}}$$

The positive solution of this quadratic equation is

$$P_{fi} = \frac{-\theta_{vg,un} + \left[\theta_{vg,un}^2 + 4\theta_{N1} K_{N1} R_{fi} T_{Na} \rho'_{fi}\right]^{1/2}}{2 \cdot \theta_{N1} K_{N1}} \tag{14.4-158}$$

where

K_{N1} = CMNL, the adiabatic liquid sodium compressibility

θ_{N1} = generalized volume fraction of liquid sodium

This equation will default to a pure liquid phase equation if the fission-gas density is zero and the $\theta_{vg,un}$ is negative.

When the latter is true, i.e. when the liquid sodium does not fit into the numerical node without compressing it, the fission-gas pressure, which is calculated from Eq. 14.4-158, is compared with the sum of the saturation pressures:

$$\begin{aligned} &\text{If } \theta_{vg,un} < 0 \text{ and } P_{fi} > P_{Nv} + P_{fv}, \\ &P_{ch} = P_{fi} \end{aligned} \tag{14.4-159}$$

$$\begin{aligned} &\text{If } \theta_{vg,un} < 0 \text{ and } P_{fi} < P_{Nv} + P_{fv}, \\ &P_{ch} = P_{fi} + P_{fv} + P_{Nv} \end{aligned} \tag{14.4-159a}$$

where P_{fi} is calculated from Eq. 14.4-158.

In the pure vapor/gas regime in which no liquid sodium is left (i.e., sodium quality equals one) the channel is calculated from

$$P_{ch} = P_{Nv}\left(T_{Na}, \rho_{Nv}\right) + P_{fi}\left(T_{Na}, \rho_{fi}\right) + P_{fv}\left(T_{fu}\right)$$

where

$$P_{Nv} = RGNA \cdot \rho'_{Na} T_{Na} / \theta_{vg,un} \tag{14.4-159b}$$

The “gas constant” *RGNA* is not really a constant but is based on an interpolation between a special “gas constant”, which leads to the sodium saturation pressure when inserted into Eq. 14.4-159b, and the actual general gas constant divided by the molecular weight of sodium vapor. This is described in more detail in section 16.4.3.5 in the *LEVITATE* description.

14.4.6 Momentum Equations in the Coolant Channel

14.4.6.1 Differential Equations for the Sodium/Vapor/Gas/Mixture and for the Moving Solid or Liquid Fuel

14.4.6.1.1 Momentum Equation for the Sodium/Vapor/Gas Mixture

The momentum equation for the mixture of liquid sodium, sodium vapor, fission gas, and fuel vapor is presented in terms of the generalized smear densities, volume fractions and sources and sinks. The step from the more basic equation, which includes the cross sectional areas of each component, to Eq. 14.4-169 below has been omitted because a similar step has been explained earlier for the mass and energy equations; see Eqs. 14.4-15 or 14.4-134. However, it should be remembered that the following equation is written for variable cross section flow. The variable cross section is included in the generalized smear densities and volume fractions.

$$\begin{aligned}
&\frac{\partial}{\partial t}\left(\rho'_{Mi}\,u_{Mi}\right)+\frac{\partial}{\partial z}\left(\rho'_{Mi}\,u_{Mi}^{2}\right)\\
&\quad=-\theta_{Mi}\frac{\partial P_{ch}}{\partial z}-\rho'_{Mi}\,g\\
&\quad-\frac{F_{Mi}\,\rho'_{Mi}}{2D_{Mi}}\cdot u_{Mi}\cdot\left|u_{Mi}\right|-f_{drag}\cdot\left(u_{Mi}-u_{fu}\right)\cdot\left|u_{Mi}-u_{fu}\right|\\
&\quad-f_{bb}\,\rho_{fu,liq}\frac{\theta_{Mi}}{2}\cdot\left[\frac{\partial}{\partial t}\left(u_{Mi}-u_{fu}\right)+u_{Mi}\frac{\partial}{\partial z}\left(u_{Mi}-u_{fu}\right)\right]\\
&\quad-S'_{Na,deet}\,u_{Mi}-S'_{Na,co}\,u_{Mi}-S'_{fv,co}\,u_{Mi}
\end{aligned}\qquad(14.4\text{-}160)$$

where the last three terms are sink terms due to sodium droplet de-entertainment onto the liquid sodium film, and sodium vapor and fuel vapor condensation on clad and structure. Source terms due to fuel evaporation and dissolved fission gas release are disregarded. All other terms will be explained only after the above equation has been modified by inserting the following mass conservation for the moving sodium/vapor/gas mixture:

$$\frac{\partial\rho'_{Mi}}{\partial t}+\frac{\partial}{\partial z}\left(\rho'_{Mi}\,u_{Mi}\right)=S'_{fi,ej}+S'_{Na,et}-S'_{Na,deet}-S'_{Na,co}-S'_{fv,co}\qquad(14.4\text{-}161)$$

where the source and sink terms on the right-hand side are due to free fission-gas equation, sodium film entrainment, sodium droplet de-entrainment onto the liquid film and sodium vapor condensation on cladding and structure. Source terms due to sodium evaporation, fuel evaporation and dissolved fission-gas release are not considered.

Equation 14.4-161 can be inserted into Eq. 14.4-160 if the first term in Eq. 14.4-160 is split. Splitting this term and inserting the mixture mass conservation equation leads to a momentum equation in which the velocity is the dependent variable and not the mass flux. It can be seen later that this is of key importance for the simultaneous

solution of the two momentum equations considered. (If mass and momentum equations for both fluids are solved simultaneously as in SIMMER-II [14-19], this splitting of the mass flux will not be necessary).

Splitting the first term in Eq. 14.4-160 and inserting Eq. 14.4-161 leads to

$$\begin{aligned}\rho'_{Mi}\frac{\partial}{\partial t}u_{Mi} = &-\frac{\partial}{\partial z}\left(\rho'_{Mi}u^2_{Mi}\right)+u_{Mi}\cdot\frac{\partial}{\partial z}\left(\rho'_{Mi}u_{Mi}\right)\\ &-\theta_{Mi}\frac{\partial P_{ch}}{\partial z}-\rho'_{Mi}g-\frac{F_{Mi}\rho'_{Mi}}{2D_{Mi}}\cdot u_{Mi}\cdot\left|u_{Mi}\right|\\ &-f_{drag}\cdot\left(u_{Mi}-u_{fu}\right)\cdot\left|u_{Mi}-u_{fu}\right|\\ &-f_{bb}\rho_{fu,liq}\cdot\frac{\theta_{Mi}}{2}\cdot\left[\frac{\partial}{\partial t}\left(u_{Mi}-u_{fu}\right)+u_{Mi}\frac{\partial}{\partial z}\left(u_{Mi}-u_{fu}\right)\right]\\ &-S'_{Na,et}u_{Mi}-S'_{fi,ej}\cdot u_{Mi}\end{aligned} \qquad (14.4\text{-}162)$$

where

f_{bb} = is a factor which is zero of the particulate and annular flow regime and has a value of one for the bubbly flow regime. This means that the apparent mass effect is considered only for the bubbly flow regime. This was done because in this latter flow regime accelerating or decelerating low-density bubbles also have to accelerate or decelerate high-density fuel of half the bubble volume (apparent mass effect). This has a significant effect on the slip between the bubbles and the continuous fuel [14-49].

$S'_{Na,et}$ = the mass of sodium entrained per unit time and per unit of smear volume

$S'_{fi,ej}$ = the mass of free fission gas being ejected into the channel per unit of time and unit of smear volume

F_{Mi} = the modified friction coefficient which is different for each flow regime:

$$F_{Mi,FR1}\ \text{is calculated in}\begin{cases}\text{Eq.14.4-82} & \text{if } \alpha_{\text{Na}} < CIVOID\\ \text{Eq.14.4-86a} & \text{if liquid sodium films present}\\ \text{Eq.14.4-91} & \text{if no liquid sodium films present}\end{cases}$$

$F_{Mi,FR3}$ = see Eq. 14.4-92

$F_{Mi,FR4}$ = 0 because there is no contact between the sodium/gas mixture and the clad or structure in the bubbly flow regime.

F_{drag} = a part of the drag force which is strongly dependent on the flow regime. For the particulate flow regime this factor is [14-49, 14-63]:

$$f_{drag,FR1} = \rho_{Mi}\,\theta_{fu}\,\frac{3}{8 f_{Pa}}\left(\frac{\theta_{Mi}}{\theta_{ch,op}}\right)^{CIA5} \cdot C_{drag} \qquad (14.4\text{-}163)$$

where

$$\theta_{fu}\,3/\left(8 r_{Pa}\right) = \frac{1}{2} \cdot \pi r_{Pa}^2 \cdot N'_{Pa}$$

$N'_{Pa} = \dfrac{\theta_{fu}}{4/3\,\pi\, r_{Pa}^3}$, which is the number of fuel particles in a unit of generalized smear volume

CIA5 is an input controlling the drag dependence on the void fraction. A value of -1.7 is recommended based on references [14-49] and [14-63].

$$C_{drag} = \begin{cases} 0.44 & \text{for } \left(\mathrm{Re}\right)_{Pa} > 500 \\ 18.5 \cdot \left(\mathrm{Re}_{Pa}\right)^{-0.6} & \text{for } \left(\mathrm{Re}\right)_{Pa} < 500 \end{cases} \qquad (14.4\text{-}164)$$

where

$$\left(\mathrm{Re}\right)_{Pa} = \frac{2 r_{Pa}\,\rho_{Mi} \cdot \left| u_{Mi} - u_{fu} \right|}{\mu_{Mi}} \qquad (14.4\text{-}165)$$

μ_{Mi} = viscosity of the sodium/gas mixture (see Eq. 14.4-83a)

The partial drag term for the annular fuel flow regime is:

$$f_{drag,FR3} = CFFRMF \cdot \rho'_{Mi} / \left(2\, D_{Mi}\right) \qquad (14.4\text{-}166)$$

where

CFFRMF includes the Reynolds number dependency of the drag and the fraction of the perimeter covered by moving fuel (see Eq. 14.4-130)

D_{Mi} = $D_{ch} \cdot \theta_{Mi} / \theta_{ch,op}$, where the D_{ch} accounts for the frozen crust. The multiplication with the ratio of volume fractions accounts for the flow

cross section reduction of the mixture due to moving fuel and sodium films. The wetted perimeter is assumed to stay unchanged. This is a reasonable assumption for a true subchannel geometry.

The partial drag term for the bubbly flow is similar to that for the particulate flow (see Eq. 14.4-163) because non-deformable bubbles are assumed in PLUTO2.

$$f_{drag,FR4} = \theta_{Mi}\,\rho_{fu,liq}\,\frac{3}{8 r_{bb}}\,C_{drag}\left(\frac{\theta_{fu}}{\theta_{ch,op}}\right)^{CIA5} \tag{14.4-167}$$

where

r_{bb} = bubble radius which cancels out when the drag coefficient (see Eq. 14.4-170) is later inserted.

C_{drag} = see discussion below and Eq. 14.4-170

Transient drag coefficients for bubbly flow are not available. Therefore a drag coefficient is used which is based on steady-state experiments. The calculation of a terminal (for steady-state) velocity can be determined by balancing the gravitational and drag forces.

$$\frac{1}{2}\,C_{drag}\,\rho_{fu}\,u_{bb,\infty}^{2}\cdot\left(\pi\,r_{bb}^{2}\right)=\left(\rho_{fu}-\rho_{Mi}\right)\cdot\,g\,\cdot\left(\frac{4}{3}\pi\,r_{bb}^{3}\right) \tag{14.4-168}$$

A terminal rise velocity obtained from the drift velocity of the bubbles for the churn turbulent regime similar to that suggested by Zuber [14-19] is used:

$$u_{bb,\infty}=1.53\frac{\theta_{ch,op}}{\theta_{fu}}\left[\frac{\sigma_{fu}\,g\left(\rho_{fu}-\rho_{Mi}\right)}{\rho_{fu}^{2}}\right]^{1/4} \tag{14.4-169}$$

In the formulation of Zuber, this is a drift velocity. For the relatively high fuel fraction assumed in the bubbly fuel flow regime in PLUTO2, the actual bubble velocity and drift velocity are not very different.

After introducing Eq. 14.4-169 into Eq. 14.4-168 one obtains:

$$C_{drag}=\frac{\sqrt{\left(\rho_{fu}-\rho_{Mi}\right)g}}{\sqrt{\sigma_{fu}}}\cdot C_{x}\cdot r_{bb}\left(\frac{\theta_{fu}}{\theta_{ch,op}}\right)^{2} \tag{14.4-170}$$

where

C_x = 1.1392 based on the above Eqs. 14.4-168 and 14.4-169. The input value of CIA6 is $C_x \cdot 3/8$ which equals 0.4272.

The great advantage of Eq. 14.4-170 is that the bubble radius, which is difficult to evaluate, appears in the numerator and therefore cancels in the drag term described in Eq. 14.4-167. However, it is somewhat questionable whether the bubbly flow in PLUTO2 is really in a churn turbulent regime. At any rate, the above formulation gives a rather high draft force, which is appropriate for a bubbly flow regime.

14.4.6.1.2 Momentum Equation for the Moving Liquid or Solid Fuel

The differential equation for the fuel momentum conservation is presented in a modified form in which the fuel mass conservation is already included. The latter applies only to the liquid or solid fuel (compare with Eq. 14.4-16)

$$\frac{\partial \rho'_{fu}}{\partial t} = -\frac{\partial \rho'_{fu} u_{fu}}{\partial z} + S'_{fu,ej} \tag{14.4-171}$$

A sink term due to fuel freezing and a source term due to frozen fuel crust release or remelting are not included in this mass conservation and in the momentum conservation because they are calculated separately in the subroutine treating the fuel plateout and crust release (PLFREZ).

By splitting the momentum storage term and by including Eq. 14.6-171 (this is similar to the derivation of Eq. 14.6-162), one arrives at:

$$\begin{aligned}
\rho'_{fu}\frac{\partial u_{fu}}{\partial t} = & -\frac{\partial}{\partial z}\left(\rho'_{fu}u_{fu}^2\right) + u_{fu}\cdot\frac{\partial}{\partial z}\left(\rho'_{fu}u_{fu}\right) \\
& -\theta_{fu}\frac{\partial P_{ch}}{\partial z} - \rho'_{fu}g - \frac{F_{fu}\rho'_{fu}}{2D_{fu}}\,u_{fu}\left|u_{fu}\right| \\
& + f_{drag}\cdot\left(u_{Mi}-u_{fu}\right)\cdot\left|u_{Mi}-u_{fu}\right| \\
& + f_{bb}\,\rho_{fu,liq}\cdot\frac{\theta_{Mi}}{2}\left[\frac{\partial}{\partial t}\left(u_{Mi}-u_{fu}\right) + u_{Mi}\frac{\partial}{\partial z}\left(u_{Mi}-u_{fu}\right)\right] \\
& + S'_{fu,ej}\cdot\left(u_{fuca}\cdot CIFUMO - u_{fu}\right)
\end{aligned} \tag{14.4-172}$$

where

drag and apparent mass forces are the same as in the mixture momentum Eq. 14.4-162 except that they act in the opposite direction,

$S'_{fu,ej}$ is the mass of fuel ejected from the failed pins per unit time per unit of generalized smear volume,

and

CIFUMO is an input value between 0 and 1. It determines how much of the axial momentum of the fuel just behind the cladding rupture is retained when the fuel is ejected into the channel. In the L8 analysis [14-15, 14-12] a

value of 1 was used. But it appears that for midplane failures, which are not rapidly expanding axially, a lower value may be more appropriate,

F_{fu} is a part of the fuel friction force between moving fuel and cladding, structure, and frozen fuel and is dependent on the fuel flow regime,

$F_{fu,FR1}$ = 0 because no friction loss between fuel particles or droplets and the walls is assumed. This is based on observations form TREAT and CAMEL out-of-pile experiments in which the particulate fuel easily travels long distances.

$$F_{fu,FR3} = \begin{cases} CIFRFU \cdot CTFRFU & \text{for } \mathrm{Re}_{fu} > CIREFU \\ \dfrac{64}{\mathrm{Re}_{fu}} \cdot CTFRFU & \text{for } \mathrm{Re}_{fu} < CIREFU \end{cases} \quad (14.4\text{-}173)$$

$$\mathrm{Re}_{fu} = \frac{\rho_{fu} \cdot |u_{fu}| \cdot D_{fu}}{\mu_{fu}}$$

μ_{fu} = *VIFULQ* is input viscosity of liquid fuel

$$D_{fu} = \frac{\theta_{fu} \cdot D_{ch}}{\theta_{ch,op} \cdot CTFRFU}$$

CTFRFU is the fraction of open channel perimeter covered by moving fuel (this includes fuel moving over crusts; see Section 14.4.3.5).

CIFRFU and CIREFU are both input parameters which should be set in a manner such that there is not a sudden jump in the friction force at Re_{fu} = CIREFU

14.4.6.2 Finite Difference Equations, Simultaneous Solution Approach, and Subroutine PLMOCO

One of the problems of using a staggered grid is that the solution of the momentum equation on the cell edges requires many variables that are defined on the cell centers. In PLUTO2, most of the needed quantities are obtained by using half the sum of the upstream and downstream quantities. Therefore, neighboring cells should have a similar length in PLUTO2, although a length ratio of less than 2 to 1 for neighboring cells is not considered to cause significant inaccuracies. In the code, all variables that are obtained by halving the sum of the upstream and downstream values contain the two-letter sequence BD (for boundary) at the end of the variable name. In the finite difference equations, no special labeling of these variables will be made.

The finite difference forms of the momentum equations are not in conservative form, although both the mass and energy equations are in conservative form. This was prompted by the experience that the calculations were not always stable (in particular for stagnation cells) when using conservative momentum equations. The latter can be easily obtained by not combining the first two terms on the right-hand side of eq. 14.4-162 and by integrating the equation from the cell midpoint below a cell boundary to the cell midpoint above it (i.e., over a "momentum cell").

In the approach in PLUTO2, the first two terms on the right-hand side of eq. 14.4-162 are combined:

$$-\frac{\partial}{\partial z}\left(\rho'_{Mi}\,u^2_{Mu}\right)+u_{Mi}\cdot\frac{\partial}{\partial z}\left(\rho'_{Mi}\,u_{Mi}\right)=-\rho'_{Mi}\,u_{Mi}\,\frac{\partial}{\partial z}u_{Mi} \tag{14.4-174}$$

All terms in Eq. 14.4-162 that include a product of velocities are finite differences in the following manner:

$$\frac{F_{Mi}\,\rho'_{Mi}}{2D_{Mi}}\cdot u_{Mi}\cdot\left|u_{Mi}\right|=\frac{F_{Mi}\,\rho'_{Mi}}{2D_{Mi}}\cdot\left(u^n_{Mi}+\Delta u_{Mi}\right)\cdot\left|u^{\,n}_{Mi}\right| \tag{14.4-175}$$

$$f_{drag}\cdot\left(u_{Mi}-u_{fu}\right)\cdot\left|u_{Mi}-u_{fu}\right|=f_{drag}\cdot\left(u^n_{Mi}+\Delta u_{Mi}-u^n_{fu}-\Delta u_{fu}\right)\cdot\left|u^n_{Mi}-u^n_{fu}\right| \tag{14.4-176}$$

$$u_{Mi}\frac{\partial}{\partial z}\left(u_{Mi}-u_{fu}\right)=\left(u^u_{Mi}-\Delta u_{Mi}\right)\cdot\frac{1}{\Delta z}\,\delta\left(u^u_{Mi}-\Delta^n_{fu}\right) \tag{14.4-177}$$

where Δ implies change over a time step at a given mesh point and δ implies change over a mesh interval at a given time.

By inserting Eqs. 14.4-174 through 14.4-177 into Eq. 14.4-162, by switching from partial derivatives to δ's and Δ's, and by collecting all terms which include Δu_{Mi} on the left-hand side yields:

$$\begin{aligned}
&\Delta u_{Mi}\cdot\left\{\frac{\rho'_{Mi}}{\Delta t}+\frac{F_{Mi}\rho'_{Mi}}{2D_{Mi}}\cdot\left|u_{Mi}\right|+f_{drag}\cdot\left|u_{Mi}-u_{fu}\right|+f_{bb}\cdot\rho_{fu,liq}\cdot\frac{\theta_{Mi}}{2}\cdot\right.\\
&\left.\left(\frac{1}{\Delta t}+\frac{\delta\left(u_{Mi}-u_{fu}\right)}{\Delta z}\right)\right\}=-\rho'_{Mi}\,u_{Mi}\,\frac{\delta u_{Mi}}{\Delta z}\\
&-\theta_{Mi}\,\frac{\Delta P_{ch}}{\Delta z}-\rho'_{Mi}\,g-\frac{F_{Mi}\rho'_{Mi}}{2D_{Mi}}\cdot u_{Mi}\cdot\left|u_{Mi}\right|\\
&-f_{drag}\cdot\left(u_{Mi}-u_{fu}\right)\cdot\left|u_{Mi}-u_{fu}\right|+f_{drag}\cdot\Delta u_{fu}\cdot\left|u_{Mi}-u_{fu}\right|\\
&+f_{bb}\,\rho_{fu,liq}\,\frac{\theta_{Mi}}{2}\cdot\left[\frac{\Delta u_{fu}}{\Delta t}-u_{Mi}\,\frac{\delta\left(u_{Mi}-u_{fu}\right)}{\Delta z}\right]\\
&-S'_{Na,et}\,u_{Mi}-S'_{fi,ej}\,u_{Mi}
\end{aligned}\qquad(14.4\text{-}178)$$

The superscripts *n*, that denote the beginning of the time step, have been dropped in this equation. Before elaborating on the spatial differencing, the elimination of the Δu_{fu}'s on the right-hand side of this equation will be described. This is achieved by inserting the finite difference form of the fuel momentum equation into the above equation. The finite difference form of the fuel momentum equation can be obtained by performing the same manipulations which were done to arrive at Eq. 14.4-178. The fuel momentum Eq. 14.4-172 reads in finite difference form:

$$\begin{aligned}
\Delta u_{fu}=\frac{AHELP}{BHELP}+\Delta u_{Mi}\cdot\left\{\frac{f_{drag}\cdot\left|u_{Mi}-u_{fu}\right|}{BHELP}\right.\\
\left.+f_{bb}\,\rho_{fu,liq}\,\frac{\theta_{Mi}}{2}\cdot\left(\frac{1}{\Delta t}+\frac{\delta\left(u_{Mi}-u_{fu}\right)}{\Delta z}\right)\cdot\frac{1}{BHELP}\right\}
\end{aligned}\qquad(14.4\text{-}179)$$

where the second term in the bracket is solely due to the apparent mass (or inertial) force and

$$\begin{aligned}
AHELP=&-\rho'_{fu}\,u_{fu}\,\frac{\delta u_{fu}}{\Delta z}-\theta_{fu}\,\frac{\Delta P_{ch}}{\Delta z}-\rho'_{fu}\,g\\
&-\frac{F_{fu}\,\rho'_{fu}}{2\,D_{vu}}\,u_{fu}\left|u_{fu}\right|+f_{drag}\cdot\left(u_{Mi}-u_{fu}\right)\cdot\left|u_{Mi}-u_{fu}\right|\\
&+f_{bb}\,\rho_{fu,liq}\,\frac{\theta_{Mi}}{2}\cdot\frac{\delta\left(u_{Mi}-u_{fu}\right)}{\Delta z}\cdot u_{Mi}\\
&+S'_{fu,ej}\cdot\left(u_{fuca}\cdot CIFUMO-u_{fu}\right)
\end{aligned}\qquad(14.4\text{-}180)$$

$$BHELP = \frac{\rho'_{fu}}{\Delta t} + \frac{F_{fu}\,\rho'_{fu}}{2\,D_{vu}} \cdot \left| u_{fu} \right| + f_{bb}\,\rho_{fu,liq}\,\frac{\theta_{Mi}}{2} \cdot \frac{1}{\Delta t} + f_{drag}\,\left| u_{Mi} - u_{fu} \right| \tag{14.4-181}$$

Equation 14.4-179 can now be inserted into Eq. 14.4-178 in order to eliminate the Δu_{fu}'s from Eq. 14.4-178. This is necessary to order to perform the simultaneous solution of the mixture and fuel momentum equations. Without this simultaneous solution of the momentum equations, the solution of this two-fluid problem is not stable. The main reason is that the drag terms in the two momentum equations, which act in opposite directions and can be quite large, would not always have the same absolute value, if not solved simultaneously. These discrepancies between the absolute values of the drag would cause serious instabilities.

By inserting Eq. 14.4-179 into Eq. 14.4-178 and collecting all the terms with Δu_{Mi} on the left-hand side, one obtains:

$$\begin{aligned} \Delta u_{Mi} \cdot \Bigg\{ & \frac{\rho'_{Mi}}{\Delta t} + \frac{F_{Mi}\rho'_{Mi}}{2D_{Mi}} \cdot \left| u_{Mi} \right| + f_{drag} \cdot \left| u_{Mi} - u_{fu} \right| \\ & - f_{drag}^2 \frac{\left(u_{Mi} - u_{fu} \right)^2}{BHELP} + BMIIN \Bigg\} \\ = & -\rho'_{Mi}\,u_{Mi}\frac{\delta u_{Mi}}{\Delta z} - \theta_{Mi}\frac{\Delta P_{ch}}{\Delta z} - \rho'_{Mi}\,g - \frac{F_{Mi}\rho'_{Mi}}{2D_{Mi}} \cdot u_{Mi} \cdot \left| u_{Mi} \right| \\ & - f_{drag} \cdot \left(u_{Mi} - u_{fu} \right) \cdot \left| u_{Mi} - u_{fu} \right| + f_{drag} \cdot \frac{AHELP}{BHELP} \cdot \left| u_{Mi} - u_{fu} \right| \\ & + AMIIN - S'_{Na,et}\,u_{Mi} - S'_{fi,ej}\,u_{Mi} \end{aligned} \tag{14.4-182}$$

where

$$AMIIN = -f_{bb}\,\rho_{fu,liq}\frac{\theta_{Mi}}{2}u_{Mi} \cdot \frac{\delta\left(u_{Mi} - u_{fu} \right)}{\Delta z} + f_{bb}\,\rho_{fu,liq}\frac{\theta_{Mi}}{2} \cdot \frac{AHELP}{\left(BHELP \cdot \Delta t \right)} \tag{14.4-183}$$

$$BMIIN = -f_{bb}\,\rho_{fu,liq}\,\frac{\theta_{Mi}}{2}\cdot\left(\frac{1}{\Delta t}+\frac{\delta\left(u_{Mi}-u_{fu}\right)}{\Delta z}\right)$$

$$-f_{bb}\,\rho_{fu,liq}\,\frac{\theta_{Mi}}{2}\,f_{drag}\cdot\left|u_{Mi}-u_{fu}\right|\cdot\left(\frac{2}{\Delta t}+\frac{\delta\left(u_{Mi}-u_{fu}\right)}{\Delta t}\right)/\,BHELP \qquad (14.4\text{-}184)$$

$$-f_{bb}^{2}\,\rho_{fu,liq}^{2}\cdot\frac{\theta_{Mi}^{2}}{4}\cdot\frac{1}{\Delta t}\cdot\left(\frac{1}{\Delta t}+\frac{\delta\left(u_{Mi}-u_{fu}\right)}{\Delta z}\right)/\,BHELP$$

AMIIN and BMIIN includes most of the terms related to the apparent mass force (the others are included in AHELP and BHELP).

Equation 14.4-182 can be solved for Δu_{Mi}. This Δu_{Mi} is then used in the fuel momentum Eq. 14.4-179 to solve for the fuel velocity increment Δu_{fu}. As discussed earlier, this simultaneous solution of the two momentum equations is of key importance for achieving a stable solution of the two-fluid problem.

An item not yet discussed is the finite differencing of the spatial derivatives. As mentioned earlier, an important feature in PLUTO2 is that the convective momentum and mass fluxes are combined 9see Eq. 14.4-174) which makes the momentum equations nonconservative but leads to stable solutions. The spatial differencing of the convective term is demonstrated for the mixture momentum flux term

$$\rho'_{Mi}\,u_{Mi}\,\frac{\Delta u_{Mi}}{\Delta z}=\begin{cases}u_{Mi,i}\,\rho'_{Mi,i-1}\left(u_{Mi,i}-u_{Mi,i-1}\right)/\Delta z_{i-1} & \text{for } u_{Mi,i}>0\\ u_{Mi,i}\,\rho'_{Mi,i}\left(u_{Mi,i+1}-u_{Mi,i}\right)/\Delta z_{i} & \text{for } u_{Mi,i}<0\end{cases} \qquad (14.4\text{-}185)$$

The finite differencing of the fuel momentum flux term is done similarly.

The mixture momentum fluxes for the lowermost and for the uppermost cells use the velocities of the sodium slug interfaces if upstream or downstream velocities are needed in the above convective flux calculation. For these nodes, the Δz_i's are the distances between the slug interfaces and the lowermost or uppermost cell boundaries at which the mixture momentum equation is solved.

The fuel velocities at the extremes of the fuel region are needed for the calculation of the convective fuel momentum fluxes at the lowermost and uppermost cell boundaries and also for the calculation of the interface locations of the fuel domain which is done in subroutine PLIF. If the fuel in the uppermost or lowermost fuel node is in a continuous fuel flow regime, the velocity of the upper or lower fuel interface will be set to the velocity of the nearest cell boundary for which the fuel velocity has been calculated by the fuel momentum equations. If the uppermost or lowermost fuel node is in a particulate flow regime, a Lagrangian momentum equation will be solved for a fuel

particle at the upper or lower end of the fuel region. The force terms in this momentum equation are equivalent to those in the regular Eulerian momentum equation (see Eq. 14.4-172), but there is, of course, no convective flux terms in this Lagrangian momentum equation.

Also needed is a spatial differencing of the gradients of the relative velocities between mixture and fuel which appear in Eqs. 14.4-183 and 14.4-184. The following upwind differencing which is keyed on the much more sensitive mixture velocity is done in the following way:

$$\frac{\Delta\left(u_{Mi}-u_{fu}\right)}{\Delta z}=\begin{cases}\left(u_{Mi,i}-u_{Mi,i-1}-u_{fu,i}+u_{fu,i-1}\right)/\Delta z_{i-1} & \text{for } u_{Mi,i}>0\\ \left(u_{Mi,i+1}-u_{Mi,i}-u_{fu,i+1}+u_{fu,i}\right)/\Delta z_{i} & \text{for } u_{Mi,i}<0\end{cases} \tag{14.4-186}$$

Subroutine PLMOCO (PLUTO2 MOMENTUM CONSERVATION) sets up all of the coefficients needed for the solution of the momentum conservation. (This is mainly because these coefficients are needed at the cell edges and have previously been set only at the midpoints. However, most interfacial drag terms were not set up earlier.) Subroutine PLMOCO also sets up the convective momentum flux terms and it performs the simultaneous solution fo the two momentum equations. Moreover, the calculation of the fuel region interface velocities, which was described in the previous paragraph, is done. Subroutine PLMOCO also calculates the velocity changes of the liquid sodium slugs above and below the interaction region. This is described in the next section.

14.4.6.3 Velocity Calculation for the Liquid Sodium Slug Interfaces

Ideally, the liquid sodium slugs should be modeled with a fully compressible treatment. Although this was done in the original PLUTO code [14-3. 14-4], it has not been incorporated in PLUTO2 because it is not considered important for whole-core calculations and because a fully compressible calculation in the liquid slugs requires the use of very small time steps. In an earlier stand-alone version of PLUTO2, an optional compressible treatment, which allows a separate time step in the liquid slugs and in the interaction region, should eventually be incorporated into SAS4A/PLUTO2 for use in expensive analyses.

In the currently available treatment in SAS4A/PLUTO2, an acoustic approach is used in the lower and upper slug until the initial pressure waves reach the subassembly inlet and exit, respectively. From then on, the liquid sodium slugs are treated with an incompressible approach.

The initial acoustic approach in PLUTO2 is only used until the pressure wave hits the nearest free surface and not during the round trip time of the expanding and receding pressure wave. The latter is commonly used for the acoustic approximation, but was not used in PLUTO2 because comparisons with the fully compressible PLUTO cod [14.3, 14-4] showed better agreement when only the time for reaching the nearest free surface was used. This time is evaluated in PLUTO2 based on the velocity of sound.

The velocity of sound in the lower slug for temperature-independent density and compressibility is:

$$u_{sonic,N1,ls} = \sqrt{1/\left(\rho_{N1,ls} \cdot K_{N1}\right)} \tag{14.4-187}$$

where

$\rho_{N1,ls}$ is the average density of the lower sodium slug at the time of PLUTO2 initialization

K_{N1} is the liquid sodium compressibility which is an input constant (see CMNL)

The time to reach the free surfaces at the inlet or outlet are calculated from:

$$\Delta t_{ac,ls} = L_{ls} / u_{sonic,N1,ls} \tag{14.4-188}$$

$$\Delta t_{ac,us} = L_{us} / u_{sonic,N1,us} \tag{14.4-189}$$

where

L_{ls} and L_{us} are the lengths of the lower and upper slug, respectively.

The calculation of the velocities of the interfaces between liquid slugs and interaction region is based on the basic physics equation stating that force is equal to the rate of momentum change. This is applied to a shock front crossing the interface that is driven by a pressure difference ΔP:

$$\frac{\Delta\left(M \cdot u_{if}\right)}{\Delta t} = -\Delta P \cdot A_{ch} \tag{14.4-190}$$

where

$$\Delta\left(M \cdot u_{if}\right) = \rho_{N1} \cdot A_{ch} \cdot u_{sonic,N1} \cdot \Delta t \cdot \left[u_{if} - u_{if}\left(t_o\right)\right] \tag{14.4-191}$$

For this equation, the mass accelerated to velocity u_{if} per Δt is the mass which was crossed by the shock wave during Δt. This mass is accelerated through a velocity increment of $[u_{if} - u_{if}(t_o)]$ due to the crossing of the shock. By inserting Eq. 14.4-191 into Eq. 14.4-190, one obtains:

$$u_{if} = u_{if}\left(t_o\right) - \frac{\Delta P}{\rho_{N1}\, u_{sonic,N1}} \tag{14.4-192}$$

For u_{if} (t_o) = 0, this would be equal to the first Rankine-Hugoniot condition for shock waves [14-56] if the actual shock velocity rather than the sonic limit were used.

The above equation is used for the velocity calculation of the lower slug interface during the acoustic period (see Eq. 14.4-188):

$$u_{if,1s}(t) = u_{if,ls}(t_o) + \frac{P_{if,ls}(t) - P_{inlet}}{\sqrt{\rho_{N1,ls} / K_{N1}}} \tag{14.4-193}$$

In this equation, the definition of the velocity of sound (14.4-187) and time-dependent interface pressure were introduced. To use a time-dependent pressure is not in the spirit of Eq. 14.4-192 which assumes a constant pressure difference. This represents the main assumption of the acoustic approximation in PLUTO2. Comparison calculations with the fully compressible PLUTO code [14.3, 14-4] have shown that it is a reasonable assumption. For the velocity calculation of the upper slug, the following is used during the acoustic period:

$$u_{if,us}(t) = u_{if,us}(t_o) + \frac{P_{if,us}(t) - P_{outlet}}{\sqrt{\rho_{N1,us} / K_{N1}}} \tag{14.4-194}$$

After the acoustic period for the lower slug is over (see Eq. 14.4-188), the incompressible calculation of the lower slug mass flow rate begins. For the upper slug, this calculation starts after the time calculated by Eq. 14.4-189 has been exceeded.

A separate incompressible slug calculation is done for the lower sodium slug (below the interaction region) and for the upper slug (above the interaction region). These slugs can occupy several axial channel zones. Each channel zone is characterized by its input flow cross section, hydraulic diameter and axial length. The sodium slugs can fully extend over several channel zones, but the uppermost segment of the lower slug and the lowermost segment of the upper slug do not fully cover a channel zone because of the presence of the interaction region. The length of the uppermost segment of the lower slug and the lowermost segment of the upper slug can vary because they have moving boundaries. A control volume approach for the momentum balance of one slug segment yields (after taking into account the assumption of a constant density in the entire lower or upper slug):

$$\begin{aligned}
\rho_{N1,i} A_{ch,i} \frac{\Delta(u_{N1,i} L_i)}{\Delta t} &= -\rho_{N1} u_{N1,i+1}^2 A_{ch,i} F_{i+1} + \rho_{N1} u_{N1,i}^2, A_{ch,i} F_i \\
&- A_{ch,i} P_{ch,i+1} + A_{ch,i} P_{ch,i} - f_{fr,i} \cdot L_i \cdot \frac{(u_{N1} | u_{N1} | \rho_{N1} A_{ch})_i}{2 D_{ch,i}} - g L_i \rho_{N1,i} A_{ch,i} \\
&- 0.5 A_{ch,i} \Delta P_{z=z_i} - 0.5 A_{ch,i} \Delta P_{z=z_{i+1}} - A_{ch,i} \Delta P_{or}
\end{aligned} \tag{14.4-195}$$

where the last three terms describe entrance and exit losses and the losses due to grid spacers in this slug segment and

L_i = length of slug segment *i*

$$\rho_{N1} = \begin{cases} \rho_{N1,ls} = \text{average sodium density for lower slug calculation} \\ \qquad \text{given by the input parameter RHSLBT} \\ \rho_{N1,us} = \text{average sodium density for lower slug calculation} \\ \qquad \text{given by the input parameter RHSLBP} \end{cases}$$

$A_{ch,i}$ = cross section of slug segment *i*

F_i = 1 except *i* designates the lower (moving) interface of the upper slug. In this case, Fi 0.

F_{i+1} = 1 except when i+1 designates the upper (moving) interface of the lower slug. In this case, $F_{i+1} = 0$.

The left-hand side of Eq. 14.4-195 can be rewritten as

$$\rho_{N1}\, A_{ch,i} \cdot \frac{\Delta\left(u_{N1,i}\, L_i\right)}{\Delta t} = \rho_{N1,i}\, A_{ch,i} \left(L_i \frac{\Delta u_{N1,i}}{\Delta t} + u_{N1,i} \frac{\Delta L_i}{\Delta t} \right) \tag{14.4-196}$$

The $\frac{\Delta L_i}{\Delta t}$ is only non-zero for the uppermost segment of the lower slug and the lowermost segment of the upper slug. For the case of these two special slug segments:

$$\frac{\Delta L_i}{\Delta t} = u_{N1,i}, \text{ for the uppermost segment of the lower slug} \tag{14.4-197}$$

$$\frac{\Delta L_i}{\Delta t} = -u_{N1,i}, \text{ for the lowermost segment of the upper slug} \tag{14.4-197a}$$

For slug segments that are neither the uppermost one of the lower slug nor the lowermost one of the upper slug, the two convective terms in Eq. 14.4-195 cancel because the velocity is the same everywhere in a slug segment. For the uppermost segment of the lower slug, only the second convective term is present in Eq. 14.4-195 and this one cancels with the last term of the right-hand side of Eq. 14.4-196. For the lowermost segment of the upper slug, only the first convective term is present in Eq. 14.4-195. This one cancels also with the last term in Eq. 14.4-196 because of Eq. 14.4-197a, which holds in this case.

After inserting Eq. 14.4-196 into Eq. 14.4-195, cancelling the convective terms and the terms with $\Delta L_i/\Delta t$ (see above discussion), and after dividing the new equation with $A_{ch,i}$, all the segment equations for each of the two slugs are added up. For the lower slug, this lead to:

$$\frac{\Delta W_{ls}}{\Delta t}\cdot\sum_{i=1}^{i=IB} L_i / A_{ch,i} = -P_{ch,IB} + P_{ch,inlet} - \sum_{i=1}^{i=IB} f_i L_i \rho_{N1,ls} \frac{u_i |u_i|}{2 D_{ch,i}} - \sum_{i=1}^{i=IB} L_i \rho_{N1,ls} g - \sum_{i=1}^{i=IB} \Delta P_{zi} + \Delta P_{or,ls} \quad (14.4\text{-}198)$$

where

W_{ls} = $\rho_{N1,ls} A_{ch,i} u_{N1,i}$, the mass flow rate which is the same in all segments of the lower slug because of the assumed incompressibility

IB = index of the uppermost segment of the lower slug

$P_{ch,IB}$ = pressure in the first node of the interaction region

ΔP_{zi} = pressure drop due to the area change between segment i-1 and segment i or due to an orifice at the bottom of segment i. This pressure drop is evaluated from

$$\Delta P_{zi} = XKORV_{i,m}\, u_{N1,i} |u_{N1,i}| \frac{\rho_{N1,ls}}{2} \quad (14.4\text{-}199)$$

where $XKORV_{i,m}$ is the input contraction or expansion coefficient for upward or downward flow. This can also be an orifice coefficient for segment i. Coefficients with m = 1 are used for upward flow; coefficients with m = 2 for downward flow, $\Delta P_{or,1s}$ is the pressure drop due to grid spacers in the channel zone KZPIN and is evaluated from the equation

$$\Delta P_{or/ls} = N_{or} \cdot XKORGD \cdot u_{N1,i} |u_{N1,i}| \frac{\rho_{N1,ls}}{2} \quad (14.4\text{-}200)$$

where

KZPIN = the channel zone which contains the pins

XKORGD = an input pressure-drop coefficient for a single grid spacer

$$N_{or} = NGRDSP \cdot \left(z_{ls,if} - z_{i=KZPIN} \right) / L_{i=KZPIN} \qquad (14.4\text{-}200a)$$

where

NGRDSP = the number of uniformly distributed grid spacers in the channel zone KZPIN which is input.

$Z_{ls,if}$ = axial location of the lower slug interface

$Z_{i=KZPIN}$ = location of the lower boundary of channel zone KZPIN

For the upper sodium slug, the incompressible momentum equation is

$$\frac{\Delta W_{us}}{\Delta t} \cdot \sum_{i=IT}^{i+IMAX} L_i / A_{ch,i} = P_{ch,IT} + P_{ch,outlet} - \sum_{i=IT}^{i=IMAX} f_i L_i \rho_{NI,us} \frac{u_i |u_i|}{2 D_{ch,i}} - \sum_{i+IT}^{i=MAX} L_i \rho_{N1,us} g - \sum_{i=IT}^{i-IMAX} \Delta P_{zi} + \Delta P_{or,us} \qquad (14.4\text{-}201)$$

where

IT = index of the lowermost segment of the upper slug

IMAX = index of the top segment of the upper slug

The reason for performing the slug momentum calculations is to determine the upper and lower interface velocities of the interaction region:

$$u_{if,ls}^{n+1} = u_{if,ls}^{n} + \Delta W_{ls} \cdot \frac{1}{\rho_{N1,ls} A_{IB}} \qquad (14.4\text{-}202)$$

and

$$u_{if,us}^{n+1} = u_{if,us}^{n} + \Delta W_{us} \cdot \frac{1}{\rho_{N1,us} A_{IT}} \qquad (14.4\text{-}203)$$

where

A_{IB} = the flow area of the uppermost segment of the lower slug

A_{IT} = the flow area of the lowermost segment of the upper slug.

14.4.6.4 PLUTO2 Time Step Determination

The PLUTO2 time step Δt_{PL} used in the numerical marching of all the in-pin and channel conservation equations is restricted by the sonic Courant conditions for both the in-pin and the channel flows. An upper limit $\Delta t_{PL,pin}$ of the PLUTO2 time step computed, based on the sonic Courant condition for the in-pin flow of the fuel and fission gas two-phase mixture, is given in section 14.2.8. In the present section, another upper limit $\Delta t_{PL,ch}$ of the PLUTO2 time step is computed based on the sonic Courant condition for the multi-component channel flow, and then the smaller of the two upper limits gives the PLUTO2 time step Δt_{PL}. The upper limit $\Delta t_{PL,ch}$ is computed to be a fraction, 0.4, (same as that used in computing $\Delta t_{PL,pin}$) of the minimum time step based on the sonic Courant condition for the channel flow.

$$\Delta t_{PL,ch} + 0.4 \cdot \min \left[\Delta z_1 / \left(V_{sonic,I} + \left| u_{MI,I} \right| \right) \right]_{I=IFMIBT,IFMITP} \tag{14.4-204}$$

The minimum in Eq. 14.4-204 is evaluated over all axial cells of the interaction region. The sonic velocity in the channel is calculated from an equation [14-28] for an adiabatic homogeneous two-phase mixture of liquid sodium and fission gas/sodium vapor. The compressibility of liquid fuel being much smaller than that of liquid sodium, the fuel is assumed to be incompressible in the calculation of the sonic velocity in the channel. The effect of fuel vapor is also not included.

$$\begin{aligned} V_{sonic}^2 = \gamma_{vg} \left(P_{fi} + P_{Nv} \right) / \Big\{ & \alpha_{vg}^2 \left(\rho_{fi} + \rho_{Nv} \right) + \alpha_{vg} \left(1 - \alpha_{vg} \right) \rho_{N1} \\ & + \left[\alpha_{vg} \left(1 - \alpha_{vg} \right) \left(\rho_{fi} + \rho_{Nv} \right) + \left(1 - \alpha_{vg} \right)^2 \rho_{N1} \right] \gamma_{vg} \left(P_{fi} + P_{NV} \right) K_{N1} \Big\} \end{aligned} \tag{14.4-205}$$

where

α_{vg} = $\theta_{vg} / (\theta_{ch,op} - \theta_{fu})$ = void fraction in the two-phase mixture of liquid sodium and fission gas/sodium vapor.

γ_{vg} = ratio of specific heat at constant pressure to that at constant volume of the fission gas/sodium vapor mixture. A value of 1.4 is assumed in the PLUTO2 code.

K_{N1} = *MNL* = adiabatic compressibility of liquid sodium.

The fission-gas pressure P_{fi} and pressure P_{Nv} due to sodium vapor are obtained as explained in Section 14.4.5 using the following equations.

$$P_{fi} = R_{fi} \, \rho'_{fi} \, T_{Na} / \theta_{vg} \tag{14.4-206}$$

$$P_{Nv} = RGNA \cdot \rho'_{Nv} \, T_{Na} / \theta_{vg} \tag{14.4-207}$$

After evaluating the two upper limits $\Delta t_{PL,pin}$ and $\Delta t_{PL,ch}$ using Eqs. 14.2-55 and 14.4-204, the PLUTO2 time step Δt_{PL} is taken to be the smaller of the two.

$$\Delta t_{PL} = \min\left[\Delta t_{PL,pin}, \Delta t_{PL,ch}\right] \tag{14.4-208}$$

If the value of Δt_{PL} obtained from Eq. 14.4-208 is less than the minimum time step given by the input parameter *DTPLIN* (suggested value $2.5\text{x}10^{-5}$ s), then Δt_{PL} is set equal to *DIPLIN*. Also, the PLUTO2 time step Δt_{PL} is not allowed to exceed a maximum value of $2\text{x}10^{-4}$ s (a number built in the code). The value of Δt_{PL} obtained in this way is rounded to an integral multiple of $1.0\text{x}10^{-5}$ s. The PLUTO2 time steps are not allowed to span the coolant dynamics time-step boundaries, or the heat-transfer time-step boundaries, or the primary loop time-step boundaries.

14.5 Temperature Calculation of Cladding, Structure, Reflector and Liquid Sodium Slugs

14.5.1 Liquid Sodium, Cladding, structure, and Reflector Temperature Calculation Outside of the Interaction Region

The expulsion of coolant from the core after PLUTO2 initiation (due to fuel-coolant interaction) results in significant preheating of cladding and other structures prior to the passage of the void interface, especially for the lower liquid slug, which has a large axial thermal gradient. Consequently, it is necessary to continue to compute the temperatures outside of the interaction zone after PLUTO2 initiation in order to provide accurate updated initial temperatures for cells being added t the integration zone (i.e., voided region). Core cladding temperatures outside of the interaction zone are computed in PLHTR, which is a modified version of the standard SAS [in heat-transfer model TSHTRV. Special routines were developed to compute the liquid coolant, structure, plenum cladding, and reflector temperatures outside of the interaction zone; a description of these subroutines follows.

Coolant temperatures are computed (in subroutine PLCOOL) based on a heat-transfer time step, as are those of the wetted structure, cladding, and reflector. The heat-transfer time step may be altered (in PLUDRV) to satisfy a Courant condition in either slug, based on the instantaneous sodium velocity.

The PLUTO coolant nodes, unlike those in the SAS boiling model, are centered in the numerical cell in order to be consistent with the PLUTO node structure in the interaction zone. The finite-difference equation, given below, is time explicit and uses donor cell differencing for the convective term:

$$\begin{aligned} &A_{ch,}\,\rho_{N1}\,C_{p,N1}\,L_i\left(T_{N1,i}^{n+1} - T_{N1}^{n}\right) \\ &\quad + \Delta M_{N1,i}\,C_{p,N1}\left(T_{N1,i}^{n} - T_{N1,i-1}^{n}\right) = H_i^{\ell}\,L_i\,\Delta t_{Ht} \quad \text{for } W_{N1} > 0 \end{aligned} \tag{14.5-1}$$

where

$A_{ch,i}$ = local flow area,

L_i = wetted length in axial cell i,

$T^n_{N1,i}; T^{n+1}_{N1,i}$ = nodal coolant temperatures at times t and $t + \Delta t$.

$\Delta M_{N1,i}$ = mass transport into axial cell I during time interval Δt.

H^{ℓ}_i = heat-transfer rate from cladding and structure per unit length.

ρ_{N1} = coolant density.

$C_{p,N1}$ = coolant specific heat.

Δt_{Ht} = heat-transfer time step.

W_{N1} = liquid sodium mass flowrate.

A similar equation is used for the case of downflow.

Normally L_i is set equal to the cell length:

$$L_i = z_{i+1} - z_i \tag{14.5-2}$$

where z_i is the elevation of the lower cell boundary. Also, the mass transport ΔM_i is usually taken to be the product of the mean flowrate W_{N1}, computed from the interface displacement, times Δt_{Ht}. Exceptions are made for cells containing the void interfaces.

Consider the mesh cell containing the upper interface of the lower slug. For this case the wetted length is given by

$$L_i = z^{n+1}_{if} - z_i \tag{14.5-3}$$

where z^{n+1}_{if} = interface elevation for the lower slug at the end of the heat-transfer time step and z_i = location of the fixed mesh cell boundary below the slug interface. For the case of expulsion (negative velocity in the lower slug), the inflow into the end cell is zero unless the interface crossed the upper boundary:

$$\Delta M_{N1,i} = \begin{cases} 0 & \text{for } z^n_{if} < Z_{i+1} \\ -A_{ch,i}\left(1-f\right)\rho_{N1,i}\left(z^{n+1}_{if} - z_{i+1}\right) & \text{for } z^n_{if} \geq z_{i+1} \end{cases} \tag{14.5-4}$$

where

f = input volume fraction CINAFO of liquid film left behind.

z_{if}^{n} = interface elevation for lower slug at time *t*.

For the case when the lower slug first reenters a cell, the coolant temperature for the end cell is set by $T_{ch,i}^{n+1} = T_{ch,i-1}^{n+1}$. In subsequent time steps, the end node temperature (for reentry or $W_{N1} > 0$) is computed with the reduced wetted length and with $\Delta M_i = W_{N1}\Delta t_{Ht}$. Similar reasoning is applied to the treatment of the segment containing the lower interface of the upper slug.

The reflector, gas plenum cladding, and structure temperatures outside of the interaction zone are computed in subroutine FLSTR using straightforward, explicit-time-differenced equations. Like the coolant calculation, these temperatures are computed every heat-transfer time step. The difference equations are based on the same nodal structure as used in the pre-PLUTO2 SAS4A calculations and used the same FORTRAN variable names, which eliminates the need to initialize these variables when PLUTO2 calculations are begun. Reinitialization is required, however, during coolant reentry.

14.5.2 Cladding and Reflector Temperature Calculation in the Interaction Region

The transient cladding, reflector, and structure temperatures within the interaction region are computed in subroutine PLTECS, which is called form subroutine PLUDRV every PLUTO time step (see Fig. 14.5-1). In the interaction region, both the cladding and reflector have three radial nodes (per axial segment), each of which has a different FORTRAN name. However, a temporary radial temperature array is defined with the numbering scheme shown in Fig. 14.5-1 for the purpose of facilitating the solution of the radial heat conduction problem.

To evaluate cladding temperatures more accurately, one desires a constantly updated fuel surface temperature (every PLUTO2 time step) rather than the one computed from PLHTR every heat-transfer time step. This updated fuel surface temperature is obtained by extending the nodal structure to overlap that of the fuel model as shown in Fig. 14.5-1. By overlapping, the fuel surface temperature is computed along with the cladding temperatures every PLUTO2 time step. To insure consistency with the fuel model, the temperature of node 2 (fuel surface) is reset along with that of node 1 every heat-transfer time step. The fuel temperature calculation in PLHTR, in turn, uses an integrated fuel-heat-loss boundary condition obtained from the cladding model.

The transient heat-transfer equation for each node is expressed in the following standard form:

$$\left(MC_p\right)_i \frac{dT_i}{dt} = \left(ha\right)_{i-1}\left(T_{i-1} - T_i\right) + \left(ha\right)_i\left(T_{i+1} - T_i\right) + Q_i^{\ell} \qquad (14.5\text{-}5)$$

where

T_i is the nodal temperature.

$MC_p)_i$ is the heat capacity of the control volume per unit length.

$(ha)_i$ is the coefficient of heat transfer from node I to I + 1 per unit length,

Q_i^{ℓ} is the control volume heat-generation rate per unit length.

The coefficients $(MC_p)_i$ and $(ha)_i$ are evaluated by the following relations:

$$\left(MC_p\right)_i = \pi\left(r_i^2 - \hat{r}_{i-1}^2\right)\rho_{i+1}\,C_{p,i-1} + \pi\left(\hat{r}_i^2 - r_i^2\right)\rho_i\,C_{p,i} \tag{14.5-6}$$

$$\left(ha\right)_i = 2\pi\, r_i\,\hat{k}_i/\left(r_{i+1} - r_i\right) \qquad \text{for}\, i \neq 2,5 \tag{14.5-7a}$$

$$\left(ha\right)_i = 2\pi\, r_i\,\hat{h}_i \qquad \text{for}\, i = 2,5 \tag{14.5-7b}$$

where ρ_i, $C_{p,i}$, and k_i are the density, specific heat, and thermal conductivity of the material between nodes i and i+1. Based on the numbering scheme shown in Fig. 14.5-1, the quantities k_3 and k_4 are set equal to the input value of the cladding thermal conductivity DCL. The products $\rho_3\,C_{\rho,4}$ and $\rho_4\,C_{p,4}$ are set equal to the input parameter CPCLRH. The mean radius $\hat{r}_i$ is defined by

$$\hat{r}_i = 1/2\,\left(r_i + r_{i+1}\right) \tag{14.5-8}$$

where r_i is the radius of node i.

Cladding melting is accounted for by using an augmented clad heat capacity, C_p', when the clad temperature falls in the melting band, where C_p' is defined by:

$$C_p' = C_p + \lambda/\Delta T_{me} \tag{14.5-9}$$

where

C_p = is the normal specific heat of the solid cladding given by the input parameter CPCL.

λ = is the latent heat of fusion which is evaluated as the difference between the input values of energies of cladding at liquidus and solidus, EGSELQ and EGSESO.

ΔT_{mc} = is the difference in the liquidus and solidus temperatures of the cladding which are input (see TESELQ and TESESO, respectively).

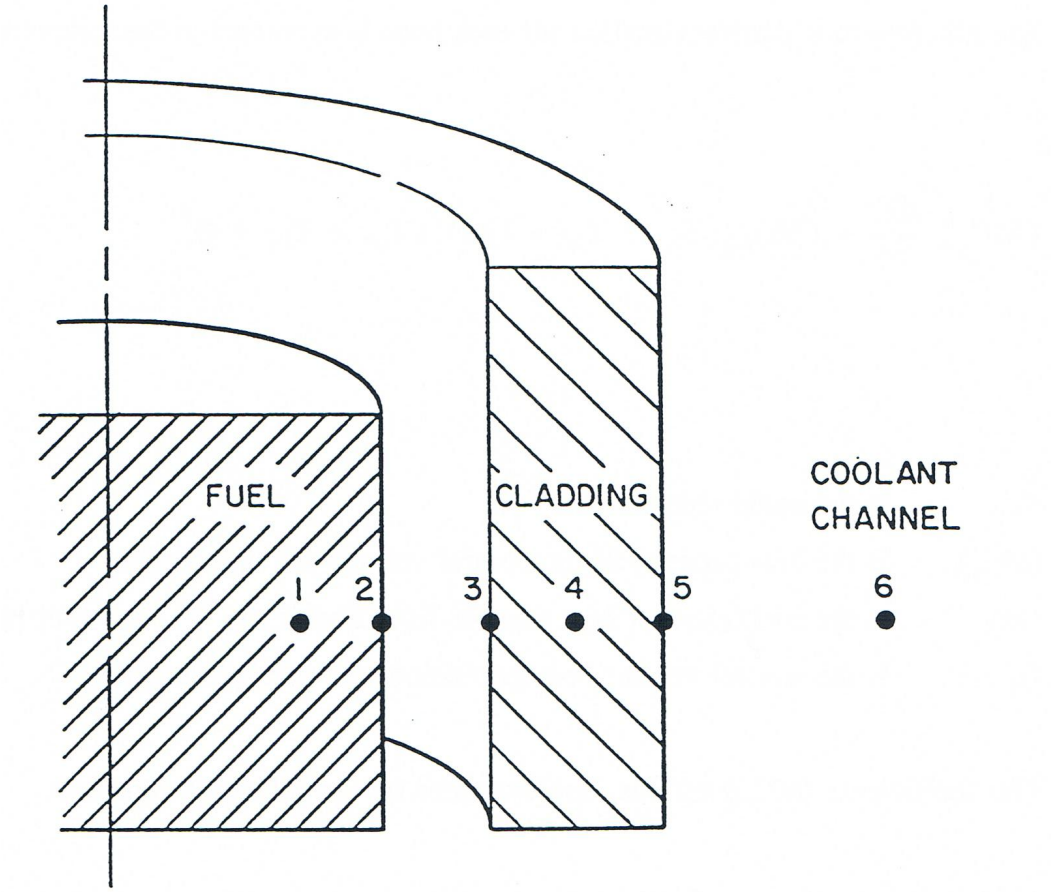

Fig. 14.5-1. Radial Node Numbering Scheme Used in Subroutine PLTECS for the Temperature Calculation of Cladding and Reflector in the Interaction Region

When entering or leaving the melting band, an adjustment o the computed temperature is required to insure that energy is properly conserved in the system. The specific heat of the cladding above the liquidus temperature is given by the input value CPSE.

The coefficient of heat transfer h_2 is set equal to the gap coefficient in the active fuel and blanket regions. In the plenum and reflector regions, however, h_2 is set equal to zero to simulate an adiabatic boundary condition at the inner cladding surface. The form of the equations for $(MC_p)_i$ and $(ha)_i$, for the reflector region is slightly modified to correspond to a slab geometry, rather than a cylindrical one.

The heat-transfer coefficient (ha), and effective sink temperature T_6 for the outer surface of the cladding and reflector are given by:

$$(ha)_5 = (ha)_{Na,cl} + (ha)_{fu,cl} + (ha)_{ff,cl} \qquad (14.5\text{-}10)$$

$$(ha)_5 \cdot T_6 = (ha)_{Na,cl} T_{Na} + (ha)_{fu,cl} T_{fu} + (ha)_{ff,cl} T_{ff} \qquad (14.5\text{-}11)$$

The three terms on the right-hand side of these equations account for heat transfer from the cladding (or structure) to each component in the channel: namely, sodium (and fission gases), moving fuel, and stationary frozen fuel.

Equation 14.5-11 is converted to a fully implicit difference equation in time. This scheme was used to obtain numerical stability when analyzing thin cladding without using excessively small PLUTO time increments. This feature will be especially useful in the analysis of ablating clad where the nodal heat capacities are shrinking to zero. The resulting difference equations for each axial slice of the core are a set of simultaneous equations for the nodal temperatures, which are solved by the Thomas algorithm for tri-diagonal coefficient matrices.

14.5.3 Structure Temperature Calculation in the Interaction Region

The temperature calculation in the subassembly hexcan wall or in the flow tube of an experiment test section normally uses the same two-node mesh structure as the remainder of the SAS4A code. However, when the SAS4A input specifies one large and one rather small node width ($w_{small} < 0.1\ w_{sr}$), the width of the small node is set to $w_{small} = 0.1\ w_{sr}$. This is done in order to avoid stability problems in the explicit temperature calculation performed in PLUTO2 or in LEVITATE. As for the pre-failure calculation of the SAS node, it is recommended that the structure node facing the coolant channel should be considerable thinner than that for the structure node facing the intersubassembly gap. This is because the node facing the coolant channel should be capable of rapidly responding to changes in the transfer from coolant or molten fuel.

In order to treat the heat transfer between two unequal nodes accurately, an approach is used in which the temperature profile in the structure is approximated by a parabola rather than a straight line between the two temperature nodes. This approach, which was originally developed for LEVITATE, has been adopted in PLUTO2. It is described in detail in Section 16.5.7.2.

14.6 Interaction with the Point Kinetics and the Primary Loop Module

14.6.1 Interaction With the Point Kinetics Module

In Section 14.1.2, the calculation in PLUTO2 of the specific power in the fuel and the total power in an original pin node was described. This was also discussed later when the heat source terms in the fuel pin and in the channel were described. The calculation of the reactivity feedbacks for channels in which PLUTO2 is active is based on fuel temperature and mass distributions and coolant voiding distributions calculated in PLUTO2 and passed to subroutine FEEDBK, where the reactivity feedbacks are calculated.

In PLUTO2, the fuel mass in the fuel pin nodes can be relatively easily calculated because the fixed Eulerian grid used for the in-pin fuel motion is part of the grid on which the material worths are defined (see Fig. 14.1-4). The calculational grid in the

coolant channel has additional cells above and below the pin grid and is therefore indexed differently. However, the axial spacing of the channel grid corresponds to that of the fuel-pin grid. A problem associated with the calculation of the fuel or sodium masses on the channel grid is the existence of partial Lagrangian cells at the edges of the interaction region. Partial Lagrangian cells such as the channel cell IFMIBT in Fig. 14.1-4 contain fuel and sodium that extend into the adjacent cell IFMIBT-1. For the purpose of the reactivity calculation this fuel and sodium are included in cell IFMIBT-1 as opposed to the approach in the hydrodynamics.

14.6.2 Coupling with the Primary Loop Module

The coupling between PLUTO2 and the primary loop module is quite simple when the PRIMAR-1 option has been chosen (i.e., input parameter IPRION set to a value less than 4). In this case, PLUTO2 uses the constant outlet coolant plenum pressure PX which is input and an inlet coolant plenum pressure which is determined by PRIMAR-1. PRIMAR-1 calculates the steady-state pump head that is multiplied by an input table or function during the transient (see section 5.9). Moreover, PLUTO2 also uses the table input for the inlet temperature history and the single input value TUPL for the reentry temperature at the outlet. However, PLUTO2 will not feed back any information to the primary loop module if the PRIMAR-1 option has been chosen.

If the PRIMAR-4 option has been chosen (IPRION=4), PLUTO2 will use the time-dependent inlet and outlet pressures which are calculated by PRIMAR-4. This is done in the following way:

$$P_{inlet}\left(t\right) = P_{inlet}\left(t_{PR1}\right) + \left(t - t_{PR1}\right) \cdot \frac{\partial P_{inlet}}{\partial t} \tag{14.6-1}$$

where

$P_{inlet}\left(t_{PR1}\right)$ is the PRIMAR-4 calculated inlet pressure at the beginning of the current primary loop time step.

$\frac{\partial P_{inlet}}{\partial t}$ is the PRIMAR-4 calculated rate or inlet pressure change during the current primary loop time step.

The outlet pressure is calculated in the same manner:

$$P_{outlet}\left(t\right) = P_{outlet}\left(t_{PR1}\right) + \left(t - t_{PR1}\right) \cdot \frac{\partial P_{outlet}}{\partial t} \tag{14.6-2}$$

PLUTO2 also uses the time-dependent inlet and outlet temperatures calculated by PRIMAR4. Since inlet and outlet temperatures change slowly, only the average values over each PRIMAR-4 step are used in PLUTO2.

When the PRIMAR-4 option has been chosen, PLUTO2 provides PRIMAR-4 with total sodium masses ejected into or received from the inlet or outlet plena during a primary loop time step:

$$\Delta M_{Na,ic,inlet} = N_{subas,ic} \int_{t_{PR1}}^{t_{PR2}} W_{Na,inlet}\, dt \tag{14.6-3}$$

and

$$\Delta M_{Na,ic,outlet} = N_{subas,ic} \int_{t_{PR1}}^{t_{PR2}} W_{Na,outlet}\, dt \tag{14.6-4}$$

where

ic = SAS4A channel number.

t_{PR1} = time at the beginning of the PRIMAR-4 time step.

t_{PR2} = time at the end of the PRIMAR-4 time step.

W_{Na} = sodium liquid and/or vapor mass flow rate.

PLUTO2 also provides PRIMAR-4 with the channel mass flow rates at the end of the primary loop time step. As long as pure liquid sodium is ejected into or received from the upper and lower plena, temporal integrals over the sodium mass flow rate times the temperature of the ejected sodium are also provided by PLUTO2. However, when the upper liquid sodium slug has been ejected out of the subassembly outlet, the additional heat added to the outlet plenum by the subsequently ejected two-phase sodium (which condenses in the plenum) and the ejected fuel during a primary loop time step is calculated by PLUTO2 for use in PRIMAR-4 (see Section 5.11.1):

$$\Delta E_{v,ic} = \left[\lambda_{Na} \cdot x_{Na} \cdot W_{Na} + u_{fu}\, \rho'_{fu} \cdot AXMX \cdot \left\{e_{fu} - EGFUTE\left(T_{Na}\right)\right\}\right] N_{sibas,ic} \cdot \left(t_{PR2} - t_{PR1}\right) \tag{14.6-5}$$

where

x_{Na}, λ_{Na} is the quality of the two-phase sodium and the enthalpy of evaporation of sodium in the highest coolant node is SAS4A channel *ic*.

EGFUTE See Eq. 14.4-150.

The quantities $\rho'_{fu}, e_{fu}, T_{Na}$ in Eq. 14.6-5 all refer to the highest coolant node HTP. A similar equation is used for the inlet plenum also. Equation 5.11-5 in Chapter 5, which calculates an estimate of the flow into or out of each SAS4A channel, requires several

coefficients for each SAS4 channel. These coefficients are calculated before boiling by the single-phase hydraulics module, then by the boiling module, and, after fuel-pin failure, they are calculated by PLUTO2 or LEVITATE, depending on which module is active in a certain channel.

14.7 Code Logic Description

14.7.1 PLUTO2 Initialization

For the initialization of PLUTO2, the flow diagrams in Fig. 14.7-1 and 14.7-2 are relevant. The flowchart in Fig. 14.7-1 shows part of the logic flow in subroutine FUINIT (FUEL MOTION INITIALIZATION) in which the decision is made whether PLUTO2 or LEVITATE should be initialized once subroutine FAILUR (which is called from the DEFORM Transient driver DFORM3 or from TSTHRM if cladding motion has already begun) has predicted pin failure. A minimum fuel melt fraction equal to the input parameter FMELTM must exist in the failing node before PLUTO2 or LEVITATE is allowed to be initiated. The decision which one of the two modules, PLUTO2 or LEVITATE, is to be initiated depends on the existence and size of a boiling region at the time of failure and whether the pins are predicted to fail into a voided or unvoided region of the channel. If there is no boiling region, as in a TOP accident, or if the pins fail into the liquid region of a partially voided channel, PLUTO2 will be initiated because of its capability of treating FCIs and sweepout of particulate fuel. If there is a large voided region in the channel, in which cladding motion may already have started, LEVITATE, which is designed for voided-channel fuel motion analysis, will be initiated. For the case of fuel pins failing into a multi-bubble boiling region, PLUTO2 will be initiated if the average void fraction in this region is below 70% at the time of pin failure. If the average void fraction is greater than 70%, it will be a LEVITATE case which has to be started by first initiating PLUTO2. In this case, the flag ILEPLI is set to 1. The flow diagram in Fig. 14.7-2 shows that a switch to LEVITATE will be immediately made in this case, once the PLUTO2 driver routine (PLUDRV) is entered.

The flow diagram shown in Fig. 14.702 shows how PLUTO2 and LEVITATE are actually initiated. In a PLUTO2 case, a check is first made to determine whether cladding motion has already begun. This is an unlikely situation that cold only come about if liquid sodium reentered into the boiling region after cladding motion had begun. This would have prevented the selection of LEVITATE. Since PLUTO2 cannot handle this situation, control is returned to subroutine FAILUR, and no fuel motion initiation will take place until the run has proceeded further and led to a more extensive boiling region that allows the initiation of LEVITATE.

In subroutine PLSAIN (PLUTO2 SAS4A COOLANT CHANNEL INITIALIZATION), the coolant mass, temperature and velocity distributions are initialized. In the case of a nonboiling channel, this is relatively straightforward, whereas it is quite complex to properly translate these quantities from the Lagrangian grid of a multi-bubble boiling module to the fixed Eulerian PLUTO2 grid.

In subroutine PLINPT (PLUTO2 *IN*PUT), the coolant channel geometry is set up, all arrays relevant for the multi-component flow in the channels are initialized, and the

geometry of the molten fuel cavity in the pins is established. The size of the latter depends on the radial and axial extent of fuel melting calculated by TSHTRN (for nonboiling cases) or TSHTRV (for cases in which boiling had already begun) and on the fuel-pin grid deformation calculated by DEFORM. The radially averaged internal fuel energy in the molten cavity is calculated based on the radial temperature profile in the cavity. The total fuel and dissolved fission-gas masses in all cavity nodes are also calculated. The latter are based on the DEFORM calculated values.

In subroutine PLSET (PLUTO2 SETUP), the molten cavity pressure, which is calculated by DEF"ORM and which can also be input (see input value PCFAIL) for parametric studies, is used to determine the mass of free fission gas in each cavity node. This was discussed earlier in more detail in Section 14.2.2. All other arrays necessary for the in-pin calculation are also initialized. Moreover, several channel arrays for the cladding and structure temperature calculations in the interaction region are initialized in this subroutine.

Subroutine PLSET1 (PLUTO2 SETUP1) initializes parameters necessary for the temperature calculation in the liquid coolant slugs, which is performed in subroutine PLCOOL. Moreover, parameters necessary for the temperature calculation in the structure, plenum cladding and reflectors outside the PLUTO2 interaction zone (which is performed in subroutine PLSTR) are initialized in PLSET1.

The flowchart in Fig. 14.7-2 also shows that LEVITAE uses most or all of the PLUTO2 initialization routines. However, LEVITATE also needs subroutine LESAIN for the case of a single large initial boiling bubble and subroutine LECLIN if cladding motion has started prior to pin failure. It can also be seen in Fig. 14.7-2 that the flag ICALC is set to 2 on the LEVITATE branch and 3 on the PLUTO2 branch. This flag controls whether the LEVITATE driver routine LEVDRV or the PLUTO2 driver routine PLUDRV will be called when the SAS4A transient driver TSTHRM is executed during the next coolant time step.

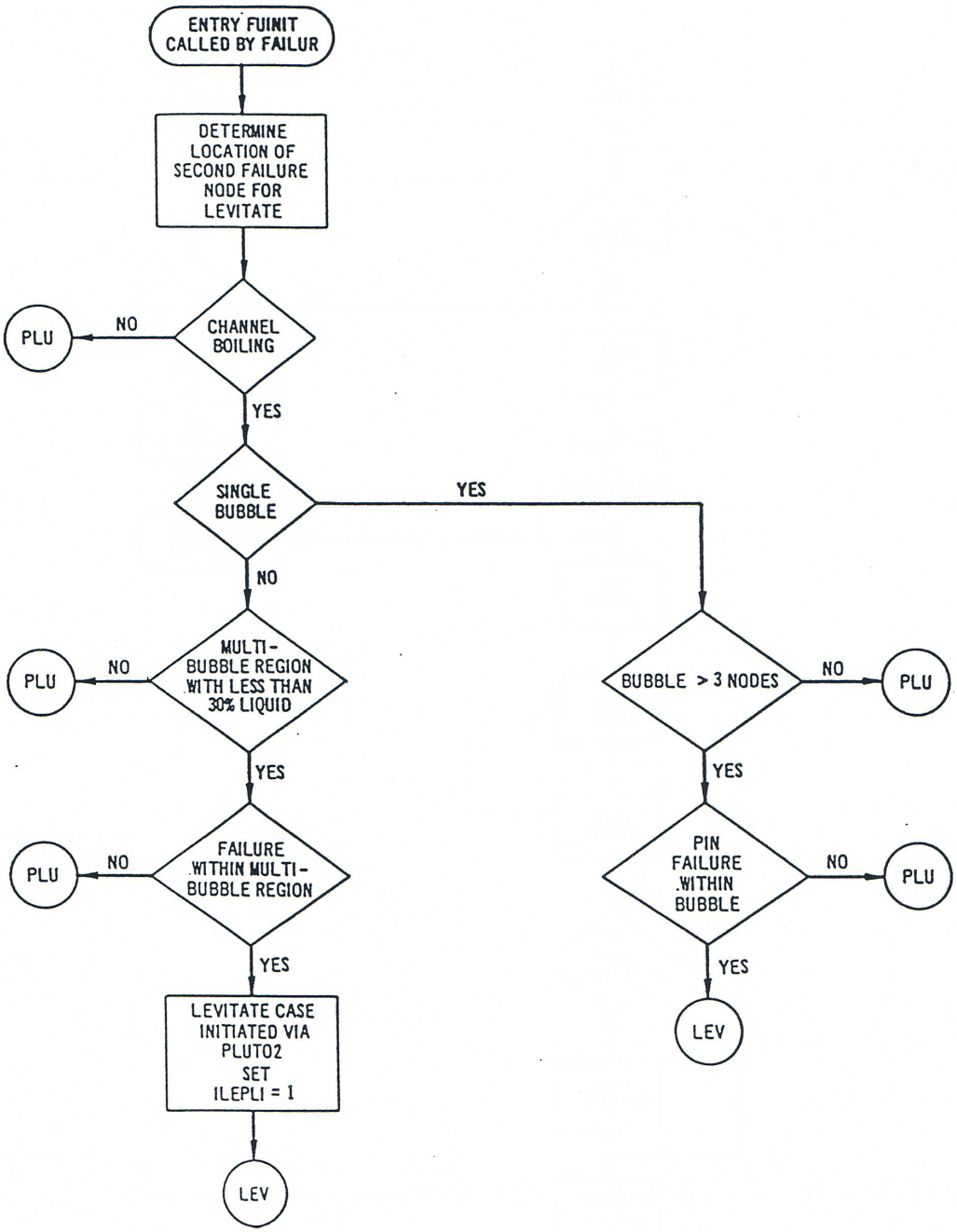

Fig. 14.7-1. First Part of the Flow Chart of Subroutine FUINIT Showing the Logic Used in Determining Whether the PLUTO2 Module of the LEVITATE Module is to be Activated. The Branch PLU or LEV Implies that the PLUTO2 Module of the LEVITATE Module is Respectively Activated. The Details of Branches PLU and LEV are Shown in Fig. 14.7-2.

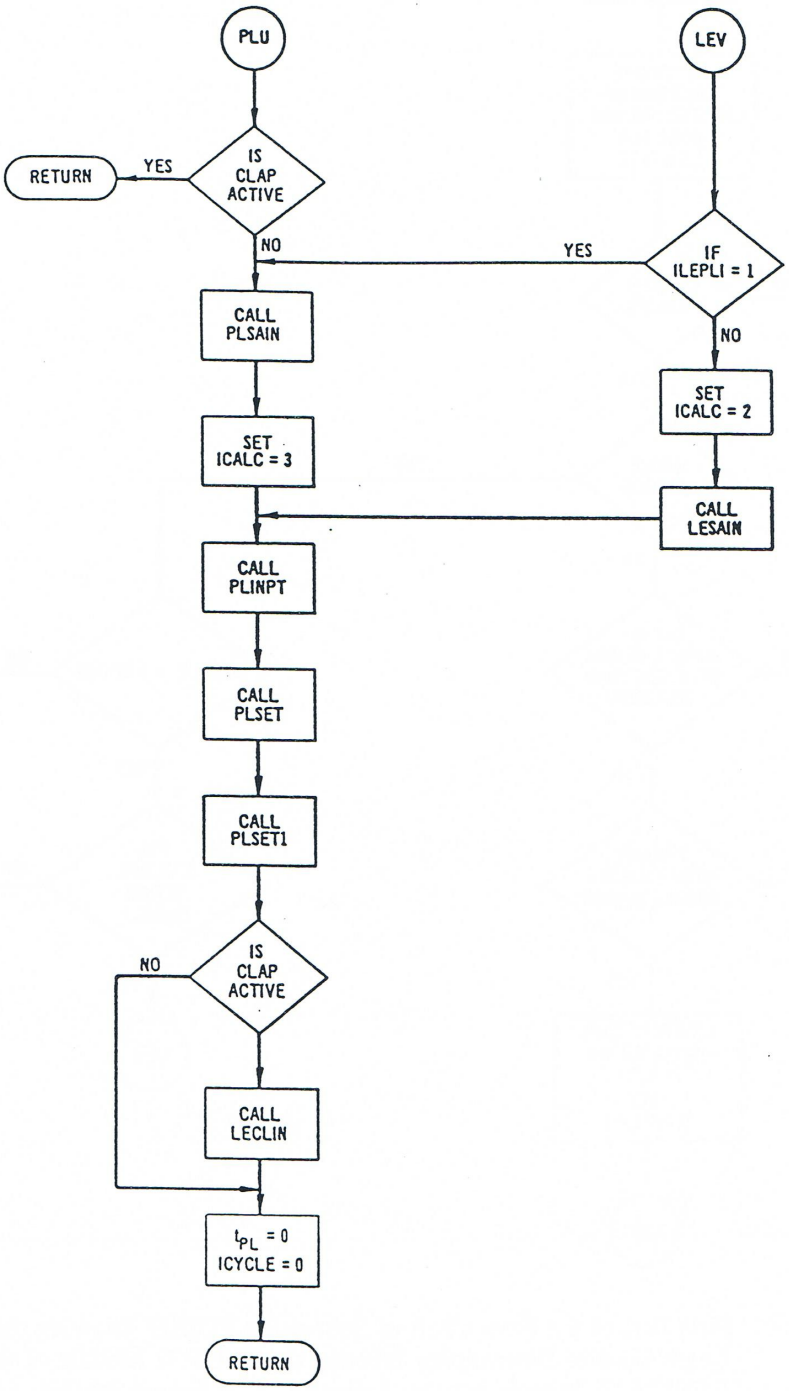

Fig. 14.7-2. Second Part of the Flow Chart of Subroutine FUINIT Showing the Initialization of the PLUTO2 and LEVITATE Modules

14.7.2 Time Step Considerations and Auxiliary Subroutines

The PLUTO2 flow logic has already been described in considerable detail in Section 14.1.2. Here, only the different time steps involved and the calling of auxiliary subroutines will be discussed.

The flow diagram of the PLUTO2 driver routine PLUDRV, which already appeared in Section 14.1.2, is also shown in Fig. 14.7-3 in order to have a complete set of PLUTO2 flow diagrams in this section.

The PLUTO2 driver routine can be called by the SAS4A transient driver TSTHRM at the beginning or at any time during a primary loop time step. The latter is common for all SAS4A calculational channels and is smaller than or equal to the main (point kinetics) time step, which is also common for all SAS4A channels.

Before PLUDRV is called for the first time in a given channel, the PLUTO2 time (TIMEPL), which is counted from the time of pin failure, is set to zero in the FAILUR routine. Moreover, the time of pin failure relative to the time of the accident initiation is recorded in the channel-dependent variable TMPLIN.

When PLUDRV is entered, TIMEPL is advanced by adding the PLUTO2 time step right after subroutine PLSET2 (which initializes temporary variables) has been called (see fig. 14.7-3). The very first PLUTO2 time-step size used is the input constant DTPLIN which is the initial and the minimum PLUTO2 time-step size. After the subroutines PLIPIN and PL2PIN have performed the in-pin calculation, a new time-step size for the in-pin motion is calculated as described in Section 14.2.8. Once all the subroutines calculating the channel fuel and sodium/gas dynamics have been called, a new time-step size for the in-pin motion is calculated as described in Section 14.2.8. Once all the subroutines calculating the channel fuel and sodium/gas dynamics have been called, anew time-step is calculated for the channel hydrodynamics (see Section 14.4.5.3). This is compared with the time-step size calculated for the in-pin motion and the smaller of the two will be used as the new PLUTO2 time-step size if it is larger than the above-mentioned input value DTPLIN. If it is smaller than DTPLIN, the latter will be used as the new PLUTO2 time-step size. Also, if it is larger than $2 \cdot 10^{-4}$ s, it will be set to this value. Moreover, if the newly determined time step extends beyond the end of a heat-transfer time step, it will be cut back such that the new PLUTO2 time will coincide with the end of the heat-transfer time step. This is possible since the heat-transfer subroutine PLHTR calculates only the fuel temperatures in the region determined by the interaction region (see Fig. 14.1-4 in section 14.1) and the fuel and cladding temperatures outside the interaction region. None of these temperatures are changing rapidly relative to PLUTO2 time-step sizes.

The determination of the heat-transfer time step is made using a series of tests. First, the initial and maximum heat-transfer time step is set to 1 ms, which is about an order of magnitude smaller than the characteristic heat-transfer time for cladding. If the initial or any later time step is larger than the current primary loop time step, it is set equal to the latter. Since the primary loop time step has to be less than or equal to the main (point kinetics) time step, it is, of course, also limited by the main time step.

The heat-transfer time step is not only used for the heat-transfer calculation of all the fuel and the cladding reflector, and the structure temperature calculation outside the interaction region, but also for the temperature calculation in the liquid sodium slugs. Since the latter involves not only heat conduction from the walls but also heat convection from the coolant cells above and below the one considered, the heat-transfer time step is also limited by a Courant condition based on the liquid slug velocity.

The flow diagram in Fig. 14.7-3 shows that PLUTO2 retains control and advances the solution using PLUTO2 time steps until the end of the primary loop time step is reached. This is different from the single-phase hydraulics driver TSCL0 and the boiling module driver TSBOIL, which return control to the SAS4A transient driver TSTHRM after every coolant time step. The latter is the basic time step in the modules controlled by TSCL0 and TSBOIL. In PLUTO2 (and LEVITATE) the coolant time step is set equal to the primary loop time step. PLUTO2 or LEVITATE thus also return control to the transient SAS4A driver at the end of this "artificial" coolant time step.

Several auxiliary subroutines used in the PLUTO2 module are not shown in the flow chart in Fig. 14.7-3. These include the function subroutine TEFUES, which calculates fuel temperatures for a given internal fuel energy and TESEEG which calculates steel temperatures for a given internal steel energy. Function subroutines EGFUTE and EGSETE perform the inverse operation for fuel and steel, respectively, i.e., calculating internal energies for a given temperature.

Several auxiliary subroutines and subroutine functions are called by the subroutine PLHTR performing the heat-transfer calculation in the solid annulus of the fuel pin and in the cladding outside the interaction region. PLHTR is a derivative of subroutine TSHTN3 described in more detail in Section 3.3.1 of Chapter 3. The most important auxiliary subroutine called by PLHTR is INVRT3, which inverts a tri-diagonal matrix. Subroutines KFUEL and KCLAD calculate the fuel and cladding conductivity, respectively. Subroutine CFUEL calculates the heat capacity of the fuel and TSHTN5 corrects fuel and cladding temperatures for the heat of fusion, if melting is occurring. Subroutine HBSMPL and function subroutine HBFND calculate the gap conductance.

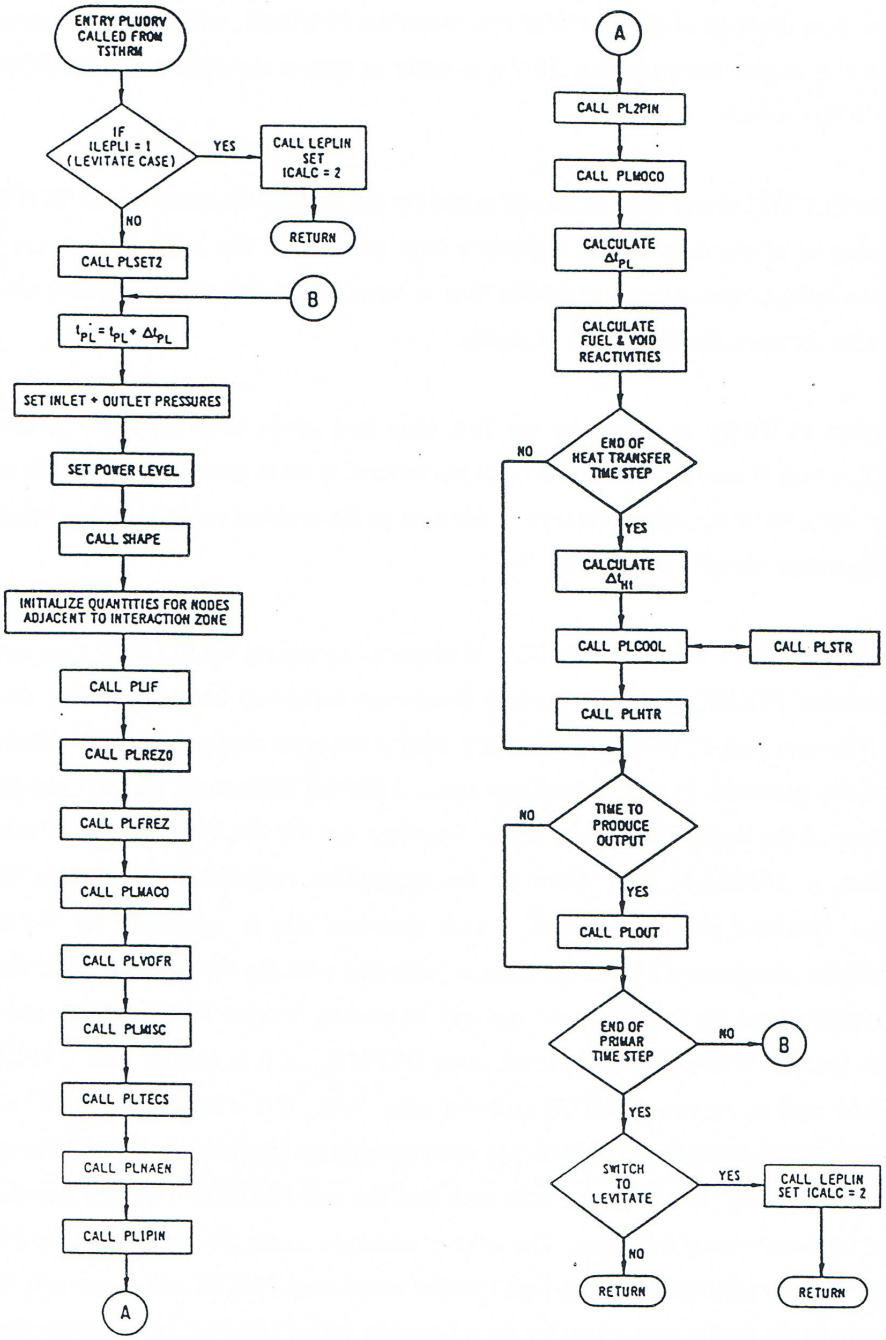

Fig. 14.7-3. Flow Chart of the PLUTO2 Driver Sub routine PLUDRV

14.8 Description of Input to and Output of the PLUTO2 Module

14.8.1 PLUTO2 Input

The SAS4A input variables required specifically by the PLUTO2 fuel motion model are given in Table 14.8-1 with their suggested values in MKS units (kilogram, meter, second, degree Kelvin). Also indicated in Table 14.8-1 are some particular sections of the documentation in which the input variables are explained, or some particular equations in which the variables are used. The first column of the table gives the location of the variable in the complete input deck of the SAS4A code. The second and the third columns give the Fortran variable names used in the code and the SAS4A input description, and the corresponding symbols, if any, used in the mathematical equations in the documentation.

14.8.2 PLUTO2 Output

The main PLUTO2 output (see Fig. 14.8-1) for a given SAS4A channel (the channel number is shown at the top of each output page) is separated into two major sections. One of these sections (output items 1 to 7 in Fig. 14.8-1) deals with the in-pin motion and the fuel and fission-gas ejection from the pins and the other section (output items 8 to 18 in Fig. 14.8-1) deals with the motion of fuel, sodium, and fission gas in the coolant channels. All output is strictly in SI units (e.g., kg, m, s, K, joules, pascals, etc.). At the time of entry to PLUTO2 module, the variables of output item 18 are printed with the message “PLUTO STARTS” and then follow output items 1 to 18.

Table 14.8-1. List of Input Variables Required by the PLUTO2 Fuel Motion Model

SAS4A Input Location	Fortran Variable	Symbol	Describing Section	Equation Number	Suggested Value in MKS Units	Comments
Block 1, INPCOM						
37	KFAILP		14.3.3		0	Mechanistic axial propagation of pin failure is opted.
38	NCPLEV		14.3.4, 14.4.3.2		3	The fuel motion calculation is switched from PLUTO2 to LEVITATE when 3 axial cladding nodes have exceeded the cladding liquidus temperature.
Block 13, PMATCM						
1124	RGAS		14.2.6	14.2-33	130.637	
1125	CINAFO			14.4-41, 14.4-42, 14.4-84		For a consistent input, the coolant film volume fraction (CINAFO) should be evaluated from cladding and structure film thicknesses WFO and WFSOO of channel 1. If CINAFO so evaluated for another channel disagrees with the above value, a consistent input is not possible.
1126	CIBBIN		14.4.3.1		0.7	See Section 14.4.3.1.
1127	CIREFU			14.4-173	2100.0	
1128	CIFRFU			14.4-173	0.02	Page 264 of Ref. [14-49].
1129	CIFUMO			14.4-172	0.5	All intra-pin axial momentum of the fuel perhaps will not be retained after ejection into coolant channel.
1130	CIVOID		14.4.3.4a		0.5	See Section 14.4.3.4.1.1.
1131	CIA1		14.4.3.b(i)	14.4-94	1.0	A recent theoretical evaluation [14-51] gives CIA1 = 3.3 to 5.0 but a preliminary calibration of the PLUTO2 module in the SAS4A version 1.0 has been done with CIA1 = 1.0
1132	CIA2		14.4.3.4b(i)	14.4-69, 14.4-98	2.0	See Section 14.4.3.4.2.1.

SAS4A Input Location	Fortran Variable	Symbol	Describing Section	Equation Number	Suggested Value in MKS Units	Comments
1133	CIA3			14.4-29, 14.4-101	0.0158	This value is good for mixed oxide fuel but not for metal alloy fuel
1134	CIA4		14.4.3.4a		0.6	CIA4 should e larger than CIVOID.
1135	CIA5			14.4-163	-1.7	Ref. [14.49, 14-63].
1136	CIA6		14.4.6.1(i)	14.4-170	0.4272	
1139	CPFU	$C_{p,fu}$		14.2-44a, 14.4-139, 14/4-143	500.0	Ref. [14-59].
1140	CDFU	k_{fu}		14.4-125	3.0	Ref [14-60].
1141	CMNL	K_{Nf}		14.4-48	4.6D-10	The compressibility of liquid sodium is very temperature-dependent and this value [14-60] corresponds to 1200 K, roughly the sodium temperature in the vicinity of pin failure at the time of failure.
1142	CDNL	$K_{N\ell}$		14.4-80	50.0	This is liquid sodium thermal conductivity at about 1200 K [14-59].
1143	CIETFU			14.4-38, 14.4-40	0.1	
1144	CDVG	k_{vg}		14.4-89	0.067	The thermal conductivity of a gas mixture is very dependent on its temperature and composition. This value of CDVG is sodium vapor thermal conductivity at 1500 K [14-61], roughly 300 K higher than the assumed sodium temperature in the vicinity of pin failure at the time of failure.
1145	VIFI				9.5D-5	This is xenon viscosity at about 1500 K extrapolated from temperature-dependent measured data [14-62] by fitting an equation of the form $T^{0.89}$ (T = xenon temperature). It is not yet used in the code.
1146	CFNACN			14.4-85	6.0D4	

SAS4A Input Location	Fortran Variable	Symbol	Describing Section	Equation Number	Suggested Value in MKS Units	Comments
1147	CFNAEV			14.4-86	6.0D5	
1148	FIFNGB			14.2-16	0.1	Also see suggested values of DEF"ORM input in Chapter 8.
1149	VINL	$\mu_{N\ell}$		14.4-83a	1.5D-4	This is liquid sodium viscosity at about 1200 K [14-61].
1150	VIVG	μ_{vg}		14.4-83a, 14.4-96	2.2D-5	This viscosity of a gas mixture is very dependent on its temperature and composition. This value of VIVG is sodium vapor viscosity at about 1500 K [14-61].
1151	EGFUSO	$e_{fu,sol}$		14.2-44, 14.4-52	1.0D6	Ref. [14-59].
1152	DZPLIN		14.4.2.3		0.02	DXPLIN must be smaller than the shortest axial mesh cell in channel.
1153	CFCOFV			14.4-98a, 14.4-117	6.0D4	This parameter is not yet used in the code.
1155	C1VIPR		14.2.4	14.2-38a	3.0D-3	
1156	C2VIPR		14.2.4	14.2-38	0.0	
1157	SUFU	σ_{fu}		14.4-169	0.45	For a consistent input, this value should equal the value input in location 1087 of block 13 [14-59].
1158	RAFPLA		14.4.3.1		2.5D-4	
1159	RAFPSM		14.4.3.1		2.5D-4	
1160	VFNALQ		14.4.3.1		0.33	See Section 14.4.3.1.
1161	EGBBLY		14.4.3.2	14.4-49, 14.4-52	EGFUSO + UFMELT(1)*0 .5	Fuel freezing is initiated when the fuel internal energy drops below the energy corresponding to 0.5 melt fraction. The value of the latter energy should be evaluated by adding 0.5 of the latent heat of fusion of fuel type 1 (location 802 of block 13) to the solidus internal energy.
1162	VIFULQ	$\mu_{fu,liq}$		14.2-29, 14.2-39, 14.4-173	4.3D-3	Ref. [14-59].
1163	VFNARE		14.4.3.1		0.8	VFNARE > VFNALQ

SAS4A Input Location	Fortran Variable	Symbol	Describing Section	Equation Number	Suggested Value in MKS Units	Comments
1164	DTPLIN	Δt_{PL}	14.2.8, 14.4.6.4	14.2-40, 14.4-28	2.5D-5	
1165	AXMX		14.2.5, 14.4.1	14.2-2, 14.4-1	1.0	Although the results of the code (except the volume fractions) are independent of the value of AXMS, the volume fractions are meaningful if AXMX is set equal to the cross-sectional if AXMS is set equal to the cross-sectional area within the outer surface of the subassembly hexcan.
1166	EPCH		14.2.4	14.2-1	1.0	
1167	TIPLMX		14.1.2 (last paragraph)		1.5	
1168	DTPLP				2.0D-3	
1169	FNMELT		14.2.2, 14.2.3	14.2-11a, 14.2-12	0.9	
1170	CIRTFS			14.2-18, 14.4-20	16.67	
1172	CIFUFZ		14.4.3.3	14.4-79	1.0	It is not yet used in the code.
1173	TIFP		14.4.3.1		0.015	It makes no difference if both fuel particle radii are equal.
1174	CIANIN		14.4.3.3	14.4-74	0.5	
1175	TEFAIL			14.3-11	TESOL(1)	It should be set equal to the solidus temperature of cladding type 1 (location 810).
1176	FNARME			14.3-10, 14.3-12	0.9	
1177	PRFAIL			14.3-13	0.0	
1178	EGMN		14.4.3.1		EGFUSO + UFMELT(1)*0.3	EGMN should be smaller than EGBBLY. It is assumed that continuous fuel flow regimes cannot be initiated below the energy corresponding to 0.3 melt fraction.
1179	HCFFMI			14.4-102, 14.4-107	1.0D5	
1180	HCFUBB			14.4-113, 14.4-116a	3.0D4	
1181	FNHTFU				0.1	It is not yet used in the code.

SAS4A Input Location	Fortran Variable	Symbol	Describing Section	Equation Number	Suggested Value in MKS Units	Comments
1184	TECLMN		14.4.3.2	14.4-51	TESOL(1)	The value should be chosen equal to the solidus temperature of cladding type 1 (location 810 of block 13) based on the consideration that cladding at solidus cannot provide support for freezing fuel.
1185	TECLRL		14.4.3.2	14.4-62	TELIQ(1)	See Section 14.4.3.2.
1186	CIHCFU		14.2.6	14.2-28	0.0158	See location 1133.
1187	HCCLMI			14.4-87, 14.4-88	1.0D5	
1188	CMFU	$K_{fu,liq}$		14.2-33	6.0D-11	The compressibility of liquid mixed oxide fuel is very dependent on temperature and the chosen value is for fuel at 4000 K [14-60].
1195	CDCL		14.5.2	14.5-7a	32.0	This value is solid cladding thermal conductivity averaged over the temperature range 1200 K to the cladding solidus temperature of 1700 K [14-59].
1196	CPCL	C_p	14.5.2	14.5-9	655.0	This value is the cladding specific heat averaged over the temperature range 1200 K to the solidus temperature of 1700 K [14-59].
1197	CPCLRH	$\rho_i C_{p,i}$	14.5.2	14.5-6	7400*CPCL	This value is obtained using the cladding specific heat CPCL (location 1196) and a cladding density of 74000 kg/m^3 averaged over the range 1200 K to the solidus temperature of 1700 K [14-59].
1198	RHSLBT	$\rho_{N\ell,\ell s}$	14.4.6.3	14.4-194, 14.4-196	728.0	This is liquid sodium density at about 1200 K [14-61].

SAS4A Input Location	Fortran Variable	Symbol	Describing Section	Equation Number	Suggested Value in MKS Units	Comments
1199	RHSLTP	$\rho_{N\ell,us}$	14.4.6.3	14.4-195, 14.4-196	0.975 * RHSLBT	It is assumed that the temperature difference between the upper and lower liquid coolant slugs is about half of the coolant temperature rise in core (ΔT_{core}), and the corresponding density difference is 2.5% for (ΔT_{core}) of about 150K. The effect of the transient heat-up of the coolant on this estimate of the input has been ignored.
1201	COEFDL(2)				9.3D-5	Ref. [14-59].
1210	EGSESO		14.5.2	14.5-9	0.834D6	Ref. [14-59].
1211	EGSELQ		14.5.2	14.5-9	EGSESO + UEMELT(1)	This value is obtained by adding the latent heat of fusion of cladding type 1 (location 816) to the solidus internal energy.
1212	CPSE		14.5.2		774.0	This is the constant value of the cladding specific heat at temperatures above the liquidus [14-59].
1214	FNSROS				0.2	The structure thickness should be divided into two mesh intervals such that the mesh interval contacting the coolant has a thickness equal to 20% of the total thickness. For consistency, this parameter must be in agreement with the input structure mesh thicknesses in locations 39-52 of block 61.
1231	SRFMLE				1.0	Also see LEVITATE input description in Chapter 16.
Block 51, INPCHN						
71	NRPI1				NPIN	All pins are assumed to fail when the fuel pin failure criterion is satisfied.
74	IPSIZE				1	
75	IBUGPL				0	
76	ICFINE				0	

SAS4A Input Location	Fortran Variable	Symbol	Describing Section	Equation Number	Suggested Value in MKS Units	Comments
77	IPRINT				0	
78	IPLOT				2	
79	IBGO				0	
80	IBSTOP				0	
81	IBNEW				0	
82	IPGO				0	
83	IPSTOP				2000	
84	IPNEW				20	
Block 65, FUELIN						
2	FMELTM		14.1.2, 14.7.1		0.2	This is required for the in-pin flow calculation of molten fuel.
19	PFFAIL				0.0	This value of PCFAIL implies that the DEFORM-IV computed molten fuel cavity pressure at pin failure time will be used in the PLUTO2 calculation.

The PLUTO2 variables that are printed in output items 1 and 2 of Fig. 14.8-1 are listed below:

ISTEP	Current main (point kinetics) time-step number.
TOTAL TIME	Time since beginning of transient. This is the regular SAS4A time.
ICYCLE	Current PLUTO2 calculational cycle for the SAS4A channel shown at the top for the page; the calculational step for the cycle number shown has just been completed at the time of a printout (see flowchart in Fig. 14.7-3).
TIMEPL	PLUTO2 time. This is counted from the time of pin failure in this channel.
DTPLU	Current PLUTO2 time-step size.

In output item 3 total masses per subassembly are shown:

SMFUPI	Current total mass of fuel in all failed pins of one subassembly.
SMFUST	Current total stationary (unmelted) fuel mass in all failed pins of one subassembly.
SMFUCA	Current total molten fuel mass in the pin cavities of all failed pins of one subassembly.
SMFICA	Current total free fission-gas mass in the pin cavities of all failed pins of one subassembly.
SMFSCA	Current total dissolved fission-gas mass in the cavities of all failed pins.

In output item 4, various other total masses for one subassembly are displayed:

SMFUME	Total mass of fuel which has melted into the molten pin cavities of all failed pins in one subassembly since the time of pin failure.
SMFIME	Total mass of the free fission gas having been added to the cavities of all failed pins in one subassembly since the time of pin failure; the total mass of dissolved fission gas having been added t the pin cavities can be calculated by multiplying SMFIME by (1-FNFIGB)/FNFIGB where FNFIGB is the input fraction of fission gas on the grain boundaries of solid fuel.
SMFSRT	Total mass of free fission gas that has been generated due to coalescence of the small (dissolved) fission-gas bubbles in all the cavities of the failed pins of one subassembly.
SMFUEJ	Total mass of fuel that has been ejected into the coolant channels since pin failure. The sum of SMFUEJ and SMFUPI should always give the total initial fuel mass of the failed pins in the subassembly considered.

SMFIEJ	Total free fission-gas mass ejected from all failed pins per subassembly.

In output item 5, several columns showing various quantities per single pin node of failure group 1 are printed:

K	Axial cell index of the pin grid; only cells which cover the molten cavity are shown. The pin gird actually extends from the bottom of the lower blanket to the top of the upper blanket.
IDISR	Gives information about cladding disruption and fuel and gas ejection. IF IDISR = 0, cladding is not ruptured; if IDISR = 2, cladding has ruptured but currently there is no ejection; if IDIST = 3, cladding has ruptured and fuel and gas ejections are going on.
DICA	Current diameter of the molten cavity in pin cell K.
AREAFR	Current are fraction of the molten pin cavity in pin cell K (i.e., cavity cross section/total fuel cross section).
FUSTAT	Stationary (solid) fuel mass in cell K. Stationary core fuel masses above and below the cavity are shown in output item 16.
FUELM	Mobile (cavity) fuel mass in cell K.
FUELSD	Fuel smear density in the cavity.
RHFUCA	Theoretical fuel density in the cavity, the fuel volume fraction in the cavity is the ratio of FUELSD to RHFUCA.
FISGM	Free fission-gas mass in the cavity part of cell K.
FISGDM	Dissolved fission-gas mass in the cavity part of cell K.
FNFIGB	Fraction of fission gas on the grain boundaries of the melting-in fuel; this fraction is instantaneously becoming free fission gas upon melt-in; it is presently a single input value.
FUEJ	Fuel mass ejected from pin cell K during the current time step.
FIEJ	Free fission-gas mass ejected from pin cell K during the current time step.

Output item 6 also prints several columns displaying variables pertaining to the in-pin motion:

K	Axial cell index of the pin grid.
I	Axial index of the corresponding channel cell.
ZZPI	Axial location of the lower cell boundary in the pin cavity.
UFPI	Fuel/fission-gas mixture velocity at the lower cell boundary. All other pin cavity quantities shown are at the cell centers.

PRCA	Total physical pressure in-cavity cell K.
PRFVPI	Fuel vapor pressure component that is based on the average fuel temperature in cavity cell K.
PRVI	Artificial viscous pressure for damping numerical oscillations behind shock fronts.
EGFUCA	Average internal fuel energy in cavity cell K.
TEFUCA	Average fuel temperature in cavity cell K.
FUMESM	Mass of fuel that has molten into cavity cell K during the current time step.
FIMESM	Mass of free fission gas that has been added to cell K during the current time step due to fuel melt-in.
SIGCL	Cladding hoop stress for cell K; a negative value indicates that the channel pressure is higher than the cavity pressure. A value of zero indicates that the cladding in this cell has failed.
UTS	Ultimate tensile strength of the cladding material at temperature TECLIN (see output item 15).

Output item 7 shows the sum of the fuel and sodium voiding reactivities and also these two reactivities separately. These reactivities are for the entire SAS4A channel under consideration which usually contains more than one subassembly (see input quantity NSUBAS). For multi-channel runs the same fuel and sodium voiding reactivities are also printed out in the short reactivity printout which appears at the end of each main (point kinetics) time step.

Output item 8 is the first row describing coolant channel variables; it prints several important integer quantities in the coolant channels (see also Fig. 14.1-4):

IFMIBT	Bottom cell of the interaction region (i.e., the region between the upper and lower sodium slugs).
IFMITP	Top cell of the interaction region.
IFFUBT	Bottom cell of the fuel region.
IFFUTP	Top cell of the fuel region.
IFFIBT	Bottom cell of fission-gas region.
IFFITP	Top cell of fission-gas region.
IFFVBT	Bottom cell of fuel vapor region.
IFFVTP	Top cell of fuel vapor region.
IFRIBT	Lowest cell containing a cladding rupture.
IFRITP	Highest cell containing a cladding rupture.

PRIN	Current inlet pressure.
PREX	Current outlet pressure.

Output item 9 shows total fuel and sodium masses in the interaction region and the fuel and sodium masses which have been ejected out of the top of the subassembly:

TOFUMA	Total fuel mass in the coolant channels of one subassembly; this should be equal to SMFUEJ (see output item4) until fuel gets ejected out of the top of the subassembly.
FUMATP	Fuel mass ejected out of the top of one subassembly.
TONAMA	Total sodium mass in the interaction region of one subassembly.
TPNAMA	Sodium mass ejected out of the top of one subassembly.

Output item 10 shows total fission-gas masses:

TOFIMA	Total mass of free fission-gas in the interaction region of one subassembly.
TODGCH	Total dissolved fission-gas mass in the interaction region of one subassembly.
TODGCL	Total dissolved fission-gas mass in the plated-out fuel on the cladding and structure (this is included in TODGCH discussed above).
FIMATP	Total free and dissolved gas masses ejected out of the top of one subassembly.

Output item 11 also shows total fission-gas masses per subassembly:

TOFIDG	Total free and dissolved fission-gas masses in all subchannels and in all failed pins of one subassembly.
TODG	Total dissolved fission-gas in all subchannels and in the cavities of all failed pins of one subassembly.
TOFI	Total free fission gas in the cavities of all failed pins and in all subchannels of one subassembly.
TOFIST	Total fission-gas mass in the stationary (unmelted) fuel of all failed pins in a subassembly (only one type of gas is currently treated in the solid part of the fuel pins in SAS4A).

Output item 12 shows channel interface locations and velocities of the various component regions (see Fig. 14.1-4 in Section 14.1):

SLIFBT(1)	Location of the upper slug interface of the lower coolant slug, which is also the location of the lower interaction zone boundary.
SLIFBR(2)	Velocity of the upper slug interface of the lower coolant slug.
SLIFTP(1)	Location of the lower slug interface of the upper coolant slug.
SLIFTP(2)	Velocity of the lower slug interface of the upper coolant slug.
FUIFBT(1)	Location of the lower boundary of the region containing fuel.
FUIFBT(2)	Velocity of the lower boundary of the region containing fuel.
FUIFTP(1)	Location of the upper boundary of the region containing fuel.
FUIFTP(2)	Velocity of the upper boundary of the region containing fuel.
FIIFBT(1)	Location of the lower boundary of the region containing free fission gas.
FIIFTP(1)	Location of the upper boundary of the region containing free fission gas.

Output item 13 shows several columns of variables pertaining to individual channels cells:

I	Axial channel index.
K	Index of pin cavity cell which is at the same elevation as channel cell I.
ZC	Location of the lower boundary of cell I.
UMCH	Velocity of the mixture of liquid sodium, sodium vapor, free fission gas and fuel vapor at the lower boundary of cell I (i.e., at ZC).
UFCH	Velocity of the liquid or solid fuel at the lower boundary of cell I (i.e., at ZC).
PRCH	Total pressure in cell I.
PRNV	Sodium vapor pressure which can be: 10^{-2} which indicates that the sodium vapor pressure is being suppressed due to a sodium liquid-phase pressure. Sodium saturation pressure if liquid is still present in cell I (i.e., THNL greater than zero – see output item 14). Gas pressure of superheated sodium vapor if no liquid sodium is left in channel cell I (i.e. if THNL is equal to zero – see output time 13).
PRFI	Free fission-gas pressure. This pressure component is equal to the total pressure for a sodium single-liquid-phase pressure situation.
PFFV	Fuel vapor pressure.

THCHOP	Open channel cross-sectional area per subassembly divided by reference area AXMS which is input. The open channel cross-sectional area is the total channel cross-section area minus the cross-sectional area of the frozen fuel crusts. THCHOP can also be interpreted as the open channel volume fraction.
THNAFM	Liquid sodium film cross-sectional area per subassembly divided by the input reference area AXMX.
THNL	Total liquid sodium cross-sectional area per subassembly divided by the input reference area AXMX.

Output item 14 contains the other area fractions and also the total component masses per axial cell I:

I	Axial channel index.
IFLAG	Indicates the type of fuel flow regime present in cell I. IFLAG = 1 indicates the particulate flow regime, IFLAG = 3 indicates partial or full annular fuel flow, and IFLAG = 4 indicates bubbly fuel flow;
THFUCH	Mobile channel fuel cross-sectional area per subassembly divided by the input reference area AXMX.
THFF	Stationary fuel crust cross-sectional area per subassembly divided by the input reference area AXMX.
THVG	Cross-sectional area of the vapor/gas flow per subassembly divided by input reference area AXMX.
FUMASS	Mobile channel fuel mass in channel cell I (a channel cell in PLUTO2 includes all subchannels of a subassembly).
FUFFMA	Stationary frozen film mass in channel cell I.
NAMASS	Total sodium mass in channel cell I.
FIMASS	Total free fission-gas mass in channel cell I.
FIDGMA	Mass of fission gas dissolved in the mobile fuel in channel cell I.
FIFFMA	Mass of fission gas dissolved in the frozen fuel crusts in channel cell I.

Output item 15 contains the variable columns giving channel, cladding, and structure temperatures in cell I:

I	Axial channel index.
IDISR	Gives information about cladding disruption and fuel and gas ejection: If IDISR = 0, cladding is not ruptured; if IDISR = 2, cladding is ruptured but currently no ejection going on; if IDISR = 3, cladding is ruptured and fuel and gas ejection are going on; IDISR also appears in output item 5.

TENA	Sodium temperature.
TEFUOS	Fuel temperature. The fuel temperature will be in the melting range if TFSOL < TEFUOS < TFLIQ (TFSIK and TFLIQ ARE INPUT). The fuel melt fraction in this case is: (TEFUOS – TFSOL)/(TFLIQ – TFSOL);
TEFFCL	Temperature of the frozen fuel crust on the cladding.
TEFFSR	Temperature of the frozen fuel crust on the structure.
TECLOS	Temperature of the cladding outer surface. The outer cladding temperature will be in the melting range if TESOL < TECLOS < TELIQ (TESOL and TELIQ are input). The cladding melt fraction in this case is: (TECLOS – TESOL)/(TELIQ – TESOL);
TECLIN	Temperature of the middle cladding node.
TESROS	Temperature of the structure surface facing the coolant channel.
TESRIN	Temperature of the structure node facing the neighboring subassembly.

Output items 16 and 17 show the pin and total fuel masses for the entire axial region containing fuel. The fuel-pin masses outside the interaction region were not shown before. The following variables are displayed:

MAFUPI	Total mass in all fuel-pin cells corresponding to channel cell I (including the stationary fuel in both the failed and unfailed pin nodes and the mobile fuel in the failed pin nodes).
MAFUTO	Sum of the total fuel in channel cell I and MAFUPI (see above). This output is valuable for comparing with one-dimensional hodoscope fuel distribution curves.

Output item 18 contains the variable columns pertaining to the temperature distribution along the entire channel including the regions outside the interaction region: It should be noted that the temperatures outside the interaction region which are shown here are calculated at the end of the last heat-transfer time step which can be fractions of a millisecond before the time of the current printout.

I	Axial channel index.
ZCOOL	Location of the lower boundary of mesh cell I.
TREFL2(2)	Inner reflector node temperature. Reflectors can be located only below or above the pin zone K2PIN.
TREFL2(1)	Temperature of the outer reflector node which is facing the coolant.
T1(NEPP)	Inner cladding surface temperature (i.e., next to the fuel).
T1(NE)	Cladding temperature of the middle cladding node.
T1(NEP)	Outer cladding surface temperature (i.e., next to the coolant).

TENA	Sodium temperature.
TSAT	Sodium saturation temperature. This is calculated only for the pin zone to detect sodium-boiling initiation.
TSTR2(1)	Temperature of the structure node facing the coolant channel.
TSTR2(2)	Temperature of the structure node facing the neighboring hexcan wall.
PRCH	Pressure in the coolant channel. This is calculated outside the fuel-pin zone only if the interaction region extends beyond it.

Output item 18 shows the message "PLUTO ENDS". This indicates that control is transferred from PLUTO2 to the SAS4A transient driver TSTHRM at the end of a primary-loop time step. The variables printed after the message "PLUTO ENDS" are not labeled in order to save space in multi-channel runs. These variables are:

ICYCLE	PLUTO2 calculational cycle.
IFMIBT	Lowermost interaction zone cell.
IFMITP	Uppermost interaction zone cell.
IFRIBT	Lowermost channel cell with failed cladding.
IFRITP	Uppermost cladding cell with failed cladding.
IFFUBT	Lowermost channel cell containing fuel.
IFFUTP	Uppermost channel cell containing fuel.
ICH	SAS4A calculational channel.
REA1	Sodium voiding reactivity for channel ICH.
REA2	Fuel reactivity for channel ICH.
TIMEPL	PLUTO2 time for channel which is counted from the time of pin failure.

The above 11 variables of output item 18 are also printed with the message "PLUTO STARTS", in the same order, at the time of entry to the PLUTO2 module, before printing output item 1.

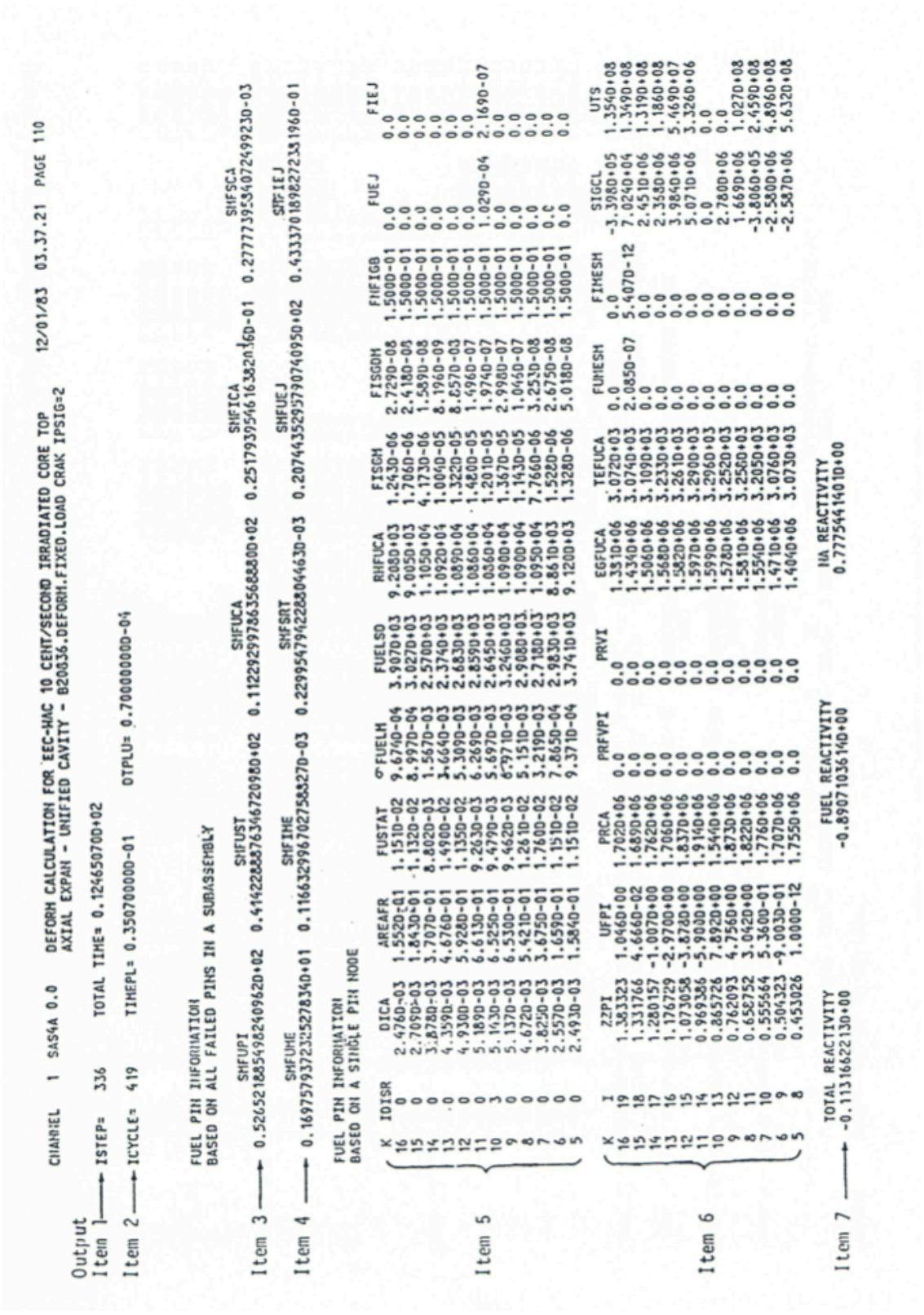

Fig. 14.8-1. Sample Output from PLUTO2 Module showing the Various Items of Output Described in Section 14.8.2

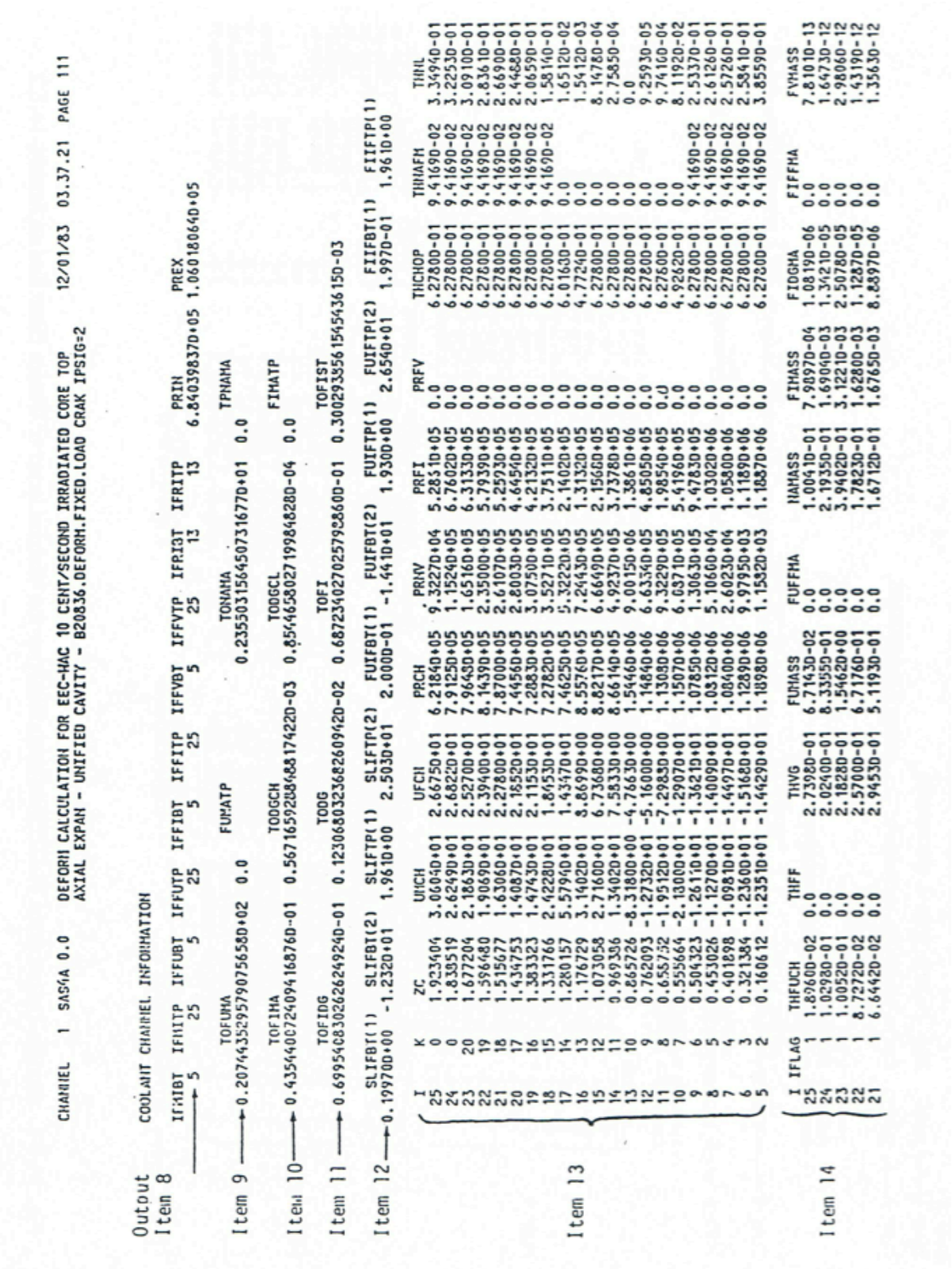

Fig. 14.8-1. Sample Output from PLUTO2 Module showing the Various Items of Output Described in Section 14.8.2 (Cont'd)

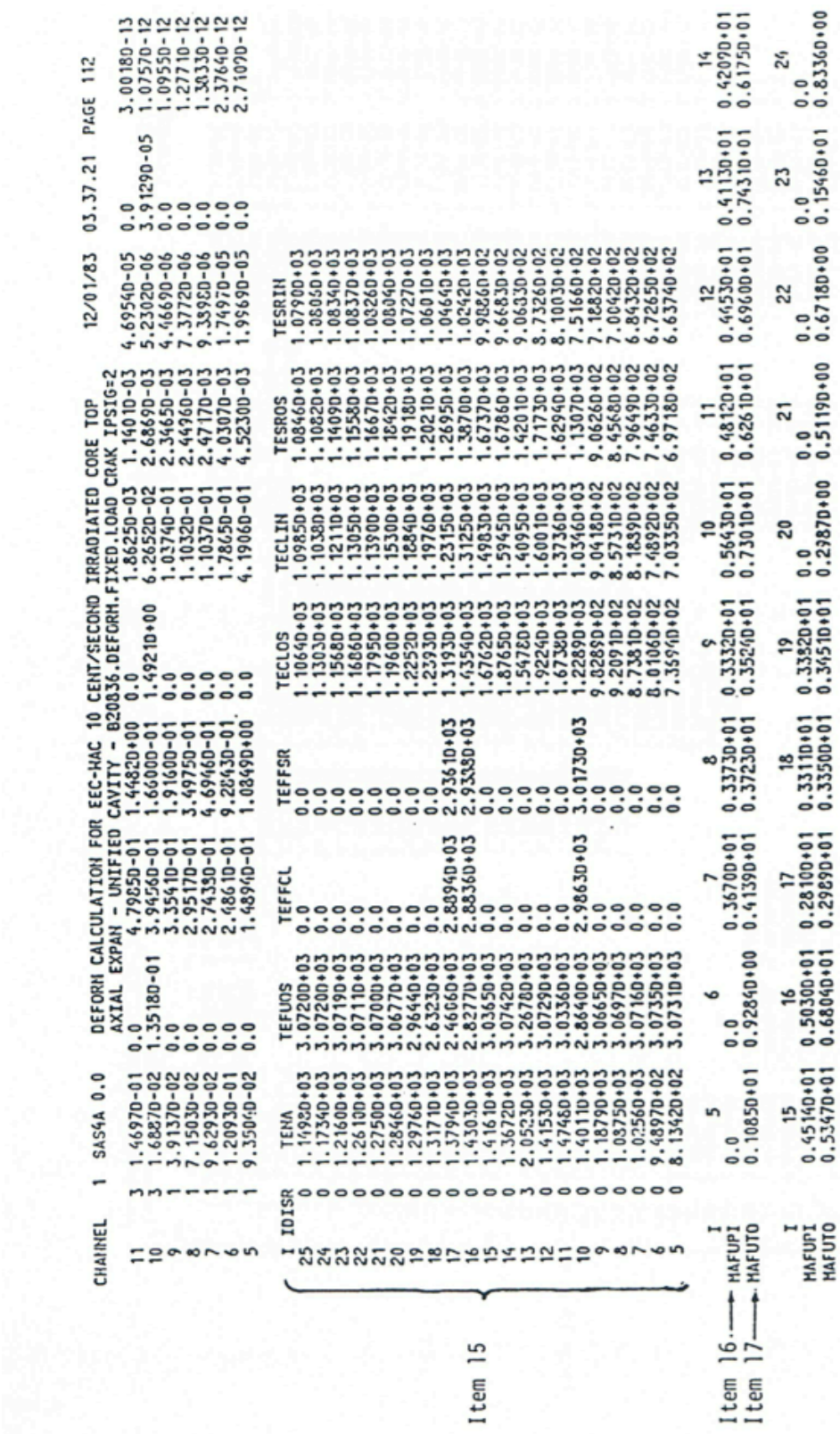

Fig. 14.8-1. Sample Output from PLUTO2 Module showing the Various Items of Output Described in Section 14.8.2 (Cont'd)

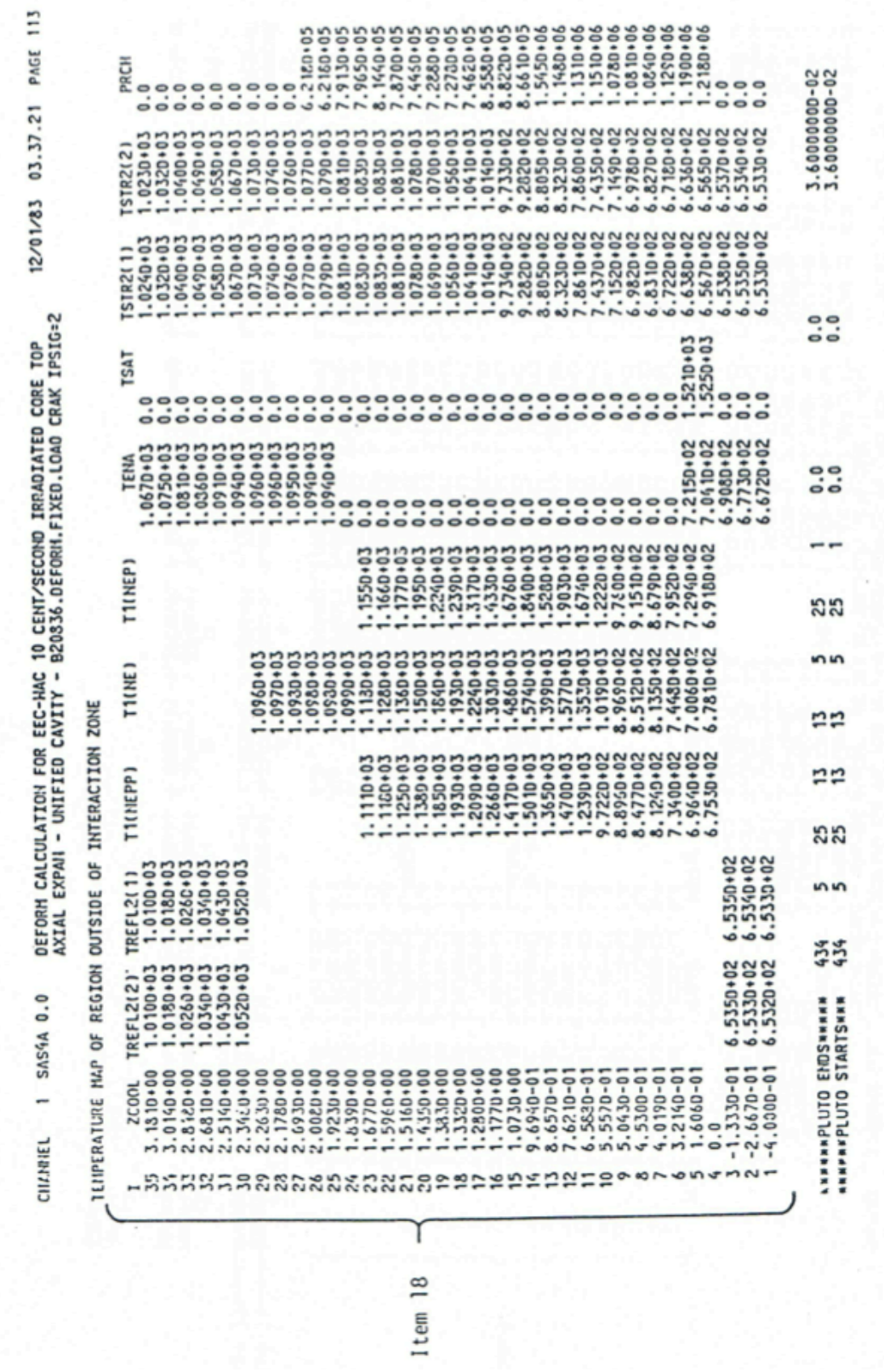

Fig. 14.8-1. Sample Output from PLUTO2 Module showing the Various Items of Output Described in Section 14.8.2 (Cont'd)

REFERENCES

14-1. L. L. Smith, et al., Unpublished information, Argonne National Laboratory, 1975.

14-2. W. R. Bohl, Unpublished information, Argonne National Laboratory, 1974.

14-3. H. U. Wider, "An Improved Analysis of Fuel Motion During an Overpower Excursion," Ph.D. Thesis, Northwestern University, Evanston, Illinois, June 1974.

14-4. H. U. Wider, et al., "An Improved Analysis of Fuel Motion During an Overpower Excursion," *Fast Reactor Safety*, CONF-740401-P3, Beverly Hills, California, p. 1541, April 1974.

14-5. A. B. Rothman, et al., "Results of Recent TOP and LOF Experiments in TREAT," *Proc. Int. Melting on Fast Reactor Safety and Related Physics*, Chicago, Illinois, CONF-761001, p. 1625, October 1976.

14-6. H. U. Wider and L. A. Semenza, "Analysis of TREAT Transient Overpower Experiments Using the PLUTO Codes," Specialists Workshop on Predictive Analysis of Material Dynamics in LMFBR Safety Experiments, Los Alamos Scientific Laboratory Report, March 1979.

14-7. P. A. Pizzica and P. B. Abramson, "A Numerical Model of Reactor Fuel and Coolant Motions Following Pin Failure," *Nucl. Sci. Eng.*, vol. 64, p. 465-479, 1977.

14-8. P. A. Pizzica, P. L. Garner, and P. B. Abramson, "A User's Guide to EPIC, a Computer Program to Calculate the Motion of Fuel and Coolant Subsequent to Pin Failure in an LMFBR," ANL-80-47, Argonne National Laboratory, Argonne, Illinois, October 1979.

14-9. D. H. Cho, R. O. Ivins, and R. W. Wright, "Pressure Generation by Molten Fuel-Coolant Interactions Under LMFBR Accident Conditions," *Proc. Conf. on New Developments in Reactor Mathematics and Applications*, Idaho Falls, March 1971.

14-10. D. P. Weber and H. U. Wider Eds., Unpublished information, Argonne National Laboratory, 1977.

14-11. H. U. Wider, "PLUTO2: A Computer Code for the Analysis of Overpower Accidents in LMFBRs," *Trans. Am. Nucl. Soc.*, vol. 27, p. 533, November 1977.

14-12. H. U. Wider, A. M. Tentner, and P. A. Pizzica, "The PLUTO2 Overpower Excursion Code and a Comparison with EPIC," *Fast Reactor Safety Meeting*, Seattle, Washington, vol. 1, p. 120, August 1979.

14-13. R. J. Page, et al., Unpublished information, Argonne National Laboratory, 1978.

14-14. R. O. McNary, et al., Unpublished information, Argonne National Laboratory, 1979.

14-15. C. H. Bowers, H. U. Wider, and A. M. Tentner, "Analysis of TREAT Transient Tests L7 and L8 with SAS3D, LEVITATE, and PLUTO2," Specialists Workshop on Predictive Analysis of Material Dynamics in LMFBR Safety Experiments, Los Alamos Scientific Laboratory, March 1979.

14-16. A. M. Tentner, H. U. Wider, and C. H. Bowers, "A Mechanistic Model of Fuel Flow Regimes and Fuel Plateout in LMFBR Overpower Accidents," *Trans. Am. Nucl. Soc.*, vol. 30, p. 448, November 1978.

14-17. A. E. Wright, et al., Unpublished information, Argonne National Laboratory, 1978.

14-18. J, K. Bigelow, G. E. Russher, and S. E. Seeman, Unpublished information, Hanford Engineering Development Laboratory, 1980.

14-19. W. A. Ragland, et al., Unpublished information, Argonne National Laboratory, 1981.

14-20. P. C. Cacciabue, et al., "Comparative Analysis of a Hypothetical 9.1 $/sec Transient Overpower Accident in an Irradiated LMFBR Core Using Different Computer Models," EUR 8018 EN, Nuclear Science and Technology, Commission of the European Community, Luxembourg, 1982.

14-21. Argonne National Laboratory, Unpublished information, 1975.

14-22. R. B. Bird, W. E. Stewart, and E. N. Lightfoot, *Transient Phenomena*, John Wiley & Sons, Inc., New York, 1960.

14-23. R. G. Deissler, "Analysis of Turbulent Heat Transfer, Mass Transfer, and Friction in Smooth Tubes at High Prandtl an Schmidt Numbers," NACA Report 1210, 1955.

14-24. A. E. Wright, et al., "Transient Overpower Test H5 on FFTF-Type Intermediate-Power Fuel," Unpublished information, Argonne National Laboratory, Illinois, June 1975. Also see A. E. Wright, et al., "Inpile Failure Threshold Experiment (H5) With Pre-Irradiated FFTF-Type Fuel," *Trans. Am. Nucl. Soc.*, vol. 18, p. 211, June 1975.

14-25. R. J. Page A. B. Rothman, and P. H. Froehle, Unpublished information, Argonne National Laboratory, 1979.

14-26. W. L. Hu, Unpublished information, Hanford Engineering Development Laboratory, 1983.

14-27. H. U. Wider, J. f. Jackson, and D. T. Eggen, "An Improved Viscous Pressure Formulation for Two-Phase Compressible Hydrodynamics Calculations," *Trans. Am. Nucl. Soc.*, vol. 17, p. 246, November 1973.

14-28. R. E. Henry, M. A. Grolmes, and H. K. Fauske, "Pressure Pulse Propagation in Two-Phase One- and Two-Component Mixtures," ANL-7792, Argonne National Laboratory, Argonne, Illinois, March 1971.

14-29. L. L. Smith, Unpublished information, Los Alamos Scientific Laboratory, 1980.

14-30. J. H. Stuhmiller and R. E. Ferguson, "Comparison of Numerical Methods for Fluid Flows," EPRI NP-1236, Electric Power Research Institute, Palo Alto, California, November 1979.

14-31. Patrick J. Roache, *Computational Fluid Dynamics*, Hermosa Publishers,

Albuquerque, New Mexico, 1976.

14-32. H. U. Wider, J. F. Jackson, and W. R. Bohl, "The Slip Flow Treatment in the PLUTO Code," *Proc. Conf. on Computational Methods in Nuclear Engineering*, Charleston, South Carolina, CONF-760413, Vol. 1, pp. II-125 to II-144, April 1975.

14-33. M. Ishii and M. A. Grolmes, "Inception Criteria for Droplet Entrainment in Two-Phase Concurrent Film Flow," *AICHE J.*, vol. 21, no. 2, p. 308-317, March 1975.

14-34. M. Ishii and M. A. Grolmes, Unpublished information, Argonne National Laboratory, 1974.

14-35. R. N. Knoopman, et al., Unpublished information, Argonne National Laboratory, 1977.

14-36. A. E. Wright, et al., Unpublished information, Argonne National Laboratory, 1976.

14-37. H. U. Wider and A. E. Wright, "Analysis of a Sodium Reentry Event in the H4 TREAT Tests," *Trans. Am. Nucl. Soc.*, vol. 22, p. 428, November 1975.

14-38. B. W. Spencer, et al., "Fuel Motion in the CAMEL TOP-Simulation LMFBR Safety Tests," *Proc. Intl. Meeting on Fast Reactor Safety*, Seattle, Washington, vol. 4, p. 1756-1765, August 1979.

14-39. Argonne National Laboratory, Unpublished information, 1980.

14-40. S. J. Board and R. W. Hall, "Recent Advances in Understanding Large Scale Vapor Explosions," *Proc. Third Specialist Meeting on Sodium/Fuel Interaction in Fast Reactors*, Tokyo, Power Reactor and Nuclear Fuel Development Corporation Report PNC N251 65-12, vol. 1, pp. 249-284, March 1976.

14-41. H. Jacobs, "Computational Analysis of Fuel-Sodium Interaction With an Improved Method," *Proc. Int. Meeting on Fast Reactor Safety and Related Physics*, Chicago, CONF-761001, pp. 926-935, October 1976.

14-42. W. A. Ragland, et al., "Interpretation of SLSF Experiment P4 Instrument Response," *Trans. Am. Nucl. Soc.*, vol. 44, p. 332-333, June 1983.

14-43. Argonne National Laboratory, Unpublished information, 1978.

14-44. S. J. Hakim, Unpublished information, Los Alamos Scientific Laboratory, 1979.

14-45. M. Epstein and G. M. Hauser, "The Melting of Finite Steel Slabs in Flowing Nuclear Reactor Fuel," *Nucl. Eng. Des.*, vol. 52, p. 411-428, 1979.

14-46. J. J. Sienicki and B. W. Spencer, Unpublished information, Argonne National Laboratory, 1981.

14-47. M. W. Maresca and O. E. Dwyer, "Heat Transfer to Mercury Flowing In-line Through a Bundle of Circular Rods," *Trans. ASME, J. Heat Transfer*, vol. 86, p. 180-186, May 1964.

14-48. John G. Collier, *Convective Boiling and Condensation*, 2nd. Ed., McGraw-Hill Book Company, New York, p. 33, 1981.

14-49. G. B. Wallis, *One-Dimensional Two-Phase Flow*, McGraw-Hill Book Company, New York, 1969.

14-50. M. M. El-Wakil, *Nuclear Power Engineering*, McGraw-Hill Book Company, New York, 1962.

14-51. Kalimullah and H. U. Wider, Unpublished information, Argonne National Laboratory, 1983.

14-52. G. L. Bordner, et al., Unpublished information, Argonne National Laboratory, 1978.

14-53. A. K. Fisher, et al., "Fuel Dynamics Loss-of-Flow Test L3," ANL-76-79, Argonne National Laboratory, Illinois, June 1976.

14-54. J. G. Eberhart, et al., Unpublished information, Argonne National Laboratory, 1976.

14-55. Argonne National Laboratory, Unpublished information, 1980.

14-56. R. Courant and K. O. Friedrichs, *Supersonic Flow and Shock Waves*, Interscience Publishers, Inc., New York, 1948.

14-57. Argonne National Laboratory, Unpublished information, Argonne National Laboratory, 1977.

14-58. M. Ishii, Argonne National Laboratory, personal communication, 1980.

14-59. Argonne National Laboratory, Unpublished information, Argonne National Laboratory, 1976.

14-60. J. K. Fink, M. G. Chasanov, and L. Leibowitz, Unpublished information, Argonne National Laboratory, 1982.

14-61. G. H. Golden and J. V. Tokar, "Thermophysical Properties of Sodium," ANL-7323, Argonne National Laboratory, Illinois, August 1967.

14-62. J. O. Hirschfelder, C. F. Curtiss, and R. B. Bird, *Molecular Theory of Gases and Liquids*, John Wiley and Sons, Inc., New York, 1954.

14-63. Kalimullah and A. M. Tentner, Unpublished information, Argonne National Laboratory, 1984.